2006

Contaminant transport processes in onsite waste disposal systems

Thidarat Bunsri
University of Wollongong

CONTAMINANT TRANSPORT PROCESSES IN ONSITE WASTE DISPOSAL SYSTEMS

A thesis submitted in fulfilment of the
requirements for the award of the degree

Doctor of Philosophy

from

UNIVERSITY OF WOLLONGONG

by

THIDARAT BUNSRI (B.Eng, M.Eng)

SCHOOL OF CIVIL, MINING AND ENVIRONMENTAL ENGINEERING

2006

THESIS CERTIFICATION

CERTIFICATION

I, Thidarat Bunsri, declare that this thesis, submitted in partial fulfilment of the requirement for the award of Doctor of Philosophy, in the School of Civil, Mining and Environmental Engineering, University of Wollongong, is wholly my own work unless otherwise referenced or acknowledged. The document has not been submitted for qualifications at any other academic institution.

_____

Thidarat Bunsri

ABSTRACT

Groundwater contamination is an important environmental problem to the present day. The groundwater pollution caused by pathogens from human excreta, particularly in developing countries is directly associated with the lack of safe drinking water and proper sanitation. A septic system is the simplest and the most economic onsite sanitation unit. It includes a tank and a drainage field. A septic tank is designed to receive domestic wastewater, especially black and grey, or a combination of both. Due to the worldwide spread of septic tank usage, it was estimated that they disposed of the largest volumes of wastewater into the ground through their drainage fields. Poorly discharged effluent often contains high concentrations of organic carbon, nutrients and pathogens. Therefore, there is a need to develop a model for estimating the migration of contaminants in a drainage field. The aim of this study was to develop a model for the transport and fate of pollutants discharged by a septic tank below the ground surface.

Firstly, a conceptual model was developed to describe removal mechanisms and the fate of contaminants such as chemical oxygen demand (COD), nitrate, phosphate and *Escherichia Coli* (*E.Coli*) in unsaturated soil conditions. The governing equations were formulated to support the established conceptual model. The migration of contaminants depends on the advection-dispersion transport and retardation processes that can be evaluated using a modified form of the Richards equation. The retardations are mainly due to adsorption and biodegradation processes that are traditionally described using the multiplicative Monod's equations and isotherm equation, respectively. Secondly, a mathematical model was developed by modifying these governing equations. The mathematical model is in the form of hyperbolic/parabolic partial differential equations with strong nonlinearity due to pressure head dependencies in the specific moisture capacity, hydraulic conductivity terms and complex retardation processes. In order to solve the mathematical model, a numerical approach was employed. The developed model was solved numerically using the Galerkin finite element method. The numerical model was coded with MATLAB software. Finally, the developed model was calibrated using the writer's laboratory data and other data obtained from case studies.

The movement of water and wastewater and the retardation of contaminants were investigated experimentally and the results of these experiments were compared with

the simulations of the developed model. Two types of porous media were used, sand and topsoil. Sand is a uniform and non-reactive porous medium which provides an effective permeability for infiltration. Topsoil is a non-uniform and reactive porous medium which provides various rates of retardation. The infiltration experiments were conducted using laboratory and pilot scale columns of 20 and 120 cm effective heights, respectively. Laboratory scale sand and soil columns were used to determine the hydraulic properties of sand and soil, the movement of water with various boundary conditions such as gravitational, static equilibrium of capillary and infiltration-redistribution flows. A pilot scale soil column was used to examine the transport of contaminants in field conditions.

The computational code used in the advective-dispersive transport (Richards' equation) was applied to the data obtained from the laboratory scale soil columns. The simulation results for the hydraulic pressure head and moisture content in both sand and soil columns matched the observed data well. The contaminant transport model could satisfactorily estimate the contaminant concentration and retardation zone. The simulation results indicate that all contaminants except *E.Coli* were reduced significantly across a 15 cm depth (elevation of 105 cm) whereas the *E.Coli* reduction zone was observed within 10 cm depth (elevation of 110 cm) of the soil column.

Eight case studies were used in the model verification processes. The developed model could effectively predict the profiles of pressure head and moisture content observed in infiltration and infiltration-redistribution systems. Furthermore, the developed model could predict the profiles of non-reactive and reactive contaminant concentrations presented in all the case studies. This indicates that the developed model is an effective alternative tool for predicting the migration of contaminants in the ground underneath a septic effluent drainage field.

ACKNOWLEDGEMENTS

I would wish to thank my supervisors, Associate Professor Muttucumaru Sivakumar and Dr. Hagare Dharmappa for their advice and continuous support for the duration of this research. Their suggestions helped to overcome many problems and reinforced the need for persistence to accomplish a satisfactory conclusion.

I also thank Associate Professor Ernest Baafi for many useful suggestions relating to the MATLAB programme. I also thank the technical staff of the School of Civil, Mining and Environmental Engineering, namely, Joanne George, Norm Gal, Ian Laird, Alan Grant and Robert Rowlan who guided and provided help, especially in the analytical techniques and the experimental set up. I am thankful to the staff of the Engineering Enquiry Centre and Engineering Faculty IT as well.

Thanks also to my scholarship advisors, Assistant Professor Jarurat Voranisarakul and Assistant Professor Wannee Puttitaworn. Funding support for this work was provided by the National Research Center for Environmental Engineering and Hazardous Waste Management (NRC-EHWM), King Mongkut's University of Technology Thonburi, Thailand and the Royal Thai Government, Ministry of Education. I also thank Associate Professor Jin Anotai, Robert Hosking and Dr. Joe Shonhardt for their help in editing this thesis.

A special thanks to my spiritual friends in the Sathya Sai Organisation of Wollongong, without their encouragement, constant warmth guidance and tender love, I could not have finished this PhD. Foremost I thank my parents for giving me life, education and unconditional support and encouragement in the pursuit of my PhD. Thanks also to my family, who took care of me with their mindfulness and love.

LIST OF PUBLICATIONS

The publications provided here are related to this PhD Thesis.

a) Refereed Journals

1. Bunsri, T., Sivakumar, M and Hagare, D. (2006). Numerical modelling of tracer transport in unsaturated porous media. Journal of Applied Fluid Mechanics (accepted).
2. Bunsri, T., Sivakumar, M. and Hagare, D. (2006). Estimating water movement through unsaturated infiltration and percolation zones underneath an effluent drainage pipe. Journal of Applied Fluid Mechanics (editor invited).
3. Sivakumar, M., Hagare, D. and Bunsri, T. (2006). Simulation of water movement through an unsaturated infiltration-redistribution system. Environmental Modelling and Assessment (under review).
4. Sivakumar, M., Hagare, D. and Bunsri, T. (2006). Application of Hydraulic Properties Functions for Richards' Equation. Geoderma (under review).
5. Bunsri, T., Sivakumar, M. and Hagare, D. (2006). The suitability of fibreglass wick application on the movement of contaminants generating from domestic wastewater. Journal of Hydrology (with editor).
6. Bunsri, T., Sivakumar, M. and Hagare, D. (2006). Modelling of *Escherichia Coli* (*E.Coli*) transport through the unsaturated porous media Journal of Contaminant hydrology (under review).
7. Hagare, D., Sivakumar, M. and Bunsri, T. (2006). The numerical simulation of water and tracer transport in soil infiltration column. Ground Water (submitted).
8. Bunsri, T., Sivakumar, M. and Hagare, D. (2006). Transport and adsorption of phosphate compounds in variably saturated soil: I. Model formulation and application. European Journal Soil Science (submitted).
9. Bunsri, T., Hagare, D. and Sivakumar, M. (2006). Transport and adsorption of phosphate compounds in variably saturated soil: II. Model calibration. European Journal Soil Science (submitted).
10. Bunsri, T., Sivakumar, M. and Hagare, D. (2006). Transport and biotransformation of organic carbon and nitrate compounds in variably saturated soil conditions: I.

Model formulation and application. Environmental Science and Technology (preparing to submit).

11. Bunsri, T., Hagare, D. and Sivakumar, M. (2006). Transport and biotransformation of organic carbon and nitrate compounds in variably saturated soil conditions: II. Model calibration. Environmental Science and Technology (preparing to submit).

b) Refereed conference

1. Bunsri, T., Dharmappa, H. and Sivakumar, M. (2003). Modelling of contaminant transport in on-site waste disposal systems. 7th Annual Environmental Research Conference, 1-4 December 2003, Victoria, Australia.
2. Sivakumar, M., Bunsri, T. and Hagare, D. (2006). Numerical modelling on contaminant transport in unsaturated porous media. The Eleventh Asian Congress of Fluid Mechanics, 22-25 May 2006, Kuala Lumpur, Malaysia.

TABLE OF CONTENTS

LIST OF FIGURES

LIST OF TABLES

LIST OF SYMBOLS

English symbols

a	Coefficient of van Genutchten's hydraulic properties model, [cm^{-1}]
A	Coefficient of Haverkamp et al.'s hydraulic properties model, [unitless]
C	Equilibrium concentration of solute phase in solution, [g/cm^3]
C^*	Mass of solute sorbed phase per dry unit weight of solid, [g/g]
C_A	Concentration in aqueous of ammonia nitrogen, [g/cm^3]
C_b	Microbial concentration, [g/cm^3]
C_{bot}	Concentration at the lower boundary, [g/cm^3]
C_b^w	Soluble microbial concentration in liquid phase, [g/cm^3]
C_b^{w*}	Microbial concentration in liquid phase that is in equilibrium with the microbial concentration in the solid phase, [g/cm^3]
$\left(C_b^w\right)_o$	Microbial concentration in influent sample, [g/cm^3]
$\left(C_b^w\right)_z$	Microbial concentration in filtered samples at depth z, [g/cm^3]
C_{int}	Initial coucentration, [g/cm^3]
C_j	Nodal concentration, [g/cm^3]
C_O	Concentration in aqueous of dissolved oxygen, [g/cm^3]
C_S	Concentration in aqueous of organic carbon/ substrate, [g/cm^3]
C_{top}	Concentration at the upper boundary, [g/cm^3]
C_b^f	Concentration of adhering microbes, [g/cm^3]
C_b^t	Total microbial concentration, [g/cm^3]
C_P	Concentration of phosphate, [g/cm^3]
C_P^S	Concentration of sorbed phosphorus, [g/g]
C_P^w	Soluble concentration of phosphorus in liquid phase, [g/cm^3]
C_P^{w*}	Concentration of phosphorus in liquid phase that is in equilibrium with the phosphorus concentration in the solid phase, [g/cm^3]
C_s^w	Concentration of limiting substrate in aqueous compartment, [g/cm^3]
D^*	Effective molecular diffusion coefficient, [cm^2/h]
D_{mol}	Molecular diffusion coefficient, [cm^2/h]
D_z	Diffusion coefficient, [cm^2/h]

E Number of elements in the system, [unitless]

g Gravitational acceleration, [m/s^2]

G Statistical curve fitting for Saxton et al.'s equation, [unitless]

H Statistical curve fitting for Saxton et al.'s equation, [unitless]

h_b Bubbling pressure, [cm]

h_C Capillary height, [cm]

i Nodal sequent, [unitless]

$I[C_O]$ Inhibition factor, [unitless]

j Nodal sequent, [unitless]

J Statistical curve fitting for Saxton et al.'s equation, [unitless]

k_B Overall rate of bacteria removal, [1/h]

k_c Rate constant bacterial adsorption, [1/h]

k_d Constant the decay rate, [1/h]

k_f Coefficient for Clapp and Hornberger equations, [unitless]

k_L Adsorption coefficient for Langmuir isotherm system, [unitless]

k_m Biomass maintenance rate, [1/h]

k_M Adsorption coefficient for Langmuir isotherm system, [cm^3/g]

k_N Microbial decay coefficient under nitrate respiration, [1/h]

k_O Microbial decay coefficient under aerobic respiration, [1/h]

k_{rw} Relative permeability, [unitless]

k_s Rate constant bacterial desorption, [1/h]

k_μ Monod constant for substrate utilization in biomass, [cm^3/g·h]

K_{AO} Ammonia nitrogen concentration under aerobic respiration at half saturation, [g/cm^3]

K_{AN} Ammonia nitrogen concentration under nitrate respiration at half saturation, [g/cm^3]

K_c Inhibition coefficient, [g/cm^3]

K_d Partitioning coefficient, [cm^3/g]

K_N Nitrate nitrogen concentration under nitrate respiration at half saturation, [g/cm^3]

K_O Oxygen concentration under aerobic respiration at half saturation, [g/cm^3]

K_{Sb} Substrate concentration at the half maximum rate under aerobic condition, [g/cm^3]

K_{SO} Substrate concentration under aerobic respiration at half saturation, [g/cm^3]

K_{SN} Substrate concentration under nitrate respiration at half saturation, [g/cm^3]

K_t Overall volumetric mass transfer coefficient for phosphate, [cm/h]

K_{zz} Fully saturated hydraulic conductivity, [cm/h]

$(K_{zz})_{cal}$ Calculated saturated permeability, [cm/h]

$(K_{zz})_{mea}$ Measured saturated permeability, [cm/h]

L Straight-line distance, [cm]

L_e Flow path distance, [cm]

m Empirical parameters for van Genutchten model, [unitless]

M_b Biomass concentration per unit volume of porous media, [g/cm^3]

M_C Specific moisture capacity, [1/cm]

MB_t Mass balance error, [unitless]

n Volume fraction of aqueous and biofilm in total volume, [cm^3/cm^3]

N Number of intervals for Poiseuille's equation, [unitless]

N_i Shape function, [unitless]

N_j Specified basis function, [unitless]

p Empirical parameters for van Genuchten model, [unitless]

P Constant for Poiseuille's equation, [unitless]

q_z Darcy's velocity in vertical direction, [cm/h]

q_C^D Portion of concentration flux due to dispersion, [g/cm·h^2]

q_C^T Portion of total concentration flux, [g/cm·h^2]

r_S Total substrate utilization, [1/h]

r_{SO} Substrate utilisation in aerobic respiration, [1/h]

r_{SN} Total substrate utilisation in nitrate respiration, [1/h]

S_s Specific storage, [1/cm]

S_w Degree of saturation, [unitless]

t Time, [h]

T_S Surface tension of water, [kg/m·s^2 or Pa]

U_W Pressure head at the capillary height, [kg·m/s^2 or Pa]

v Pore velocity, [cm/h]

v_i Average linear velocity in the *i* direction, [cm/h]

X Safe distance between drainage field and pumping well, [m]

Y_b Heterotrophic microbial yield coefficient, [unitless]

Y_O Heterotrophic yield coefficient for aerobic bacteria, [unitless]

Y_N Heterotrophic yield coefficient for nitrifying bacteria, [unitless]

z Vertical direction, [cm]

Greek symbols

α Haverkamp model curve fitting coefficient, [unitless]

β Haverkamp model curve Fitting coefficient, [unitless]

σ Coefficient of Clapp and Hornberger equations, [unitless]

ϕ Porosity, [unitless]

γ Haverkamp model curve fitting coefficient, [unitless]

ξ Coefficient of Clapp and Hornberger equations, [unitless]

η Effectiveness of biofilm, [unitless]

κ Retardation factor, [unitless]

λ First order biodegradation rate, [1/h]

λ_b Metabolism rate for microbes, [1/h]

λ_N Constant for nitrate biodegradation, [1/h]

λ_S Constant for substrate biodegradation, [1/h]

μ_b Microbial maximum specific growth rate, [1/h]

μ_O Maximum specific growth rate for aerobic bacteria, [1/h]

μ_N Maximum specific growth rate for nitrifying bacteria, [1/h]

θ Volumetric water content, [cm^3/cm^3]

θ_r Residual moisture content, [cm^3/cm^3]

θ_s Saturated moisture content, [cm^3/cm^3]

θ_{10} Volumetric moisture content at 10 kPa, [cm^3/cm^3]

ρ_B Soil bulk density, [g/cm^3]

ρ_w Density of water, [g/cm^3]

ν_y Stochiometric coefficient, [unitless]

ω Coefficient relating to the tortuosity, [cm/cm]

ψ Hydraulic pressure head, [cm]

ψ_{bot} Hydraulic pressure head at the lower boundary, [cm]

ψ_e Air entry pressure potential, [kg/m·s^2 or Pa]

ψ_f Pressure head at the wetting front, [cm]

ψ_{int} Initial pressure head, [cm]

ψ_j Nodal pressure head, [cm]

$\psi_0(z)$ Known distributions of pressure heads at time $t = 0$, [cm]

ψ_S Air entry pressure head, [cm]

ψ_{top} Hydraulic pressure head at the upper boundary, [cm]

LIST OF ABBREVIATIONS

1D	one dimensional model
2D	two dimensional model
3D	three dimensional model
AC	activated carbon
APHA	American Public Health Association
AS	Australian Standards
ASTM	American Society for Testing and Materials International
AWTS	aerated wastewater treatment systems
BOD	biochemical oxygen demand
CEC	cation exchange capacity
cfu	coliform faecal unit
COD	chemical oxygen demand
DO	dissolved oxygen
E.Coli	*Escherichia Coli*
EC	electical conductivity
EC_e	electroconductivity of soil saturated extract
EC (1:5)	electrical conductivity of a 1 to 5 soil/water suspension
FDM	finite different method
FEM	finite element method
GF/C	glass fibre filter paper
GWT	groundwater table
HV	Haverkamp et al.'s hydraulic properties model
HWSF	Human waste storage facility
HWTD	Human waste treatment device
Inorg-P	Inorganic phosphorus compounds
LWA	light weight aggregate
MATLAB	MATrix LABoratory programme
MO	microorganism
NH_4-N	ammonia nitrogen
NO_3-N	nitrate nitrogen
ODE	ordinary differential equation
Org-C	organic carbon compounds

Org-N	organic nitrogen compounds
Org-P	organic phosphorus compounds
PCAP	passive capillary sampler
PDE	partial differential equation
PO_4-P	phosphate phosphorus
R^2	residual square
RASFD	recirculating aerobic sand filter devices
REV	representative elementary volume
SS	suspended solids
TKN	total Kjeldahl nitrogen
TN	total nitrogen
TP	total phosphorus
USDA	United States Department of Agriculture
VG	van Genuchten's hydraulic properties model

TERMINOLOGY USED TO DESCRIBE MUNICIPAL EFFLUENT TRANSPORT IN GROUNDWATER

Adsorption- a sorbed phase concentration of molecules or ions on surface.

Adsorption isotherm- the measure of changes in amount of a substance adsorbed at different concentration at a constant temperature.

Aerobic- the conditions contain dissolve or free oxygen.

Anaerobic- the conditions absent dissolved or free oxygen.

Anaerobic digestion-a decomposition process occurs in the absence of oxygen.

Advection- movement of contaminants caused by the flow of infiltration.

Biological film-a film that forms on the inert material surfaces, it functions as biological filter.

Biotransformation processes- the biological processes influence to the chemical or substrate structures.

Capillary pressure- the attraction of water due to capillary force.

Chemical sorption- the formation of chemical bonds between sorbate and sorbent surface. This could be also call chemisorption.

Darcy's velocity- a superficial velocity (specific discharge) is a function of hydraulic gradient and permeability.

Datum- the reference elevation. The datum is usually chosen at the lowest point, which the lowest gravitational potential is observed.

Denitrification-nitrate transformation into nitrogen gaseous. This process occurs, if soil becomes oxygen deficient.

Dispersion- the movement caused by irregular mixing of water during advection and the concentration gradient.

Faecal coliform-a type of bacteria that lives in a gut of warm-blooded animals.

Filtration- the entrapment of large solid particles.

Gravitational flow- the downward flow of water due to the gravity.

Hydraulic conductivity- the fluid flow rate per unit time per unit cross sectional area of porous media.

Homogenous -the same porous media properties in a considered representative volume.

Ion exchange- the replacement of ion between the chemical and mineral surface.

Matric pressure- the attraction of water to solids in the subsurface. Matric pressure potential arises from both adsorption and capillary water in soil pores.

Nitrification-a transformation of inorganic ammonia into nitrate.

Nutrients-the essential chemical elements that support animal and plant growth. Nitrogen and phosphorus compound are the major essential nutrient for plant growth. Excess nutrients encourage a nuisance algae and aquatic plants growth that posts the human health impact.

Organic matter-the compounds consisting carbon skeletons; it may appear in dissolved, suspended and colloidal form.

Percolation-a water descends through soil profile.

Permeability-the relative fluid flow through porous media; this relates to particle grain size and media properties.

Porosity- a dimensionless ratio of pore volume over total volume.

Porous media- the geometrical that water can penetrate, such as sand, silt, clay, soil, or rock.

Precipitation- geochemical reactions results in a contaminant transporming from a dissolved from to an insoluble form.

Relative hydraulic conductivity-the estimated hydraulic conductivity associated the degree of saturation.

Retardation- principally chemical and biological mechanisms that slow down the movement of contaminants.

Saturated hydraulic conductivity- the hydraulic conductivity measured at saturation soil condition, which has no entrapped air.

Saturated zone-the soil laye that all pore spaces are full of water.

Specific storage-a volume of released water from unit volume of aquifer; it is measured in unit of decline hydraulic head.

Specific moisture capacity-a changing of volumetric moisture content over pressure head.

Suction head- a negative pressure head due to capillary force.

Tracer- distinguishable constituents carried by feeding solution that gives information concerning the soil-water system.

Unsaturated zone-the subsurface soil layer locates above the water table.

Vadose zone-the unsaturated zone locates between the root zone and saturated zone.

Void ratio-a ratio of void volume over solid volume.

Volumetric moisture content- a ratio water volume over total volume of porous media.

Water content- a ratio of water mass over solid mass.

Water table-the surface of fluid pressure in porous media; it equals atmospheric.

DEDICATION

This thesis is dedicated to my dear mother, Thipwimol Bunsri, who has supported me with unlimited love.

CHAPTER 1

INTRODUCTION

1.1 Overview

The modern environmental movement began in the 1960s where the key issue was reducing pollution from smoke stacks and sewer pipes. The second movement began in the late 1970s when environmentalists focused on toxic compounds, especially hazardous waste disposal and site remediation. The third movement began in the late 1980s with farmers, businesses, homeowners, and others, questioning environmental laws and regulations. Some environmental laws stated that some pollutants could be contained in air, water, or soil, at levels greater than their allowable values. Regardless of what the laws and the regulations required, long-term environmental problems were not completely solved. These facts reflected public concern and awareness about the quality of the environment (Sparks 1995).

Even though the provisions of the environmental laws and the regulations were publicly proclaimed, there continued to be a number of inorganic and organic contaminants that were being discharged into the environment. Some of these contained toxic substances and pathogens that generated acute health problems. Land use applications, such as landfills, gravel yards, and absorption fields, seemed to be the final destination of all the disposed contaminants. In fact over 200 chemical substances have been observed in groundwater alone, all of which have potentially adverse affects on human health (U.S. EPA 1990).

As mentioned, groundwater contamination has been an important issue from the 1980s to the present day. To solve this environmental problem, many symposia and conferences on the topic have been held and the number of forums seems to increase each year. For example, more than 90 such conferences were held around the world in 2004 (Boulding and Ginn 2004). Groundwater contamination often leads to critical health problems caused by pathogens from human excreta, particularly in developing countries. According to the World Summit on Sustainable Development (WSSD)

(2002) and Earth Summit (2002), approximately 1.2 billion people lacked safe drinking water, or 20% of world population, 2.4 billion people lacked adequate sanitation, or 40% of world population, and 6000 children die every day from water borne diseases. As a result the United Nations established a framework for action on water and sanitation. Vision 21 on Water and Sanitation seeks "a clean and healthy world: a world in which every person has safe and adequate water and sanitation and lives in a hygienic environment" (WSSD 2002).

Domestic wastewater and sewage sludge were identified as major sources of groundwater contaminants. The disposal of both domestic wastewater and sewage sludge could pollute the groundwater if the soil's retardation capacity is exceeded. The U.S. EPA (1983a) reported that 40 to 50% of domestic sludge generated every year was disposed or onto the land. Local residential disposal units, especially septic tank systems, added contaminants to the groundwater unless they were properly designed and maintained (Department of Local Government 1998 and U.S. EPA 1990).

Onsite sewage management systems in Australia have been receiving significant attention since the failures in the New South Wales systems were reported. The increase of failures suggests that many systems did not achieve environmental and public health requirements. Increasing public awareness forced the NSW Government to promulgate the Local Government Act 1993 and the Environmental Planning and Assessment Act 1979. This stated that "onsite and centralised sewage systems should respond on the basis of being ecological sustainable and their impact on public health" (NSW Department of Local Government 1998).

A survey by Geary (1992) and O'Neill (1993) on the performance of onsite waste disposal systems reported that more than 40% could not remove nutrients and actively added to water management problems in the catchment. The Public Inquiry into the Management of Sewage By-Products in NSW Coastal Zone reported that the failure of a sewage treatment system located in New South Wales was in the range of 50-90% (Codd 1997). The cumulative effects of the failure of a large number of onsite systems in sensitive locations could significantly impact areas downstream, especially coastal areas. The outbreak of oyster and shellfish contamination in New South Wales was a serious health issue (Hackney and Pierson 1994, AWT Ensight 1997 and White 2001).

A well-known outbreak in 1978 involved faecal contamination in the Georges River and caused viral gastroenteritis (ANZECC/ARMCANZ 2000). In addition, the outbreak in 1997 of *Hepatitis* A in Wallis Lake (NSW), affected approximately 274 people. The *Hepatitis* A virus affected approximately 444 people throughout Australia in 1999 and while the source of waste remained unidentified, this outbreak was found incidentally when the high failure rate of onsite sewage systems (33%) was reported (Brooker 1999).

1.2 Septic tank system

A septic system is one of the simplest methods for treating and disposing of domestic wastewater where municipal sewers are not available. The first septic system in Australia was installed in South Australia in 1901, and by 1908 approximately 35 septic tanks were in use. This increased rapidly to 2000 in 1920, and then to 25000 by 1940. By 1968, around 5000 tanks per year were installed (South Australian Health Commission 1968). Since then they were used in most parts of Australia.

A septic system consists of a tank and a drainage field. It is designed to receive domestic wastewater, especially black and grey, or a combination of both. Wastewater is stored and treated anaerobically for a short period of time. Floatable sewage such as oil, grease and faecal constituents rises to the top but heavier sewage sinks to the bottom. Both floatable and settleable sludges were decomposed anaerobically by microbes, and then form the layers of brownish white scum. Between these scum layers, it is a clarified effluent which is discharged into the drainage field via an outlet in the tank (Kaplan 1991). The criteria for the septic system design, installation, maintenance, and operation is given in the Australian and New Zealand Standard (AS/NZS 1547) (Australian/New Zealand Standard 2000).

1.3 Effluent disposal and contaminants transport

Due to the worldwide spread of septic tanks, it was estimated that they disposed of the largest volumes of wastewater into the ground (U.S. EPA 1977). Although they were well designed, installed, maintained, and operated, some could not treat domestic wastewater effectively because they suffered from a poor location and/or an inadequate

drainage system (Butler and Payne 1995). Poor quality treated effluent often contained high concentrations of organic carbon compounds, nutrients, and pathogens (U.S. EPA 1990, Butler and Payne 1995 and WSSD 2002). The major problems arising from disposing of septic tank effluent were potential eutrophication (algae bloom), chemical pollution and risks to public health (Australian Water Resources Council (1983) cited in Hamilton et al. 1992). Excess organic carbon compounds could impact groundwater quality. Nitrogen compounds are oxidised by microbes to form nitrate and excessive nitrate in drinking water is a major cause of methemoglobinemia (blue baby disease) in infants, and it is concerned as a pro-carcinogen. The nitrate can also promote eutrophication in surface water. Excess phosphate can also add substantially to eutrophication. The pathogenic organisms present in the septic tank effluent can affect human health (U.S.EPA 1986).

The system considered in this research mainly focused on the drainage area, which was the end of the domestic wastewater disposal. Soil in a drainage field is either saturated or unsaturated. The layer of soil above the groundwater table is in the unsaturated zone where air and water occupy the pores. This zone contains dissolved oxygen which can serve aerobic biodegradation processes. The layer of soil below the groundwater table is in the saturated zone where water fills the pores fully. Both anoxic and aerobic conditions occur in this zone and the microbes use intermediate organic substances or other minerals as terminal electron acceptors (MacQuarrie and Sudicky 2001).

The extent to which contaminants migrate in groundwater relies on the transport processes and retardation. Transport of contaminants refers to the advection and dispersion mechanisms. Advection is caused by wastewater flow, which carries the contaminants along the flow path. Dispersion is caused by irregular mixing and molecular diffusion. Retardation refers to the various reactions which can slow the movement of contaminants (Fetter 1992, Sparks 1995, Schnoor 1996 and Boulding and Ginn 2004). The contaminants might be retarded by soil microbes and minerals. Organic carbon and nitrogen compounds could be degraded by soil microbes. Phosphate compounds can be retarded by soil minerals and pathogens can be removed by soil filtration process. The effectiveness of these reactions depends upon the physical, chemical and biological properties of the soil. These reactions might not be enough to

retard the contaminants completely, if the contaminants contained in effluent are too concentrated (U.S. EPA 1986 and Kaplan 1991).

The migration of contaminants underneath a drainage field is a complicated process where many active parameters, including advection, dispersion, and retardation should be considered. It is necessary to develop a model to evaluate the fate and concentration of contaminants, and to find better solutions to this serious groundwater pollution problem.

1.4 Modelling concept

Monitoring and remediation of onsite waste disposal systems have proven to be costly and time consuming. Therefore contaminant transport modelling is necessary for decision-making purposes. Modelling is basically developed for three purposes (Schnoor 1996):

(a) To clearly understand the transport and fate of pollutants by quantifying the possible movement, reaction and speciation;

(b) To determine the impact of the concentration and exposure of contaminants to the groundwater: past, present, or future; and

(c) To predict the future impacts and discover alternative ways to prevent, manage, or take action on these impacts.

A septic tank contaminant transport model was a composition of transport and retardation processes. The construction process began with a conceptual, mathematical, and numerical model, and finished with calibration and verification. The conceptual model was established to describe the mechanisms occurred in the considered system. The retardation and transport of contaminants within a controlled volume were qualitatively explained. The mathematical model was obtained by modifying the equations or the formulations associated with the conceptual model. The exact solution of a complex mathematical model is very difficult, thus, a numerical approach was applied to provide an approximate solution. The numerical model was coded using MATLAB (MATrix LABoratory) software. Due to the advantages of computing technology, the calculation process was very fast and effective. The approximate

solution could be estimated accurately using this developed computational code. The calibration and verification of the model was done using experimental data and historical case studies from the literature. Calibration and verification of the model indicated that it corresponded well to estimate migration of contaminants in a drainage field.

1.5 Aim and objectives

The aim of this study was to investigate the transport and ultimate fate of pollutants discharged by septic tank systems. The specific objectives were:

(a) Develop conceptual models to explain the removal mechanisms and fate of contaminants in unsaturated soil conditions;

(b) Modify the governing equations to support the conceptual models established;

(c) Develop a numerical model to solve the governing equations and produce computational codes;

(d) Calibrate the developed model using data from previously published research;

(e) Investigate laboratory and pilot scale soil column experiments and calibrate the model developed; and

(f) Evaluate the limitations of the model derived from the prediction of contaminants transport.

1.6 Scope

To achieve these objectives this study was carried out phase by phase.

(a) Development of a conceptual model

Development of a conceptual model was established according to the fundamentals of geochemical science/engineering to gain an overview of contaminants migrating from a septic tank. The processes were as follows:

- Review existing literature in the field of septic tank contaminants transport;
- Identify the majority of contaminants that seriously impact the environment;
- Review the possible soil-contaminant interactions and describe the dominant interaction between each of the contaminants identified;

- Consider the possible flow patterns of effluent into a drainage field, including the affects of the gravitational, static capillary equilibrium and infiltration-redistribution systems;
- Define the governing equations to support contaminants transport and retardation. Richards' and hydraulic properties equations were applied to describe the advective-dispersive transport process. Multiplicative Monod's and Langmuir isotherm equations were applied to describe the biodegradation and sorption processes, respectively; and
- Establish the assumptions necessary to identify the boundaries of the problems and simplify them into a determinable scale.

(b) Development of mathematic and numerical models

The development of mathematical and numerical models quantitatively described the conceptual model. The processes were:

- Modify the governing equations to obtain a mathematical model for contaminant transport with retardation processes;
- Apply the finite element method (FEM) to solve the mathematical model, and obtain a numerical model; and
- Produce a computational code to determine the approximate solutions of the numerical model.

(c) Model Calibration

Calibration was needed to determine the model reliability and be confident of the simulation results. The model was calibrated with historical case studies and experiments. The experimental set up is described below:

(d) Experimental set up

Two porous media were utilised, including a medium grained river sand (particle size 250-500 μm), and a sample of topsoil (particle size <2.00 mm). The sand could be characterised as non-reactive porous media whereas the topsoil could be characterised as reactive porous media. The characteristics of these two materials were examined in the Soil Laboratory and Environmental Engineering Laboratory at the University of Wollongong. All the wastewater samples were analysed quantitatively in the

Environmental Engineering Laboratory at the University of Wollongong. The experimental set up and methodology were as follows:

- Batch tests were investigated to examine specific parameters including hydraulic properties of sand and soil, kinetic coefficients of soil phosphate adsorption and reduction of contaminants onto fibreglass wick filaments; and
- Continuous tests included laboratory and pilot scale column tests. Laboratory scale tests were conducted to determine the contaminant transport under advection and dispersion processes. Pilot scale tests were used to evaluate the transport and retardation of reactive contaminants in the unsaturated soil condition.

1.7 Chapter organisation and schematic of the thesis

This research was mainly focused on modelling the contaminants transport in unsaturated soil conditions. The research framework described in this thesis is presented below:

Chapter 1- Introduction. This chapter contained an overview of the research. Contributions of this research were previewed. Chapter 2- Transport and Fate of Contaminants Released from Septic Tanks. This part explains the characteristics of untreated domestic wastewater and the application of an onsite treatment unit. Additionally, the characteristics of the treated domestic wastewater and its possible impacts on the quality of the groundwater, as well as the migration and fate of reactive contaminants that occur underneath the drainage area were reviewed.

A conceptual model was developed to describe the migration and reaction of specified contaminants contained in the effluent at a qualitative scale. The governing equations were defined as presented in Chapter 3- Development of A Conceptual Model. These governing equations were then combined and modified into a mathematical model. An FEM numerical technique was used to solve this derived mathematical model. The computational codes of the numerical model were prepared using MATLAB software. The development process for the mathematical and numerical model is described in Chapter 4- Development of A Mathematical and A Numerical Model. Chapter 5- Experimental Set Up describes work to calibrate and verify the model. This chapter

presents analytical methods for testing soil and wastewater parameters and preliminary design of soil columns and procedures of batch and continuous tests.

Chapter 6- Preliminary and Batch Tests, presents the results and discussions of soil and wastewater characteristics, sand and soil hydraulic properties, kinetic coefficient of phosphorus adsorption and the suitability of the fibreglass wick to soil sampling technique. Transport by the advection process in various boundary conditions and the impact of soil background concentration and thickness to the dispersion process are discussed in Chapter 7- Laboratory Scale Soil Column Tests. Chapter 8- Pilot Scale Soil Column Tests presents the effectiveness of soil in wastewater purification. This included the simulation of contaminants transport with retardation in a pilot scale soil column and the estimation of contaminant reduction zones. Chapter 9- Model Applications and Case Studies focuses primarily on the practical use of the model. The developed model was calibrated with historical data from previous research. Its performance is evaluated with a statistical test. The outcome of this research, including improvement and further motivation, is presented in Chapter 10- Conclusions and Recommendations for Further Work.

A schematic diagram presenting the structure of this thesis is shown in Figure 1.1. It may be separated into 3 sections, literature review, model development, and model calibration and verification. The literature review section is presented in Chapter 2. The model development section is given in Chapter 3 and 4. The model calibration section is contained in Chapters 5 to 9.

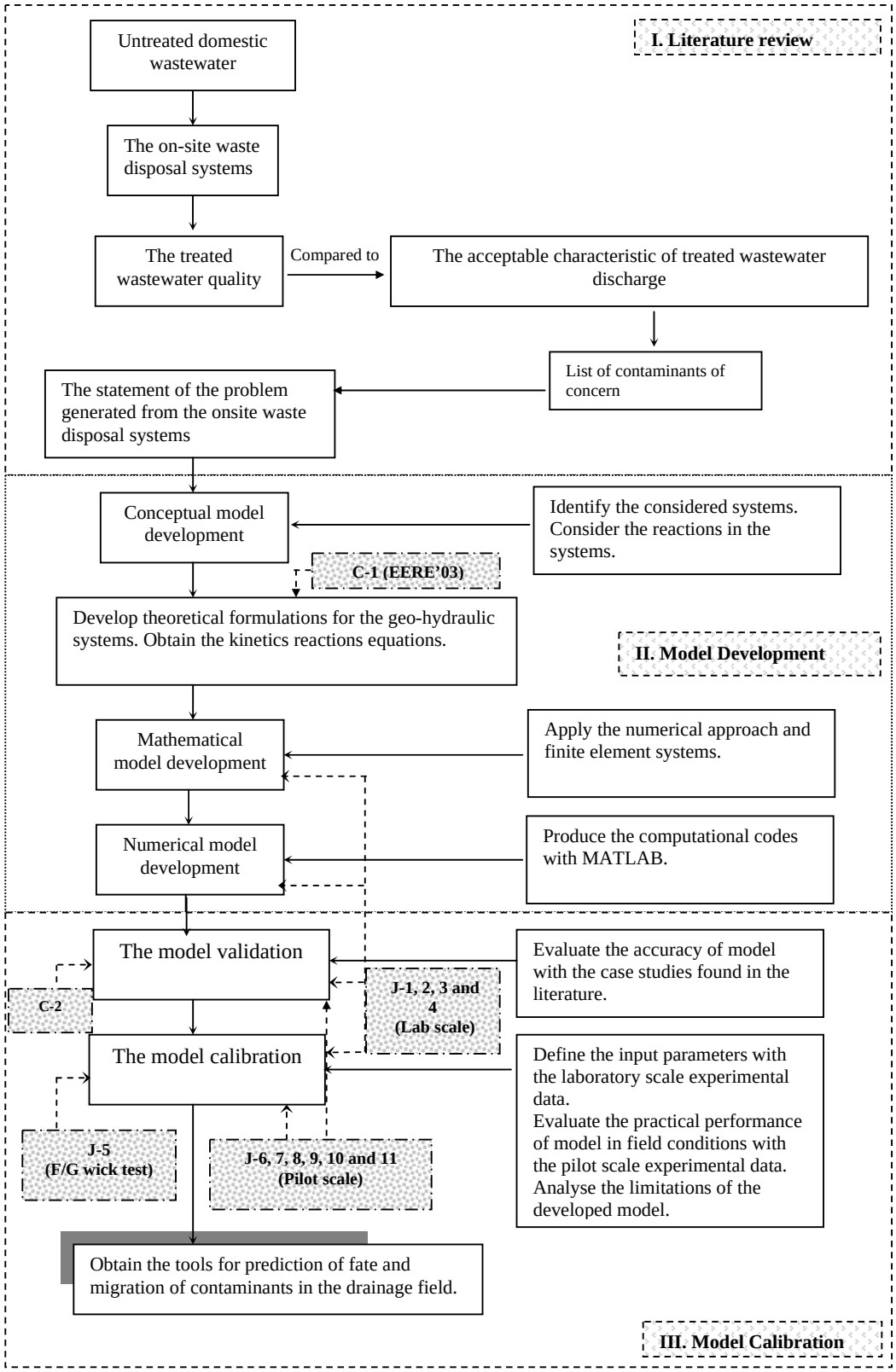

Note: J is refereed journals and C is refereed conferences.

Figure 1.1 Structure of this research

CHAPTER 2

TRANSPORT AND FATE OF CONTAMINANTS RELEASED FROM SEPTIC TANKS

2.1 Introduction

Domestic wastewater often contains contaminants that must be treated and removed before it is discharged into the environment. In remote or urban areas where centralised sewerage systems may not be available, onsite treatment systems may be applied to treat this wastewater. A septic tank is an economic and popular onsite treatment unit that is typically applied to domestic wastewater, especially black water from toilets.

The volume of domestic wastewater varies throughout the day and the quality also varies depending on the range of household products used. The qualitative characteristics of domestic wastewater are distinguished by their physical, chemical, and biological compositions (Noss 1989). Fluctuations in the quantity and quality of domestic wastewater could affect the performance of a septic tank. A failed septic tank could discharge poor quality effluent which may pose risks to human health and the environment (Geary 2003). Further as treated wastewater passes to the vadose zone, its quality may be improved by a complex series of physical, chemical, and biological processes (Brouwer 1983, Canter and Knox 1985 and Kaplan 1991).

This chapter includes two parts namely, source and pathway of groundwater contaminants. The first part describes the characteristics of untreated domestic wastewater; the management and treatment process and the specific contaminants remaining in treated domestic wastewater. The second part focuses on the transport and fate of these contaminants along the drainage field.

2.2 Characteristics of untreated domestic wastewater

Domestic wastewater is generated from four main sources, the kitchen, the bathroom (includes basin, bath and shower), the laundry, and the toilet. This wastewater could be

separated into three categories based on the contents of the contaminants (NSW Department of Local Government 1998).

(a) Black water refers to human excreta containing wastewater from toilets;

(b) Grey water is sullage without contamination from human excreta, eg, kitchen, bath, shower, and laundry wastewater; and

(c) A combination of black and grey water.

The quality and quantity of untreated wastewater depends on the availability of a reticulated water supply; the number of people in a household; the water conservation practices maintained by the household; the waste management practices used, and the volume of water consumed by the appliances and fixtures used. The characteristics of untreated domestic wastewater are given in Table 2.1. Non-reticulated water supply systems could reduce the volume of wastewater generated. Although the amount of black water was less than grey, the level of contaminants would be much higher. The three major constituents in domestic wastewater were organic compounds, nutrients, and pathogens (NSW Department of Local Government 1998).

Table 2.1 Characteristics of typical untreated domestic wastewater
(NSW Department of Local Government 1998)

Parameter	Range	Grey water %	Black water %
Flow- non reticulated water supply	100-140 L/p/d	65	35
Flow-reticulated water supply	150-300 L/p/d	65	35
Biochemical oxygen demand (BOD)	200-300 mg/L	35	65
Suspended solids (SS)	200-300 mg/L	40	60
Total nitrogen (TN)	20-100 mg/L	20-40	60-80
Total phosphorus (TP)	10-25 mg/L	50-70	30-50
Faecal coliform	10^3-10^{10} cfu/100 mL	medium-high	high

Table 2.2 presents the quality of untreated domestic wastewater overseas (Australian Water Resource Council Research Project 79/118 1983 cited in Hamilton et al. 1992). The qualities of domestic wastewater observed in Australia and overseas are quite similar. It might be assumed that, despite the sources being different, the quality of domestic wastewater does not change significantly.

Table 2.2 Quality of domestic wastewater from oversea reports
(Australian Water Resource Council Research Project 79/118 1983)

Source	Comments	Parameters (mg/L)										
		SS	BOD	COD	Nitrogen				Phosphorus			Faecal coliform (cfu /100mL)
					Total	Organic	NH_4	NO_3	Total	Organic	Inorganic	
Tchobanoglous (1973)	General figures	225	200	450	40		25		10			
Pahren (1978)	Lit. Review sewage USA.	30-350	30-600	100-1000	20-85	5-32	8-50	0-3	4-50	1-5	8-13	
Viraraghavan (1976)	Mean values over time	200	520	1000			47	0.1	14			$3.0x10^4$
Viraraghavan (1976)	Value exceeded only 15% of the time	320	670	1650			75	0.19	32			$6.6x10^5$

Many pollutants contained in untreated wastewater could potentially affect human health and pollute the environment. The residents are not allowed to discharge their raw wastewater directly to lands and/or to other receiving waters. Hence a suitable sewage management scheme was introduced to improve the quality of wastewater which could substantially reduce the impacts on humans and the environment (NSW Department of Local Government 1998).

2.3 Phases of managing domestic wastewater

The Local Government Act 1993, section 68(1) states that the human waste treatment device (HWTD), the human waste storage facility (HWSF) and/or drains connected to any such device or facility should be installed and/or constructed in every house. A successfully designed onsite waste disposal system has to be approved by the Local Government (NSW Department of Local Government 1998). The system is described as:

- *Phase 1: Waste Capture and Conveyance*

Drains –Wastewater from the fittings (toilet, bidet, hand-basin, shower, bath, kitchen and laundry) are collected and carried to a HWTD or HWSF.

Alternatively, human excreta containing wastewater can be directly flushed into a HWTD without the use of drains.

- *Phase 2: Waste Treatment or Storage*

Wastewater is treated, stored, polished, and disposed of with a HWTD.

Human excreta containing wastewater is treated and stored in a HWSF.

- *Phase 3: Waste Use or Disposal*

Drains – Treated wastewater is disposed of into a natural soil filtration system. They include ancillary systems such as constructed wetlands, amended soil, mounds and soil absorption, and irrigation systems.

Suspended solids (SS) are reduced in the first phase. The second phase provides the primary, secondary, or tertiary treatment processes. The final effluent gets purified with soil filtration or ancillary systems in the last phase. Table 2.3 describes a conventional onsite treatment unit (NSW Department of Local Government 1998).

Table 2.3 Onsite sewage management systems
(NSW Department of Local Government, 1998)

Sources	Phase 1	Phase 2	Phase 3	Human waste treatment device or storage facility
Black water and grey water	Drain	HWTD	Drain	• Septic tank/ collection well • Aerated wastewater treatment system • Wet composting toilet • Wastewater ejection unit • Common effluent system pre-treatment device • Recirculating sand filter device
Blackwater		HWTD	Drain	• Septic closet • Waterless composting toilet
Blackwater		HWTD		• Chemical toilet • Combustion toilet
Grey water excluding kitchen	Drain	HWTD	Drain	• Grey water treatment device
Blackwater		HWTD		• Pan • Cesspit

There are many types of onsite treatment unit as shown in Table 2.3 such as septic tanks, aerated wastewater treatment systems (AWTS), waterless composting toilets, recirculating aerobic sand filter devices (RASFD), wet composting toilets and

combustion toilets (Kaplan 1991 and NSW Department of Local Government 1998). Septic tanks seem to be the simplest and most economic unit that were widely applied to treat domestic wastewater (Geary 2003). More than 23 million homes in the United States rely on onsite wastewater disposal systems (Noss 1989). Department of Local Government in New South Wales (2001 cited in Geary 2003) reported that 280,000 houses in New South Wales used onsite wastewater systems and approximately 74% of them were septic tanks.

2.4 Septic tank

The design criteria for septic tanks, including performance, installation, maintenance and modes of operation, are described in the Australian and New Zealand Standard (AS/NZS 1547 2000). After receiving black water, sewage is separated physically based on the density. Low density sewage such as oil, grease, and faecal coliform floats on the surface and high density sewage settles at the bottom of the tank. Both flotable and sinkable sewage are decomposed anaerobically and become the brownish white layer of scum. Scum must be removed periodically to maintain an effective volume in the tank. Between the layers of scum, clarified sewage can overflow to a drainage field via an outlet pipe (Kaplan 1991). Figure 2.1 shows the cross section of a conventional septic tank (NSW Department of Local Government 1998).

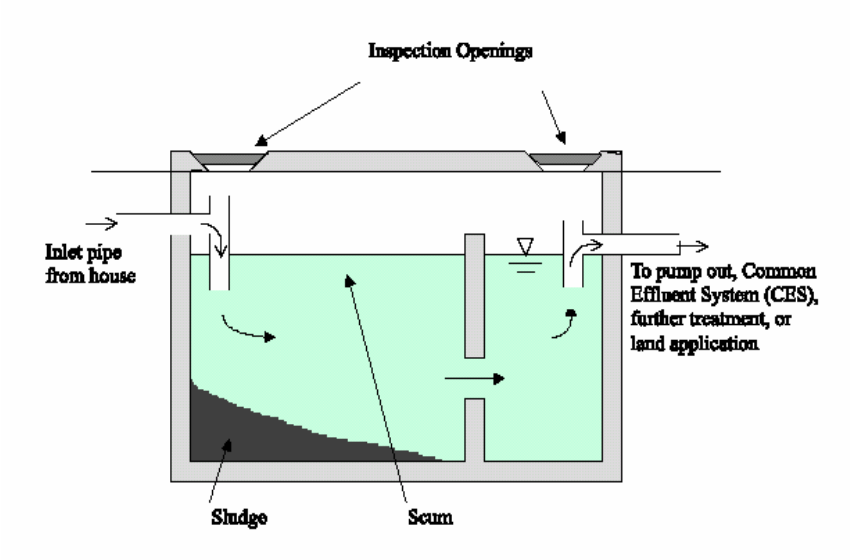

Figure 2.1 Cross section of a septic tank (NSW Department of Local Government 1998)

The reactions that take place in a septic system are shown in Table 2.4. These are the anaerobic digestion processes that provide primary treatment (Wilhelm et al. 1994).

Table 2.4 Important reactions in a septic system (Wilhelm et al. 1994)

Zone	Reactions
Anaerobic zone (septic tank and biological mat)	*Organic molecule hydrolysis:* Proteins+ H_2O →Amino acids Carbohydrates + H_2O → Simple sugars Fats + H_2O → Fatty acids and glycerol *Ammonium release:* Urea $[CO(NH_3^+)_2]$ + H_2O → $2NH_4^+ + CO_2$ Amino acids + H_2O → NH_4^+ + Organic compounds *Fermentation:* Amino acids, simple sugars → H_2, acetate (CH_3COO^-), other organic acids *Anaerobic oxidation:* Fatty acids + H_2O → H_2, CH_3OO^- *Sulfate reduction:* SO_4^{2-} +$2CH_2O$*+ $2H^+$ → $H_2S + 2CO_2 + 2H_2O$ *Methanogenesis:* CH_3OO^- (acetate) + H^+ → $CH_4 + CO_2$ $CO_2 + 4H_2$ → $CH_4 + 2H_2O$

Note: * Organic matter is simplified as CH_2O throughout. Actual organic matter contains C of various states of oxidation and other elements such as N, P and S, and therefore actual reaction products vary.

The quality of wastewater treated by septic tanks in Australia and overseas is summarised in Table 2.5 (Brouwer 1983). A comparison between treated (Table 2.5) and untreated domestic wastewater (Table 2.1 and 2.2) indicates that the quality of wastewater is improved as:

- Approximately 18-70% of SS were removed by gravitational and biodegradation processes
- The ratios of BOD/COD in both untreated and treated wastewater were 0.48 and 0.43, respectively. These ratios were in the possible range of 0.4-0.6 as reported by Metcalf and Eddy (2003). The effluent discharged from an onsite unit obtained 46 and 40% reduction of BOD and COD, respectively
- Approximately 75-80% and 20-50% of organic nitrogen (Org.-N) and ammonia nitrogen (NH_4-N) were removed from raw wastewater, respectively. Effluent contained low concentration of nitrate

- Organic phosphorus was significantly converted to inorganic phosphorus. Total phosphorus reduced approximately 38-50%; and
- Faecal coliforms were substantially removed, with the removal efficiency of 99.99%.

Table 2.5 Quality of septic tank effluent (Brouwer 1983)

References	Concentration (mg/L) except Faecal Coliforms (cfu/100mL)									
		C-source		N-source				P-source		
	SS	BOD	COD	TN	Org. N	NH_4-N	NO_3-N	TP	Inorg. P	Faecal Coliform
Overseas:										
U.S. EPA (1978)	44-54	129-147	310-344	41-49		28-34	0-0.9	12-14	10-12	$3x10^5$-10^6
Dudley and Stephson (1973)				45	10	35	0.5	25		
Biggar and Corey (1969)				35	10	25	0.15			
Popkin and Bendixen (1968)				30	5.6	24.6	0.2			
Viraraghavan (1976); mean value over time. Ontario	165	280	550			92	0.02	10.5		$1.6x10^5$
Viraraghavan (1976); value exceeded only 15% of the time.	250	350	800			105	0.04	14.0		$2.6x10^6$
Brandes (1977); toilet only. Ontario	65-100	36-260				105-150	0.1-0.5	19-20	14-19	$1.8x10^5$-7.410^5
Otis and Boyle (1976); general figures.	60	150		±55	±17	±39		±15	±12	
Kristiansen (1980); general figure. Norway				15-25	±3-5	±12-20		12-20		
Australia:										
Bruty and Mann (1977); systems Melbourne	32	175								
Robinson (1977); one household, Melbourne	121	496								$4.1x10^6$
Robinson (1977); one household, Melbourne	60	151								$3.8x10^6$
Brouwer et al. (1979); toilet only Melbourne				430-573				31.8-33.3		
Department of Health Victoria (1976); Melbourne						72		16		
Hawkins (pers.comm.); municipal plant, Melbourne	91-122	122-143						10-12		
Hawkins (pers.comm.); municipal plant, Melbourne	110-550	275-445						25-42		

Expected quality of treated wastewater by a typical septic tank is given in Table 2.6 (NSW Department of Local Government 1998).

Table 2.6 Expected quality of wastewater treated by a septic tank
(NSW Department of Local Government, 1998)

Parameters	Concentration
Biochemical oxygen demand (BOD)	150 mg/L
Suspended solids (SS)	50 mg/L
Total nitrogen (TN)	50-60 mg/L
Total phosphorus (TP)	10-15 mg/L
Faecal coliform	10^5-10^7 cfu/100 mL

When the effluent quality shown in Table 2.5 is compared to the expected quality shown in Table 2.6, it is clear the septic tanks generate poor quality effluent and do not meet the expected quality. In the worst cases, SS and BOD were ten and three times higher than the allowable discharged concentration, respectively. TN and TP were two and ten times worse than expected concentrations, respectively. Hence, the failures of septic tanks had often been identified as a source of groundwater contamination, especially in sensitive areas (Canter and Knox 1985 and Hamilton et al.1992).

Successful domestic wastewater treatment relied upon the septic tank and soil absorption system. Septic tanks and soil drainage fields have a life expectancy of 25 and 5-15 years, respectively, that the drainage field reaches its maximum capacity before the end of the septic tank life. Hence an old drainage system was a highlight of the failure of onsite treatment systems (NSW Department of Local Government 1998). As a result, the guidelines for land to be used for effluent irrigation (NSW EPA 1995) stated “new residential sub-divisions with onsite sewage management require 4000-5000 m^2 per household, minimum, to reduce the impact of pollution in medium to long term” (The Environmental Protection Authority (EPA) 1995 cited in NSW Department of Local Government 1998).

2.5 Specific groundwater contaminants emanating from septic tanks

According to Australian Water Resources Council (1983) (cited in Hamilton et al. 1992), the major problems arising from disposing of septic tank effluent were

eutrophication, chemical pollution, and risks to public health. These problems related to several contaminants including organic carbon, nitrogen, phosphorus compounds and pathogens.

Even though a septic tank did not discharge any toxic organic carbon compounds, ordinary compounds could stimulate the growth of microbes and nitrification. High concentrations of organic carbon may reduce the amenity and quality of the environment (NSW Department of Local Government 1998).

Septic tank effluent often contained high concentrations of nitrogen compounds, which could eventually be transformed to nitrate. Nitrate was listed in the group of acute chemical contaminants in drinking water because nitrate has been related to methemoglobinemia in infants. Nitrate contaminated drinking water has also been linked to gastric cancer mortality rates and non-Hodgkin's lymphoma (Killingstad et al. 2002). The US Safe Drinking Water Act 1974 approved critical levels of nitrate at 10 mg/L (Sparks 1995). Besides, nitrate was a limiting nutrient for phytoplankton activity in marine systems that could induce eutrophication in estuarine areas (Harman et al. 1996).

Although phosphorus compounds were non-toxic substances, they could decrease the quality of water resources. Phosphate could stimulate the growth of aquatic plants and algae, which can lead to eutrophication (Hamilton et al. 1992, Sawyer et al. 1994 and Zanini et al. 1998).

In addition, septic tank effluent also contains a variety of microbes, such as viruses, bacteria, nematodes and worms, which can cause serious health problems (Winneberger 1984). Hence the transport and fate of contaminants carried on the drainage field is very important and will be described fully in the following section.

2.6 Contaminants transport processes

Classification of the sub-surface flow condition is given in Figure 2.2. The soil drainage field is classified into unsaturated (vadose or aeration) and saturated (groundwater) zones. Firstly, the unsaturated zone is located above the groundwater table, which could

be separated into the soil water zone, the intermediate vadose zone, and the capillary zone. The depth of the soil water zone could be estimated from the maximum depth to which plant roots can penetrate, called the root zone. The intermediate zone is relatively dry but will contain some residual moisture. It will also contain a significant amount of air in pore spaces. Gravitational flow can slowly fill the vacant soil pores. This zone is also called the infiltration zone. The capillary zone is a transition zone between the unsaturated and the saturated zone. Capillary action will occur due to the attractive forces of soil pore water and the surface tension of water. The height of the capillarity zone depends on the diameter of the pores, the smaller the diameter the greater the capillary height. Secondly, the saturated zone is located below the groundwater table. The soil pores in this zone will be full of water (Boulding and Ginn 2004).

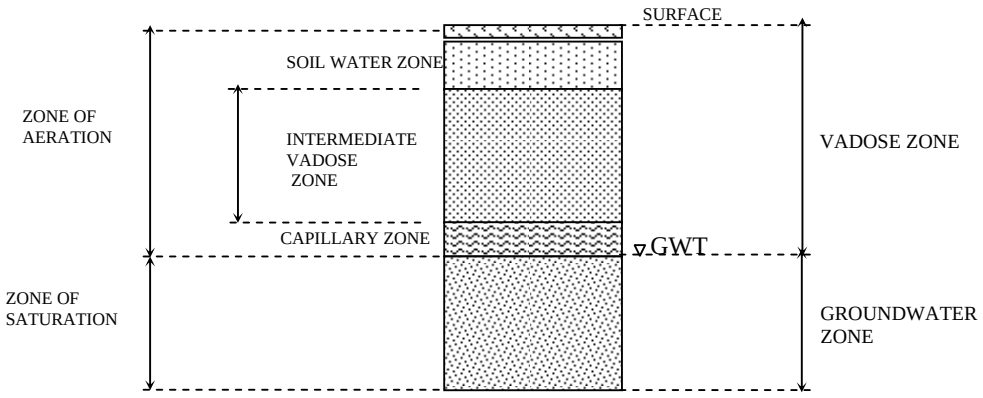

Figure 2.2 Classification of soil conditions
(adapted from Boulding and Ginn 2004)

The extent that contaminants migrate in ground depends upon the movement of wastewater, which is the best carrier. Contaminants can migrate slowly due to advection and dispersion processes (Boulding and Ginn 2004).

2.6.1 Advection transport

Most of the contaminants can be completely dissolved in the wastewater and can be accounted for as a homogenous bulk solute. Transport by advection relies on a bulk liquid movement. Contaminants may be carried at the same velocity and direction as the

flow of bulk solute. Flow of bulk liquid through soil pores would be normally by laminar flow and the velocity would be very low (Boulding and Ginn 2004).

2.6.2 Dispersion transport

Transport by dispersion consists of hydrodynamic dispersion and molecular diffusion. Hydrodynamic dispersion is caused by the variation in hydraulic conductivity and porosity. Molecular diffusion is driven by the concentration gradient. Even though there is no movement of bulk liquid, molecular diffusion will still be occurring if there is a gradient of concentration between the two positions (Boulding and Ginn 2004). These dispersion-diffusion processes can spread the contaminants. Transport by advection and dispersion is illustrated in Figure 2.3.

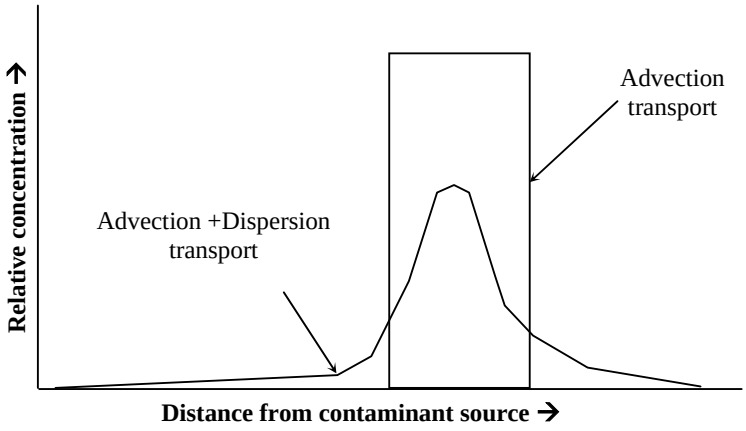

Figure 2.3 Patterns of contaminant transport processes
(adapted from Boulding and Ginn 2004)

2.7 Fate of contaminants

During transport, contaminants can react with soil microbes and minerals. Their fates could be changed considerably along the transport path and this will be discussed in more detail in the remainder of the chapter.

2.7.1 Organic carbon compounds

Organic carbon compounds are the primary sources of carbon for biomass metabolism and growth. Microbes prefer to digest organic carbon compounds until their concentrations become extremely low. Organic carbon substrates are classified into many levels. A primary substrate could be consumed first and then a secondary substrate could be used, and so on (Bouwer and McCarty 1984, Borden et al 1986 and Borden and Bedient 1986). When microbes consume the various substrates, and if organic carbon compounds are completely biodegraded, carbon dioxide gas and water would be the final products. An increase of dissolved carbon dioxide might affect the solubility of the aqueous carbonate mineral and the pH buffer system (Robertson and Cherry 1992).

Microbes obtain energy from the terminal electron acceptor in redox reactions. When oxygen is used as the electron acceptor, the process is known as aerobic respiration. The oxidised inorganic compounds such as nitrate, sulphate and carbon dioxide can also function as electron acceptors for some microbes, this process is known as anaerobic respiration (Sawyer et al. 1994). The limitation of dissolved oxygen can inhibit the growth of aerobic microbes and the consumption of organic carbon (McCarty et al. 1981).

The number of microbes can control the rate of organic carbon consumption. The equilibrium of biomass concentration could be observed in a stationary phase. Biomass could increase and/or decrease depending on environmental conditions such as temperature, pH, and moisture. Dead biomass could be consumed as organic substrates by other living cells (Widdowson et al 1988). Besides, microbes are insoluble, so they could be adsorbed easily onto the surface of the soil particles (MacQuarrie et al. 1990). When microbes are free to move, they could be filtered by the soil matrix (Harvey et al. 1984). The adhering microbes could then form a biological zone that could effectively consume the organic carbon compounds (MacQuarrie et al. 1990).

2.7.2 Nitrogen compounds

Approximately 80% of the nitrogen discharged from septic tanks is an inorganic substance with ammoniacal nitrogen dominating (30-111 mg/L) (Winneberger 1984, Walker et al. 1973 and Weiskel and Howes 1992). Ammonium ions can react with soil minerals. In enriched manganese soil, an ion exchange process can be activated immediately. The absorbed ammonium ions can be further biodegraded by nitrifying microbes (Ptacek 1998). Besides, ammonia could also be oxidised by autotrophic nitrifying bacteria under aerobic conditions and become nitrate, when the effluent was exposed to air (Sawyer et al. 1994). Coarse textured soil could provide a high degree of ammonia reduction because dissolved oxygen can rapidly move through the soil pores. This can be simplified such that the coarser the soil, the higher the degree of ammonia reduction (MacQuarrie et al. 2001).

The ammonia can remain in the effluent and is not completely removed by these reactions if its concentration is very high. Ammonia could be further consumed by another group of nitrifying bacteria, and the final product will be nitrate (Ptacek 1998 and MacQuarrie et al. 2001). A study of sandy Wisconsin soils reported that ammonia was transformed into nitrate. The elevated concentrations of nitrate at the depths of 0.3 and 69 m below the soil surface were 40 and 10 mg/L, respectively (Walker et al. 1973). Whelan (1988) studied the migration of nitrogen compounds in the drainage field, which was constructed on calcareous sand (Xerosamment) in Australia. Ammonia was almost completely oxidised by autotrophic nitrifying bacteria and transformed into nitrate. The concentration of nitrate increased dramatically from the surface to a depth of 50 cm.

Nitrification processes not only release nitrate, but also hydrogen ions. The hydrogen ion can potentially reduce the pH of the system from 9 to 5.5. This remarkable change in the pH can destroy the microbial activity (Whelan 1988 and Robertson and Cherry 1992). The nitrate compounds might be further degraded under anoxic/anaerobic conditions in the saturated zone (MacQuarrie et al. 2001). However, denitrification was very difficult in this zone because the remaining concentration of organic carbon compounds was normally low. The microbes could not further consume, so, the

anaerobic biodegradation was inhibited. So too, the microbes did not further consume any nitrate for their metabolism (Desimone and Howes 1996).

Bunnell et al. (1999) determined the efficiency of removing nitrogen from a drainage field using a pressure dosing septic system and a standard septic system. The effluent drainage process in the pressure dosing septic system was operated with a pumped tank, whereas the standard septic system was operated with gravitational flow. Both drainage fields received effluent that contained predominantly ammonia. The concentrations of NH_4 and Org.-N in both systems reduced rapidly, as the effluent passed through the soil surface. Conversely, nitrate increased with the depth of soil in the drainage field. This confirmed that ammonia oxidation and nitrification led to a dramatic increase in nitrates present.

Robertson et al. (2000) collected field data and revealed that some septic systems generated nitrate over the critical level (10 mg/L). The nitrate concentrations observed are reported in Table 2.7. The barriers were able to remove some amounts of nitrate, however, they might not be sufficient for high concentrations in wastewater, as observed at the Killarney site referred to the table.

Table 2.7 Nitrate concentration before (in) and after (out) treatment in different types of drainage field barriers (Robertson et al. 2000)

Location	Site description	Type of barrier in drainage field	Nitrate concentration (mg/L)	
			In	Out
Killarney	Conventional septic system, hydraulic retention time of 40 days, 0.68 m^3 in volume	0.5-1.0 inch of waste cellulose solids mixed with silty, fine sand	57.0[A]	11.6
Borden	Hydraulic retention time of 15 days, 9 m^3 in volume	0.5-1.0 inch of waste cellulose solids mixed with silty, fine sand	1.2[A,B]	0.2
Long Point Wall	Average hydraulic retention time of 13 days	Excavated sand material mixed with approximately 20% by volume of coarse hardwood sawdust	33.9[A]	2.9
North Campus Reactor	Hydraulic retention time of 3-7 hours, 1.9 m^3 in volume	Coarse wood mulch derived from local tree debris	4.8[A]	2.0

Note [A] Averaged values of all obtained data for six to seven years operation (1992 to 1998/1999).
[B] Untreated septic tank effluent

2.7.3 Phosphorus compounds

Table 2.8 presents the yearly averages for each septic tank. It may be observed that the septic tanks generated soluble phosphorus in a range of 0.6-2.2 mg/L. After passing the coarse gravel lined wetlands, the concentration in effluent was 0.5-1.3 mg/L. Thus, it was concluded that comparatively little phosphorus was removed by passing through these coarse gravel lined wetlands (Neralla et al. 2000).

Table 2.8 Yearly average concentrations for samples of soluble phosphorus in septic tanks (inf.) and subsurface constructed wetland (eff.) (Neralla et al. 2000)

Location	No. of people	No. of septic tanks	Septic tank total volume (L)	Flow estimate (m^3/d)	Gravel size (cm)	Soluble P (mg/L)	
						Inf.	Eff.
College station	2	2	3785	0.57	1.6	0.6±0.2	0.5±0.2
Bryan	4	2	3785	1.14	1.6	0.6±0.4	0.7±0.3
D'Hanis	3	1	3785	0.85	1.9	2.2±0.4	1.1±0.9
Stephenville	2	1	4371	0.57	0.95	1.1±0.5	0.8±0.3
Houston	3	2	3785	0.85	1.6	1.3±0.3	1.3±0.3
Tomball	3	1	3785	0.85	1.6	1.7±0.2	1.2±0.2
Dublin	2	1	3785	0.57	1.9	0.8±0.4	0.6±0.2
Weslaco	2	1	2839	0.57	0.95	1.1±0.3	0.7±0.2

Septic tanks can discharge phosphorus in the form of orthophosphate ($H_2PO_4^-$ and HPO_4^{2-}) (Robertson 1995 and Robertson and Blowes 1995). Orthophosphate compounds may be adsorbed onto the soil minerals, especially reactive iron, aluminium, and calcium compounds. Low concentrations of phosphate ions (less than 5 mg/L) could be adsorbed onto the iron and aluminium minerals in strong acidic to neutral conditions, and also it could be adsorbed onto calcium minerals in neutral to alkaline systems (Wilhelm et al. 1994). During nitrification, a hydrogen ion is generated and the acidity of the system increases. This acidity could actually lead to dissolution of carbonate minerals. As the rate of carbonate dissolution increases, the rate of phosphate adsorption decreases (Zanini et al. 1998).

Phosphate attenuation (PO_4^{3+}) may be retarded by precipitation on the positively charged mineral sources such as ferric (oxy) hydroxides, aluminium compounds and calcite. The conversion of ammonium ion to nitrate can occur near the percolation pipe in an oxidative environment. The Ferrous (Fe^{2+}) can be converted to ferric ions (Fe^{3+}) in

this environment. The precipitation of ferric (oxy) hydroxide and ferric phosphate was observed by Wilhelm et al. (1996). In an acidic soil with pH below 5, neutralisation can be driven by the dissolution of gibbsite. This can cause the release of aluminium ions that could stimulate the precipitation of phosphate in the form of aluminium phosphate. If the pH becomes neutral, the precipitation of calcium phosphate could occur instead (Zanini et al. 1998).

Harman et al. (1996) confirmed that the phosphate removal rate due to adsorption was much higher than precipitation, and thus, the adsorption reaction was the most important mechanism for retarding of phosphate. Robertson (1995) monitored the migration of phosphate in onsite systems. The phosphate migration rate depended on the characteristics of the soil, thickness of the unsaturated zone, applied loading rate, and age of the septic systems. Several studies of the migration of phosphate in the sub-surface found that it could be attenuated over short distances of several metres below the surface (Harman et al. 1996 and Baker 1996). Robertson and Harman (1999) observed phosphate plumes in 2 and 4-year operating onsite treatment systems and found the concentrations of phosphate were 0.4 and 5 mg/L, respectively. Whelan and Barrow (1984a and 1984b) also observed that phosphate migrated very quickly in sandy soil that contained little clay, aluminium oxide, ferrous oxide, and organic matter.

Some opportunities also exist for bypass flow in the drainage field. Especially in coarse soil, a soluble phosphate could migrate directly to groundwater without any retardation (Pierzynski et al. 2000). If phosphate compounds reach the groundwater, they may migrate downstream in the general direction of the groundwater flow. Mobilisations of phosphate in aquifers are likely to be controlled by site specific factors including the amount of soil minerals, composition of percolated wastewater and the buffering capacity of soil. The complexity of these factors might lead to difficulties in predicting the phosphate plume in aquifers. Since the migration of phosphate in the long term is different site by site, the phosphate plume could be estimated only in a local scale (Zanini et al. 1998).

2.7.4 Faecal coliforms

The study of pathogens discharged from septic tanks focuses on *E.Coli* because it is an indicator organism which originates from faecal waste (sewage) (Jewett et al. 1995). The number of total and faecal coliforms in septic tank effluent is reported in Table 2.9 (Neralla et al. 2000). The gravel lined drainage fields were too coarse to reduce any coliforms through filtration.

Table 2.9 Yearly average for total and faecal coliform numbers in septic tank effluent (Neralla et al. 2000)

Location	No. of people	No. of septic tanks	Septic tank total volume (L)	Flow estimate (m^3/d)	Gravel size (cm)	Total coliforms (log cfu/ 100mL)	Faecal coliforms (log cfu/ 100mL)
College station	2	2	3785	0.57	1.6	6.5±0.9	5.6±1.5
Bryan	4	2	3785	1.14	1.6	6.7±1.3	5.4±1.4
D'Hanis	3	1	3785	0.85	1.9	6.6±0.4	6.2±0.7
Stephenville	2	1	4371	0.57	0.95	6.1±0.6	5.5±1.2
Houston	3	2	3785	0.85	1.6	7.3±0.7	6.8±0.9
Tomball	3	1	3785	0.85	1.6	6.5±0.5	6.1±0.6
Dublin	2	1	3785	0.57	1.9	6.5±0.6	5.2±1.2
Weslaco	2	1	2839	0.57	0.95	7.1±0.6	6.8±1.6

Filtration and adsorption were potential mechanisms for bacterial and viral retardation (Hagedorn 1981, Jewett et al. 1995, Cuyk et al. 2001 and McKay et al. 2002). Vinod and Bokil (1982) have researched the most suitable media for removing bacteria. The media were prepared by mixing various ratios of sand, silt, and clay. The results indicated that the composite soil consisting of 60% sand and 40% soil (particle size 75 μm) was the most efficient means for removing microbes.

Filtration and adsorption relied on the particle size of the media and the flow rate of the wastewater. Fine grained media and low flow rates could induce a biological clogging zone, and provided the highest retardation of microbes (Stevik et al. 1999a and 1999b). Kaplan (1991) claimed that microbes could not be filtrated by any coarse grained soils. Microbes smaller than 3 microns were found at depths of 0.3-90 m (1-300 feet) and 840 m (2800 feet) below the surface of a sandy and gravel aquifers, respectively. Vaughn et al. (1983) observed that the viruses discharged from septic tanks could be found at the

depths of 3.6 and 67 m in drainage fields located on fine and coarse soil layers, respectively.

The lack of nutrients and organic matter could stimulate microbial decay (Canter and Knox 1985). Parker and Mee (1982) studied the movement of *Samonella Adelaide* and faecal coliforms in two drainage fields constructed on a layer of coarse sand. The decay of the microbes was estimated from LD_{10} which refers to the lowest lethal dose that only 10% of total microbes were killed. The LD_{10} of faecal coliform and *Samonella Adelaide* were 64 and 46 days, respectively. These values refer to the worst living conditions. Retardation of contaminants in saturated and unsaturated soil are summarised in Table 2.10.

Table 2.10 Details of the removal mechanisms in unsaturated and saturated zones

Contaminant	Mechanism	Equation	Reference
Nitrogen	*Unsaturated zone:* biodegradation	$NH_4^+ + 2O_2 \rightarrow NO_3^- + 2H^+ + H_2O$	Wilhelm et al. (1994)
	buffering systems	$H^+ + HCO_3^- \rightarrow H_2CO_3$ $CaCO_3 + H^+ \rightarrow Ca^{2+} + HCO_3^-$ $CaCO_3 + CO_2 + H_2O \rightarrow Ca^{2+} + 2HCO_3^-$	
	Saturated zone: biodegradation	$4NO_3^- + 5CH_2O + 4H^+ \rightarrow 2N_2 + 5CO_2 + 7H_2O$	Wilhelm et al. (1994)
Phosphorus	*Unsaturated zone:* metal precipitation/ adsorption*	$Fe^{3+} + H_2PO_4^- + 2H_2O \Leftrightarrow FePO_4 \bullet 2H_2O + 2H^+$(pH 4.5- 5) $3Fe^{2+} + 2PO_4^{3-} + 8H_2O \Leftrightarrow Fe_3(PO_4)_2 \bullet 8H_2O$ (pH 4.5- 5) $Al^{3+} + H_2PO_4^- + 2H_2O \Leftrightarrow AlPO_4 \bullet 2H_2O + 2H^+$ (pH 4.5- 5) $5Ca^{2+} + 3HPO_4^{2-} + H_2O \Leftrightarrow Ca_5(PO_4)_3(OH) + 4H^+$ (pH 7-8)	Robertson (1995) Zanini et al. (1998)
	Saturated zone: metal precipitation/ desorption *	$Fe^{3+} + H_2PO_4^- + 2H_2O \Leftrightarrow FePO_4 \bullet 2H_2O + 2H^+$(pH 4.5- 5) $3Fe^{2+} + 2PO_4^{3-} + 8H_2O \Leftrightarrow Fe_3(PO_4)_2 \bullet 8H_2O$ (pH 4.5- 5) $Al^{3+} + H_2PO_4^- + 2H_2O \Leftrightarrow AlPO_4 \bullet 2H_2O + 2H^+$(pH 4.5- 5) $5Ca^{2+} + 3HPO_4^{2-} + H_2O \Leftrightarrow Ca_5(PO_4)_3(OH) + 4H^+$(pH 7-8)	Robertson (1995) Zanini et al. (1998)
Organic carbon	*Unsaturated zone:* biodegradation	$CH_2O + O_2 \rightarrow CO_2 + H_2O$	Wilhelm et al. (1994)
	Saturated zone: biodegradation	$4NO_3^- + 5CH_2O + 4H^+ \rightarrow 2N_2 + 5CO_2 + 7H_2O$	Wilhelm et al. (1994)
Microbes	*Unsaturated zone:* Metabolic processes (Assimilation/ Dissimilation)	$8CH_2O + 3O_2 + NH_3 \rightarrow C_5H_7NO_2$**$+ 3CO_2 + 6H_2O$ $C_5H_7NO_2 + 8H_2O \rightarrow 5CO_2 + NH_3 + 20H^+ + 20e^-$	Orhon and Artan (1994)

Note * A number of phosphate minerals are thermodynamically stable in groundwater environments, particularly those associated with the metal cations $Fe^{2+} > Fe^{3+} > Al^{3+} > Ca^{2+}$, respectively (Robertson 1995).

** The biomass chemical formula.

2.8 Summary

Untreated domestic wastewater is a high strength wastewater that contains many contaminants including organic, inorganic substances and pathogens. These contaminants could potentially impact on human health and environmental quality. Thus, untreated wastewater should not be permitted to discharge to the environment.

Raw domestic wastewater can be effectively treated by conventional septic tanks if they work properly. However, there was a great concern on the failure of septic systems in which poor quality effluent containing contaminants with extremely high concentrations can be released to the environment. Major contaminants emanating from the failed septic tanks include organic carbon, nitrate, phosphate compounds and faecal coliforms and in many cases their concentrations were found to be higher than allowable levels. As soon as these contaminants reached the groundwater, they could be responsible for health and environmental impacts.

When contaminants enter the drainage field, advection and dispersion could spread the contaminants and extend their travel time. Physical, chemical, and biological reactions can improve the quality of wastewater discharged from septic tanks. Land application alone might not be enough to protect the groundwater resource, if high concentrations of contaminants are released from a septic tank and/or the drainage field is poorly located. The migration of contaminants needs to be estimated. A better solution would be to develop a predictive model. This is best done by formulating a conceptual model and is described in the next chapter.

CHAPTER 3

DEVELOPMENT OF A CONCEPTUAL MODEL

3.1 Introduction

A conceptual model for contaminant transport in unsaturated soil is proposed for the process that takes place from the time the contaminated water is discharged into a drainage field until it reaches the groundwater. The model consists of both contaminant transport and retardation processes. Firstly, the contaminant transport process is described according to the geological and soil hydraulic properties, which could be used to predict the probable movement of wastewater. Secondly, the contaminant retardation process is defined based on the geochemical and biological reactions.

The conceptual model is compared to the available commercial models for estimating the fate and/or migration of contaminant to select the most suitable model. There were many limitations on the existing models. A suitable model for microbial transport could not be achieved. The related governing equations for contaminant transport and retardation are reviewed to quantitatively describe the established model. Transport of contaminants can be described based on the processes of advection and dispersion. Retardation of contaminants can be defined as the interactions between soil and contaminants.

3.2 Development of a conceptual model

A conceptual model of transport with retardation of contaminants associated with septic tank effluent is presented in Figure 3.1. A septic tank is best suited to an area with a low groundwater table and moderately permeable soil. There exists residential areas which are outside the service of a centralised sewage treatment system that use septic tanks even though the geological conditions may not be suitable. The worse case concerns are those areas located in a high groundwater table, with high soil permeability. The drainage field presented here contained unsaturated and saturated zones. The retardation mostly occurred in the unsaturated zone. The concentration of contaminants potentially

reaching the groundwater table depended on the unsaturated zone. Hence, the conceptual model focused mainly on the transport and retardation of contaminants in the unsaturated zone. The boundary of the system considered begins at the septic tank effluent drainage pipe and ends at the groundwater table as shown in Figure 3.1.

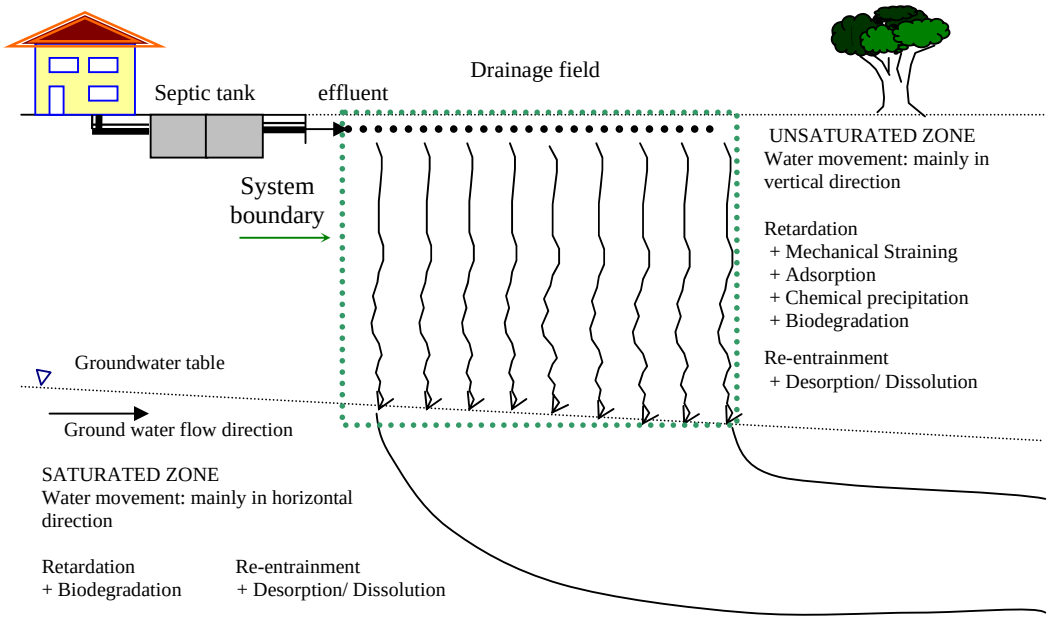

Figure 3.1 Conceptual model

Septic tank effluent percolates vertically in an unsaturated zone and the contaminants are carried by advection and dispersion. The effluent added in to the drainage field moves downwards due to gravitational force, whereas, groundwater moves upwards due to capillary force. The flow presented here is under the influence of infiltration-redistribution forces. Groundwater normally contains low concentration of contaminants, and it is assumed that the groundwater did not add any contaminants in the system. However, groundwater might dilute the concentration of contaminants.

Dynamic interactions between soil and contaminants in an unsaturated zone are complex. Thus, only dominant reactions are considered in order to simplify retardation as presented in Table 3.1.

Table 3.1 Dominant reactions for retardation of contaminants in septic tank effluent

Contaminant	Physical reaction	Chemical reaction	Biological transformation
Nitrate-nitrogen	-	-	Nitrification/ Denitrification
Phosphate-phosphorus	-	Adsorption	-
Organic carbon compounds	-	-	Biodegradation
Microbes	Filtration	Adsorption	Cell decay

The assumptions made in developing the conceptual model are:

(a) Soil was homogeneous and incompressible;

(b) Soil had a mix of microbial cultures activated and acclimatised to contaminants. Septic tank effluent contained no hazardous chemicals, and hence there was no inhibition of biological processes;

(c) There was no rainfall and the groundwater table was constant, so there was no smearing zone of contaminants;

(d) Septic tank effluent was loaded into the drainage field with a constant discharge rate and its characteristics did not vary significantly; and

(e) All chemical interactions were fast enough to validate the chemical equilibrium assumptions.

The conceptual model established here is further compared with the available commercial or existing models in order to select the most suitable model.

3.3 Commercial models of soil-contaminant transport

The soil contaminant transport models that are available in the literature including the commercially available models have been reviewed and a summary is presented in Table 3.2.

Table 3.2 Summary of available models for septic tank effluent transport in soil

Models	Monitored contaminants				Soil Conditions	Dimensions	Available	Remarks	References
	N	P	Org. C	MO*					
CHEMTRN	←Users define equilibrium constants and stoichiometric coefficients →				Saturated	1D	http://www.nea.fr/abs (Nuclear Energy Agency)	Last modified 29 May 1986.	Miller et al. (2001)
PRZM3	Y	N	N	N	Unsaturated	1D	http://viso.ei.jrc.it/focus/gw/model/PRZM http://www.epa.gov/ceampubl/DOS/PRZM3/INSTALP3.EXE	This software operates in DOS. Most references for PRZM applications use this software to predict fate of pesticides in soils.	Russell and Reinken (1984)
MacQuarrie et. al. (2001)	Y	N	Y	N	Unsaturated/ saturated	3D	-	This model had been applied at Cambridge site, Ontario, Canada. Water table at this site was high, thus, unsaturated condition was neglected.	MacQuarrie et al. (2001)
Kinzelbach et. al. (1991)	Y	N	Y	Y	Saturated	2D	-	This model concerns the increase of microbial mass in denitrification process. The author provided the governing equation, but the details of model did not show in this article.	Kinzelbach et al. (1991)
Zanini et.al. (1998)	N	Y	N	N	Unsaturated	-	-	This article provided conceptual model and experimental data. The governing equations, and numerical model did not investigate.	Zanini et al. (1998)
Ginn et.al. (2002)	N	N	N	Y	Saturated	3D	-	The authors provided the governing equations of microbial transportation, bio-film formation and metabolic effects on microbial.	Ginn et al. (2002)
MacQuarrie et.al. (1990)	N	N	Y	Y	Saturated	3D	-	The microbial mass was kept constant in this model. The transportation was set in 3D, but the biodegradation rate was set in 1D.	MacQuarrie et al. (1990)
Zysset et.al. (1994)	N	N	N	Y	Saturated	1D	-	The authors gave the governing equations for bio-film system in groundwater. Nitrate and organic carbon were concerned as soluble substrates to maintain the microorganism growth.	Zysset et al. (1994)
Baek et.al. (1989)	N	N	N	Y	Unsaturated	1D	-	This article provided the governing equations for BIOSOIL model. However, this model was not referred in textbook and U.S. Geological Survey Report.	Baek et al. (1989)

Note * MO is microbe.

Most models could also support the transport of contaminants in either unsaturated or saturated soil conditions. The models developed for reactive contaminants transport in saturated soil conditions include CHEMTRAN, the model of Kinzelbach et al. (1991), Ginn et al. (2002), MacQuarrie et al. (1990) and Zysset et al. (1994). CHEMTRAN was the most flexible model because the users could define any contaminants considered. However, the model did not provide any kinetic coefficients which made it inconvenient to use. The model of Kinzelbach et al. (1991) could be applied to the transport of nitrogen, organic carbon compounds, and microbes. The model of Ginn et al. (2002) only mentioned the transport of microbes, whereas the model of MacQuarrie et al. (1990) could support the transport of organic carbon compounds and microbes. The models developed for reactive contaminants transport in unsaturated soil conditions include PRZM3, the model of Zanini et al. (1998) and Beak et al. (1989), which can support the transport of pesticides, phosphorus and microbes, respectively.

The available commercial and other existing models reviewed could not be directly applied to the problem in hand as they do not take into account the transport and retardations of microbes in the unsaturated zone. Hence there is a need to develop a mathematical model using fundamental principles to predict contaminant transport through unsaturated porous media that incorporates the transport and retardation of microbial actions.

3.4 Governing equations for contaminants transport

The governing equation for multi-component transportation of contaminants in porous media under variable saturation conditions could be expressed in a general form as follows (Schnoor 1996).

$$\underset{(accumulation)}{\frac{\partial C}{\partial t}} = \underset{(dispersion)}{\frac{\partial}{\partial z}\left(D_z \frac{\partial C}{\partial z}\right)} - \underset{(advection)}{\frac{\partial}{\partial z}(q_z C)} - \underset{(sorption)}{\frac{\rho_B}{\theta}\left(\frac{\partial C^*}{\partial t}\right)} \pm \underset{(reaction)}{\sum_{m=1}^{n} r_m} \qquad (3\text{-}1)$$

where

θ = The volumetric water content [$L^3 L^{-3}$]

C^* = The concentration of a considered constituent in sorbed phase [M L^{-3}]

D_z = The dispersion coefficient [L^2 T^{-1}]

r_m = The physical, chemical and biological reaction rate [M L^{-3} T^{-1}]

In accordance with the mass balance concept, advection and dispersion terms are used to estimate the mass of contaminants that flow through a representative elementary volume (REV) of a porous medium. Sorption and other reactions define the source/sink terms (Schnoor 1996). This governing equation is in a form of a hyperbolic/parabolic partial differential equation (PDE) and consists of many idealised parameters such as D_z, q_z and r_m. Parameters D_z and q_z can be determined using Richards' equation and r_m can be expressed as a function according to the defined reactions. The details of these equations are given in the following sections.

3.4.1 Richards' equation

The non-linear flow velocity in the unsaturated zone was evaluated using either changing of pressure head or moisture content. Pressure head based Richard's equation was used to estimate the non-linear Darcy's velocity (Bear 1972, Bear and Verrujit 1987 and Huyakorn et al. 1984).

$$\frac{\partial}{\partial z}\left[K_{zz}k_{rw}\left(\frac{\partial \psi}{\partial z}+1\right)\right]=\phi\frac{\partial S_w}{\partial t} \tag{3-2}$$

where

K_{zz} = The saturated hydraulic conductivity [L T^{-1}]

k_{rw} = The relative permeability [unitless]

ψ = The pressure head [L]

ϕ = The porosity [unitless]

S_w = The degree of saturation [unitless]

z = The depth in the vertical direction (positive upward) [L]

The specific moisture capacity (M_C) is ideally defined as the changing of volumetric content over the changing of pressure head ($\frac{\partial \theta}{\partial \psi}$). The right-hand side of Equation 3-2 could be rearranged as a function of M_C and $\frac{\partial \psi}{\partial t}$ as follows (Huyakorn et al. 1984):

$$\phi \frac{\partial S_w}{\partial t} = \phi \frac{\partial S_w}{\partial \psi} \frac{\partial \psi}{\partial t} \cong \frac{\partial \theta}{\partial \psi} \frac{\partial \psi}{\partial t} = M_C \frac{\partial \psi}{\partial t} \tag{3-3}$$

Therefore Equation 3-2 could be rewritten as (Huyakorn et al. 1984):

$$\frac{\partial}{\partial z}\left[K_{zz} k_{rw} \left(\frac{\partial \psi}{\partial z} + 1 \right) \right] = M_C \frac{\partial \psi}{\partial t} \tag{3-4}$$

where

M_C = The specific moisture capacity [L^{-1}]

The first term of Equation 3-4 contained an unsaturated Darcy's equation, q_z. This was formulated as follows (the negative sign means a downward flow) (Huyakorn et al. 1984):

$$q_z = -K_{zz} k_{rw} \left(\frac{\partial}{\partial z} [\psi + z] \right) \tag{3-5}$$

where

q_z = Darcy's velocity in vertical direction [$L\ T^{-1}$]

By inserting a series of tensiometers in different parts of a drainage field, the profiles of pressure head could be observed as shown in Figure 3.2. The negative pressure head determined in the unsaturated soil layer was due to suction head, zero pressure head occurred at the groundwater table and the positive pressure head presented in the saturated soil layer was due to hydraulic head (gravitational head plus pore-water pressure head) (Fredlune and Rahardjo 1940).

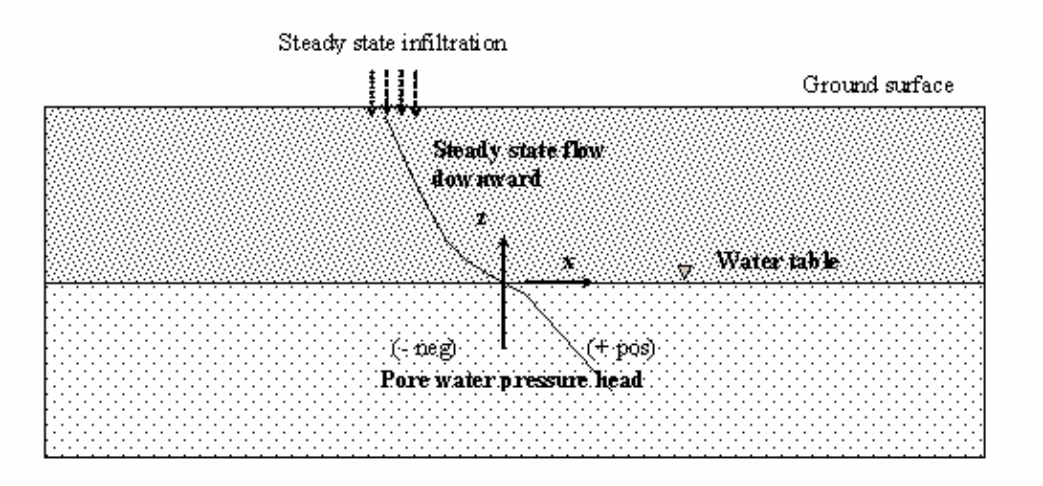

Figure 3.2 Profiles of pore pressure under a steady state flow of infiltration (adapted from Fredlune and Rahardjo 1940)

Figure 3.3 presents possible pressure head profiles at varying Darcy's velocities. If the velocity is constant $(\partial\psi / \partial z = 0)$, the simplest pressure head profiles (case 3) are obtained. When $\partial\psi / \partial z$ is negative with $-K_{zz}k_{rw} < q_z < 0$, this will lead to vertical downward flow (case 1). If $\partial\psi / \partial z$ is positive with $q_z < -K_{zz}k_{rw}$, water moves downward with suction head (case 2). The upward flow is yielded (case 4), if Darcy's velocity is greater than zero. However, most cases in the unsaturated zone, the water will experience a downward flow (Warrick et al. 1991).

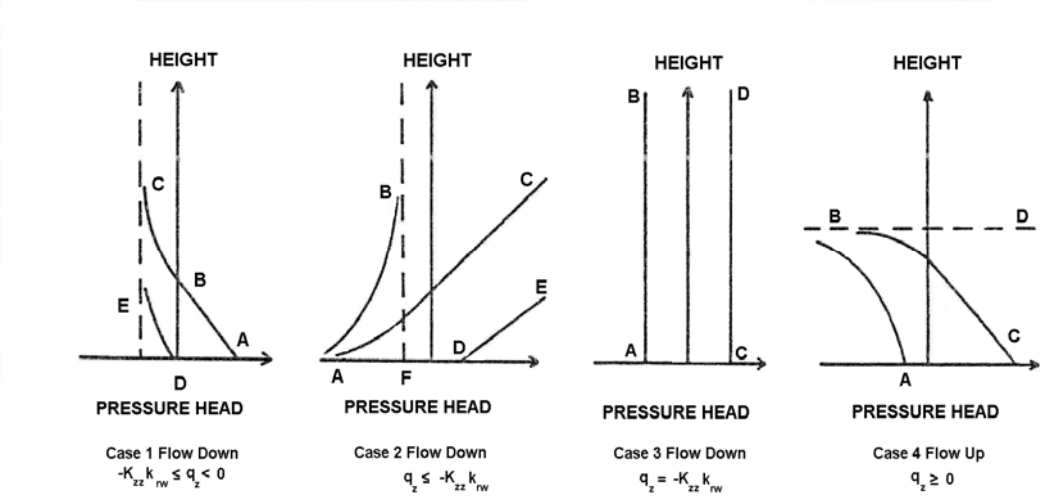

Figure 3.3 Possible pressure head profiles at varying Darcy's velocities (Warrick et al. 1991)

The dispersion, D_z consisted of hydrodynamic dispersion and molecular diffusion, and it could be obtained from Fick's Law (Fetter 1992).

$$D_z = \omega v_i + D^* \tag{3-6}$$

where

D^* = An effective molecular diffusion coefficient [$L^2\ T^{-1}$]

ω = A coefficient relating to tortuosity [unitless]

v_i = The average linear velocity in the vertical direction $\left(= \frac{q_z}{\theta}\right)$ [$L\ T^{-1}$]

Tracer testing was the best way to estimate the dispersion coefficients. Tracers used included potassium bromide, sodium chloride, tritium, fluorescein, and Rhodamine WT dyes (Schnoor 1996). Scheidegger (1960) conducted laboratory and field scale tracer tests to estimate the dispersion and travel time of particles in soils. The results suggested that the dispersion relied on depth and the pore size of soils. Deeper soil layers and smaller soil pores generated higher dispersion and longer travel times.

Variables M_C and $K_{zz}k_{rw}$ presented in Richard's and Darcy's equations were estimated using the hydraulic properties equations.

3.4.2 Hydraulic properties equations

The hydraulic properties equations used in this research included those of Haverkamp et al. (1977), van Genuchten (1980) and Saxton et al. (1986). The details of these equations were given as follows:

Haverkamp et al.'s equations (HV)

Haverkamp et al. (1977) fitted the properties of homogeneous soil in unsaturated conditions by the least square method. The equations were given as:

$$\theta = \frac{\alpha(\theta_s - \theta_r)}{\alpha + |\psi|^{\beta}} + \theta_r \tag{3-7}$$

$$K_{zz} k_{rw} = K_{zz} \left(\frac{A}{A + |\psi|^{\gamma}} \right) \tag{3-8}$$

where

θ_r = A residual moisture content [L^3 L^{-3}]

θ_s = A saturated moisture content [L^3 L^{-3}]

A, α, β, γ = The curve fitting coefficient [unitless]

Examples of water retention curves obtained from HV are presented in Figure 3.4.

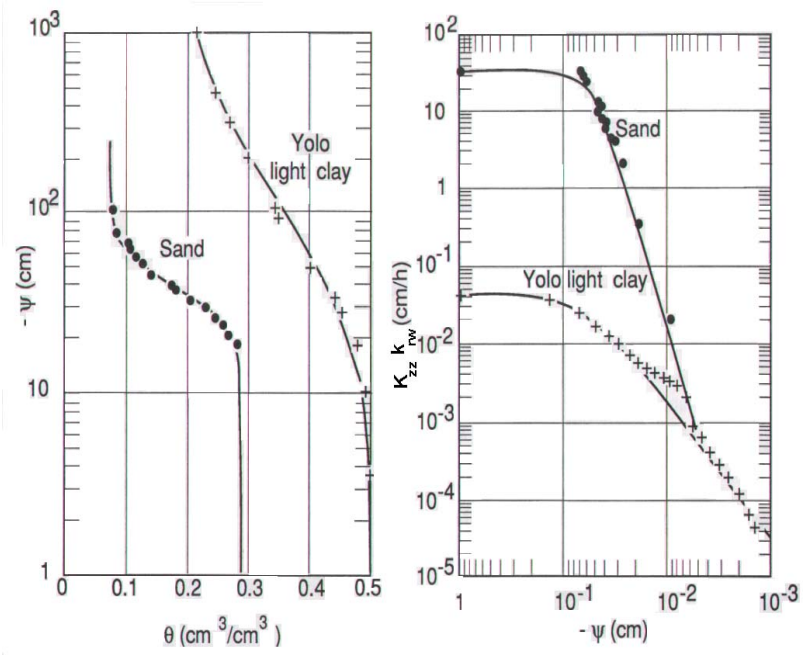

Figure 3.4 Water retention curves fitted by HV equations (Haverkamp et al. 1977)

Variable M_C could be estimated by differentiating Equation 3-7, yielding:

$$M_C = -\frac{\alpha\beta(\theta_s - \theta_r)|\psi|^{\beta-1}}{\left(\alpha + |\psi|^{\beta}\right)^2} \tag{3-9}$$

The coefficients for HV were provided in Table 3.3 (Haverkamp et al.1977) for two soil types.

Table 3.3 Empirical coefficients for HV equations (Haverkamp et al. 1977)

Soil type	Saturation conductivity, Kzz (cm/h)	Saturated moisture content, θs	Residual moisture content, θr	α (cm^{-1})	β	A	γ
Sand	34.0	0.287	0.075	$1.611x10^{6}$	3.96	$1.175x10^{6}$	4.74
Yolo Light Clay	$4.428x10^{-2}$	0.495	0.124	739.0	4.00	124.6	1.77

van Genuchten's equations (VG)

van Genuchten (1980) derived the hydraulic properties equations based on the equation of Brooks and Coley (1964). The hydraulic properties equations were presented as follows:

$$\theta = \theta_r + \frac{\theta_s - \theta_r}{\left(1+\left(a|\psi|\right)^p\right)^m} \tag{3-10}$$

$$k_{rw} = \frac{\left[1-\left(a|\psi|\right)^{p-1}\left[1+\left(a|\psi|\right)^p\right]^{-m}\right]^2}{\left[1+\left(a|\psi|\right)^p\right]^{m/2}} \tag{3-11}$$

where

a = The soil water retention function [L^{-1}]

m and p = The empirical parameters, $\left(m = 1-\left(1/p\right)\right)$ [unitless]

An example of water retention curve fitted by VG is presented in Figure 3.5.

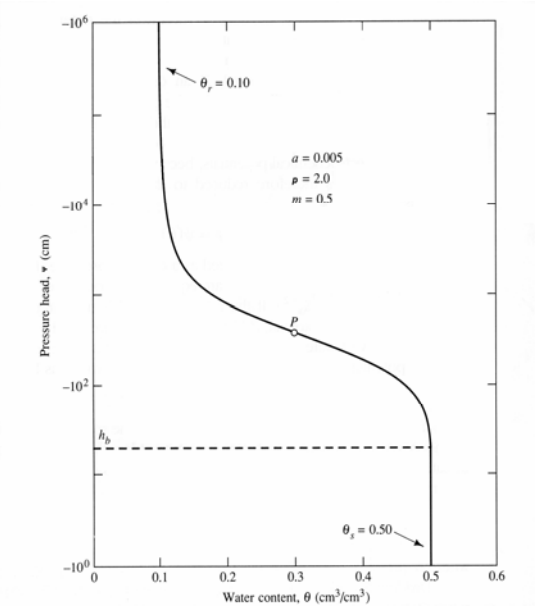

Figure 3.5 Determination of empirical coefficients for VG equations (Fetter 1992)

Variable M_C could be derived from VG equations (Equation 3-10) as follows:

$$M_C = \frac{-a^p (p-1)(\theta_s - \theta_r)|\psi|^{p-1}}{\left\{1+(a|\psi|)^p\right\}^{m+1}} \tag{3-12}$$

The possible values for the coefficients presented in VG equations were given in Table 3.4. The coefficients were sorted by soil textures in accordance with USDA textural classes (U.S. Department of Agriculture 2001) (Carsel et al. 1988).

Table 3.4 Recommended empirical coefficients for VG equations (Carsel et al. 1988)

Soil Type	Saturated Moisture Content, θ_S	Residual Moisture Content, θ_r	a (cm^{-1})	p
Clay*	0.38	0.068	0.008	1.09
Clay loam	0.41	0.095	0.019	1.31
Loam	0.43	0.078	0.036	1.56
Loam sand	0.41	0.057	0.124	2.28
Silt	0.46	0.034	0.106	1.37
Silt loam	0.45	0.067	0.020	1.41
Silty clay	0.36	0.070	0.005	1.09
Silty clay loam	0.43	0.089	0.010	1.23
Sand	0.43	0.045	0.145	2.68
Sandy clay	0.38	0.100	0.027	1.23
Sandy clay loam	0.39	0.100	0.059	1.48
Sandy loam	0.41	0.065	0.075	1.89

Note: *Agricultural soil, less than 60% clay.

Saxton et al.'s equations

The hydraulic properties could be estimated from the soil texture using a method generalised by Saxton et al. (1986). The textural class was assessed according to the USDA system. The water retention curve was fitted with linear regression and the formulations were presented in S.I. unit as follows:

1) The applied tension 10 to 1500 kPa (or 102.1 to 15315 cm H_2O)

$$\psi = \psi_e \left[\frac{(\theta - \theta_r)}{(\theta_s - \theta_r)} \right]^H \tag{3-13}$$

by assuming $\theta_r = 0$; will give

$$\psi = J\theta^G \tag{3-14}$$

where

ψ = The soil water pressure [kPa]

ψ_e = The air entry pressure [kPa]

θ = The volumetric moisture content [cm^3 cm^{-3}]

θ_s = The saturation volumetric moisture content [cm^3 cm^{-3}]

θ_r = The residual volumetric moisture content [cm^3 cm^{-3}]

H = The statistical curve fitting value (from 44 soil samples and R^2 =0.99)

$\left(= -3.140 - 0.00222(\%clay)^2 - 3.484\times10^{-5}(\%sand)^2(\%clay)\right)$

J = The statistical curve fitting value (from 44 soil samples and R^2 =0.99)

$\left(= \exp[-4.396 - 0.0715(\%clay) - 4.880\times10^{-4}(\%sand)^2 - 4.285\times10^{-5}(\%sand)^2(\%clay)]100.0\right)$

2) The applied tension ψ_e to 10 kPa (or ψ_e to 102.1 cm H_2O)

$$\psi = 10.0 - \frac{(\theta - \theta_{10})(10.0 - \psi_e)}{(\theta_s - \theta_{10})} \tag{3-15}$$

where

θ_{10} = The volumetric moisture content at 10 kPa $\left(= \exp\left(\frac{[2.302 - \ln J]}{G}\right)\right)$ [cm^3/cm^3]

$\psi_e = 100.0[-0.108 + 0.341\theta_s]$

and

$\theta_s = 0.332 - 7.251\times10^{-4}(\%sand) + 0.1276[\log(\%clay)]$

3) The applied tension 0.0 kPa to ψ_e (or 0.0 cm H_2O to ψ_e)

$$\theta = \theta_s \tag{3-16}$$

Variables $K_{zz}k_{rw}$ were estimated as follows:

$$K_{zz}k_{rw} = 2.778\times10^{-6}\{\exp[12.012 - 0.0755(\%sand) + \left[-3.8950 + 0.03671(\%sand) - 0.1103(\%clay) + 8.7546\times10^{-4}(\%clay)^2\right](1/\theta)]\} \quad (3\text{-}17)$$

where

$K_{zz}k_{rw}$ = The unsaturated hydraulic conductivity [m s^{-1}]

Kunze et al.'s equation

Kunze et al. (1968) established a relative permeability function based on Poiseuille's equation. The coefficient of relative permeability was obtained from the relationship between the matrix suction and volumetric moisture content. The equation was given as follows:

$$k_{rw}(\theta)_i = \frac{(K_{zz})_{mea}}{(K_{zz})_{cal}} \frac{{T_S}^2 \rho_w g}{2\mu_w} \frac{{\theta_S}^P}{N^2} \sum_{j=i}^{m} \left\{(2j+1-2i)\left(|-\psi|\right)_j^{-2}\right\} \quad i=1, 2,\ldots, m \quad (3\text{-}18)$$

where

$k_{rw}(\theta)_i$ = Calculated coefficient of permeability for a specified volumetric moisture content; θ_i, corresponding to the i^{th} interval [unitless]

i = Interval on the water retention curve [unitless]

j = Counter number from i to m [unitless]

$(K_{zz})_{mea}$ = Measured saturated coefficient of permeability [L T^{-1}]

$(K_{zz})_{cal}$ = Calculated coefficient of permeability [L T^{-1}]

T_S = Surface tension of water [M L^{-1} T^{-2}]

ρ_w = Water density [M L^{-3}]

g = Gravitational acceleration [L T^{-2}]

μ_w = Absolute viscosity of water [M L^{-1} T^{-1}]

P = A constant which accounts for the interaction of pores of various sizes, usually assumed to be 2.0 (Green and Corey 1971 cited in Fredlune and Rahardjo 1940) [unitless]

m = Total number of intervals between the saturation volumetric water content and the residual volumetric water content [unitless]

N = Total number of intervals computed between saturation and residual volumetric moisture content $\left(N = \frac{m\theta_s}{(\theta_s - \theta_r)} \right)$ [unitless]

An example of estimating of relative permeability using Kunze's equation is illustrated in Figure 3.6.

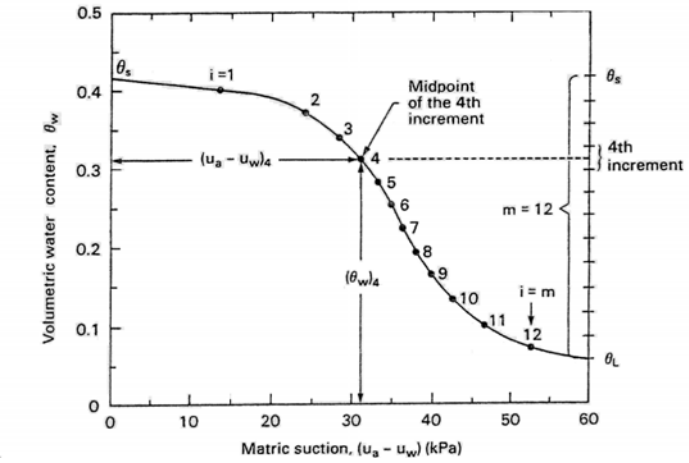

Figure 3.6 Graphical estimation of relative permeability (Fredlune and Rahardjo 1940)

3.4.3 Soil contaminant reactions

The governing equations for contaminant retardations were defined as follows:

Nitrogen and organic carbon compounds

The total rate of organic carbon compounds (substrate) utilisation, r_S was a combination of the substrate utilisation rate due to aerobic and nitrate respiration (Widdowson et al.1988).

$$r_S = r_{SO} + r_{SN} \tag{3-19}$$

where

r_S , r_{SO} and r_{SN} = The total substrate utilisation, substrate utilisation under aerobic respiration and substrate utilisation under nitrate respiration, respectively [T^{-1}]

Using a modified Monod's equation, the substrate utilisation rates could be derived as follows (Widdowson et al. 1988):

$$r_{SO} = \frac{\mu_O}{Y_O}\left[\frac{C_S}{K_{SO}+C_S}\right]\left[\frac{C_O}{K_O+C_O}\right]\left[\frac{C_A}{K_{AO}+C_A}\right] \quad (3\text{-}20a)$$

$$r_{SN} = \frac{\mu_N}{Y_N}\left[\frac{C_S}{K_{SN}+C_S}\right]\left[\frac{C_N}{K_N+C_N}\right]\left[\frac{C_A}{K_{AN}+C_A}\right]I[C_O] \quad (3\text{-}20b)$$

where

μ_O and μ_N = The maximum specific growth rate for aerobic and denitrifying bacteria, respectively [T^{-1}]

Y_O and Y_N = A heterotrophic yield coefficient for aerobic and denitrifying bacteria, respectively [unitless]

C_S , C_O and C_A = The concentration in aqueous of organic carbon, oxygen and ammonia, respectively [M L^{-3}]

K_{SO} , K_O and K_{AO} = Half concentration of substrate, oxygen and ammonia nitrogen under aerobic respiration, respectively [M L^{-3}]

K_{SN} , K_N and K_{AN} = Half concentration of substrate, nitrate and ammonia nitrogen under nitrate respiration, respectively [M L^{-3}]

$I[C_O]$ = The inhibition factor ($I[C_O]=\left[1+\frac{C_O}{K_c}\right]^{-1}$) [unitless]

K_c = The coefficient of inhibition [M L^{-3}]

Sierra and Renault (1998) measured dissolved oxygen (DO) in soils. A sample of which was classified as Gleyic Luvisol and the location was near Citeaus ($47^o09' N,\ 5^o05' E$) in the valley of the Sâone, in France. The concentration of DO relied upon soil moisture content, soil temperature, and the rate of microbial respiration. DO decreased, when moisture

content increased. It was observed that DO decreased from 1.19 to 0.56 mg/L (or 0.17 to 0.08 %) after a heavy rainfall (intensity 34 mm for 72 hours). During summer, DO of the topsoil (0.2 m below surface) was 2.5 times higher than in winter. A high population and activity of microbes was also found in summer. Evaporation increased during summer, and loss of moisture content induced an increase in DO. Averaged DO in all seasons at the depths of 0.2, 0.5, 0.75 and 1.5 m (below the surface) were 0.84, 0.53, 0.23 and 0 mg/L (or 0.12, 0.075, 0.033 and 0%), respectively.

DO in the soil was actually relatively low ($[C_O]$<0.5 mg/L). The value of K_C was 0.01-0.05 mg/L, and the possible inhibition factor $I[C_O]$ was 0.091 (Widdowson et al. 1988). High DO was sometimes found in a low temperature area. DO at a Cambridge site was 6.0 mg/L and the average temperature was 12 ^oC. On this site, K_C was 1.0 mg/L which provided a $I[C_O]$ of 0.143 (MacQuarrie et al. 2001). DO in this research was assumed to be 0.2-2.0 mg/L according to Widdowson et al. (1988). This is one third of the Cambridge site. The K_C was assumed to be 0.10-0.20 and the inhibition to be 0.05-0.5. The inhibition was weighed on the K_C at 0.175 and the inhibition factor was 0.0802. The nitrate respiration was 8 % of the total respiration.

Harvey et al. (1984) determined the kinetic coefficients for nitrifying and denitrifying bacteria. These coefficients are given in Table 3.5 (Wanner and Gujer 1986 and Benefield and Molz 1984, cited in Widdowson et al. 1988):

Table 3.5 Kinetic parameters for organic carbon and nitrate retardation

(Harvey et al. 1984 cited in Widdowson et al. 1988)

Parameter	Value	Parameter	Value
M_b (mg/cm^3)	5.65×10^{-4}	K_{SO} (mg/cm^3)	0.040
μ_O (1/day)	3.1	K_{SN} (mg/cm^3)	0.040
μ_N (1/day)	2.9	Ko (mg/cm^3)	0.00077
Y_o	0.45	K_N (mg/cm^3)	0.00260
Y_N	0.5	K_{AO}(mg/cm^3)	0.0010
k_o (1/day)	0.02	K_{AN} (mg/cm^3)	0.0010
k_N (1/day)	0.02		

The substrate and nitrate retardation could be arranged as follows (Widdowson et al. 1988):

$$\frac{\partial(C_S)}{\partial t} = \frac{M_b r_S}{\theta} \tag{3-21}$$

and

$$\frac{\partial(C_N)}{\partial t} = \frac{M_b r_N}{\theta} \tag{3-22}$$

where

M_b = Concentration of biomass per unit volume of porous media [M L^{-3}]

The production rate of biomass was not constant. The total biomass in the system could be assumed based on the difference between its production and decay rate as follows (Widdowson et al. 1988):

$$\frac{\partial M_b}{\partial t} = [(Y_S r_{SO} - k_O) + (Y_N r_{SN} - k_N I[C_O])]M_b \tag{3-23}$$

where

k_O and k_N = The microbial decay coefficient for aerobic, and nitrate respiration, respectively [T^{-1}]

Phosphorus compounds

Phosphorus adsorption was formulated as follows (Shah et al. 1975):

$$\rho_B \frac{\partial C_P^s}{\partial t} = K_t \left(C_P^w - C_P^{w*}\right) \tag{3-24}$$

where

C_P^s = The concentration of adsorbed phosphorus [M M^{-1}]

K_t = The overall volumetric mass transfer coefficient [L T^{-1}]

C_P^{w*} = The concentration of phosphorus in liquid phase that is in equilibrium with the concentration of phosphorus in the solid phase [M M^{-1}]

$(C_P^w - C_P^{w*})$ = A driving force for transferring phosphorus from liquid to solid phase [M L^{-3}]

The Langmuir isotherm equation was the best fit of phosphorus adsorption (Shah et al. 1975). Variable C_P^{w*} presented in Equation 3-24 was modified as follows (Schnoor 1996 and Watts 1997):

$$C_P^{w*} = \frac{k_L k_M C_P^w}{1 + k_M C_P^w} \tag{3-25}$$

where

k_L = The coefficient (Langmuir rate constant) [unitless]

k_M = The maximum phosphate adsorption capacity on soil [L^3 M^{-1}]

Faecal coliforms

The overall reaction rates of microbial kinetics were the summation of production, maintenance, decay, adsorption and desorption. The retardation equation was given as (Zysset et al. 1994):

$$n\frac{d(C_b^f)}{dt} = n\nu_y \eta k_\mu C_S C_b^f - nk_d C_b^f + \theta k_c C_b^w - nk_s C_b^f \tag{3-26}$$

where

n = The fraction of aqueous volume and biofilm in total volume (= porosity) [unitless]

C_b^f = The concentration of adhering microbes [M L^{-3}]

C_b^w = The concentration of free swimming microbes [M L^{-3}]

C_S = The concentration of limiting substrate in aqueous compartment [N L^{-3}]

ν_y = The stoichiometric coefficient [M N^{-1}]

η = An effectiveness of biofilm [unitless]

k_μ = Monod's constant for substrate utilisation in biomass [$L^3 M^{-1} T^{-1}$]

k_d = The constant the decay rate [T^{-1}]

k_s and k_c = The constant desorption (detachment) and adsorption (attachment) rate, respectively [T^{-1}]

The unit N is the quantity of microbes involved.

The equilibrium of immobile and mobile *E.Coli* was given as follows (Zysset et al. 1994 and Stevik et al. 1999b):

$$C_b^w \rightarrow C_b^f \tag{3-27}$$

Equation 3-27 could be developed as a first order kinetics equation as follows (Characklis et al. 1990).

$$\frac{\partial C_b^f}{\partial t} = k_B \theta \cdot C_b^w \tag{3-28}$$

where

k_B = An overall rate constant of bacterial removal processes in biological filter systems (including adsorption; k_c and desorption rate; k_s) [T^{-1}]

Using the initial kinetic rate, Equation (3-28) was simplified as follows (Stevik et al. 1999b):

$$\left(C_b^w\right)_z = \left(C_b^w\right)_o e^{-k_B t} \tag{3-29}$$

where

$\left(C_b^w\right)_o$ = *E.Coli* concentration in wastewater at the filter surface [$N L^{-3}$]

$\left(C_b^w\right)_z$ = *E.Coli* concentration at depth z [$N L^{-3}$]

t = Time for wastewater flows down to depth z

Stevik et al. (1999a) has conducted column experiments to study the effects of physical and chemical properties of filter media on the removal of *E.Coli* and their results are presented in Figure 3.7, which had an overall kinetics rate constant; k_B of 0.105 hour^{-1} (2.52 day^{-1}) with the initial concentration; $\left(C_b^w\right)_o$ of 3.4833x10^8 cfu/100mL. The authors had defined the constant k_B as overall *E.Coli* removal. This might not be correct because the columns were kept in dark and cool (temperature 7±1 ^{o}C) conditions that certainly would have minimised the growth of *E.Coli*. Schnoor (1996) reported the kinetic coefficient for decay of coliforms in a river (fresh water) was 0.5-5 day^{-1}.

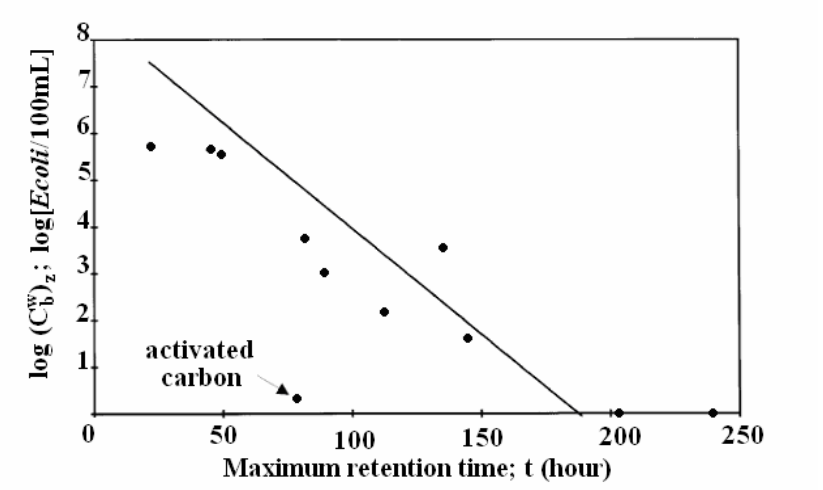

Figure 3.7 *E.Coli* concentration verus minimum wastewater retention time (Stevik et al. 1999b)

Schijven et al. (2002) determined the kinetic coefficients of viruses in aquifers using two types of bacteriophages MS2 and PRD1. The applied dosages were 2.5x10^{12} and 2.5x10^{13} cfu/100mL, respectively. The kinetics coefficients were calculated using data taken from six observation wells. The results are given in Table 3.6.

Table 3.6 Kinetic coefficients of bacteriophages MS2 and PRD1 (Schijven et al. 2002)

Bacterio-phage	Parameter	Unit	Well						Average kinetic coefficient
			W1	W2	W3	W4	W5	W6	
MS2	k_c	1/day	4.1	3.2	2.8	2.0	1.3	0.8	**2.367**
	k_s	1/day	0.00087	0.0016	0.0026	0.0018	0.00052	0.0030	**0.0017**
	k_g	1/day	0.03	0.03	0.03	0.03	0.03	0.03	**0.03**
	k_d	1/day	0.085	0.092	0.092	0.092	0.092	0.092	**0.092**
PRD1	k_c	1/day	4.0	3.1	2.2	1.5	1.3	0.7	**2.133**
	k_s	1/day	0.00077	0.0011	0.0018	0.0025	0.0021	0.0034	**0.0019**
	k_g	1/day	0.12	0.12	0.12	0.12	0.12	0.12	**0.12**
	k_d	1/day	0.071	0.067	0.067	0.067	0.067	0.067	**0.068**

Note: k_g was the kinetic growth rate.

Average MS2 and PRD1 kinetic decay rates were 0.092 and 0.068 day^{-1}, respectively. These rates were much lower than the *E.Coli* decay rates observed in a river. The average kinetic adsorption rates of MS2 and PRD1 were approximately 2.37 and 2.13 day^{-1}, respectively. By comparison, the adsorption rate is much higher than the kinetic decay rate. Thus, the sorption process plays a significant role in the microbial retardation. The adsorption rates of these bacteriophages are also closer to the kinetic filtration rate of *E.Coli* proposed by Stevik et al. (1999b).

3.5 Summary

A conceptual model was developed to predict all the known processes for transport and retardation of contaminants. Firstly, the transport processes were driven by advection and dispersion mechanisms. Secondly, the majority of retardations were investigated in the unsaturated zone. Organic carbon and nitrate nitrogen compounds could be retarded by biotransformation under aerobic and/or anoxic conditions. Phosphate could be adsorbed onto the soil minerals. *E.Coli* could be filtered, adsorbed and decayed through the porous media.

The available commercial and other research models reviewed were widely used to predict the fate of contaminants in either the unsaturated or saturated zones. However, none of these models satisfactorily suited for the transport of contaminants of septic effluent under unsaturated soil. This has lead to the development of the present conceptual model. The related equations for transport and retardation were reviewed from current theories and they were used in the developing of this conceptual model. Transport due to advection-dispersion was described using Richards' equation. Retardations were described using multiplicative Monod's equations for aerobic and nitrate respiration, the Langmuir adsorption isotherm for phosphorus sorption, and adsorption and first order decay for *E.Coli.*

The mathematical model was further developed by modifying these governing equations, and then it was solved using numerical techniques. The numerical model was coded using the MATLAB programme. Details of the development of the mathematical and the numerical solution will be presented in the next chapter.

CHAPTER 4

DEVELOPMENT OF MATHEMATICAL AND NUMERICAL MODELS

4.1 Introduction

The processes for development of mathematical and numerical models for contaminant transport coupling retardation are described in this chapter. A mathematical model was obtained by modifying the governing equations presented in the previous chapter. The mathematical model contained a system of a non-linear hyperbolic/parabolic partial differential equations (PDE). The model was found to be very complex and exact solutions could not be obtained. Therefore, a numerical approach was used to evaluate approximate solutions for the mathematical model.

Galerkin's finite element method (FEM) and Green's theorem were applied to convert the PDE contained in the mathematical model to an ordinary differential equation (ODE). Various initial and boundary conditions were defined to solve the numerical model. The schematic of the iteration process was yielded using a single Picards' iteration technique. The numerical model was coded using the MATLAB programme.

4.2 Development of a mathematical model

A mathematical model for contaminants transport and retardation was derived by substituting the governing equations presented in previous chapter into the mass balance equation (Equation 3-1) (Kirkner and Reeves 1988, Reeves and Kirkner 1988, Fetter 1992 and Schnoor 1996). The derivation of the mathematical model of each contaminant is shown in the following sections.

4.2.1 Nitrogen and organic carbon compounds

By referring to the rate of kinetic reaction (Equation 3-21) for organic carbon compounds biodegradation, the equation for transport of organic carbon compounds is written as follows:

$$\frac{\partial C_S}{\partial t} = -\frac{\partial}{\partial z}(q_z C_S) + \frac{\partial}{\partial z}\left(D_z \frac{\partial C_S}{\partial z}\right) - M_b \frac{\mu_O}{Y_O}\left[\frac{C_S}{K_{SO}+C_S}\right]\left[\frac{C_O}{K_O+C_O}\right]\left[\frac{C_A}{K_{AO}+C_A}\right] \quad (4\text{-}1)$$

One simulation case considered the ammonia nitrogen was excessive so $\left[\frac{C_A}{K_{AO}+C_A}\right]$ became 1.0. Dissolved oxygen (DO) in the system was held constant at 2.0 mg/L, thus $\left[\frac{C_O}{K_O+C_O}\right]$ becomes constant. The organic carbon compound concentration, C_S (0.226 mg/cm^3) was much greater than half the maximum rate of substrate concentration, K_{SO} (0.040 mg/cm^3). This led to a pseudo first order equation by assuming $K_{SO}+C_S \approx C_S$ (Widdowson et al. 1988). Then, Equation 4-1 could be simplified as follows:

$$\frac{\partial C_S}{\partial t} = -\frac{\partial}{\partial z}(q_z C_S) + \frac{\partial}{\partial z}\left(D_z \frac{\partial C_S}{\partial z}\right) - M_b \lambda_S C_S \quad (4\text{-}2)$$

where

λ_S = A constant corresponding to $\frac{\mu_O}{Y_O}\left[\frac{C_O}{K_O+C_O}\right].\left[\frac{C_A}{K_{AO}+C_A}\right]$

Based on a macroscopic mass balance, the aqueous-phase microbial concentration equaled the volumetric moisture content (Zysset et al. 1994). Equation 4-2 could be modified as follows:

$$\frac{\partial C_S}{\partial t} = -\frac{\partial}{\partial z}(q_z C_S) + \frac{\partial}{\partial z}\left(D_z \frac{\partial C_S}{\partial z}\right) - \theta \lambda_S C_S \quad (4\text{-}3)$$

Referring to the rate of nitrate consumption (Equation 3-22), the nitrate transport equation can be formulated as follows:

$$\frac{\partial C_N}{\partial t} = -\frac{\partial}{\partial z}(q_z C_N) + \frac{\partial}{\partial z}\left(D_z \frac{\partial C_N}{\partial z}\right) - M_b \frac{\mu_N}{Y_N}\left[\frac{C_S}{K_{SN}+C_S}\right]\left[\frac{C_N}{K_N+C_N}\right]\left[\frac{C_A}{K_{AN}+C_A}\right] I[C_O] \qquad (4\text{-}4)$$

The half saturation concentrations of substrate, K_{SN}, nitrate, K_N and ammonia, K_{AN} utilisation under nitrate respiration were too small (0.040, 0.003 and 0.001 mg/cm^3, respectively) when compared with concentrations of substrate and ammonia (0.226 and 1.0 mg/L, respectively). So, terms $\left[\frac{C_S}{K_{SN}+C_S}\right]$, $\left[\frac{C_N}{K_N+C_N}\right]$ and $\left[\frac{C_A}{K_{AN}+C_A}\right]$ became pseudo first order kinetic. The kinetic term for ammonium retardation was closer to 1.0 (Widdowson et al. 1988). Equation 4-4 could be simplified as:

$$\frac{\partial C_N}{\partial t} = -\frac{\partial}{\partial z}(q_z C_N) + \frac{\partial}{\partial z}\left(D_z \frac{\partial C_N}{\partial z}\right) - M_b C_S C_N \lambda_N \qquad (4\text{-}5)$$

where

λ_N = A constant term relating to $\frac{\mu_N}{Y_N}\left[\frac{C_A}{K_{AO}+C_A}\right] I[C_O]$

Based on the macroscopic microbial population balance (Zysset et al. 1994), the nitrate transport was simplified as follows.

$$\frac{\partial C_N}{\partial t} = -\frac{\partial}{\partial z}(q_z C_N) + \frac{\partial}{\partial z}\left(D_z \frac{\partial C_N}{\partial z}\right) - \lambda_N \theta C_S C_N \qquad (4\text{-}6)$$

4.2.2 Phosphorus compounds

According to the phosphorus retardation (Equation 3-24 and 3-25), the kinetic equation was obtained as follows:

$$\frac{\partial C_P^{w*}}{\partial t} = \frac{k_L k_M \frac{\partial C_P^w}{\partial t}}{\left(1 + k_M C_P^w\right)^2} \tag{4-7}$$

Substituting Equation 4-7 into Equation 3-1 provided the following:

$$\left(1 + \frac{\rho_B k_L k_M}{\theta\left(1 + k_M C_P^w\right)^2}\right)\frac{\partial C_P^w}{\partial t} = -\frac{\partial}{\partial z}\left(q_z C_P^w\right) + \frac{\partial}{\partial z}\left(D_z \frac{\partial C_P^w}{\partial z}\right) \tag{4-8}$$

The distribution coefficient, K_d was defined as follows:

$$K_d = \frac{k_L k_M}{\left(1 + k_M C_P^w\right)^2} \tag{4-9}$$

The first term of Equation 4-8 was defined as the retardation factor κ and yielded:

$$\kappa = 1 + \frac{\rho_B K_d}{\theta} \tag{4-10}$$

Phosphate could be divided into immobile and mobile phases (Shah et al. 1975). The soluble phosphate, C_P could be assumed as a volumetric portion of moisture (Fetter 1992). The transport of phosphate was obtained as follows:

$$\frac{\partial(\theta \kappa C_P)}{\partial t} = -\frac{\partial}{\partial z}\left(q_z C_P\right) + \frac{\partial}{\partial z}\left(D_z \frac{\partial C_P}{\partial z}\right) \tag{4-11}$$

4.2.3 *E.Coli*

Refer to Equation 3-28, the concentration of *E.Coli* related to the substrates consumed. Substrate utilisation during metabolisation processes was defined using the first order Monod's kinetics equation as follows (Zysset et al. 1994).

$$\frac{\partial C_S}{\partial t} = -\frac{\mu_b}{Y_b}\left[\frac{C_S}{K_{Sb} + C_S}\right] \cdot C_b^t - k_m C_b^t \tag{4-12}$$

where

C_S = The carbonaceous substrate concentration [M L^{-3}]

C_b^t = The total microbial concentration [M L^{-3}]

μ_b = The microbial maximum specific growth rate [T^{-1}]

Y_b = A heterotrophic microbial yield coefficient [unitless]

C_s = The substrate concentration [M L^{-3}]

K_{Sb} = The substrate concentration when the rate of utilisation is half the maximum rate under aerobic condition [M L^{-3}]

k_m = A biomass maintenance rate [T^{-1}]

Production of new biomass and maintenance of existing cells were presented on the right side as the first and second terms of Equation 4-12, respectively. The substrate concentration, C_S was too small when compared to the concentration of half the maximum substrate utilization, K_{Sb}. Hence, a pseudo first order kinetic equation was generated as follows (Zysset et al. 1994):

$$\frac{\partial C_S}{\partial t} = -k_\mu C_S C_b^t - k_m C_b^t \tag{4-13}$$

where

$$k_\mu = \frac{\mu_b}{Y_b}$$

By substituting Equation 4-13 into Equation 3-1, the substrates consumed by *E.Coli* was formulated as follows:

$$\frac{\partial C_S}{\partial t} = \frac{\partial}{\partial z}\left(D_z \frac{\partial C_S}{\partial t} \right) - \frac{\partial}{\partial z}(q_z C_S) - \theta \lambda_S C_S \tag{4-14}$$

where

$$\lambda_S = \frac{\partial C_S}{\partial t}$$

Based on the mass balance equation, the concentration of *E.Coli* may equal to the concentration of substrate that they consumed. Therefore, the *E.Coli* transport equation was governed as follows:

$$\frac{\partial(\kappa\theta C_b)}{\partial t} = \frac{\partial}{\partial z}\left(D_z \frac{\partial C_b}{\partial z}\right) - \frac{\partial}{\partial z}(q_z C_b) - \lambda_b \theta \kappa C_b \tag{4-15}$$

where

$\kappa = 1 + \frac{\rho_B k_B}{\theta}$;

$\lambda_b = (k_\mu - k_m) \cdot C_b^t$; and

$C_b^t = \kappa C_b$

A general form of the mathematical model for contaminant transport coupling retardations could be written as follows (Huyakorn et al. 1985):

$$\underset{(dispersion)}{\frac{\partial}{\partial z}\left(D_z \frac{\partial C}{\partial z}\right)} \quad \underset{(advection)}{-\frac{\partial}{\partial z}(q_z C)} \quad = \quad \underset{(accumulation)}{\frac{\partial}{\partial t}(\theta \kappa C)} \quad + \quad \underset{\left(1^{st} order \quad decay\right)}{\lambda \theta \kappa C} \tag{4-16}$$

The retardation factor, κ equals 1.0 for organic carbon and nitrate compound transport equations. The biodecay factor, λ equals 0.0 for phosphate compounds transport equation. Only microbial transport contains all of these factors. The advection term in Equation 4-16 contained two independent variables, q_z and C. The differentiation of the product of $q_z \cdot C$ yields:

$$\frac{\partial}{\partial z}(q_z C) = C \frac{\partial q_z}{\partial z} + q_z \frac{\partial C}{\partial z} \tag{4-17}$$

The derivation of Darcy's velocity over distance presented in Equation 4-17 was defined using the continuity equation as follows (Huyakorn et al. 1985):

$$-\frac{\partial q_z}{\partial z} = \frac{\partial \theta}{\partial t} \tag{4-18}$$

The continuity equation when placed into Equation 4-17, yielded:

$$\frac{\partial}{\partial z}(q_z C) = C\frac{\partial \theta}{\partial z} + q_z \frac{\partial C}{\partial t} \tag{4-19}$$

Accumulation term $\frac{\partial}{\partial t}(\theta\kappa C)$ presented in Equation 4-16 could be expressed as:

$$\frac{\partial}{\partial t}(\theta\kappa C) = \kappa C\frac{\partial \theta}{\partial t} + \theta\kappa\frac{\partial C}{\partial t} + \theta C\frac{\partial \kappa}{\partial t} \tag{4-20}$$

Referring to $\kappa = 1 + \frac{\rho_B K_d}{\theta}$, the time derivative was derived as follows:

$$\frac{\partial \kappa}{\partial t} = \frac{\theta\frac{\partial(\rho_B K_d)}{\partial t} - \rho_B K_d \frac{\partial \theta}{\partial t}}{\theta^2} \tag{4-21}$$

Substituting Equations 4-19, 4-20 and 4-21 into Equation 4-16, result in:

$$\frac{\partial(\theta\kappa C)}{\partial t} = C\left[\kappa - \frac{\rho_B K_d}{\theta}\right]\frac{\partial \theta}{\partial t} + \theta\kappa\frac{\partial C}{\partial t} + C\frac{\partial(\rho_B K_d)}{\partial t} \tag{4-22}$$

By definition, $\kappa - \frac{\rho_B K_d}{\phi\theta} = 1$, the first term on right side of Equation 4-22 could be simplified as follows:

$$\frac{\partial(\theta\kappa C)}{\partial t} = C\frac{\partial \theta}{\partial t} + \theta\kappa\frac{\partial C}{\partial t} + C\frac{\partial(\rho_B K_d)}{\partial t} \tag{4-23}$$

Assuming that $\frac{\partial(\rho_B K_d)}{\partial t}$ was negligible (Huyakorn et al. 1985), the last term on Equation 4-23 could be simplified as follows:

$$\frac{\partial(\theta\kappa C)}{\partial t} = C\frac{\partial \theta}{\partial t} + \theta\kappa\frac{\partial C}{\partial t} \tag{4-24}$$

Substituting Equation 4-24 into 4-16, and obtained:

$$\frac{\partial}{\partial z}\left(D_z \frac{\partial C}{\partial z}\right) - q_z \frac{\partial C}{\partial z} = \theta\kappa\left[\frac{\partial C}{\partial t} + \lambda C\right] \tag{4-25}$$

The governing mathematical model was a non-linear parabolic-hyperbolic PDE. It cannot be solved by simple techniques and an exact solution would be difficult to obtain. There are two ways to solve this model including the Laplace transform and a numerical approach. If there was no retardation and biodecay ($\kappa = 1.0$ and $\lambda = 0.0$) in the considered system, the analytical results could be obtained using Laplace transforms (Nützmann et al. 2002). The analytical solutions of the non-reactive contaminant transport in unsaturated soil with various boundary conditions are given in Appendix-A. However, the developed model contained the retardation term that could not be solved using Laplace transforms. The model was solved using a numerical approach.

4.3 Development of a numerical model

A numerical approach was applied to estimate approximate solutions of this proposed model. The processes of development of a numerical model are presented in the following sections.

4.3.1 Contaminant transport in variably saturated soil conditions

Applying Galerkin's finite element method, the concentration of each constituent at each element could be obtained as the product of the nodal concentration at time "t"and the shape function "N_j". The approximate solution was defined as follows (Segerlind 1984, Huyakorn et al. 1985 and Clement et al. 1998):

$$C(z,t) = \sum_{j=1}^{m} N_j(z) C_j(t) \tag{4-26}$$

where

$N_j(z)$ = The shape function [unitless]

$C_j(t)$ = The values of elemental concentration at time t [M L^{-3}]

The finite difference discretionary scheme is presented in Figure 4.1. The number of nodes in the system was assigned sequentially to the flow direction. It started from the column surface and ended at the column base. The datum was located at the column base.

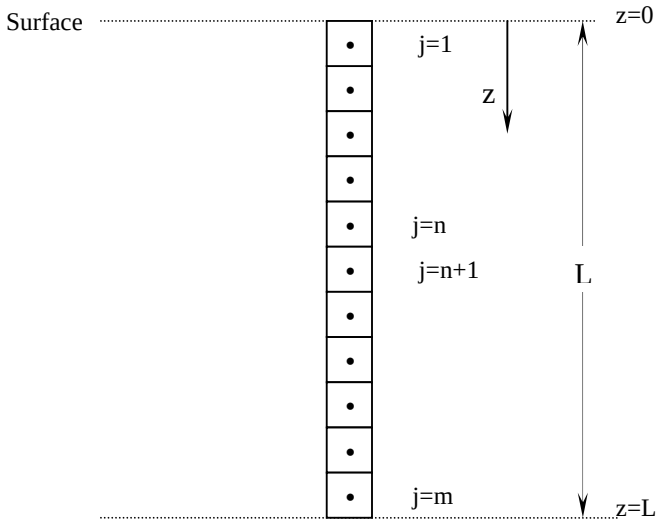

Figure 4.1 Scheme of finite discretion

The mathematical model presented in Equation 4-25 could be modified as follows:

$$L[C]=\frac{\partial}{\partial z}\left(D_z\frac{\partial C}{\partial z}\right)-q_z\frac{\partial C}{\partial z}-\theta\kappa\left[\frac{\partial C}{\partial t}+\lambda C\right] \tag{4-27}$$

The weighting function, N_i was added into the integration form as follows:

$$\int_{z=0}^{z=L} N_i L[C]dz = 0 \tag{4-28}$$

where

$[0, L]$ = The extent of the vertical direction (one dimension) domain

The subscript "i" denoted the sequent of element in the domain, it flowed as same as the subscript "j" presented in Figure 4.1.

Equation 4-27 was substituted into Equation 4-28, and Equation 4-29 was obtained:

$$\int_{z=0}^{z=L} N_i\frac{\partial}{\partial z}\left(D_z\frac{\partial C}{\partial z}\right)dz-\int_{z=0}^{z=L} N_i q_z\frac{\partial C}{\partial z}dz-\int_{z=0}^{z=L} N_i\theta\kappa\left[\frac{\partial C}{\partial t}+\lambda C\right]dz=0 \tag{4-29}$$

The first derivative term in Equation 4-29 was yielded as follows:

$$\int_{z=0}^{z=L} N_i \frac{\partial}{\partial z}\left(D_z \frac{\partial C}{\partial z}\right)dz = \int_{z=0}^{z=L} N_i D_z \frac{\partial^2 C}{\partial z^2}dz + \int_{z=0}^{z=L} N_i \left(\frac{\partial D_z}{\partial z}\right)\left(\frac{\partial C}{\partial z}\right)dz \tag{4-30}$$

Green's theorem (bypass integral technique) was applied to the second derivative term of Equation 4-29. Term U and dV were established as follows:

$$\textit{Bypass integral formulation}: \int_{z=0}^{z=L} UdV = UV\Big|_{z=0}^{z=L} - \int_{z=0}^{z=L} VdU \tag{4-31}$$

$$U = N_i \frac{\partial C}{dz} \qquad dU = \left[N_i \frac{\partial^2 C}{\partial z^2} + \left(\frac{\partial C}{\partial z}\right)\left(\frac{\partial N_i}{\partial z}\right)\right]dz$$

$$dV = \frac{\partial D_z}{\partial z}dz \qquad V = D_z$$

These integral functions were formatted as follows:

$$\int_{z=0}^{z=L} N_i \left(\frac{\partial D_z}{\partial z}\right)\left(\frac{\partial C}{\partial z}\right)dz = N_i D_z \left(\frac{\partial C}{\partial z}\right)\Big|_{z=0}^{z=L} - \int_{z=0}^{z=L} N_i D_z \frac{\partial^2 C}{\partial z^2}dz - \int_{z=0}^{z=L} D_z \left(\frac{\partial C}{\partial z}\right)\left(\frac{\partial N_i}{\partial z}\right)dz \tag{4-32}$$

Substituting Equations 4-30 and 4-32 into Equation 4-29 yields:

$$N_i D_z \left(\frac{\partial C}{\partial z}\right)\Big|_{z=0}^{z=L} - \int_{z=0}^{z=L} D_z \left(\frac{\partial C}{\partial z}\right)\left(\frac{\partial N_i}{\partial z}\right)dz - \int_{z=0}^{z=L} N_i q_z \frac{\partial C}{\partial z}dz - \int_{z=0}^{z=L} N_i \theta\kappa\left[\frac{\partial C}{\partial t} + \lambda C\right]dz = 0 \tag{4-33}$$

By referring to the approximate solution (Equation 4-26), the time and space derivatives of concentration were derived as follows:

$$\frac{\partial C}{\partial t} = N_j \frac{\partial C_j}{\partial z}$$
$$\frac{\partial C}{\partial z} = C_j \frac{\partial N_j}{\partial z} \tag{4-34}$$

These derivatives were replaced into Equation 4-33:

$$\int_{z=0}^{z=L}\left(D_z\frac{\partial N_i}{\partial z}\frac{\partial N_j}{\partial z}+N_i\frac{\partial N_j}{\partial z}q_z\right)C_j dz+\int_{z=0}^{z=L}N_iN_j\theta\kappa\left[\frac{\partial C_j}{\partial t}+\lambda C_j\right]dz-N_iD_z\left(\frac{\partial C}{\partial z}\right)\Bigg|_{z=0}^{z=L}=0 \tag{4-35}$$

Equation 4-35 was reformed to an ordinary differential equation (ODE), and the algebraic matrix systems were defined as follows:

$$\{[P_{ij}]+[R_{ij}]\}C_j+[Q_{ij}]\frac{\partial C_j}{\partial t}=\{S_i\} \tag{4-36}$$

where

$$[P_{ij}]=\sum_e\int_{z=0}^{z=L}\left(D_z\frac{\partial N_i}{\partial z}\frac{\partial N_j}{\partial z}+N_i\frac{\partial N_j}{\partial z}q_z\right)dz;$$

$$[Q_{ij}]=\sum_e\int_{z=0}^{z=L}N_iN_j\theta\kappa dz;$$

$$[R_{ij}]=\sum_e\int_{z=0}^{z=L}N_iN_j\theta\kappa\lambda dz;\ \ and$$

$$\{S_i\}=N_iD_z\left(\frac{\partial C}{\partial z}\right)\Bigg|_{z=0}^{z=L}$$

4.3.2 Richards' equation

The approximate solution of Richards' equation was assumed as follows (Wang and Anderson 1982, Coley 1983, Segerlind 1984 and Paniconi et al.1991):

$$\psi(z,t)=\sum_{j=1}^{m}N_j(z)\psi_j(t) \tag{4-37}$$

where

$N_j(z)$ = The specified basis functions [unitless]

$\psi_j(t)$ = The unknown coefficients with corresponding to the value of nodal pressure head [L]

The subscript "j" is defined to denote a nodal sequence.

The sequence of the nodal concentrations was arranged in a similar manner as the nodal concentration given in Figure 4-1. Richards' equation was written in a form of $L[\psi]=0$ as follows.

$$L[\psi]=M_C\frac{\partial\psi}{\partial t}-\frac{\partial}{\partial z}\left[K_{zz}k_{rw}\left(\frac{\partial\psi}{\partial z}+1\right)\right] \tag{4-38}$$

The approximate solutions were evaluated using Galerkin's finite element method. The integral formed was given as follows:

$$\int_{z=0}^{z=L} L[\psi]N_i\,dz=0 \tag{4-39}$$

Substitute Equation 4-38 into Equation 4-39, and yielded:

$$\int_{z=0}^{z=L} N_i M_C\frac{\partial\psi}{\partial t}dz-\int_{z=0}^{z=L} N_i\left[K_{zz}k_{rw}\left(\frac{\partial\psi}{\partial z}+1\right)\right]dz=0 \tag{4-40}$$

The second term of Equation 4-40 could be arranged as follows:

$$\frac{\partial}{\partial z}\left[K_{zz}k_{rw}\left(\frac{\partial\psi}{\partial z}+1\right)\right]=K_{zz}k_{rw}\frac{\partial^2\psi}{\partial z^2}+\left(\frac{\partial\psi}{\partial z}\right)\left(\frac{\partial K_{zz}k_{rw}}{\partial z}\right)+\frac{\partial K_{zz}k_{rw}}{\partial z} \tag{4-41}$$

Equation 4-41 was substituted into Equation 4-40, and obtained:

$$\int_{z=0}^{z=L} N_i M_C\frac{\partial\psi}{\partial t}dz-\int_{z=0}^{z=L} N_i K_{zz}k_{rw}\frac{\partial^2\psi}{\partial z^2}dz-\int_{z=0}^{z=L} N_i\left(\frac{\partial\psi}{\partial z}\right)\left(\frac{\partial K_{zz}k_{rw}}{\partial z}\right)dz-\int_{z=0}^{z=L} N_i\frac{\partial K_{zz}k_{rw}}{\partial z}dz=0 \tag{4-42}$$

Applying bypass integrating technique to the third and the fourth term presented in Equation 4-42 provides:

$$U=N_i\left(\frac{\partial\psi}{\partial z}\right) \qquad dU=\left[\left(\frac{\partial N_i}{\partial z}\frac{\partial\psi}{\partial z}\right)+N_i\frac{\partial^2\psi}{\partial z^2}\right]dz$$

$$dV=\frac{\partial K_{zz}k_{rw}}{\partial z}dz \qquad V=K_{zz}k_{rw}$$

So;

$$\int_{z=0}^{z=L} N_i\left(\frac{\partial \psi}{\partial z}\right)\left(\frac{\partial K_{zz}k_{rw}}{\partial z}\right)dz = N_i K_{zz}k_{rw}\left(\frac{\partial \psi}{\partial z}\right)\Big|_{z=0}^{z=L} - \int_{z=0}^{z=L} K_{zz}k_{rw}\left(\frac{\partial \psi}{\partial z}\frac{\partial N_i}{\partial z}\right)dz$$
$$- \int_{z=0}^{z=L} N_i K_{zz}k_{rw}\frac{\partial^2 \psi}{\partial z}dz \qquad (4\text{-}43)$$

and

$$U = N_i \qquad dU = \frac{\partial N_i}{\partial z}dz$$
$$dV = \frac{\partial K_{zz}k_{rw}}{\partial z}dz \qquad V = K_{zz}k_{rw}$$

So too;

$$\int_{z=0}^{z=L} N_i \frac{\partial K_{zz}k_{rw}}{\partial z}dz = N_i K_{zz}k_{rw}\Big|_{z=0}^{z=L} - \int_{z=0}^{z=L} K_{zz}k_{rw}\frac{\partial N_i}{\partial z}dz \qquad (4\text{-}44)$$

Equations 4-43 and 4-44 were placed into 4-42 to provide:

$$\int_{z=0}^{z=L} N_i M_C \frac{\partial \psi}{\partial t}dz - N_i K_{zz}k_{rw}\left(\frac{\partial \psi}{\partial z}+1\right)\Big|_{z=0}^{z=L} + \int_{z=0}^{z=L} K_{zz}k_{rw}\left(\frac{\partial \psi}{\partial z}\frac{\partial N_i}{\partial z}\right)dz + \int_{z=0}^{z=L} K_{zz}k_{rw}\frac{\partial N_i}{\partial z}dz = 0 \qquad (4\text{-}45)$$

Referring to the approximate solution (Equation 4-36), where time and space derivatives of ψ were expressed as follows:

$$\frac{\partial \psi}{\partial t} = N_j \frac{\partial \psi_j}{\partial t}$$
$$\frac{\partial \psi}{\partial z} = \psi_j \frac{\partial N_j}{\partial z} \qquad (4\text{-}46)$$

Equation 4-46 was substituted into Equation 4-45, the numerical solution of Richards' equation was yielded as follows:

$$\int_{z=0}^{z=L} N_i M_C \frac{\partial \psi_j}{\partial t} dz - N_i K_{zz} k_{rw} \left(\frac{\partial \psi}{\partial z} + 1 \right) \Bigg|_{z=0}^{z=L} + \int_{z=0}^{z=L} K_{zz} k_{rw} \psi_j \left(\frac{\partial N_i}{\partial z} \frac{\partial N_j}{\partial z} \right) dz + \int_{z=0}^{z=L} K_{zz} k_{rw} \frac{\partial N_i}{\partial z} dz = 0 \quad (4\text{-}47)$$

Equation 4-47 was converted to an ODE, and the algebraic matrix systems were defined as follows:

$$\left[A_{ij} \right] \psi_j + \left[B_{ij} \right] \frac{\partial \psi_j}{\partial t} = \{ E_i \} \quad (4\text{-}48)$$

where

$$\left[A_{ij} \right] = \sum_e \int_{z=0}^{z=L} K_{zz} k_{rw} \left(\frac{\partial N_i}{\partial z} \frac{\partial N_j}{\partial z} \right) dz;$$

$$\left[B_{ij} \right] = \sum_e \int_{z=0}^{z=L} N_i N_j M_C dz; \quad \textit{and}$$

$$\{ E_i \} = N_i K_{zz} k_{rw} \left(\frac{\partial \psi}{\partial z} + 1 \right) \Bigg|_{z=0}^{z=L} - \sum_e \int_{z=0}^{z=L} K_{zz} k_{rw} \frac{\partial N_i}{\partial z} dz$$

The vector matrix $\{E_i\}$ could be written in a form of Darcy's flux boundary condition as follows:

$$\{ E_i \} = -N_i q_z \Big|_{z=0}^{z=L} - \sum_e \int_{z=0}^{z=L} K_{zz} k_{rw} \frac{\partial N_i}{\partial z} dz \quad (4\text{-}49)$$

The stiffness matrices presented in these numerical solutions must be interpolated using interpolation functions. These functions were derived in the following section.

4.4 Element interpolation functions

One element contained two nodes, one on the top (Node 1), and the other at the base (Node 2). The shape of the element interpolation function was a linear function as shown in Figure 4.2. The linear interpolation function, $f(z)$ contained two constants; a_1, and a_2. The constant a_1 was defined as the interception of the function and constant

a_2 referred to as the slope of the interpolation function. The linear interpolation function was given as follows (Segerlind 1984):

$$f(z) = a_1 + a_2 z \tag{4-50}$$

where

a_1 and a_2 = The constants which could be evaluated from the point elements

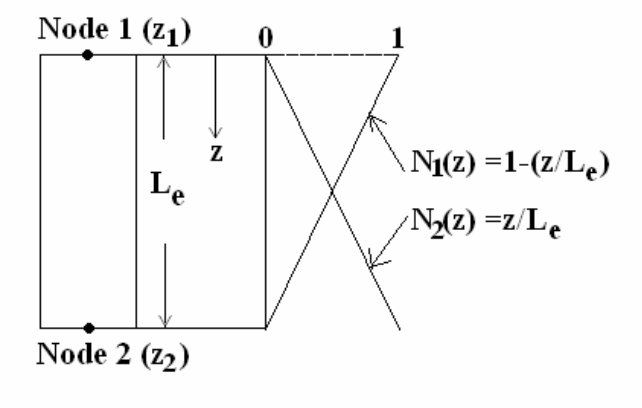

Figure 4.2 Element interpolation function (Segerlind 1984)

The linear interpolation between these two nodes could be simplified as follows (Segerlind 1984):

$$f(z_1) = a_1 + a_2 z_1 \tag{4-51a}$$

and

$$f(z_2) = a_1 + a_2 z_2 \tag{4-51b}$$

where

z_1 and z_2 = The coordination on z-axis

The element interpolation functions, $f(z_1)$ and $f(z_2)$ were modified to be a matrix of the constraints, as follows (Segerlind 1984):

$$\begin{Bmatrix} f(z_1) \\ f(z_2) \end{Bmatrix} = \begin{bmatrix} 1 & z_1 \\ 1 & z_2 \end{bmatrix} \begin{Bmatrix} a_1 \\ a_2 \end{Bmatrix} \tag{4-52}$$

The coefficient a_1 and a_2 was obtained by matrix inversion as follows (Segerlind 1984):

$$\begin{Bmatrix} a_1 \\ a_2 \end{Bmatrix} = \frac{1}{L_e}\begin{bmatrix} z_2 & -z_1 \\ -1 & 1 \end{bmatrix}\begin{Bmatrix} f(z_1) \\ f(z_2) \end{Bmatrix} \tag{4-53}$$

where

L_e = The length of a small element that was measured from upper node to lower node; ($= z_2 - z_1$); [L]

The constraints, a_1 and a_2 were substituted into Equation 4-50. The linear interpolation function, $f(z)$ could now be rewritten as follows (Segerlind 1984).

$$f(z) = \frac{1}{L_e}(z_2 - z)f(z_1) + \frac{1}{L_e}(z - z_1)f(z_2) \tag{4-54}$$

The linear interpolation function was also modified to produce the simple element shape function as (Segerlind 1984):

$$f(z) = N_1^e f(z_1) + N_2^e f(z_2) \tag{4-55}$$

The shape functions at the upper (Node1) and lower node (Node 2) could be written as (Segerlind 1984):

$$N_1^e = \frac{1}{L_e}(z_2 - z), \quad N_2^e = \frac{1}{L_e}(z - z_1) \quad \text{for } z_1 \leq z \leq z_2 \tag{4-56a}$$

or

$$N_1^e = 1 - \frac{z}{L_e}, \quad N_2^e = \frac{z}{L_e} \quad \text{where } z_1 = 0 \text{ and } z_2 = 1 \tag{4-56b}$$

The derivative of these shape functions over an element length could be derived as (Segerlind 1984):

$$\frac{dN_1^e}{dz} = -\frac{1}{L_e}, \quad \frac{dN_2^e}{dz} = \frac{1}{L_e} \tag{4-57}$$

The nodal differentiated terms with respect to z for a one-dimensional element (Equations 4-56 and 4-57) were applied to derive the stiffness matrices. The element interpolation functions were yielded as follows.

$$\int_{z=0}^{z=L}\begin{bmatrix}\frac{\partial N_i}{\partial z}\frac{\partial N_j}{\partial z} & \frac{\partial N_i}{\partial z}\frac{\partial N_j}{\partial z}\\ \frac{\partial N_i}{\partial z}\frac{\partial N_j}{\partial z} & \frac{\partial N_i}{\partial z}\frac{\partial N_j}{\partial z}\end{bmatrix}dz=\frac{1}{L_e}\begin{bmatrix}1 & -1\\ -1 & 1\end{bmatrix} \qquad with \qquad i=1,2 \quad j=1,2 \tag{4-58a}$$

$$\int_{z=0}^{z=L}\begin{bmatrix}N_iN_j & N_iN_j\\ N_iN_j & N_iN_j\end{bmatrix}=\frac{L_e}{6}\begin{bmatrix}2 & 1\\ 1 & 2\end{bmatrix} \qquad with \qquad i=1,2 \qquad j=1,2 \tag{4-58b}$$

$$\int_{z=0}^{z=L}\begin{bmatrix}N_i\frac{\partial N_j}{\partial z} & N_i\frac{\partial N_j}{\partial z}\\ N_j\frac{\partial N_i}{\partial z} & N_j\frac{\partial N_i}{\partial z}\end{bmatrix}=\frac{1}{2}\begin{bmatrix}-1 & 1\\ -1 & 1\end{bmatrix} \qquad with \qquad i=1,2 \qquad j=1,2 \tag{4-58c}$$

$$\int_{z=0}^{z=L}\begin{bmatrix}\frac{\partial N_i}{\partial z}\\ \frac{\partial N_i}{\partial z}\end{bmatrix}dz=\begin{bmatrix}-1\\ 1\end{bmatrix} \qquad with \qquad i=1,2 \tag{4-58d}$$

$$\int_{z=0}^{z=L}\begin{bmatrix}N_i\\ N_i\end{bmatrix}dz=\frac{L_e}{2}\begin{bmatrix}1\\ 1\end{bmatrix} \qquad with \qquad i=1,2 \tag{4-58e}$$

and

$$\left(\begin{Bmatrix}N_i\\ N_i\end{Bmatrix}\frac{df(z)}{dz}\right)\Bigg|_{z=0}^{z=L}=\begin{Bmatrix}-\frac{df(0)}{dz}\\ \frac{df(L_e)}{dz}\end{Bmatrix} \qquad with \qquad i=1,2 \tag{4-58f}$$

The stiffness matrices were presented in the numerical solutions of both contaminant transport and Richards' equations. They could be written as follows:

The contaminant transport model:

$$\begin{aligned}
\left[P_{ij}\right] &= \sum_e \int_{z=0}^{z=L} \left(D_z \frac{\partial N_i}{\partial z}\frac{\partial N_j}{\partial z} + N_i \frac{\partial N_j}{\partial z} q_z \right) dz = \sum_e \frac{D_z}{L_e}\begin{bmatrix} 1 & -1 \\ -1 & 1 \end{bmatrix} + \sum_e \frac{q_z}{2}\begin{bmatrix} -1 & 1 \\ -1 & 1 \end{bmatrix} \\
\left[Q_{ij}\right] &= \sum_e \int_{z=0}^{z=L} N_i N_j \theta\kappa dz = \sum_e \frac{\theta\kappa L_e}{6}\begin{bmatrix} 2 & 1 \\ 1 & 2 \end{bmatrix} \\
\left[R_{ij}\right] &= \sum_e \int_{z=0}^{z=L} N_i N_j \theta\kappa\lambda dz = \sum_e \frac{\theta\kappa\lambda L_e}{6}\begin{bmatrix} 2 & 1 \\ 1 & 2 \end{bmatrix} \\
\left\{S_i\right\} &= N_i D_z \left(\frac{\partial C}{\partial z}\right)\Big|_{z=0}^{z=L} = \sum_e D_z \begin{Bmatrix} -\dfrac{dC(0)}{dz} \\ \dfrac{dC(L_e)}{dz} \end{Bmatrix}
\end{aligned} \tag{4-59}$$

Richards' equation:

$$\begin{aligned}
\left[A_{ij}\right] &= \sum_e \int_{z=0}^{z=L} K_{zz} k_{rw} \left(\frac{\partial N_i}{\partial z}\frac{\partial N_j}{\partial z} \right) dz = \sum_e \frac{K_{zz} k_{rw}}{L_e}\begin{bmatrix} 1 & -1 \\ -1 & 1 \end{bmatrix} \\
\left[B_{ij}\right] &= \sum_e \int_{z=0}^{z=L} N_i N_j M_C dz = \sum_e \frac{M_C L_e}{6}\begin{bmatrix} 2 & 1 \\ 1 & 2 \end{bmatrix} \\
\left\{E_i\right\} &= -N_i\, q_z\big|_{z=0}^{z=L} - \sum_e \int_{z=0}^{z=L} K_{zz} k_{rw} \frac{\partial N_i}{\partial z} dz = -\sum_e \begin{Bmatrix} -q_z(0) \\ q_z(L_e) \end{Bmatrix} - \sum_e K_{zz} k_{rw} \begin{bmatrix} -1 \\ 1 \end{bmatrix}
\end{aligned} \tag{4-60}$$

To cover the whole system, these small elements were connected as illustrated in Figure 4.3. There were two small elements in this system, the upper element was called "Element 1", and the adjacent element was called "Element 2". The lower node of Element 1 was connected with the upper node of Element 2. This system contained three nodes. The interpolation functions at the middle node (Node 2) obtained from "Elements 1" and "Element 2" must be the same. Therefore, the stiffness matrices of the system can be obtained as follows:

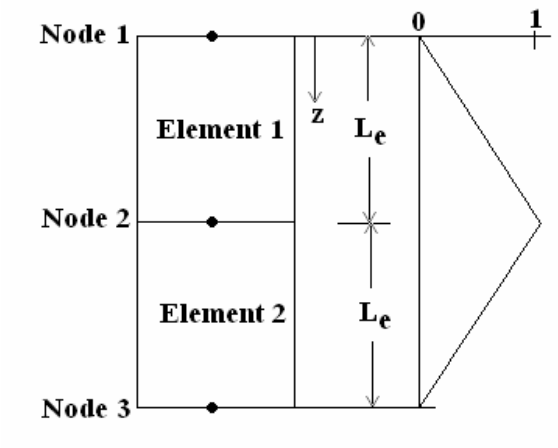

Figure 4.3 Scheme of element connection

The contaminant transport model:

$$\begin{aligned}
\left[P_{ij}\right] &= \sum_e \frac{D_z}{L_e}\begin{bmatrix} 1 & -1 & 0 \\ -1 & 2 & -1 \\ 0 & -1 & 1 \end{bmatrix} + \sum_e \frac{q_z}{2}\begin{bmatrix} -1 & 1 & 0 \\ -1 & 0 & 1 \\ 0 & -1 & 1 \end{bmatrix} \\
\left[Q_{ij}\right] &= \sum_e \frac{\theta\kappa L_e}{6}\begin{bmatrix} 2 & 1 & 0 \\ 1 & 4 & 1 \\ 0 & 1 & 2 \end{bmatrix} \\
\left[R_{ij}\right] &= \sum_e \frac{\theta\kappa\lambda L_e}{6}\begin{bmatrix} 2 & 1 & 0 \\ 1 & 4 & 1 \\ 0 & 1 & 2 \end{bmatrix} \\
\left\{S_i\right\} &= \sum_e D_z\begin{Bmatrix} -\dfrac{dC(0)}{dz} \\ 0 \\ \dfrac{dC(L)}{dz} \end{Bmatrix}
\end{aligned} \tag{4-61}$$

Richards' equation:

$$\begin{aligned}
\left[A_{ij}\right] &= \sum_e \frac{K_{zz}k_{rw}}{L_e}\begin{bmatrix} 1 & -1 & 0 \\ -1 & 2 & -1 \\ 0 & -1 & 1 \end{bmatrix} \\
\left[B_{ij}\right] &= \sum_e \frac{M_C L_e}{6}\begin{bmatrix} 2 & 1 & 0 \\ 1 & 4 & 1 \\ 0 & 1 & 2 \end{bmatrix} \\
\left\{E_i\right\} &= -\sum_e \begin{Bmatrix} -q_z(0) \\ 0 \\ q_z(L) \end{Bmatrix} - \sum_e K_{zz}k_{rw}\begin{bmatrix} -1 \\ 0 \\ 1 \end{bmatrix}
\end{aligned} \tag{4-62}$$

According to the continuity flow equation, the nodal velocity at the end of element "*n*" and the beginning of element "$n+1$" must be equalled or $q_z(L)-q_z(0)=0$ and $\frac{dC(L)}{dz}-\frac{dC(0)}{dz}=0$. The initial and boundary conditions for contaminant transport model and Richard's equations were specified in the next section.

4.5 Initial and boundary conditions

The initial condition was defined as the starting condition of the system at *t=0*. The boundary conditions were classified into upper and lower boundaries that were located on the top and bottom of columns, respectively (Huyakorn and Pinder 1983). In this research the upper boundary was the condition at the discharge point and the lower boundary was the condition at the water table or the column base. The boundary and initial conditions for the contaminant transport model and Richards' equation included the known concentration of contaminant and pressure head, respectively (Bear 1979 and Huyakorn and Pinder 1983).

4.5.1 Contaminant transport in variably saturated soil conditions

The initial concentration in the entire domain $[0, L]$ at time t = 0 was defined as follows (Bear 1979, Huyakorn and Pinder 1983, Huyakorn, et al. 1985, Ségol 1993 and Clement et al. 1998):

$$C_j(z,0) = C_0(z) \tag{4-63}$$

where

$C_0(z)$ = The known distributions of solute concentration at time t = 0 [ML^{-3}]

The boundary concentration on the edge of domain $[0, L]$ at time "*t*" was defined using the Dirichlet boundary condition (Bear 1979, Huyakorn and Pinder 1983, Huyakorn, et al. 1985, Ségol 1993 and Clement et al. 1998).

$$C_j(z,t) = C(z,t) \qquad on \qquad z_1 < z < z_2 \tag{4-64}$$

The specific dispersive flux on the edge of domain $[0, L]$ at time "*t*" was employed using Neumann boundary condition. The dispersive flux was defined as $\frac{\partial C}{\partial z}$, (Bear 1979, Huyakorn and Pinder 1983, Huyakorn, et al. 1985, Ségol 1993 and Clement et al. 1998).

$$D_z \frac{\partial C}{\partial z} = q_C^D \qquad on \qquad 0 \le z \le L \tag{4-65a}$$

and

$$D_z \frac{\partial C}{\partial z} - q_z C = q_C^T \qquad on \qquad 0 \le z \le L \tag{4-65b}$$

where

q_C^D = The portion of the boundary flux attributable to concentration due to dispersion [M L^{-1} T^{-2}]

q_C^T = The portion of the boundary flux attributable to total concentration [$ML^{-1}T^{-2}$]

4.5.2 Richards' equation

The initial pressure heads in the entire domain $[0, L]$ at time t = 0 was established as (Coley 1983, Paniconi et al. 1991 and Ségol 1993):

$$\psi_j(z,0) = \psi_0(z) \tag{4-66}$$

where

$\psi_0(z)$ = The known distributions of pressure heads at time t = 0 [L]

There was a limitation on measurement of pressure head on the surface. The tensiometer cannot be exposed to the atmosphere, as the air bubbles may accumulate inside the tip of the meter and they could disturb the signal reading. Hence, the initial pressure head on the surface was estimated using the equations of Clapp and Hornberger (1978) (cited in Dingman 1994) given as follows.

$$|\psi(\theta)| = |\psi_S| \phi^{\sigma} \theta^{-\sigma} \tag{4-67a}$$

$$|\psi(S)| = |\psi_S| S^{-\sigma} \tag{4-67b}$$

and

$$K_{zz}k_{rw}(\theta) = K_{zz}\phi^{-\xi}\theta^{\xi} \tag{4-67c}$$

where

ψ_S = The air entry pressure head [L]

S_w = The degree of saturation [unitless]

σ and ξ = The empirical parameters [unitless]

Clapp and Hornberger (1978) found that $\xi \approx 2\sigma + 3$. Table 4.1 presents the possible values for the parameters used in Clapp and Hornberger (1978)'s equations.

Table 4.1 Possible parameter values used in the equation of Clapp and Hornberger (1978) (cited in Dingman 1994)

Soil texture	ϕ	K_{zz} (cm/s)	$\lvert\psi_S\rvert$ (cm)	ξ
Sand	0.395 (0.056)	$1.72\text{x}10^{-2}$	12.1 (14.3)	4.05 (1.78)
Loamy sand	0.410 (0.068)	$1.56\text{x}10^{-2}$	9.0 (12.4)	4.38 (1.47)
Sandy loam	0.435 (0.086)	$3.47\ \text{x}10^{-3}$	2.8 (3.0)	4.90 (1.75)
Silt loam	0.485 (0.059)	$7.20\text{x}10^{-4}$	78.6 (51.2)	5.30 (1.96)
Loam	0.451 (0.078)	$6.95\text{x}10^{-4}$	47.8 (51.2)	5.39 (1.87)
Sandy clay loam	0.420 (0.059)	$6.30\text{x}10^{-4}$	29.9 (37.8)	7.12 (2.43)
Silty clay loam	0.477 (0.057)	$1.70\text{x}10^{-4}$	35.6 (37.8)	7.75 (2.77)
Clay loam	0.476 (0.053)	$2.45\text{x}10^{-4}$	63.0 (5.0)	8.52 (3.44)
Sandy clay	0.426 (0.057)	$2.17\text{x}10^{-4}$	15.3 (17.3)	10.4 (1.64)
Silty clay	0.492 (0.064)	$1.03\text{x}10^{-4}$	49.0 (62.1)	10.4 (4.45)
Clay	0.482 (0.050)	$1.28\text{x}10^{-4}$	40.5 (39.7)	11.4 (3.70)

Note: A number in a parenthesis refers to the standard deviation.

Boundary condition for gravitational system

The pressure head in the entire domain $[0, L]$ at time "*t*" was established using the Dirichlet boundary condition as follows (Bear 1979, Huyakorn and Pinder 1983, Coley 1983, Paniconi et al. 1991 and Ségol 1993):

$$\psi_j(z,t) = \psi(z,t) \qquad on \qquad z_1 < z < z_2 \tag{4-68}$$

The infiltration boundary (wetting front) could be estimated using equation of Green-Ampt (1911) (cite in Dingman 1994). The equation was given as follows:

$$|\psi_f| = k_f |\psi_S| \tag{4-69}$$

where

k_f = The effective pressure head at the wetting front $(=1/(1+3/\xi))$; [unitless]

The normal flux of pressure (q_z), which could support the derivative of variables $(\frac{\partial\psi}{\partial z}, \frac{\partial\theta}{\partial z})$ was defined using Neumann boundary condition (Bear 1979, Huyakorn and Pinder 1983, Coley 1983, Paniconi et al. 1991 and Ségol 1993).

$$-K_{zz} k_{rw} \left[\frac{\partial\psi}{\partial z} + 1 \right] = q_z \qquad on \qquad 0 \le z \le L \tag{4-70}$$

Boundary conditions for the redistribution system

The boundary conditions were evaluated according to the physical model of capillarity attraction. The zone of negative pressure could be observed with depth of capillary height, h_C. The capillary height was from the water level inside the capillary tube. The capillary height could be estimated as follows (Freudlune and Rahardjo 1940):

$$U_W = -\rho_W h_C g \tag{4-71}$$

where

U_w = The hydraulic pressure head at the capillary height [M L T^{-2}]

ρ_W = The water density [M L^{-3}]

h_C = The capillary height [L]

g = The gravitational acceleration [L T^{-2}]

The physical model of capillarity and the graphical plot of equilibrium of capillary pressure force in unsaturated soil are presented in Figures 4.4 and 4.5, respectively. The variables presented in Figure 4.4 included "T_S", "r_S"and "α". These were the surface

tension, the radius of capillary tube and the contact angle, respectively. The variable "U_a" presented in Figure 4.5 was the atmospheric pressure. It normally equalled to 0 cm H_2O.

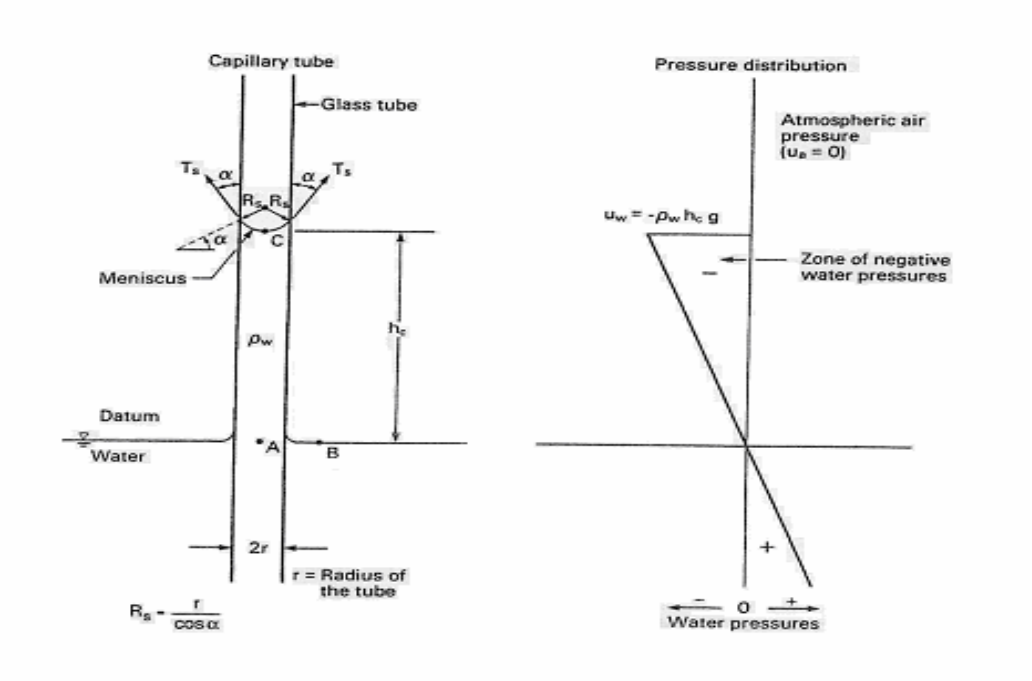

Figure 4.4 Physical model of capillarity inside the capillary tube (Fredlune and Rahardjo 1940)

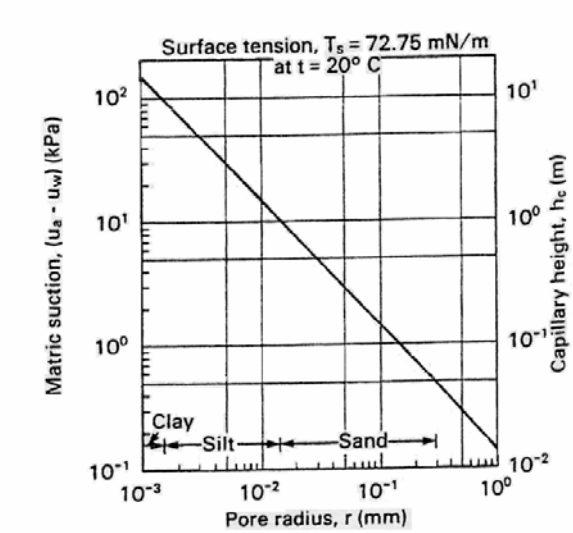

Figure 4.5 Relationship between pore radius, matric suction and capillary height (Fredlune and Rahardjo 1940)

4.6 Model solving techniques

Paniconi et al. (1991) applied six iteration techniques to solve Richards' equation including iterative Newton, iterative Picard, linearised Newton, linearised Picard, implicit factored and three level Lee's schemes. Among these techniques, Picard's iterative technique was the simplest and most powerful technique. So, this technique was applied to solve the numerical solution of contaminant transport and Richards' equations in this research.

4.6.1 Iteration procedure for contaminant transport model

The time dependent concentration predicted by the numerical contaminant transport model (Equation 4-38) could be derived as follows (Wang and Anderson 1982, Paniconi et al. 1991 and Ségol 1993):

$$\left\{\frac{\partial C}{\partial t}\right\} = \frac{1}{\Delta t}\left(\{C\}^{t+\Delta t} - \{C\}^{t}\right) \tag{4-72}$$

where

Δt = The length of the time step [T]

$\left\{\frac{\partial C}{\partial t}\right\}$ = A column matrix, which refers to $C_j = C_j(t)$

The superscript "t"and "$t = \Delta t$" represented the previous and current time levels, respectively.

Thus an approximation of the time derivative at a particular node "*j*" can be explained as follows (Wang and Anderson 1982, Paniconi et al. 1991 and Ségol 1993):

$$\frac{\partial C_j}{\partial t} = \frac{C_j^{t+\Delta t} - C_j^{t}}{\Delta t} \tag{4-73}$$

The term "$\left\{\frac{\partial C}{\partial t}\right\}$" can be simplified with this vector symbol "$\{C\}$". The iterative schematic could be obtained using a single Picard iteration technique as follows (Wang and Anderson 1982, Paniconi et al. 1991 and Ségol 1993):

$$\left(\frac{1}{2}\left(\left[P_{ij}\right]+\left[R_{ij}\right]\right)+\frac{1}{\Delta t}\left[Q_{ij}\right]\right)\left(\{C\}^{t+\Delta t}-\{C\}^{t}\right)=\{S_i\}-\left(\left[P_{ij}\right]+\left[R_{ij}\right]\right)\{C\}^{t} \tag{4-74}$$

4.6.2 Iteration procedure for Richards' equation

The numerical solution of Richards' equation is presented in Equation 4-47, the time derivative of pressure head can be derived as follows (Wang and Anderson 1982, Paniconi et al. 1991 and Ségol 1993):

$$\left\{\frac{\partial \psi}{\partial t}\right\}=\frac{1}{\Delta t}\left(\{\psi\}^{t+\Delta t}-\{\psi\}^{t}\right) \tag{4-75}$$

where

$\left\{\frac{\partial \psi}{\partial t}\right\}$ = A column matrix, which refers to time-dependent hydraulic pressure head

$(\psi_j=\psi_j(t))$

The time derivative approximation at a particular node "*j*" can be explained as follows (Wang and Anderson 1982, Paniconi et al. 1991 and Ségol 1993):

$$\frac{\partial \psi_j}{\partial t}=\frac{\psi_j^{t+\Delta t}-\psi_j^{t}}{\Delta t} \tag{4-76}$$

The term "$\left\{\frac{\partial \psi}{\partial t}\right\}$" can be simplified with the vector symbol "$\{\psi\}$". The iterative scheme obtained using a single Picard's method was governed as follows (Wang and Anderson 1982, Paniconi et al. 1991 and Ségol 1993):

$$\left(\frac{1}{2}\left[A_{ij}\right]^{t}+\frac{1}{\Delta t}\left[B_{ij}\right]^{t}\right)\left(\{\psi\}^{t+\Delta t}-\{\psi\}^{t}\right)=\{E_i\}-\left[A_{ij}\right]^{t}\{\psi\}^{t} \tag{4-77}$$

Celie et al. (1990) estimated the pressure head profiles using Richards' equation. The numerical model was developed using both finite difference model (FDM) and FEM. The model developed using FEM had given an oscillation of pressure head that was

near the infiltration front. This oscillation pressure head could be reduced by applying a diagonal time matrix (mass lumping technique). The water balance (MB_t) was defined based on a diagonal time matrix. This was investigated to evaluate the error within the calculation process if existed. The water balance equation for the finite element technique is presented as follows (Celie et al. 1992 and Ségol 1993):

$$MB\left(t^{n+1}\right)=\frac{\sum_{i=1}^{E-1}\left(\theta_i^{n+1}-\theta_i^0\right)\Delta z+\left(\theta_0^{n+1}-\theta_0^0\right)\frac{\Delta z}{2}+\left(\theta_E^{n+1}-\theta_E^0\right)\frac{\Delta z}{2}}{\sum_{k=1}^{n=1}\left(q_{zo}^n-q_{zL}^n\right)\Delta t} \tag{4-78}$$

where

q_{zo} *and* q_{zL} = The boundary fluxes associated with z_0 *and* z_L, respectively [L T^{-1}]

E = The number of element [unitless]

Superscripts "n" *and* "n+1" refer to the previous and current iteration step, respectively.

The flow chart of the model solution process is provided in Figure 4.6. Firstly, Richards' equation was solved. The approximated solution of pressure head (ψ_j), moisture content (θ), Darcy's velocity (q_z) and pore velocity (v) were obtained. Secondly, these solutions were substituted into the advection and dispersion terms presented in the contaminant transport model. The concentration profiles and the reduction zone were evaluated. Finally, the simulation results were reported.

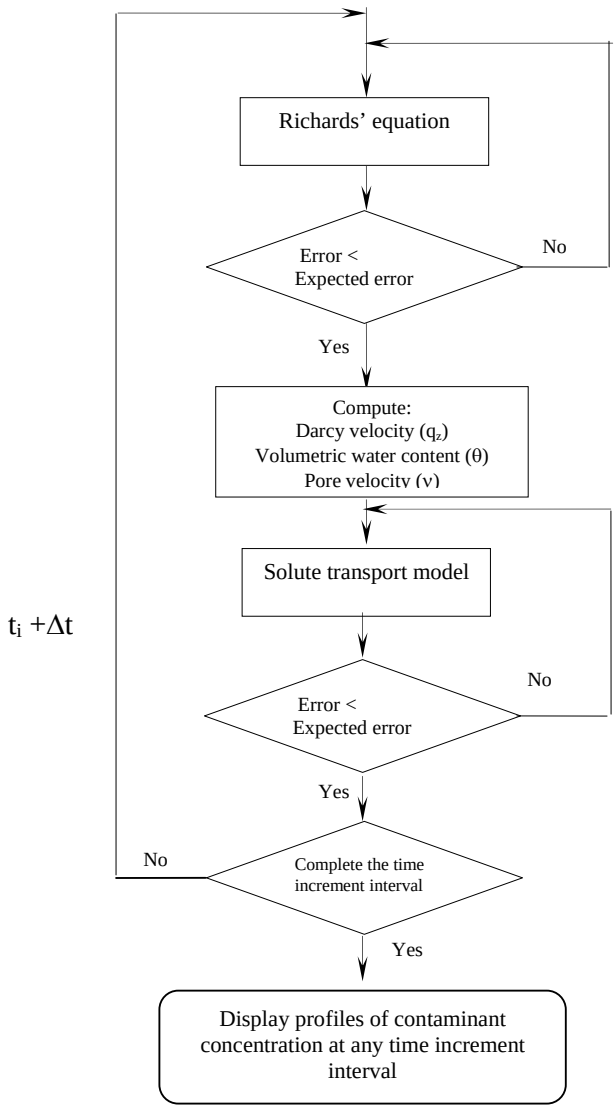

Figure 4.6 Schematic flowchart of the solution for the model developed

4.7 Development of the computational codes

The algorithm is described in the next section. The computational codes are given in Appendix-B.

4.7.1 Algorithm for Richards' equation

1. Input the geometry of the considered area (depth z) and the number of nodes in the considered area, to compute the nodal space (Δz).

2. Compute and store element properties such as the elemental depth, nodal coordinate, nodal connective.

3. Select the hydraulic properties equations: HV, VG and Saxton's function. Input the coefficients for hydraulic properties. Compute relative permeability (k_{rw}), and specific moisture capacity (M_C).

4. Input the initial and boundary conditions.

5. Compute and store the weighting function (N_i) and its derivative (dN_i/dz) for each node of the element.

6. Compute and store the shape function (N_j) and its derivative (dN_j/dz) for each node of the element.

7. Compute the element matrix and vectors for Richards' equation $[A_{ij}]$, $[B_{ij}]$ and $\{E_i\}$.

8. Assemble the element matrix to the global matrix $[A_{ij}]^e$, $[B_{ij}]^e$and $\{E_i\}^e$.

9. Store the global matrix $[A_{ij}]^e$, $[B_{ij}]^e$ and $\{E_i\}^e$ for the component on scratch files.

10. Compute the initial nodal pressure head (ψ_0) according to the capillary pressure head (ψ_c).

11. Input the initial time (t_0), the final time (t_f) and the number of time step, as well as compute the time increment (Δt).

12. Set the starting node "***j* = 0**" and starting time "***t* = 0**" as well as set iteration count. "**count =0**".

13. **While** "$t < t_f$" do Steps 14 to 26.

14. **For** "***j* =1**" to the "**n th**" node, do Steps 15 to 26.

15. Compute term $B = \frac{1}{\Delta t}\sum_{i=1}^{nnode}\left[B_{ij}\right]\{\psi\}^t$

16. Set up the allowance maximum error (E_{max})

17. **For** "***j* =1**" to the "***n***" node, do Steps 18 to 26 for each component.

18. Retrieve the global matrices $[A_{ij}]^e$, $[B_{ij}]^e$ and $\{E_i\}^e$ from the scratch files.

19. Update the term "***B***" according to the boundary conditions during $[t, t+\Delta t]$.

20. **If** "***j*=1**" go to Step 22

21. **Elseif** "***j*=*n***" go to Step 22

22. $\{\psi\}^{t+\Delta t} = \{\psi_0\}$

23. **Else**, solve the nodal pressure head $\{\psi\}^{t+\Delta t}$ according to

$$\left(\frac{1}{2}\left[A_{ij}\right]^t + \frac{1}{\Delta t}\left[B_{ij}\right]^t\right)\left(\{\psi\}^{t+\Delta t} - \{\psi\}^t\right) = \{E_i\} - \left[A_{ij}\right]^t\{\psi\}^t$$

24. Compute the error; Error = $\left\| \{\psi\}^{t+\Delta t} - \{\psi\}^{t} \right\|$

25. **If** "**Error ≥E_{max}**" hold $\{\psi\}^{t} = \{\psi\}^{t+\Delta t}$ and then go to Step 14

26. **Else**, compute the iteration count according to

$count = count + 1$

$t = t + 1$

and then, go to Step 13.

27. Compute the nodal Darcy flux (q_z) according to $q_z = -K_{zz} k_{rw} \frac{\partial(\psi + z)}{\partial z}$

28. Display the option modes, including "**(a) continue the solute transport model**", "**(b) re-run the programme for the new site**", and "**(c) quit the programme**".

29. **If** Option = "**a**" go to ***Contaminant transport model***

Elseif, Option = "**b**" rerun ***Richards' equation***

Else, Display the input and output

End.

4.7.2 Algorithm for contaminant transport model

1. Recall the input coefficient from Richards' equation and calculate Darcy's velocity (q_z) and pore velocity (υ). Add the required inputs for contaminant reaction including biodegradation rate (λ), retardation coefficient (κ), soil bulk density (ρ_B) and distribution coefficient (K_d).

2. Input the initial and boundary conditions.

3. Recall the weighting function (N_i) and its derivative (dN_i/dz) as well as the shape function (N_j) and its derivative (dN_j/dz) for each node of the element from Richards' equation.

4. Compute the element matrix and vectors for the solute transport equation $[P_{ij}]$, $[Q_{ij}]$, $[R_{ij}]$ and $\{S_i\}$.

5. Assemble the element matrices to the global matrix $[P_{ij}]^e$, $[Q_{ij}]^e$,$[R_{ij}]^e$and $\{S_i\}^e$.

6. Store the global matrix $[P_{ij}]^e$, $[Q_{ij}]^e$,$[R_{ij}]^e$and $\{S_i\}^e$ for the component on scratch files.

7. Input the initial nodal concentration (C_i).

8. Input the initial time (t_0), the final time (t_f) and the number of time step, as well as compute the time increment (Δt).

9. Set the starting node "***j* = 0**" and starting time "***t* = 0**", as well as set the iteration "count =0".

10. **While** "$t < t_f$" do Step 11 to 22.

11. **For** "***j* =1**" to the "**n th**" node, do Steps 12 to 22

12. Compute term $P = \frac{1}{\Delta t}\sum_{i=1}^{nnode}\left[\left[P_{ij}\right]+\left[R_{ij}\right]\right]\{C\}^t$

13. Set up the allowance maximum error (E_{max})

14. **For** "***j* =1**" to the "**n th**" node, do Steps 15 to 22 for each component.

15. Retrieve the global matrix $[P_{ij}]^e$, $[Q_{ij}]^e$,$[R_{ij}]^e$and $\{S_i\}^e$ from the scratch files.

16. Update the term P according to the boundary conditions [t, $t+\Delta t$].

17. **If** "***j*=1**" node go to Step 18

18. $\{C\}^{t+\Delta t} = \{C_i\}$

19. **Else**, solve the nodal concentration $\{C\}^{t+\Delta t}$ according to

$$\left(\frac{1}{2}\left(\left[P_{ij}\right]+\left[R_{ij}\right]\right)+\frac{1}{\Delta t}\left[Q_{ij}\right]\right)\left(\{C\}^{t+\Delta t}-\{C\}^t\right)=\{S_i\}-\left(\left[P_{ij}\right]+\left[R_{ij}\right]\right)\{C\}^t$$

20. Compute the error; Error = $\left\|\{C\}^{t+\Delta t}-\{C\}^t\right\|$

21. **If** "**Error ≥*E*$_{max}$**" hold $\{C\}^t = \{C\}^{t+\Delta t}$ and then go to Step 13

22. **Else**, compute the iteration count according to

$count = count + 1$

$t = t + 1$

and then, go to Step 10.

23. Display the input and output solution for the water movement model and/or the solute transport model.

24. Display the option modes including "**(a) re-run the programme for the new site**" and/or "**(b) new contaminant constitute**" and "**(c) quit the programme**".

25. **If** Option = "**a**" go to ***Richards' equation***

Elseif, Option = "**b**" rerun the ***contaminant transport model***

Else, Display the input and output

End.

4.8 Summary

A mathematical model was developed by modifying the governing equation presented in the previous chapter. This developed model included two parts, namely transport and retardation. The transport processes presented in the mathematical model depended upon the advection and dispersion processes. The transport process is non-linear and varies with time and is related to Darcy's and pore water velocities. These velocities were estimated using Richards' equation. The retardation processes were described using the multiplicative Monod, the Langmuir adsorption and the microbial metabolism equations. The mathematical model was in the form of a PDE. It was transformed to the ODE using Galerkin's method and a numerical solution was achieved. The FEM was applied to generate a symmetrical stiffness matrix. A single Picard's iteration supported the calculation strategies of this numerical model. The MATLAB programme was applied to produce the computational codes for the model.

The developed model will be calibrated with experimental data and historical case studies. The experimental set up will be described in the next chapter.

CHAPTER 5

EXPERIMENTAL SET UP

5.1 Introduction

The details of experimental set up are described in this chapter. The experiments were both continuous and batch tests. The continuous tests included laboratory and pilot scale tests. Laboratory scale soil column tests were used to observe contaminant transport due to advection and dispersion processes. Pilot scale soil column tests were used to observe contaminant transport with reactions similar to the field conditions. The batch tests were conducted to estimate the coefficients of soil hydraulic properties, phosphorus adsorption, and the suitability of fibreglass candlewick methods in the sampling of pore water.

5.2 Soil sample preparation

The two soil samples utilised were medium grained sand and topsoil. A sample of medium grained sand was prepared from river sand with a particle size of 250-500 μm (micron). The sample of topsoil was collected near the Building 4-Engineering, at University of Wollongong. The topsoil was air dried and sieved to eliminate rocks, plant roots, leaves and earthworms. The largest particle size of the soil was less than 2.0 mm.

5.3 Methods for testing soil

Random samples were selected according to the AS 1289 Method of Testing Soils for Engineering Purposes. This included AS 2589.1 Method 1: Preparation of Disturbed Soil Sample for Testing and ASTM D421-85 Standard Practice for Dry Preparation of Soil Samples for Particle-size Analysis and Determination of Soil Constants. The testing parameters and their analytical methods are given in Table 5.1.

Table 5.1 Methods for testing soil

Parameter	Method	Reference
Physical properties:		
particle size distribution	Sieving in combination with hydrometer method	AS 1289.3.6.2-1995 and Gee and Bauder (1986)
soil classification	The textural triangle nomenclature	Brady (1974) and USDA (2001)
hydraulic conductivity (cm/h)	Standard test method for permeability of granular soil	AS 1289.6.7.3-1999
bulk density (kg/m^3)	Sand replacement method using a sand cone pouring apparatus	AS 1741.4-2000 and Bowles (1992)
specific gravity	Soil particle density	AS 1289.3.5.1-1995
soil water content (%)	Oven drying method	AS 1289.2.1.1-1992
soil porosity (%)	Volume-mass relationship	Fedlune and Rahardjo (1940)
Chemical properties:		
soil organic matter (%)	Walkley-Black procedure	Nelson and Sommers (1982)
soil pH	Electrode pH meter method	AS 1289.4.3.1. (1977)
soil total phosphorus (ppm)	Total Phosphate (Digestion)	Olsen and Sommers (1982)
soil total nitrogen (ppm)	Regular Kjeldahl method	Bremner and Mulvaney (1982)
soil exchangeable cation, (meq/100 g)	Ammonium acetate method	Thomas (1982)

5.4 Wastewater sample preparation

Raw household wastewater was collected from the Bellambi Sewage Treatment Plant (Bellambi STP). This treatment plant receives domestic wastewater from households around Bellambi, Corrimal, Towradgi and Fairy Meadow. The Bellambi STP has primary treatment containing a fine screen followed by chemical assisted sedimentation (CAS) and disinfection processes. The discharge rate of this wastewater treatment plant was 23 ML/day based on an average daily dry weather discharge. This treatment plant serves a population of 85,000 (Sydney Water 2005).

In this research samples of wastewater were collected after fine screen filtration. During this process coarse solids were removed so the wastewater only contained suspended solids. The sample was kept in a 20 L storage tank under anaerobic conditions for 3-4 days before feeding to the column of soil. This storage tank also served as a pre-sedimentation tank.

5.5 Methods for testing wastewater

The wastewater sample was collected, preserved and stored according to APHA (1998) Standard Methods for Testing Water and Wastewater. A list of parameters, testing methods and references are given in Table 5.2.

Table 5.2 Method for testing wastewater

Parameter	Method	Reference
Physical properties:		
Electrical conductivity (μmhos/cm)	Water Electrical conductivity	Rayment and Higginson (1992)
Chemical properties:		
Nitrogen compounds:		
Total Kjeldahl nitrogen (mg/L)	Semi-micro Kjeldahl method	Rayment and Higginson (1992)
Nitrate-nitrogen (mg/L)	Sodium Salicylate development using standard solution	Yang et al. (1998)
Ammonium-nitrogen (mg/L)	Colorimetric, Automated Phenate	U.S. EPA (1983b)
Phosphate-phosphorus (mg/L)	Vanadomolybdophospheric acid colorimetric method	Rayment and Higginson (1992)
Chemical oxygen demand (mg/L)	Closed reflux, colorimetric method	APHA(1998)
Dissolved oxygen (mg/L)	DO electrode method	APHA(1998)
pH	pH electrometric method	APHA(1998)
Suspended solids (mg/L)	Oven Dry-105 ^{o}C, 24 hours	APHA(1998)
Biological properties:		
E.Coli (cfu/100mL)	Escherichia coli (*E.Coli*) in water by membrane filtration using modified membrane-Thermotolerant Escherichia Coli Agar (Modified mTEC)	U.S.EPA (2005)

5.6 Preliminary soil column design

The design parameters of the soil columns are given in Table 5.3. The design details are provided in Appendix-C.

Table 5.3 Design parameters of the laboratory and pilot scale sand/soil columns

Parameter	Unit	Value	Reference
Fine to medium grain sand			
Bulk density	kg/m^3	1.8	Robertson (1995)
Effective porosity		0.4	Rawls et al. (1983)
Relative saturation		0.375	Lee et al. (1998)
Hydraulic conductivity	cm/h	11.78	Rawls et al. (1983)
Topsoil			
Bulk density	kg/m^3	1.25	Watts (1997)
Effective porosity		0.4	Rawls et al. (1983)
Relative saturation		0.240*	Broadbridge and White (1988) and White and Broadbridge (1988)
Hydraulic conductivity	cm/h	0.34	Green-Ampt (1911)

Note: * Average from the air-dry moisture content divided by saturated moisture content ($\theta/\theta s$)

5.7 Continuous flow experiments

Continuous flow tests consist of the advection transport and dispersion transport in a laboratory scale soil column and contaminants transport with reactions in a pilot scale soil column.

5.7.1 Advection transport in a laboratory scale soil column

The laboratory scale soil columns were fabricated using a plexi-glass tube with an inside diameter of 6.9 cm and a total height of 30 cm (effective height 20 cm). Jet fill tensiometer model 2100F moisture probes were used to measure negative pore pressure. The datum was defined at the base of the column (positive upward). Five tensiometers were inserted at depth 2.5, 6.5, 10, 14.0 and 17.5 cm. above the datum. Rubber plugs were inserted into the observation ports to prevent leakage. The tensiometer was

connected to data logger model DT 500 DataTaker. A 10 volts DC transformer supplied power to the data logger. The fabricated column is illustrated in Figure 5.1.

Figure 5.1 Fabricated laboratory scale soil column

The laboratory soil column where the flow tests were carried out could be classified into three categories including the gravitational, the equilibrium of static capillary, and the infiltration and redistribution systems. These are shown in Figure 5.2. The details of the experimental set up were as follows:

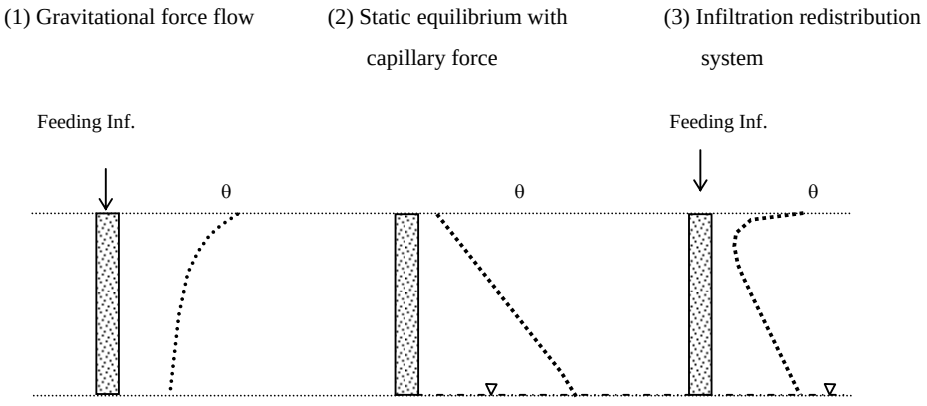

Figure 5.2 Modes of laboratory scale unsaturated column studies

The gravitational infiltration system

The infiltration columns were initially packed with dry sand and soil. Sand and soil columns were filled with packing bulk densities of 1.8 and 1.25 g/cm^3, respectively. Tap water was fed with a peristaltic pump to sand and soil column. The feeding rates were 66.1 and 7.18 cm^3/h, respectively. The moisture content of sand and soil samples were monitored at each 4-cm.

The static equilibrium capillary force system

The columns were initially packed with dry sand and soil. Sand and soil columns were packed with the bulk densities of 1.8 and 1.25 g/cm^3, respectively. Tap water was added into the storage tank. The columns were placed into the water storage tank. The water level was located at the column base. The moisture content sand/soil samples were monitored for every 4-cm intervals.

The infiltration-redistribution system

The columns were initially packed with dry sand and soil. Sand and soil columns were packed with bulk densities of 1.8 and 1.25 g/cm^3, respectively. The columns were placed into the water storage tank similar to the columns for testing flow under static equilibrium capillary force. The columns were brought to an equilibrium condition while tap water was added to the surface of the sand and soil columns at the rates of 66.1 and 7.18 cm^3/h; respectively. The moisture contents of sand and soil samples were determined for every 4-cm interval.

5.7.2 Dispersion transport in a laboratory scale soil column (tracer tests)

The experimental set up for tracer test was undertaken in the same way as the apparatus presented in the laboratory soil column tests- the gravitational system and the hydraulic properties test. The only difference was the addition of NaCl tracer solution. The concentration of sodium ion was determined by measuring EC (1:5). EC of a 1:5 extract of soil and water was applied. Air –dried soil weighing 20 g was mixed into 100 mL of deionised water. The vessel was covered with a watch glass and the solution is shaken for 1 hour and then allowed to settle for 20-30 minutes (Rayment and Higginson 1992).

The soil contained ions such as sodium (Na^+), magnesium (Mg^{2+}), calcium (Ca^{2+}), potassium (K^+), ammonium (NH_4^+) chloride (Cl^-), sulfate (SO_4^{2-}), and bicarbonate (HCO_3^-). These interferences might have increased the measured concentration of the tracer applied (Sparks 1995). In this study, the topsoil sample could contain the background ions which could adversely affect the measured tracer concentration. The concentration of the NaCl tracer applied must be considered together with the presence of the background ions. The thickness of the soil layer also impacts on the spreading of the tracer. Three tracer tests were conducted under various conditions as presented in Table 5.4.

Table 5.4 Details of tracer tests

Tests	Packing depth (cm)	NaCl conc. (mg/L)	Feeding rate (cm^3/h)	Location of tensiometers (cm)	Location of EC (1:5) measurement (cm)
Tracer test 1	5	200	7.18	2.5	0.5, 1.5, 2.5, 3.5, 4.5
Tracer test 2	5	500	7.18	2.5	0.5, 1.5, 2.5, 3.5, 4.5
Tracer test 3	20	500	7.18	2.5, 6.5,14.0,17.5	2.0,6.0,10.0,14.0,18.0

5.7.3 Contaminant transport with reactions in a pilot scale soil column

The pilot scale column test was conducted to observe the contaminant transport with retardation in the unsaturated zone. The pilot scale columns were fabricated from plexiglass tubes with an inside diameter of 10.4 cm and total height of 136 cm, which included 120 cm for packing and 16 cm for freeboard. The details of the fabricated soil columns are illustrated in Figures 5.3 and Figure 5.4, respectively.

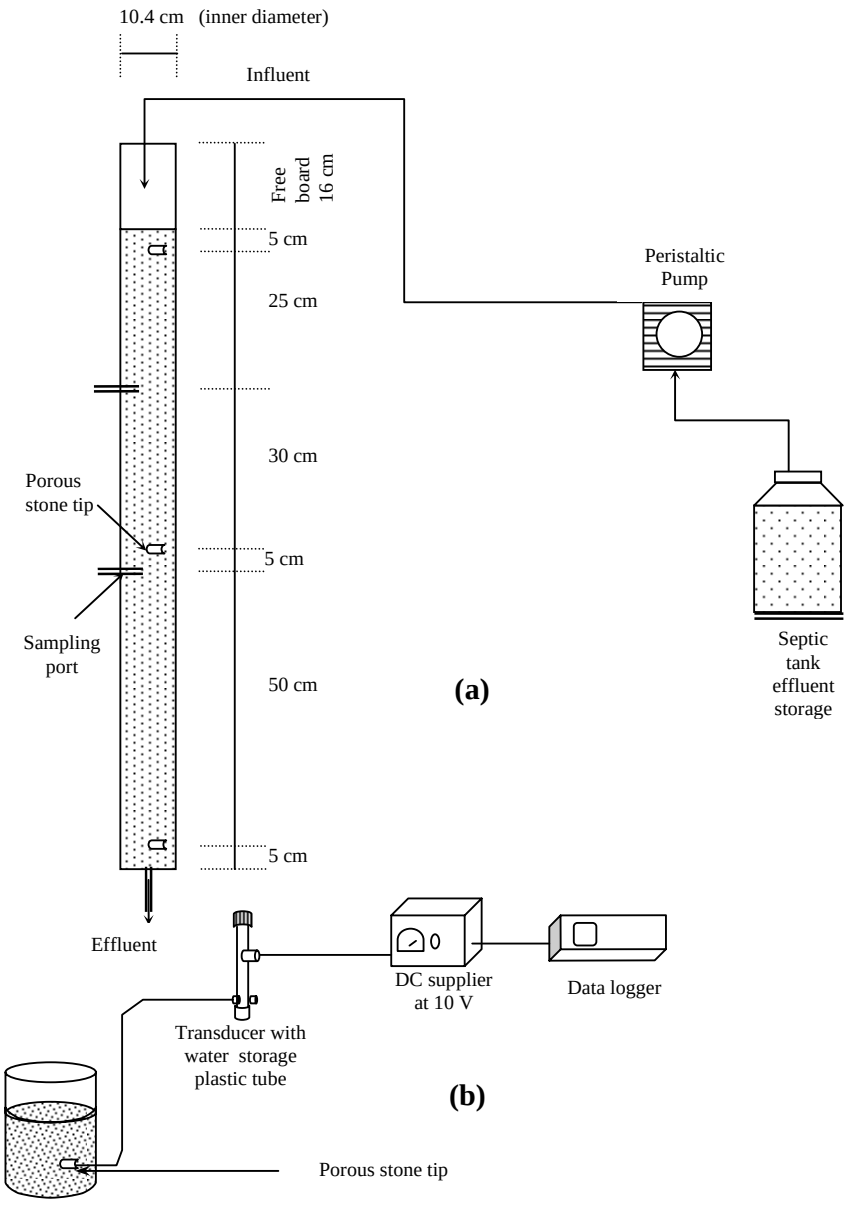

Figure 5.3 Diagram for pilot scale soil experimental set up
(a) soil column set up and (b) tensiometer set up

Figure 5.4 Pilot scale experimental set up

This pilot scale column was initially packed with dry soil to give a bulk density of 1.25 g/cm^3. Five tensiometers were used to measure the pore pressure. They were located at 5, 32.5, 60, 87.5, and 115 cm above the datum (column base). When the tensiometers reached equilibrium conditions, domestic wastewater was added via a peristaltic pump. The calculated effluent feed rate required was 16.3 cm^3/h. At this flow rate setting, the peristaltic pump could not operate to lift the water to the top of column (136 cm high). Therefore, the feeding rate was increased to 17.8 cm^3/h. A distribution plate was placed on the surface to distribute the effluent uniformly. The passive capillary sample technique was applied using a fibreglass wick and the concentration profiles at the packing depths of 120, 65, and 30 cm (above the datum) were observed.

5.8 Batch experiments

Batch tests were used to determine the soil hydraulic properties, the advection and dispersion transport in unsaturated soil conditions, the kinetic coefficients of soil-phosphate adsorption and the suitability of fibreglass wicks in wastewater sampling.

5.8.1 Soil hydraulic properties test

The test was modified from the Haverkamp et al. (1977), which was described as "…[The] experiments were done in the laboratory using a plexiglass column, 93.5 cm long and 6-cm inside diameter (ID) uniformly packed with sand to a bulk density of 1.66 g/cm^3. The column was equipped with tensiometers at depths of 7, 22, 37, 52, 67 and 82 cm below the soil surface. Each tensiometer had its own pressure transducer. The changes of water content at different depths were obtained by gamma ray attenuation using a source of 100 mCi of Americium-241. A constant water pressure was maintained at the lower end of the column and a constant flux was imposed at the soil surface (z=0). The hydraulic conductivity-water content relationship of the soil was obtained by analysis of the water-content and water-pressure profiles during transient flow (Watson 1966 and Vachaud and Thony 1971). The soil water-pressure-water content relationship was obtained at each tensiometer depth by correlating tensiometer readings and water content measurement during experiments."

There are many laboratory methods for testing water retention. The dynamic method was found to be similar to Haverkamp et al.'s experiments. This method was suitable for low suction pressure (<0.1MPa). The water retention data could be obtained from relatively dry to relatively wet soil samples. This method was described as follows (Klute 1986).

"…Alternatively, in principle, if one can measure the water content and metric pressure head as a function of time at a given point in a soil water flow system, a dynamic water retention function can be obtained by repairing the values of water content and pressure head at a given time. The flow may be either steady or unsteady."

The soil hydraulic properties test was undertaken as illustrated in Figure 5.5. The columns were initially packed with sand and soil samples. The packing depth was 5 cm. The bulk densities of sand and soil columns were controlled at 1.80 and 1.25 g/cm^3, respectively. Time series data of pressure head was measured using a single tensiometer that was inserted at the depth of 2.5 cm above the column base. Tap water was poured through the sand and soil columns at the rates of 66.1 and 7.18 cm^3/h, respectively. The water content was determined every 1-cm interval, using the gravitational method. The relative permeability was determined using Kunze's equation.

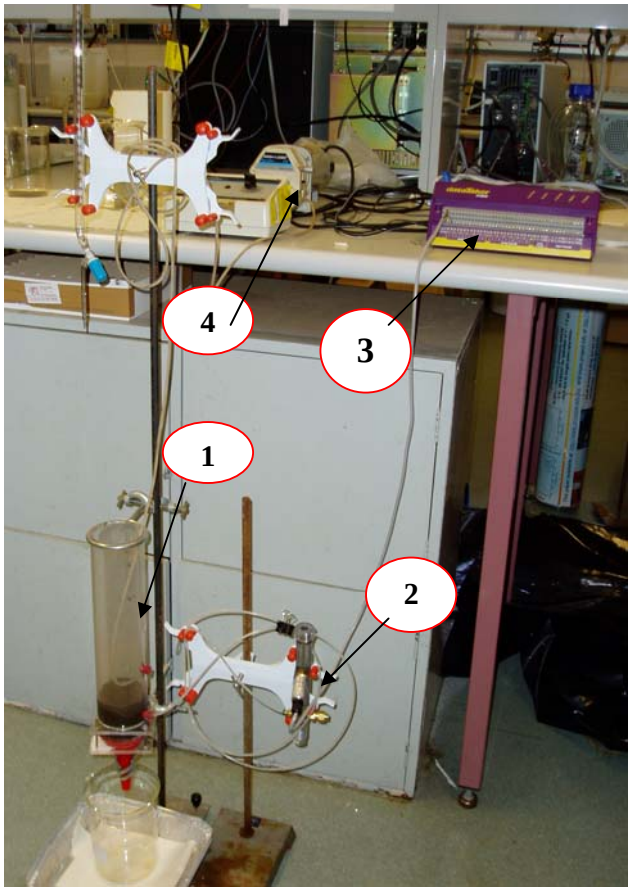

Items:

1. Sand/soil column
2. Tensiometer
3. Data logger
4. Peristaltic pump

Figure 5.5 Soil hydraulic properties test

5.8.2 Phosphorus adsorption test

Phosphorus adsorption experiments were set up using a procedure modified from Watts (1997). Firstly, the equilibrium time was evaluated. There were two sets of experiments that included one blank test. A 2-g sample of air-dry soil was placed into a 100-mL Erlenmeyer flask and 40 mL of 10 mgP /L solution was added. The flask was placed in an incubator shaking machine and kept at room temperature (23 ^{o}C). The shaking speed was set to 150 rpm, and shaken for 1, 2, 3, 4, 5, 6, 7, 8 and 24 hours. The phosphorus concentration was analysed by the soluble phosphorus method (Olsen and Sommers 1982). Each soil mixture was filtered through Whatman paper number 42. The phosphorus concentration was detected using a UV-Visible spectrophotometer at a wavelength of 470 nm. For the blank, the same procedure was applied, except that 40

mL of deionised water was added instead of the phosphate solution. All the flasks were kept in the shaker for the same period as those used for testing.

Secondly, after the equilibrium time was specified, the isotherm was determined. Sample of 0.25, 0.5, 0.75, 1.0, 1.25, 1.50 and 1.75 g of soil were placed into 100-mL Erlenmeyer flasks containing 40 mL of either with or without 10 mgP/L for testing and control sets, respectively. These flasks were put into the shaking incubator and mixed until equilibrium time was achieved. Phosphate concentrations were analysed according to the procedures outlined before.

5.8.3 Reduction of contaminants on fibreglass wick

Soil water samples were collected using a fibreglass wick no. 1381 (1.27 cm in diameter) that was supplied by Pepperell Braiding Company. Many researchers have shown that a fibreglass wick did not absorb and react to organic compounds, viruses, and colloids (Holder et al. 1991, Polentika et al. 1992, Rimmer et al. 1995 and Czigány et al. 2005) and it did not disturb the moisture content (Boll 1992, Rimmer et al. 1995 and Gee et al. 2004). However, these statements did not cover the case of wastewater.

The wick braiding process might add some impurities to the fibreglass wick. To prevent this, the wicks were treated with the procedure described by Holder et al. (1991). The impurities were completely removed by combustion at 400 ^{o}C for 4 hours. The cleaned wick was cut into 40 cm length which would cause the least disturbance to pressure head and moisture content (Knutson et al. 1993). The prepared wick is shown in Figure 5.6.

Figure 5.6 Treated fibreglass wick

Tests of reduction of contaminants on fibreglass wick were adapted from Czigány et al. (2005). The experimental set up was illustrated in Figure 5.7. The fibreglass wicks were placed into plastic funnels. The top 4.5 cm was unwoven and individual braids were spread in the funnel. Half of the total wick was placed inside the funnel to keep it in place. The wastewater was fed through the funnel at a constant rate of 17.8 cm^3/h. The top of the funnel was covered with plastic wrap to prevent evaporation and natural aeration. The wastewater storage vessel was placed on a magnetic stirrer and stirred constantly while being poured. The contaminants of interest consisted of nitrate, TKN, ammonia-nitrogen, soluble phosphate, suspended solids and *E.Coli*.

Figure 5.7 Test of reduction of contaminants on fibreglass wick

5.9 Summary

Samples of medium grained sand and topsoil were collected and their characteristics were determined using the procedures from AS/NZS, USDA, and other methods derived from the literature. Raw domestic wastewater and its filtrated samples were analysed according to the APHA standard methods. Sand and soil columns were fabricated for the laboratory and pilot scale testing using the design criteria from the AS/NZS standard and other literature.

Tests were undertaken in two modes, one a continuous flow test and the other a batch test. Further, the continuous tests were classified into laboratory and pilot scale tests. Laboratory scale soil column tests were carried out to observe the contaminant transport behaviour by advection and dispersion. Pilot scale soil column tests were investigated to observe the contaminants transport with retardation. Batch experiments were investigated to determine the soil hydraulic properties, adsorption of phosphorous, and the suitability of fibreglass wicks for sampling the pore water.

The results obtained from these experiments will be discussed in Chapters 6 to 8.

CHAPTER 6

PRELIMINARY AND BATCH TESTS

6.1 Introduction

The preliminary tests were carried out to determine the characteristics of sand and soil and properties of domestic wastewater. Batch tests presented in this chapter included the determination of soil hydraulic properties and phosphate adsorption coefficients and the suitability of the fiberglass wicks for soil water sampling. The results obtained from these tests are discussed in this chapter.

6.2 Characteristics of sand and soil

The physical appearances of sand and soil are presented in figure 6.1. The medium grained sand was light yellow whereas the topsoil sample was dark brown.

Figure 6.1 Samples of medium grain sand and soil

The physical and chemical properties of sand and soil samples are given in Table 6.1. The laboratory data is presented in Appendix-D. Sand was high in density, rigid and had high permeability. It contained low mineral and organic matter. Conversely, soil was quite loose, mix grained and had low permeability. It contained high Cation Exchange

Capacity (CEC), Electrical Conductivity (EC), organic matter, nitrogen and phosphorus compounds that originated from degraded organic materials.

Table 6.1 Characteristics of sand and soil samples

Parameters	**Materials**	
	Sand	**Topsoil**
Physical properties		
Particle size analysis		
- sand (%)	100	37.51
- silt (%)	0	43.79
- clay (%)	0	18.70
Textural classification	sand	loam
Hydraulic conductivity (cm/h)	6.466	0.662
Specific gravity	2.65	2.55
Bulk density (g/cm^3)	1.79	1.28
Void ratio	0.49	0.74
Porosity	0.33	0.43
Moisture content (%)	0.121	5.00
Chemical properties		
pH (1:5)	6.874	7.134
Cation exchange capacity (meq/100 g)	0.142	17.49
Organic carbon (%)	0.026	5.15
Organic matter (%)	0.397	9.61
Total nitrogen (mg/g soil)	0.086	1.76
Total phosphorus (mg/g soil)	0.246	3.41
EC (1:5) (mohs/cm)	0.002	0.13

6.3 Characteristics of domestic wastewater

The physical appearances of pre-settled wastewater and soil-filtrated samples are shown in Figure 6.2. The settled wastewater was quite clear. It contained some amount of suspended solids. The soil-filtrated samples were very clear and their colour was pale yellow. The characteristics of the pre-settled wastewater are provided in Table 6.2. The results of laboratory analysis are given in Appendix-E.

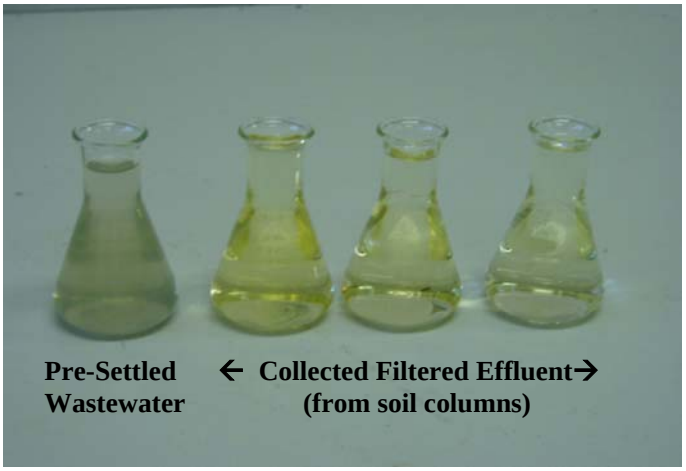

Figure 6.2 Samples of domestic wastewater and filtered effluent

Table 6.2 Characteristics of wastewater in a pre-sediment tank

Parameter	Number of samples	Range of conc.	Average conc.	Deviation*
Physical Properties				
EC (μmohs/cm)	24	483-1648	955	267
Temperature (^{o}C)	24	19- 26	23	1.8
Chemical Properties				
pH	24	6.6-7.6	7.3	0.22
SS (mg/L)	26	15-116	50	27
DO (mg/L)	16	0.00-0.57	0.17	0.17
COD (mg/L)	24	168-326	249	34
TKN (mg/L)	17	33-87	56	11
NH_4-N (mg/L)	24	23-80	49	14
Org-N (mg/L)	17	0.4-28	12	8
NO_3-N (mg/L)	24	0.17-2.3	1.1	0.58
PO_4-P (mg/L)	24	2.2-9.2	4.7	1.6
Biological Properties				
Faecal Coliforms (cfu/100 mL)	13	$5.70x10^5$-$4.14x10^6$	$2.05x10^6$	$1.15x10^6$

Note: * Standard deviation was evaluated using the non-bias method.

The electrical conductivity, EC was 483-1648 μmohs/cm. In common septic systems, the ECs were reported to be in the range of 1150-1350 μmohs/cm (UWS laboratory cited in Geary 2003). The actual value of EC of wastewater depends on the source of water supply, the amount of dilution from rainfall and infiltration into sewers (if any) as

well as on the amount of soluble ions added using household use. A lower average value obtained in this study is typical of the domestic wastewater from a centralised wastewater collection system. The concentration of dissolved oxygen, DO concentration was 0.00-0.57 mg/L with an average value of 0.17 mg/L. This suggested that the storage tank was operated under anaerobic conditions similar to that encountered in septic tank effluent. For example the effluent discharged from a typical septic tank contained DO with the concentration of 0.2-0.6 mg/L (UWS laboratory cited in Geary 2003).

As settled wastewater was kept under anaerobic conditions, the pH of the wastewater sample might be expected to drop significantly due to the fermentation process (Sawyer et al. 1994). Nevertheless, the pH of pre-settled wastewater was approximately 6.6-7.6, and was close to neutral. This indicated that the wastewater contained pH buffer constituents such as bicarbonate and carbonate, and the buffer constituents might be present in excess of that destroyed by the acid released by the fermentation process. The suspended solids, SS concentration was in the range of 15-116 mg/L with an average value of 50 mg/L. It varied greatly. This might be a result of dilution related to rainfall as well as pre-sedimentation of the wastewater. This wastewater however contained high organic carbon as measured by the chemical oxygen demand, COD. The COD concentration varied from 168 to 294 mg/L. The estimated concentration of biochemical oxygen demand, BOD was 67-176 mg/L based on the COD/BOD ratio at 0.4-0.6, which was proposed by Metcalf and Eddy (2003).

The domestic wastewater also contained high concentrations of nutrient constituents. The concentrations of total Kjeldahl nitrogen, TKN and ammonia nitrogen, NH_4-N were 56 and 49 mg/L, respectively. The ratio of NH_4-N/TKN was approximately 0.87. This indicated that the nitrogen in the wastewater was mainly in the form of ammonia. The NH_4-N concentration observed here was lower than that reported by the Department of Health in Victoria (1976 cited in Brouwer 1983), that was 72 mg/L. In addition, the concentration of nitrate nitrogen, NO_3-N was 1.1 mg/L and is similar to the normal concentration of nitrate of approximately 0.9 mg/L encountered in domestic wastewater (U.S.EPA 1978 cited in Brouwer 1983). The pre-settled wastewater contained soluble phosphate, PO_4-P with a concentration of 2.2-9.2 mgP/L. The soluble phosphate in the settled wastewater varied widely. The significant change of phosphorus concentration might due to the use of heavy duty synthesis detergents that sometimes contain over

50% of phosphate (Sawyer et al. 1994). The soluble phosphate observed from the pre-settled wastewater was much higher than the critical level (0.005 mg/L) which could potentially stimulate the algal bloom (Sawyer et al. 1994). The faecal coliform was found to be $2.05x10^6$ cfu/100 mL, this value was in a normal range. Department of Local Government (1998) reported that the faecal coliform was found with the range of 10^5-10^7 cfu/100mL in septic tank effluent.

The characteristics of this domestic wastewater varied over time. Low concentrations of wastewater were often observed during periods of rainfall that might be a result of dilution.

6.4 Determination of soil hydraulic properties

The hydraulic properties of sand and soil were observed in batch tests. The laboratory data are presented in Appendix-F.

6.4.1 Sand water retention curve

The observed hydraulic properties data are presented in Figure 6.3.

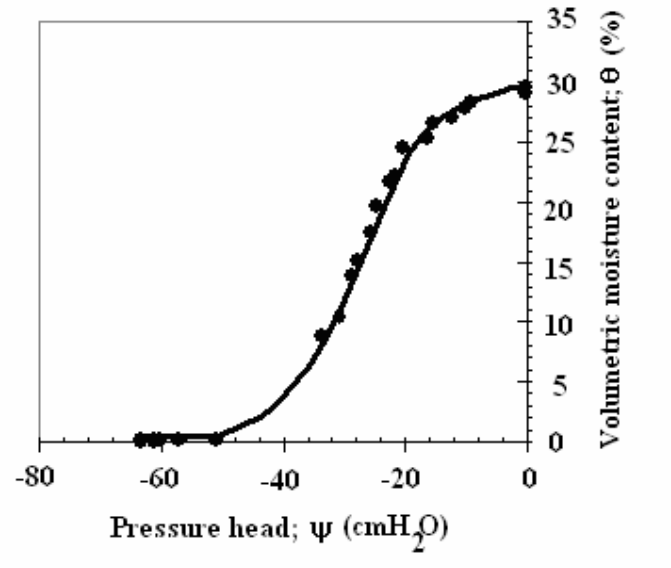

Figure 6.3 Pressure head versus volumetric moisture content in sand

This plot generated saturated, θ_s and residual moisture content, θ_r that were 0.3 and 0.001, respectively. The possible range of θ_s and θ_r of sand was 0.30-0.40 and 0.05-0.10, respectively (Broadbridge and White 1988). Both values were in the possible range.

The fingerprint of an unstable front in sand is presented in Figure 6.4. The uniform sharp dried front approached the tensiometer for 55 minutes, with the pressure head of –3.02 cmH_2O. The reading was constant until filtration was stopped (after 500 minutes). The constant pressure head after the wetting front passes indicated that the water moved downward, and the sand column was in equilibrium of inflow-outflow. This constant pressure head equalled the fully saturated permeability (Dingman 1994 and Bauters et al. 1998).

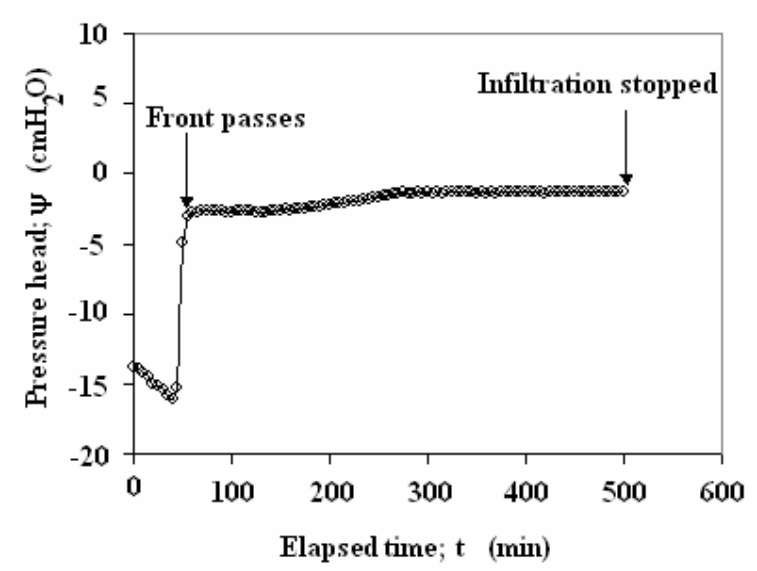

Figure 6.4 Time series of the pressure head in sand

The relative permeability, $K_{zz}k_{rw}$ was determined using Kunze's equation (Equation 3-18) (Fredlune and Rahardjo 1940). The calculated permeability, $(K_{zz})_{cal}$ was obtained using Darcy's equation with the result being 1.225×10^{-5} m/s (or 4.4082 cm/h). The measured permeability, $(K_{zz})_{mea}$ was 1.796×10^{-5} m/s (or 6.4656 cm/h). The tests were conducted at 23 ^{o}C (room temperature). Water surface tension, T_S was 7.23×10^{-5} kN/m, water density, ρ_w was 997.57 kg/m^3 and viscosity, μ_w was 9.41×10^{-4} N-s/m^2 (Fredlune

and Rahardjo 1940). The graphical plot of pressure head (ψ) versus relative permeability ($K_{zz}k_{rw}$) is illustrated in Figure 6.5.

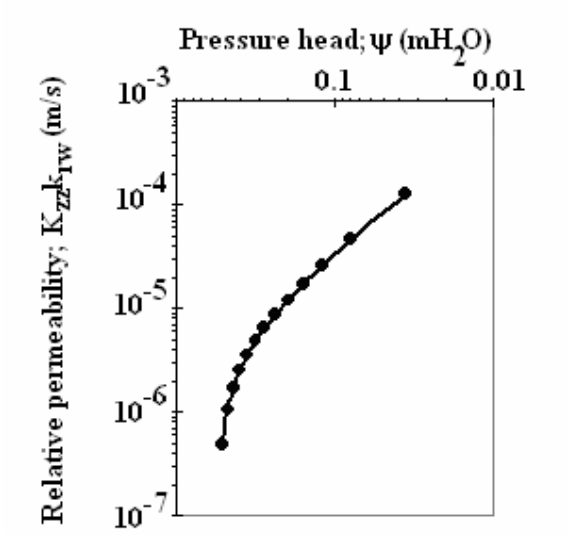

Figure 6.5 Hydraulic conductivity versus pressure head in sand

The term, $K_{zz}k_{rw}$ was 5x10^{-7}-1.5x10^{-4} m/s (or 0.18-54 cm/h). The ratio of $K_{zz}k_{rw}/K_{zz}$ indicates that parameter k_{rw} was 0.03-7.8. A realistic unsaturated condition was selected to produce a water retention curve. Only data from unsaturated soil condition $(0 \le k_{rw} \le 1)$ was considered.

Firstly, a water retention curve was fitted using van Genuchten's equations (Equation 3-10 and 3-11). The water retention curve obtained is presented in Figure 6.6. The empirical coefficients are given in Table 6.3. These coefficients were found to be in the acceptable range. However, the equations did not fit the observational data well, when sand was relatively dry (θ <0.1). This error might have been generated in the measurements. The jet filled tensiometer was sensitive to presence of air bubbles. When soil was relatively dry, air bubbles could pass through a porous tip of the tensiometer. These bubbles could potentially disturb the reading signal (Fredlune and Rahardjo 1940).

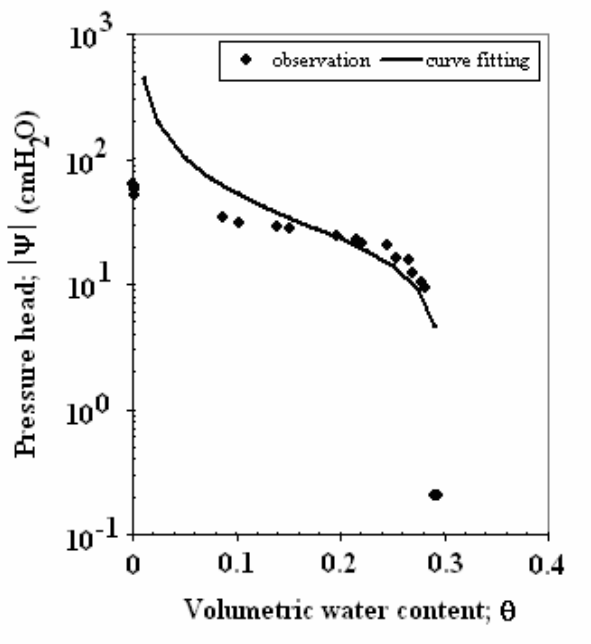

Figure 6.6 Water retention curve of sand sample fitted by VG equations

Table 6.3 VG empirical coefficients of sand

Sand hydraulic parameters	Carsel et al. (1988)	Calculation value
Saturated sand volumetric water content; θ_s	0.43	0.30
Residual sand volumetric water content; θ_r	0.045	0.07
Soil water retention function a (1/cm)	0.145	0.0446
Empirical parameter p	2.68	2.1636
Empirical parameter m	0.6269	0.5378

Secondly, the data was fitted using the Haverkamp et al. equations (Equation 3-7 and 3-8). The water retention curve is presented in Figure 6.7. The empirical coefficients were given in Table 6.4. There were significant differences between the literature and experimentally observed values. These differences may be due to the difference of particles size of sand used between this research and Haverkamp et al.'s tests.

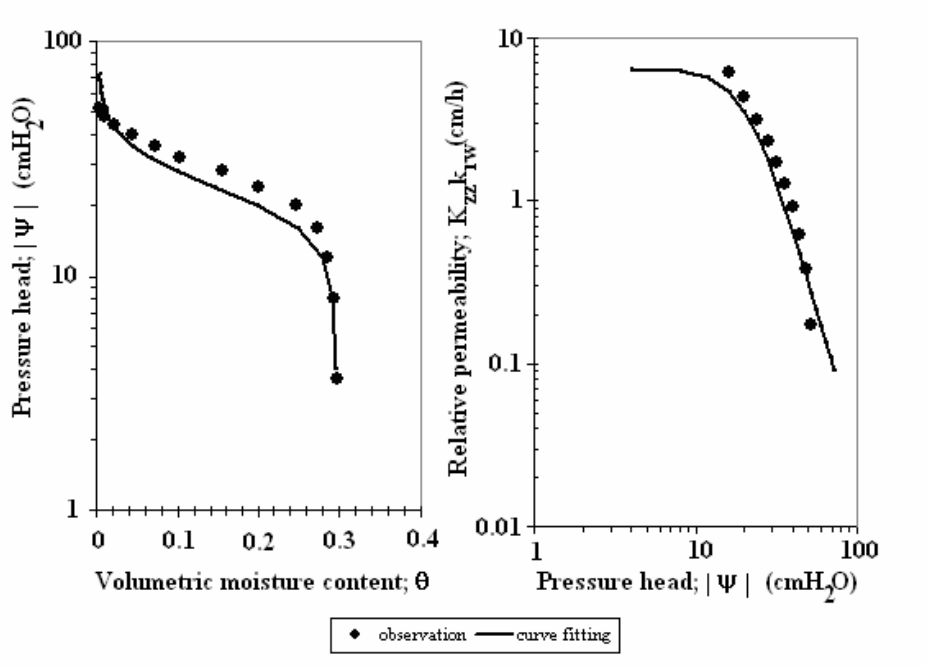

Figure 6.7 Water retention curves of sand sample fitted by HV equations

Table 6.4 HV empirical coefficients of sand

Sand hydraulic parameters	Haverkamp et al. (1977)	Calculation value
Saturated sand volumetric water content; θ_s	0.287	0.30
Residual sand volumetric water content; θ_r	0.075	0.07
Empirical parameter A	1.175×10^6	4.04×10^4
Empirical parameter α	1.161×10^6	6.83×10^5
Empirical parameter β	3.96	4.2424
Empirical parameter γ	4.74	3.4765

6.4.2 Soil water retention curve

The plot of pressure head (ψ) versus moisture content (θ) is given Figure 6.8. The results indicated that ψ increased slightly when θ was less than 0.12. After this point, ψ increased sharply and the soil column reached fully saturated conditions.

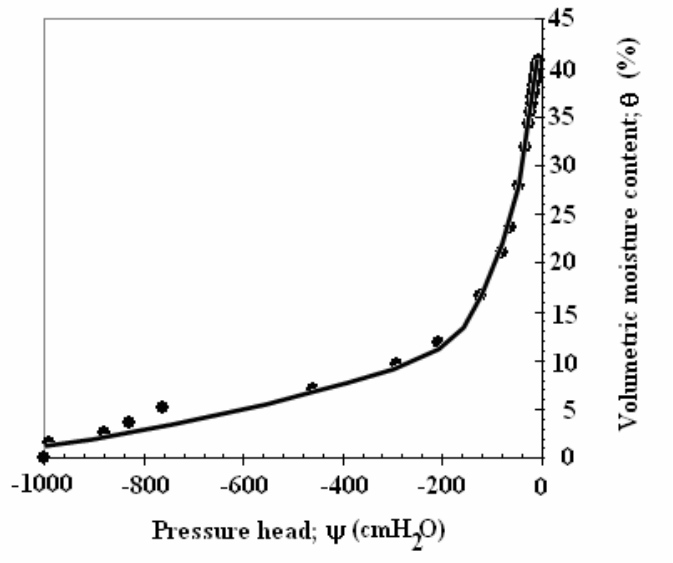

Figure 6.8 Pressure head versus volumetric moisture content in soil

The fingering phenomenon of wetting front infiltration through soil is shown in Figure 6.9. The uniform wetting front was observed after 35 minutes. The pressure head was constant at –2.48 cmH_2O. After stopping infiltration, the pressure head still remained the same as the front passed. The pressure head oscillates sharply before the front passes. The high pressure head gradient at this part led to high Darcy's velocity (Bauters et al. 1998). It can be seen that the front pass took only a short period to reach to the observation point.

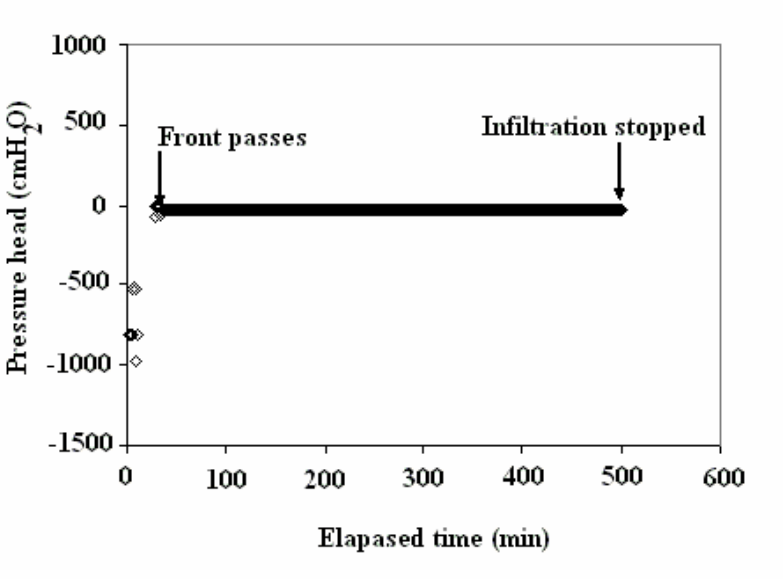

Figure 6.9 Time series of the pressure head in soil

The term $K_{zz}k_{rw}$ was estimated using Kunze's equation. The soil column was operated under the same temperature as the sand column. Thus, the parameters T_S, ρ_w and μ_w were same values as the sand column. The variable $(K_{zz})_{cal}$ was 1.84x10^{-6} m/s (or 0.6624 cm/h). The variable, $(K_{zz})_{mea}$ was determined from the feeding rate of the peristaltic pump, which was 1.32x10^{-6} m/s (or 0.4756 cm/h). The plot of $K_{zz}k_{rw}$ versus θ is given in Figure 6.10.

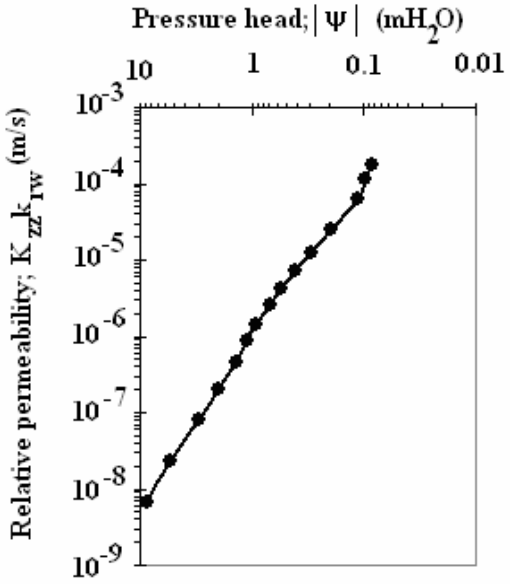

Figure 6.10 Hydraulic conductivity versus pressure head in soil

The terms $K_{zz}k_{rw}$ was 8x10^{-9}-2x10^{-4} m/s (or 2.88x10^{-3}-72 cm/h). The ratio of $K_{zz}k_{rw}/K_{zz}$ varied from 0.004 to 108. The k_{rw} observed using this ratio showed a wide variation that might result from a less uniform distribution of particles (Fetter 1992). The composition of the soil was a mixture of clay, silt and sand. The fine particles of clay and silt could resist the movement of water for a long time. Both underflow and overflow could be observed in the soil column (Bauters et al. 1998).

Firstly, the water retention curve was fitted using the van Genuchten (1980) equations as presented in Figure 6.11. The empirical coefficients are given in Table 6.5. A good fit was obtained between the observed and the calculated results. The coefficients were closer to the value given by Carsel et al. (1988).

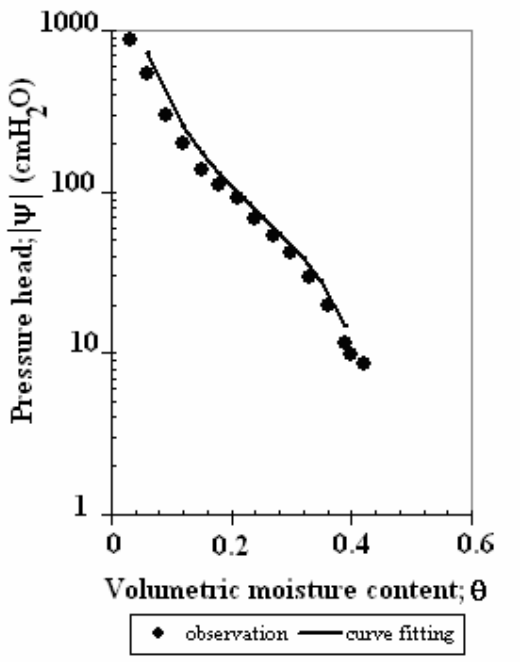

Figure 6.11 Water retention curve of soil sample fitted by VG equations

Table 6.5 VG empirical coefficients of soil

Soil hydraulic parameters	Carsel et al. (1988)	Calculation value
Saturated soil volumetric water content; θ_s	0.43	0.42
Residual soil volumetric water content; θ_r	0.078	0.04
Soil water retention function *a* (1/cm)	0.036	0.0249
Soil water retention function *p*	1.56	1.6740
Empirical parameter *m*	0.359	0.4026

Secondly, the hydraulic properties data were fitted using the Haverkamp et al. (1977) equations. The water retention curve is presented in Figure 6.12. The data could be fitted well using HV equations. The empirical coefficients are given in Table 6.6. Only the empirical coefficients of light Yolo clay were available from the literature. These coefficients were totally different. However, the empirical coefficients A, α, β and γ in the soil samples utilised were between sand and Yolo clay.

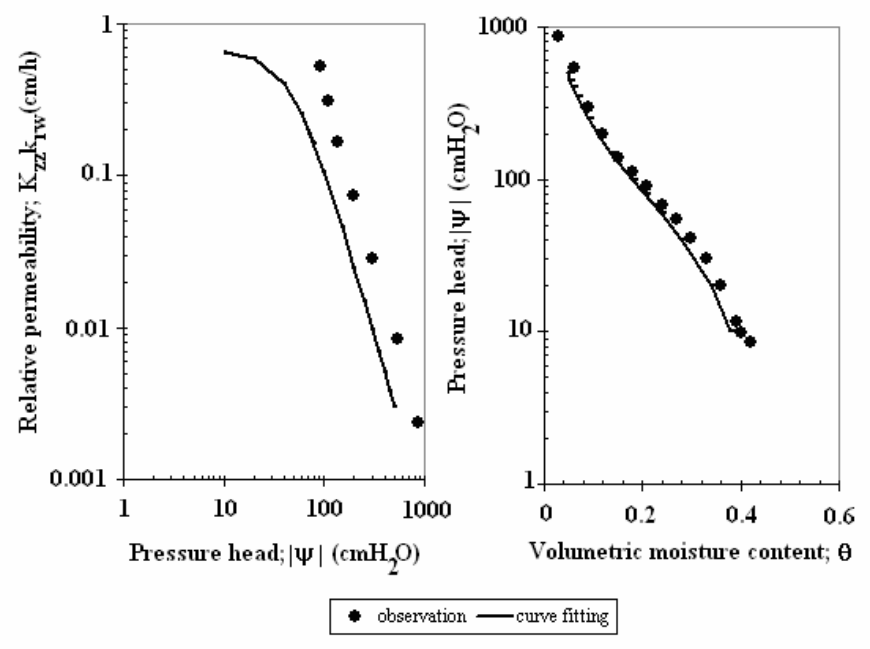

Figure 6.12 Water retention curves of a soil sample fitted by HV equations

Table 6.6 HV empirical coefficients of soil

Soil hydraulic parameters	Haverkamp et al. (1977)	Calculation value
Samples	Yolo light clay	Loam
Saturated sand volumetric water content; θ_s	0.495	0.42
Residual sand volumetric water content; θ_r	0.124	0.04
Empirical parameter A	124.6	8.27×10^3
Empirical parameter α	739	1.20×10^2
Empirical parameter β	4.00	1.1045
Empirical parameter γ	1.77	2.3181

Both HV and VG equations could fit most of the experimental data. However, the differences were believed to stem from the nature of measurement using an initially saturated tensiometer. The truncation error generated from the measurement was also acceptable. Observation indicates that the VG equations were less sensitive to an increase of moisture content than the HV equations. This might relate to the parameters defined in the VG equations that excluded the relative hydraulic conductivity. The coefficients obtained from both equations will be utilised to calculate the specific moisture content, M_C presented in Richards' equation.

6.5 Determination of soil phosphate sorption coefficients

Figure 6.13 presents a plot of the phosphate concentration versus observation time. The soluble phosphate reached the adsorption equilibrium within 8 hours. This concentration reduced slowly until 24 hours elapsed. The phosphate removed was approximately 80% of the initial phosphate concentration. The final phosphate concentration was found to be 1.9 mgP/L. An equilibrium time of phosphate sorption was 24 hours. The observation data were given in Appendix-G.

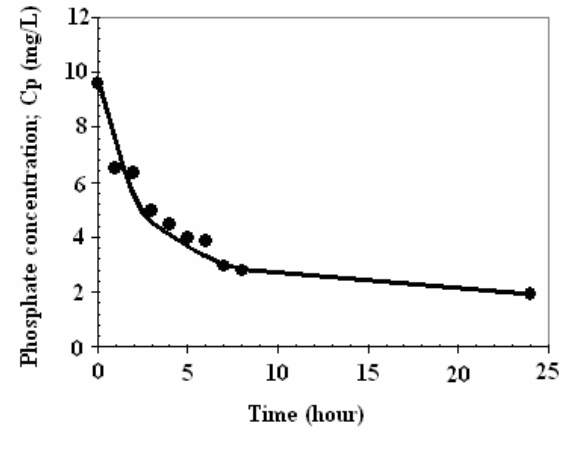

Figure 6.13 Phosphate adsorption equilibrium time

Figure 6.14 presents the plot of phosphate concentration versus weight of soil. The results indicated that more phosphate was adsorbed if more soil was added.

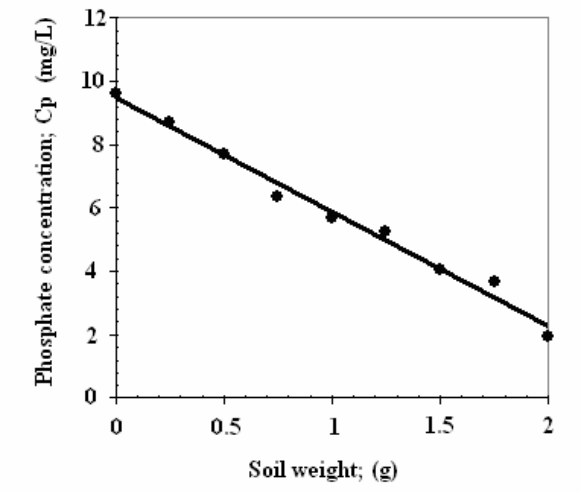

Figure 6.14 Soluble phosphate versus soil weight

The adsorption isotherms were fitted using linear sorption and Langmuir's and Freundlich's equations. The best fit was selected from the greatest regression (R^2-value). Among these isotherms, Langmuir's equation was the best fit. The adsorption isotherm is presented in Figure 6.15.

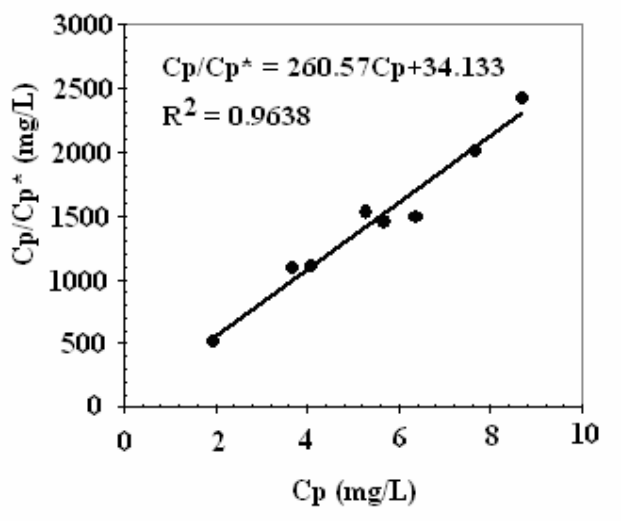

Figure 6.15 Langmuir plot of soil-phosphorus adsorption isotherm

The kinetic coefficients k_M and k_L and Langmuir isotherm equation were obtained as follows.

$$C^* = \frac{k_L k_M C}{1 + k_M C} \qquad = \frac{0.029297 C_P}{1 + 7.634 C_P} \tag{6-1}$$

Therefore the retardation factor was:

$$r_P = 1 + \frac{\rho_B}{n}\left(\frac{0.029297}{(1 + 7.634 C_P)^2}\right) \tag{6-2}$$

The phosphate concentration in domestic wastewater was very low (4.7mg/L or 4.7×10^{-9} g/cm^3). The phosphate adsorption rate obtained in this soil was 1.091 (based on the soil bulk density of 1.25 g/cm^3 and the porosity of 0.4). To simplify the system, the term $(1 + 7.634 C_P)^2 \approx 1.00$ the first order kinetic rate was assumed as:

$$r_P = 1 + \frac{\rho_B (0.029297)}{n} \tag{6-3}$$

By comparison, the kinetic retardation rate obtained from Equation 6-3 was greater than the one obtained from Equation 6-2, only 8.24×10^{-6} %. This difference was negligible.

6.6 Suitability of fibreglass wick for soil water sampling technique

The fibreglass wick could develop natural capillary tension. It could be applied as passive capillary samplers (PCAPs). The wick was woven from fibreglass, which behaves as a porous media. The additional filtration mechanism from fibreglass filaments might impact on the constituents in the soil pore water. Thus, the reduction of contaminants was considered in this section. The experimental data are provided in appendix-G.

6.6.1 Absorption of wastewater in fibreglass wick

Figure 6.16 presents the flow rate, the accumulated and the discharging volume of the influent and effluent through the fibreglass wick.

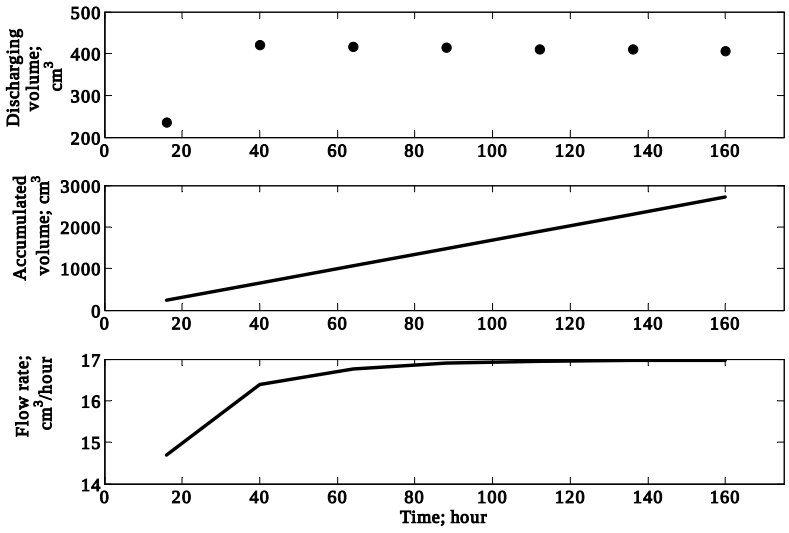

Figure 6.16 Discharging and accumulated effluent volume and flow rate over time

A closed system was set up in this experiment. The loss of feeding wastewater influent due to evaporation was very low. The inflow and outflow in the system were 2848 and

2716 cm^3, respectively. Based on the water balance, water lost was approximately 132 cm^3. This may have been absorbed in the filaments of fibreglass wick. The absorption was only 4.6% of the total feeding wastewater. This indicates that the fibreglass wick was hydrophobic material that did not retard the flow of wastewater. The effluent outflow rate increased over time. It was 14.7, 16.4, 16.8 and 16.9 cm^3/h within 16, 40, 64 and 88 hours, respectively. The outflow rate was remained constant at 17.0 cm^3/h, until the test was finished. The wastewater could have accumulated in the fibreglass wick at the equilibrium of inflow and outflow to value of 58.4 cm^3. By calculation, the travel time of wastewater in this 40-cm long fibreglass wick was 3.4 hours.

6.6.2 Reduction of suspended solids in fibreglass wick

The physical appearances of raw wastewater and filtered samples are illustrated in Figure 6.17.

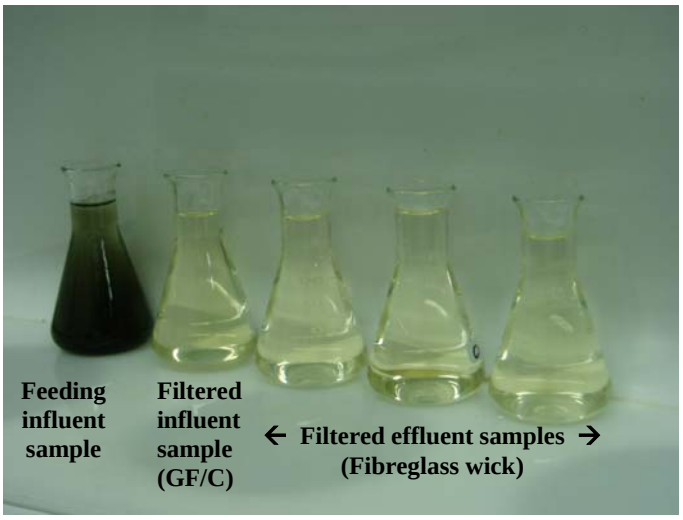

Figure 6.17 Wastewater influent and filtered samples

As raw wastewater passed through the fibreglass wick, the SS was completely removed. Obviously, filtered samples were very clear and its colour was pale yellow. This was the same colour as in a sample filtered through glass fibre filter paper (GF/C). It was the true colour of wastewater that originated from impurities. The SS reduction is given in Figure 6.18. The concentration of SS found in the filtered sample was less than 0.2 mg/L whereas in the raw wastewater sample it was 60-280 mg/L.

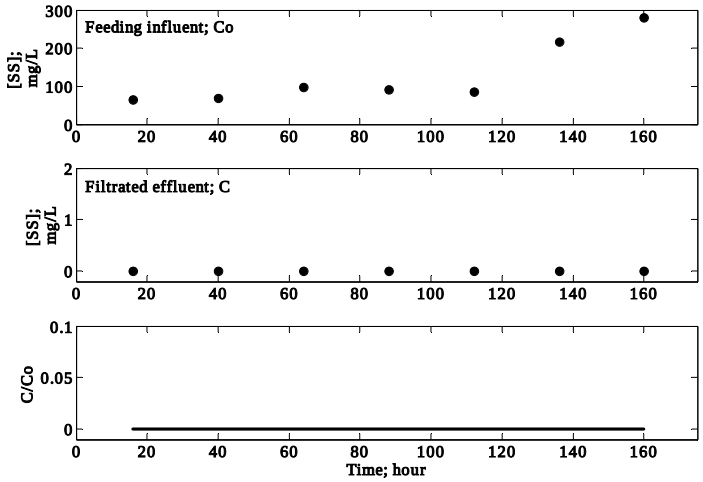

Figure 6.18 Reduction of SS through the fibreglass wick

6.6.3 Effect of fibreglass wick filtration processes on pH and EC

Figure 6.19 presents pH and EC profiles over the observation time. pH of feeding wastewater was neutral to slightly alkaline, however the pH's of the filtered samples were moderately alkaline. An increase in pH might relate to the nature of the wastewater containing ammonia and hydroxide. The EC value did not significantly change during the filtration processes. It was confirmed that the soluble salts did not react with the fibreglass wick.

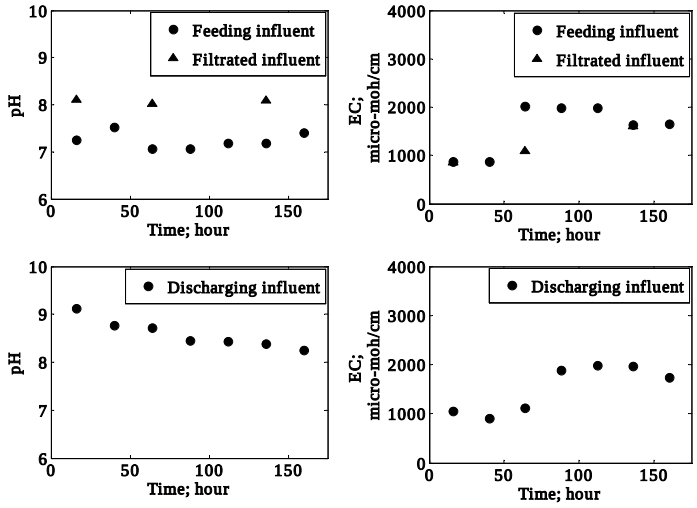

Figure 6.19 Changes of pH and EC with time during the fibreglass wick filtration process

6.6.4 Reduction of nitrogen compounds in fibreglass wick

The ammonia concentration profiles are presented in Figure 6.20. The ammonia concentration, reduced only 1-3 mg/L, after percolating through the fibreglass wick. The reduction was equivalent to 3-7% of the feeding concentration. Due to the short retention time, the loss of ammonia might result from ammonia-releasing processes. The increase of pH in the filtered samples might relate to ammonia reduction. At pH above 8.0, the ammonia could be liberated freely (Sawyer et al. 1994).

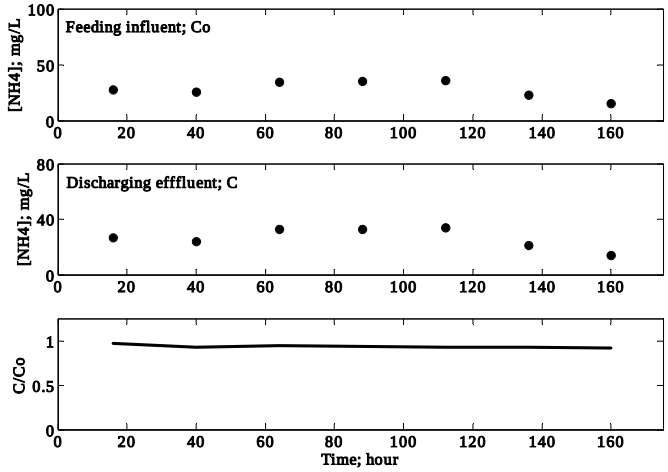

Figure 6.20 Reduction of ammonia through the fibreglass wick

The change of nitrate concentration is given in Figure 6.21. The nitrate concentrations in the influent varied from 0.5 to 1.0 mg/L. The effluent contained nitrate with concentrations of 0.6-0.9 mg/L. The concentration increased 0.1-0.3 mg/L in the effluent sample. By comparison, the ammonia concentration decreased 1-3 mg/L. This suggested that only 3% of nitrate increased from the ammonia oxidation processes. However this number was very small and was negligible.

The balance of nitrogen might be evaluated from the Total Kjeldahl Nitrogen, TKN. Concentration profiles of TKN are presented in Figure 6.22. Low concentrations of TKN were found in the filtered samples. These samples contained only the soluble TKN as the SS were completely removed by fibreglass filaments. Concentrations of soluble TKN of GF/C paper filtered samples (C_F) were 40-52 mg/L. The ratio $(C_O-C_F)/C_O$ confirmed that 94% of TKN was contained in the SS. The C/C_F ratio was 1.1 which

showed that soluble TKN contained in the fibreglass wick and GF/C paper filtered samples were same. Thus, the fibreglass wick did not remove any soluble TKN from the raw wastewater.

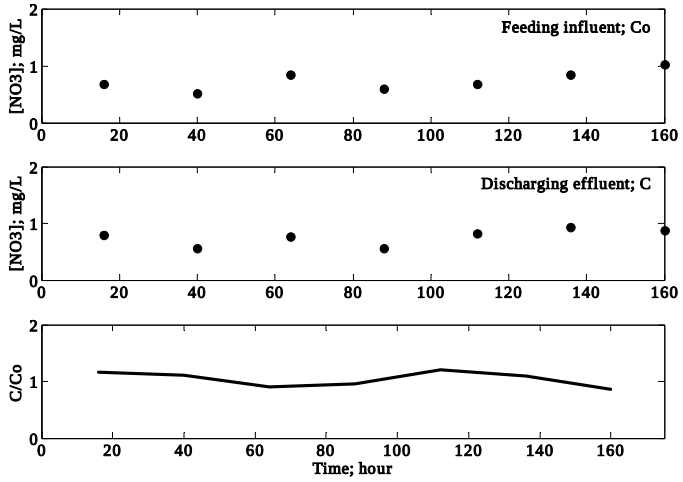

Figure 6.21 Reduction of nitrate through the fibreglass wick

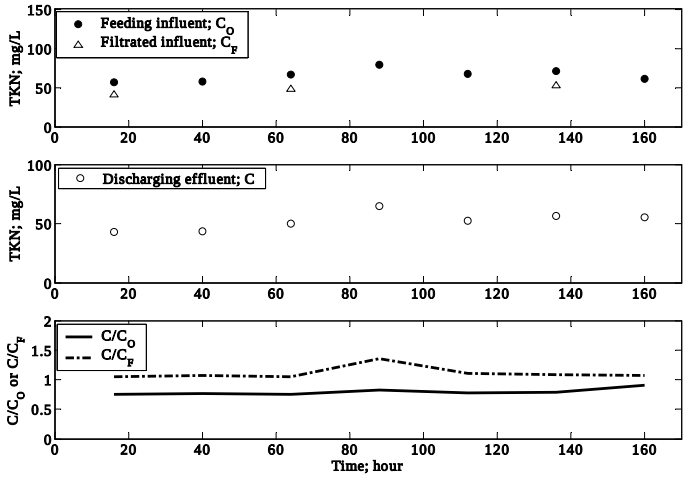

Figure 6.22 Reduction of TKN through the fibreglass wick

Figure 6.23 shows the change to the organic nitrogen, Org.-N with time. The Org.-N concentrations in influent and effluent samples were 238-660 and 16-41 mg/L, respectively. Soluble Org.-N concentration was estimated from GF/C paper filtered samples which were 13-19 mg/L. The ratio of C/C_F was 1.2. This value indicates that the fibreglass wick and GF/C paper filtered samples were same. The fibreglass wick did

not impact on the soluble Org.-N. The ratio of $(C_O-C_F)/C_O$ reveals that 60% of Org.-N was contained in the SS.

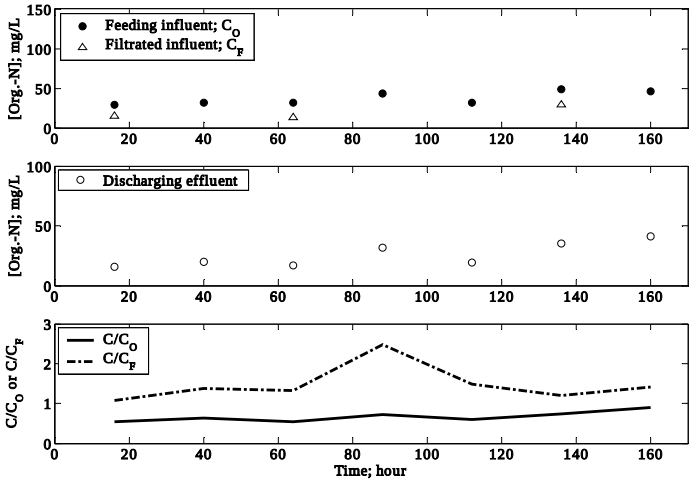

Figure 6.23 Reduction of organic nitrogen through the fibreglass wick

6.6.5 Reduction of COD in fibreglass wick

The concentration of Chemical Oxygen Demand, COD measured in influent and effluent samples varied in the ranged of 230-660 and 230-246 mg/L, respectively. The COD concentration found in the influent sample included organic SS that increased the total COD. Soluble COD in the influent was determined from GF/C filtered samples. The averaged soluble COD concentration was 228 mg/L. The ratio of C/C_F was found to be 1.0. The fibreglass wick and GF/C paper filtered samples were the same in quality. Fibreglass wick did not absorb any soluble COD. This finding agreed well with Holder et al.'s experiments (1991) showing that the fibreglass wick did not absorb any organic compounds. The ratio of $(C_O-C_F)/C_O$ suggested that 27% of COD was contained in the SS. Thus, removing of the SS potentially contributes to a reduction of COD, if high levels of organic SS are contained in the raw wastewater. The results are presented in Figure 6.24.

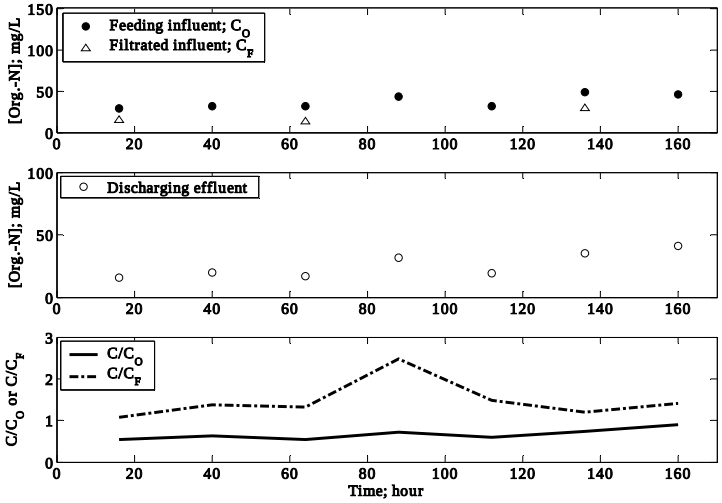

Figure 6.24 Reduction of COD through the fibreglass wick

6.6.6 Reduction of phosphate compounds in fibreglass wick

The reduction of soluble phosphate is presented in Figure 6.25.

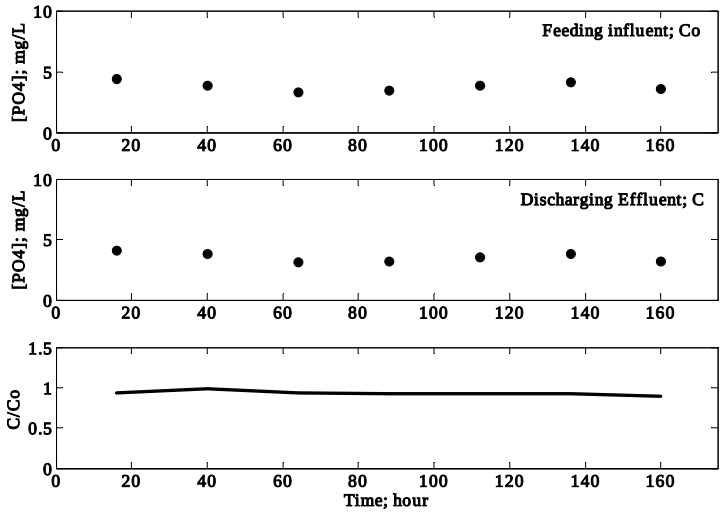

Figure 6.25 Reduction of phosphate through the fibreglass wick

The average concentrations of phosphate in the influent and effluent were 3.8 and 3.5 mg/L, respectively. The phosphate reduction might result from precipitation and electrochemical processes. The fibreglass filament contained silica, and these particles were negatively charged. The positive ions were potentially collected by the negative

charge of the filament (Czigány et al. 2005). Coincidentally, the phosphate ion (PO_4^{3-}) has highly negative charges and could be deposited on the edge of silica covered fibre. Fibreglass wicks could remove phosphate up to approximately 7% of the initial concentration. This reaction may contribute to a reduction of soluble phosphate.

6.6.7 Reduction of *E.Coli* in fibreglass wick

The reduction of *E.Coli* by the fibreglass wick is shown in Figure 6.26. The numbers of *E.Coli* in influent and effluent were $2.89x10^6$ and $6.95x10^4$ cfu/100mL, respectively. Low numbers of *E.Coli* in filtered samples related to the removal of SS. The *E.Coli* remaining in the filtered wastewater was estimated from GF/C paper filtered samples and was $5.04x10^4$ cfu/100mL. The ratio of C/C_F indicated that the fiberglass wick could remove *E.Coli* at 45% less efficiency than the GF/C paper. This might result from the density of these filter materials. GF/C paper was denser than the fiberglass wick (Whatman 2005). Certainly, it gave higher removal efficiency than the fiberglass wick did. The ratio $(C_O-C_F)/C_O$ confirmed that 96% of *E.Coli* were attached on the organic SS. *E.Coli* preferred to be attached on SS as they could obtain the substrates for their living cells (Sparks 1995).

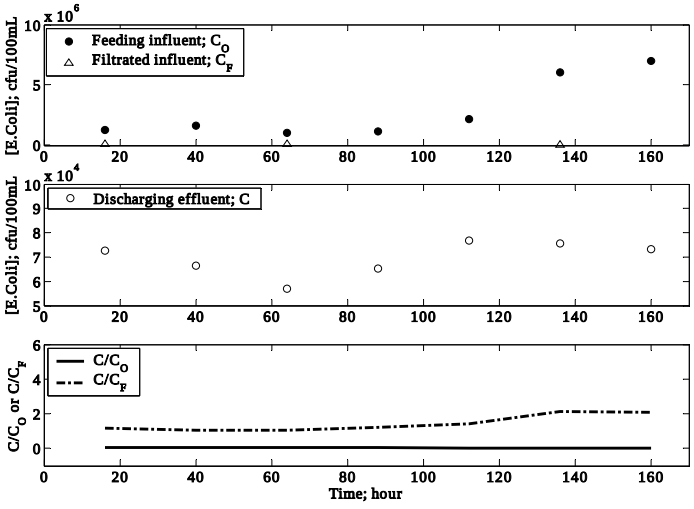

Figure 6.26 Reduction of *E.Coli* through the fibreglass wick

The fibreglass wick did not react with any soluble contaminants and it did not absorb any wastewater. The quality of filtered samples obtained from the fibreglass wick was the same as the filtered sample obtained from GF/C paper. The fibreglass wick was

found to be suitable for conducting the experiments with wastewater containing very low organic SS concentrations.

6.7 Summary

The characteristics of the media and the wastewater used in this research were described in the preliminary tests. Sands were the uniform, non-reactive porous media and soils were the non-uniform, reactive porous media. The domestic wastewater used in this research contained high concentrations of organic carbon, nitrogen, phosphorus compounds and *E.Coli*. Most water quality parameters were found to be similar to effluents from typical septic tanks. However, the wastewater quality depended on the weather. Rainfall dilutes the wastewater and thus changes its characteristics.

The batch tests described the hydraulic properties of the media, phosphate adsorption and the contaminant reduction on fiberglass wicks. The hydraulic properties of sand and soil were fitted using Haverkamp et al. (1977) and van Genuchten (1980) equations. Both equations corresponded to the laboratory determined hydraulic properties of sand and soil. The coefficients of hydraulic properties were in the possible range. The study of phosphate adsorption suggested soil could retard phosphate effectively. The coefficients of the phosphate adsorption were governed by Langmuir's isotherm equation, as this was the best fit. The properties of fibreglass wicks were tested. The results indicated that fiberglass wicks were suitable to sample soluble contaminants from soil pores. They did not absorb wastewater and transmitted the filtered wastewater quickly.

CHAPTER 7

LABORATORY SCALE SOIL COLUMN TESTS

7.1 Introduction

The results obtained from the laboratory scale tests of sand and soil columns are presented and discussed in this chapter. The experiments contained the studies of advection and dispersion transport. The developed models using Richards' equation and non-reactive contaminant transport were applied to simulate the laboratory data. The simulations corresponded well to these observations. Flow in various conditions resulted in different Darcy's velocities that led to non-linear and time varying transport processes.

7.2 Advection transport in the laboratory scale sand column

The column tests were classified into three types of flow as follows: gravitational infiltration, static equilibrium of capillary force, and infiltration-redistribution system. The detailed results are given in Appendix-H.

7.2.1 Gravitational infiltration system

The simulation of advection transport in a gravitational system was undertaken using Richards' equation. The input parameters are given in Table 7.1.

Table 7.1 Input parameters for water movement through a sand infiltration column

Parameters	Values
Domains	20 cm
Boundary conditions	Refer to the pressure head reading
Hydraulic properties	Refer to coefficients of HV and VG
Time domain	8 hours
Number of time step; *nt*	Varies from 300 to1200 steps per hour
Nodal spacing; *dz*	0.25 cm

Firstly, the HV equation was applied to support the calculation of M_C presented in Richards' equation. The simulations of hydraulic pressure head profiles are given in Figure 7.1. The simulation matched well with the observation. The averaged Darcy's velocity on the column surface at 0.5, 1.0, 2.0 and 3.0 hours were -0.0081, -0.0328, -0.0814 and -0.1227 cm/h, respectively. As time increased, Darcy's velocity increased. The increase of velocity was non-linear and time varying. The wetting fronts reached the elevations of 17.5, 10.0 and 5.0 cm within 0.5, 2.0 and 3.0 hours, respectively. The estimated travel time of water that passed through the 20-cm deep sand layer was 4.0 hours.

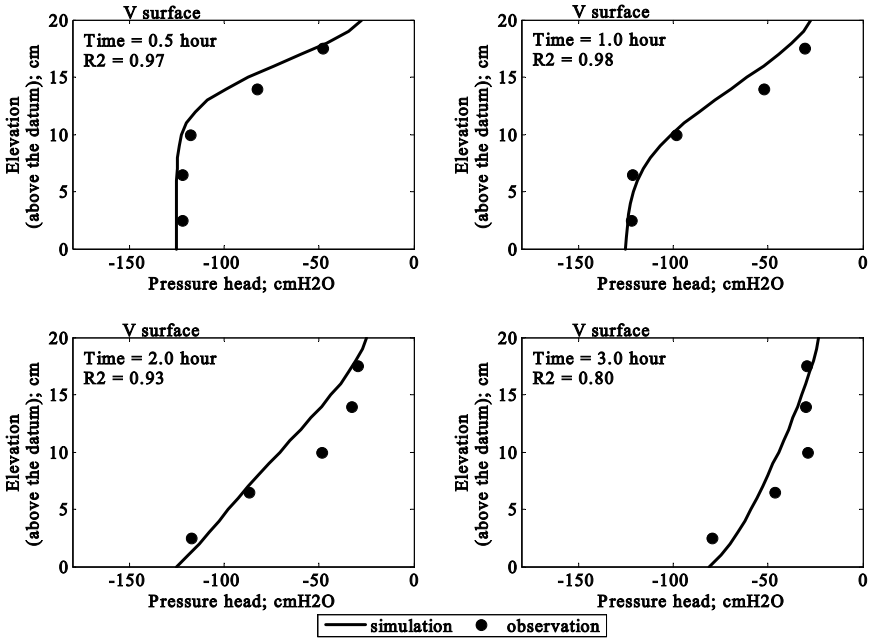

Figure 7.1 Pressure head profiles in a sand infiltration column simulated using Richards' and HV equations (datum at the column base).

The moisture content profiles are presented in Figure 7.2. There was a significant error in the prediction of moisture content. The simulations were much lower than the observations. This might be due to the moisture content being governed as indicated by the hydraulic properties equations. The moisture contents observed were 0.1-0.2. At this range of moisture content, the hydraulic properties equation could generate moisture contents that were 19-39% lower than the measured moisture content resulting in an underestimation. Coincidently, the residual squares indicated that the differences

between the simulations and observations were in the range 18-34%. In addition, the HV equations did not support to the water movement through initially dry soil (Haverkamp et al. 1977). The travel time of the water could not be estimated when these unclear wetting fronts were indicated.

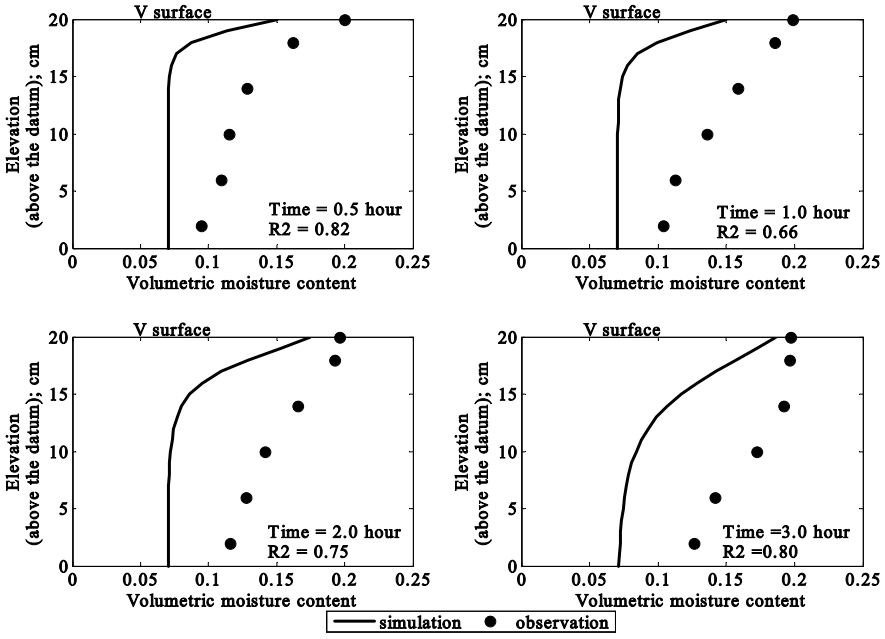

Figure 7.2 Moisture content profiles in a sand infiltration column simulated using Richards' and HV equations (datum at the column base).

The distribution of pressure head over time is shown in Figure 7.3. There was good agreement between the identified boundaries and the numerical solutions. Based on the hydraulic properties of sand, an equilibrium of inflow and outflow should be obtained when the pressure head, ψ was -1.8x10^{-3} cmH_2O (K_{zz}=1.8x10^{-3} cm/s). However, the maximum pressure head observed was -29.5 cmH_2O. This pressure head was closer to the capillary pressure of -26.4 cmH_2O (Wurbs and James 2001). This might indicate that water inside the soil pores was in a stable condition under the influence of both surface tension and gravitational forces (Freudlune and Rahardjo 1940). So, excess water moved downward according to gravitational force. The water would pass through the 20-cm deep sand layer within 4.0 hours.

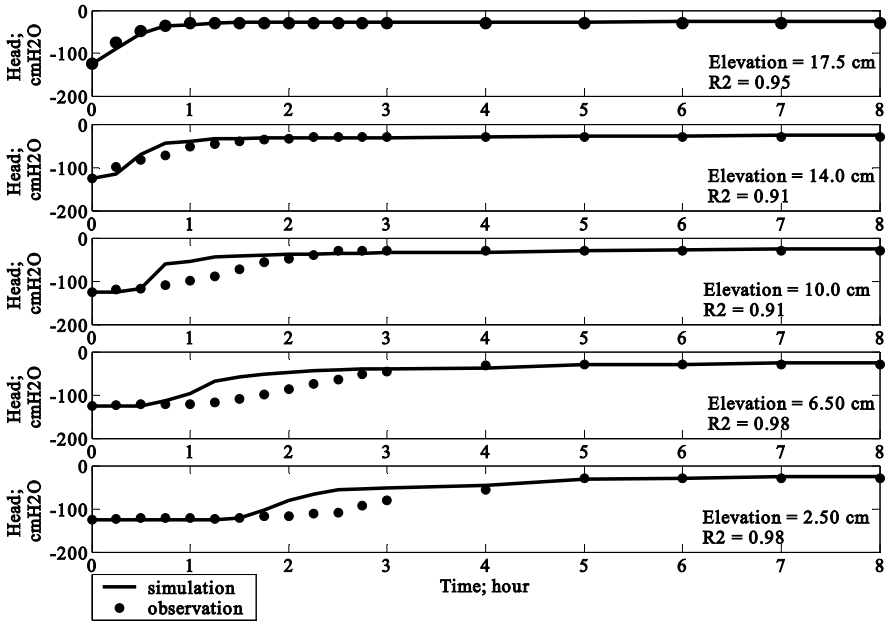

Figure 7.3 Simulation of time series of elevated pressure head in a sand infiltration column using Richards' and HV equations (datum at the column base).

Secondly, Richards' and the VG equations simulated the pressure head profiles in the column tests. The results are presented in Figure 7.4. The averaged Darcy's velocity at the column surface at 0.5, 1.0, 2.0 and 3.0 hours, was -0.0064, -0.0316, -0.0801 and -0.1216 cm/h, respectively. These velocities were close to the previous simulation that used the HV equations. Darcy's velocity was also non-linear and time varying. The simulation clearly described the wetting front movement. The saturation zone was at the elevations of 17.5, 10.0 and 2.5 cm at 0.5, 1.0 and 3.0 hours, respectively. The estimated travel time of water in this 20-cm deep sand layer was 3.8 hours.

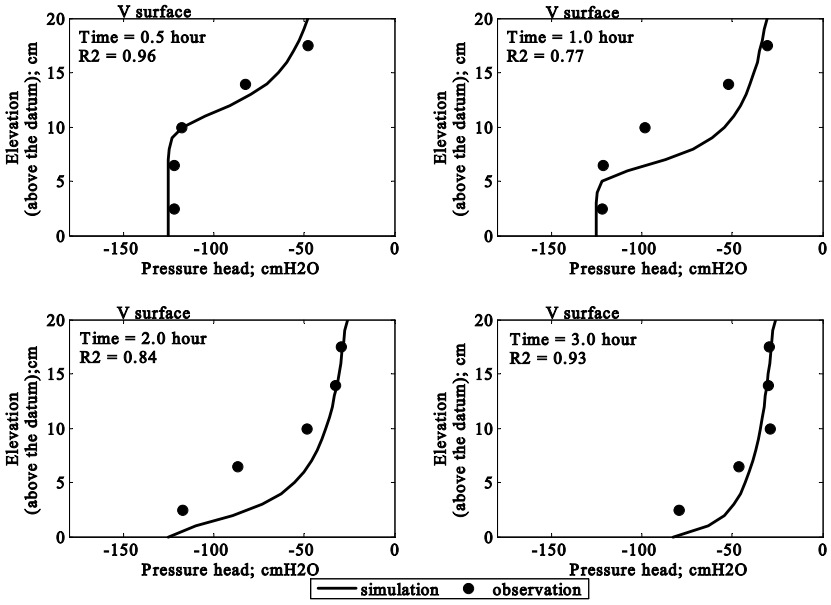

Figure 7.4 Pressure head profiles in a sand infiltration column simulated using Richards' and VG equations (datum at the column base).

Richards' and VG equations were applied to simulate the moisture content profiles. The simulations are given in Figure 7.5.

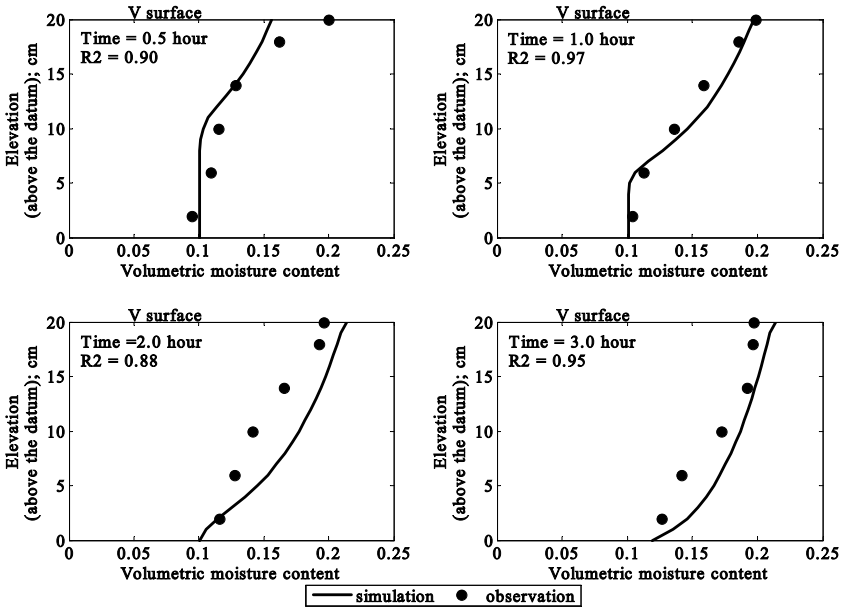

Figure 7.5 Moisture content profiles in a sand infiltration column simulated using Richards' and VG equations (datum at the column base).

The simulations corresponded well to the observations. As water was added to the column surface, the moisture content increased gradually. The wetting front was observed at the elevations of 15.0, 7.5 and 2.5 cm within 0.5, 1.0 and 2.0 hours, respectively. The estimated travel time of water through the 20-cm deep sand layer was 3.8 hours. Pressure head and moisture content profiles generated the same estimated travel time.

Figure 7.6 presents the pressure head distribution over time. The simulations matched well with the observations. The whole column reached full saturation within 4 hours. The maximum storage capacity was 0.33 and the maximum pressure head was -29.5 cmH_2O. It was observed that the maximum storage capacity equalled the porosity. This indicated that the feeding water could fill all pores (Cullen and Everett 1995).

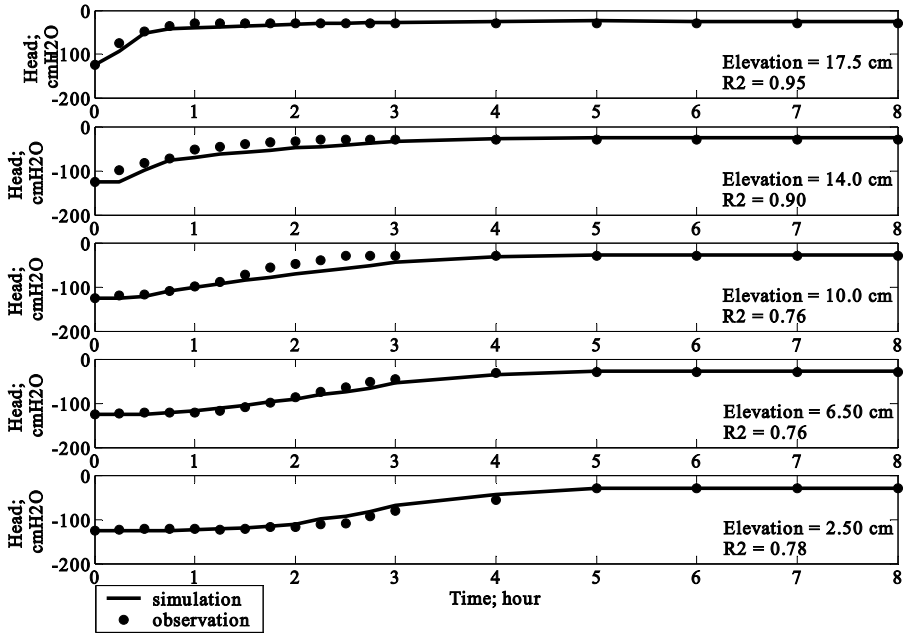

Figure 7.6 Simulation of time series of elevated pressure head in a sand infiltration column using Richards' and VG equations (datum at the column base).

The travel time of water through the 20-cm deep sand layer was better estimated by the pressure head profiles. Simulations obtained using Richards' and HV and VG equations generated the estimated travel times of 4.0 and 3.8 hours, respectively.

7.2.2 Static equilibrium capillary force system

The pressure head and moisture content distributions under static equilibrium of capillary forces were estimated using the capillary height equation (Equation 4-71). The input parameters are given in Table 7.2.

Table 7.2 Input parameters for static equilibrium of a sand column

Parameters	Values
Domains	20 cm
Boundary conditions	Refer to the pressure head reading
Hydraulic properties	Refer to coefficients of HV and VG
Time domain	3 hours
Number of time step; *nt*	Varies from 300 to 1200 steps per hour
Nodal spacing; *dz*	0.25 cm

The simulated hydraulic pressure head and moisture content profiles are illustrated in Figure 7.7.

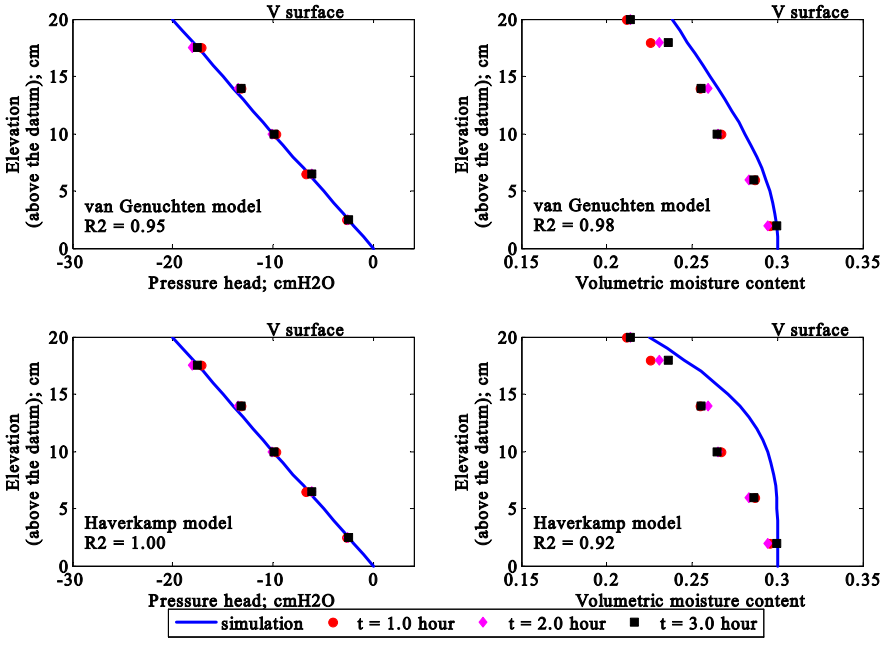

Figure 7.7 Static equilibrium of capillary force in a sand column (datum at the column base).

The pressure heads increased linearly from the column base to the surface. The maximum pressure head was 0 cmH_2O at the datum. The minimum pressure head was found at the surface of the column with the figure of -20 cmH_2O. The volumetric moisture content increased from 0.13 at the surface to 0.30 at the base of the column. The column achieved the equilibrium condition after the first hour. The capillary height, h_C was 20-24.6 $cmH_2O\left(\rho_w = 998 \;\; kg/m^3 and \;\; g = 9.81 \;\; m/s^2\right)$. The gradient of the hydraulic pressure head equalled 1.00. The trendline of pressure head profiles observed in the column was the same as for the physical model of capillarity.

7.2.3 Infiltration-redistribution system

The simulations of water movement in the infiltration-redistribution system were governed using Richards and HV or VG equations. The input parameters are given in Table 7.3. The pressure head at the upper boundary was assumed at the fully saturated condition. Using the Clapp and Hornberger (1978) equation, the pressure head at the upper boundary was -12.1±14.3 cmH_2O. This simulation applied -5.0 cm H_2O for the upper boundary pressure head. It was adequate to generate downward flow. The pressure head at the sharp front was evaluated using the equation of Green-Ampt (1911) (cited in Dingman 1994). The value was found to be -6.95± 8.0 cmH_2O, when the infiltration conductivity, k_f was 0.57.

Table 7.3 Input parameters for water movement through an infiltration and redistribution system in a sand column

Parameters	Values
Domains	20 cm
Boundary conditions	Initial conditions refer to the statical equilibrium of capillary force. The boundaries rely on the pressure head reading.
Hydraulic properties	Refer to coefficients of HV and VG
Time domain	3 hours
Number of time step; *nt*	Varies from 300 to 1200 steps per hour
Nodal spacing; *dz*	0.25 cm

The first simulations of water movement in the infiltration-redistribution system were obtained by using Richards' and HV equations. The results are presented in Figure 7.8. Averaged Darcy's velocity at 0.5, 1, 2 and 3 hours were -0.00041, -0.00084, -0.00109 and -0.00139 cm/h, respectively. Water percolated in this system more slowly than the gravitational system. This might result from redistribution that could retard the downward flow of water (Cullen and Everett 1995).

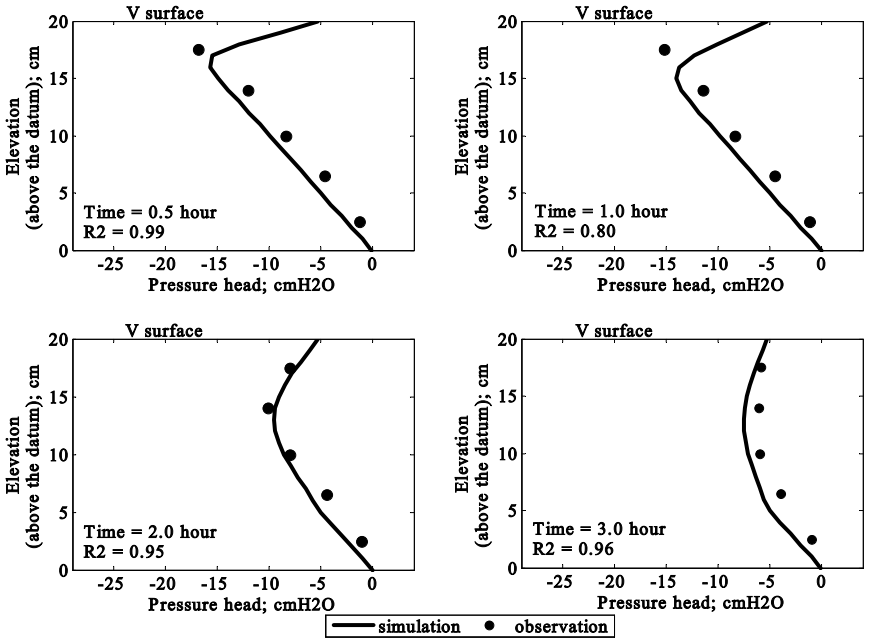

Figure 7.8 Pressure head profiles in a sand infiltration-redistribution column simulated using Richards' and HV equations (datum at the column base).

The simulations of moisture content are presented in Figure 7.9. Sand moisture content profiles were in a narrow range of 0.27-0.3. This indicated that the sand was relatively wet and the column was nearly in a fully saturation condition. The whole column may have been full of water, after 3 hours continuous feeding.

The second simulation for water movement in the infiltration-redistribution system was conducted using Richards and VG equations. The hydraulic pressure head profiles are given in Figure 7.10. Water percolated through this system very slowly. Darcy's velocities were -0.00147, -0.00231, -0.00290 and -0.00707 cm/h, at 0.5, 1.0, 2.0 and 3.0 hours, respectively.

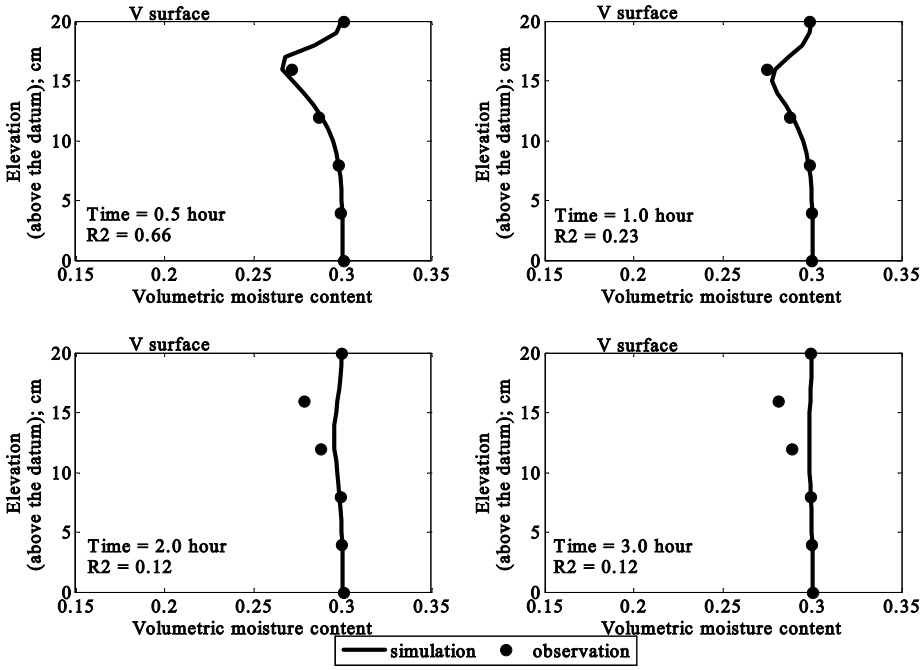

Figure 7.9 Moisture content profiles in a sand infiltration-redistribution column simulated using Richards' and HV equations (datum at the column base).

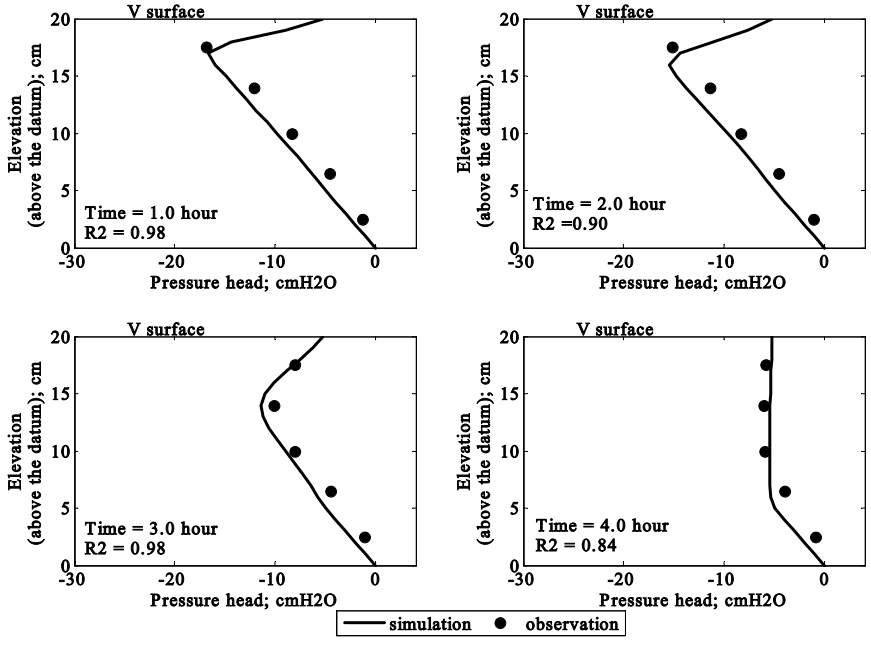

Figure 7.10 Pressure head profiles in a sand infiltration-redistribution column simulated using Richards' and VG equations (datum at the column base).

The volumetric moisture content profiles are presented in Figure 7.11. The simulations generated similar moisture content profiles to the observed data. Almost three quarters of the columns were full of water that rose due to the capillary force. The driest point of sand column appeared at the elevation of 17.5 and 13.5 cm, at 1.0 and 2.0 hours, respectively. The shape of the moisture content profiles was the same as for the pressure head.

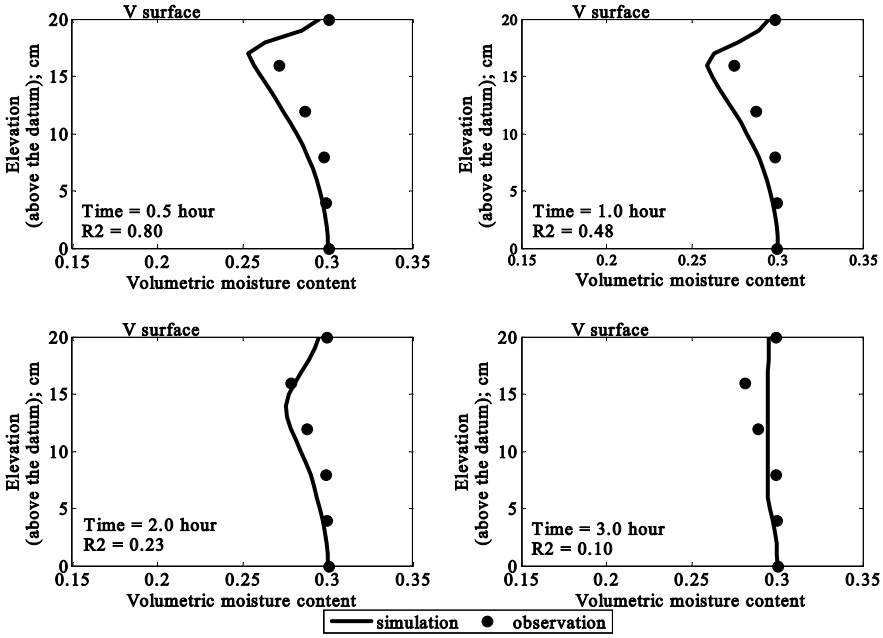

Figure 7.11 Moisture content profiles in a sand infiltration-redistribution column simulated using Richards' and VG equations (datum at the column base).

7.3 Advection transport in the laboratory scale soil column

The soil column tests were also separated into three parts as for the sand column tests. The observation results are given in Appendix-H.

7.3.1 Gravitational infiltration system

In this experiment, water percolated very slowly. The observations of the wetting fronts are presented in Figure 7.12. The saturated zone was formed after 8 hours of feeding, and this zone extended gradually. The whole column became fully saturated after 3 days of continuous feeding.

(a) (b) (c)

Figure 7.12 Movement of the wetting front in a soil column

(a) 24 hours, (b) 48 hours and (c) 72 hours

The movement of water in this infiltration soil column was simulated. The input parameters are given Table 7.4.

Table 7.4 Input parameters for water movement through a soil infiltration column

Parameters	Values
Domains	20 cm
Boundary conditions	Refer to the pressure head reading
Hydraulic properties	Refer to coefficients of HV and VG equations
Time domain	52 hours
Number of time step; *nt*	Varies from 600 to 2400 steps per hour
Nodal spacing; *dz*	0.25 cm

The first simulation was undertaken using Richards' and the HV equations. The pressure head profiles are presented in Figure 7.13. Darcy's velocities on the upper boundary at 8.0, 16.0, 24.0 and 52.0 hours, were $-4.6\text{x}10^{-6}$, $-4.6\text{x}10^{-3}$, $-5.8\text{x}10^{-3}$ and $-2.2\text{x}10^{-2}$cm/h, respectively. Darcy's velocity increased non-linearly over time. They were lower than the saturation hydraulic conductivity (0.662 cm/h). This indicates that

the movement of water through the soil infiltration column was still in a transient flow condition.

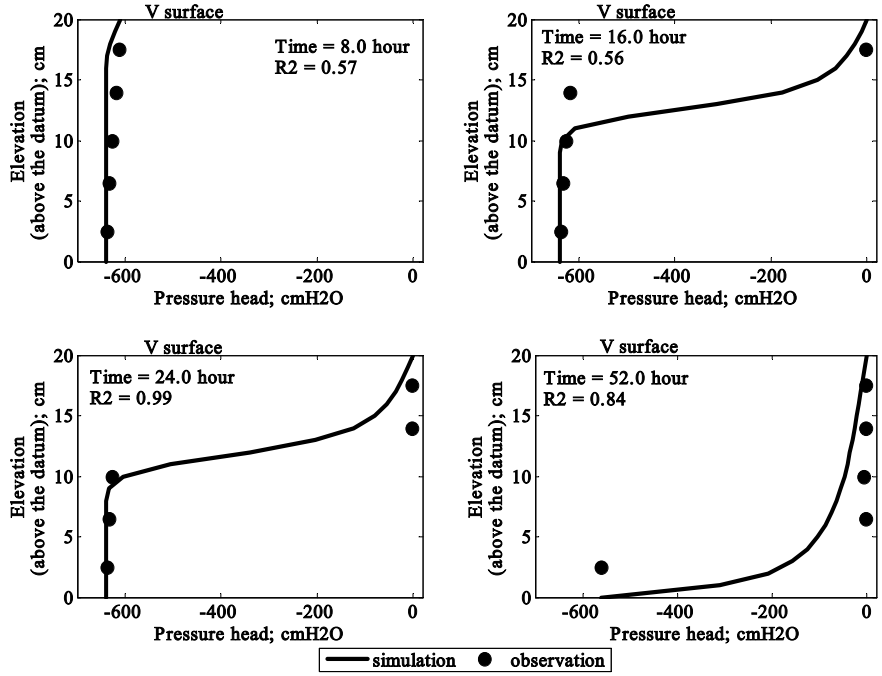

Figure 7.13 Pressure head profiles in a soil infiltration column simulated using Richards' and HV equations (datum at the column base).

After 16, 24 and 52 hours of continuous feeding, the saturation zone was observed at elevations of 16, 15 and 6.5 cm, respectively. The travel time of water through a 20 cm deep soil column was approximately 64-66 hours. The travel time was very long. The soil had a high porosity and its water storage capacity was also high. The maximum storage capacity was 0.43. This value was close to the porosity of the soil. Thus, the time to achieve the equilibrium of inflow and outflow in soil took longer than for sand.

The simulations of moisture content profiles are given in Figure 7.14. The results did not clearly indicate the wetting front. Similar to the sand column test, the HV equations underestimated the moisture content. This might confirm that the HV equations did not estimate the moisture content efficiently in an initially dry soil condition. So, the estimated travel time of water through this soil column could not be obtained from these moisture content profiles.

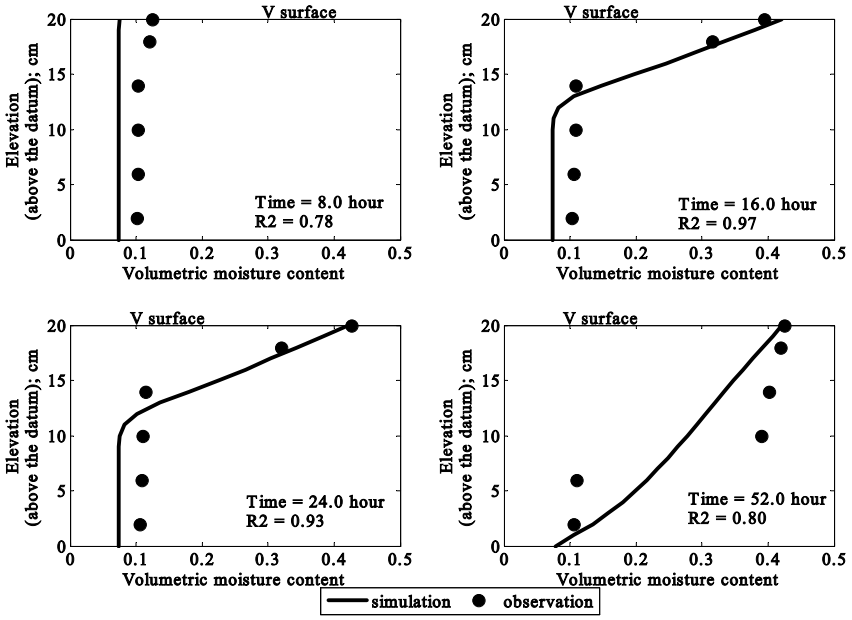

Figure 7.14 Moisture content profiles in a soil infiltration column simulated using Richards' and HV equations (datum at the column base).

The elevated pressure head over time was simulated. The results are shown in Figure 7.15.

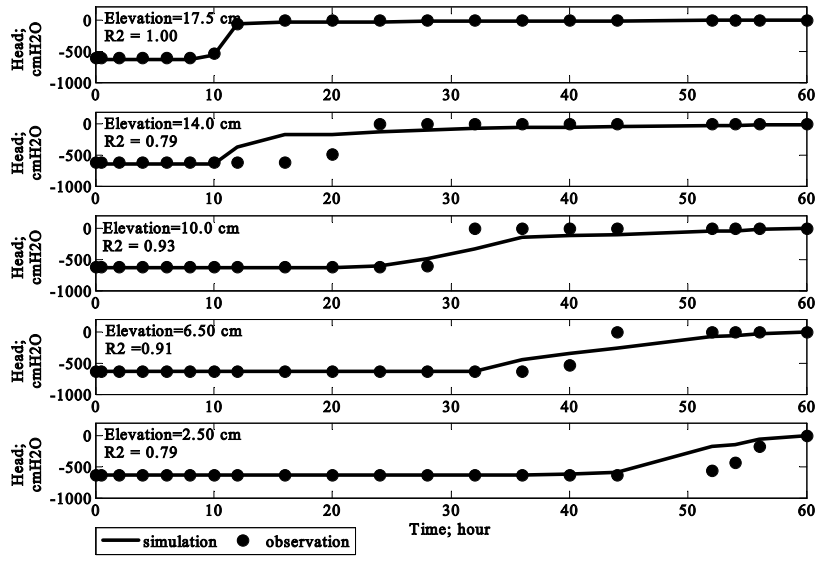

Figure 7.15 Simulation of time series of elevated pressure head in a soil infiltration column using Richards' and HV equations (datum at the column base).

The wetting front was observed at the elevations of 17.5, 14 and 2.5 cm within 12, 16 and 52 hours, respectively. The whole column was expected to reach a fully saturated condition within 60 hours. The maximum pressure head at the wetting front was -0.005 cmH_2O. It was close to the fully saturated hydraulic conductivity (-1.84×10^{-4} cm/s). This suggested that the soil column nearly reached the equilibrium of inflow-outflow.

The second simulation of water movement in a soil infiltration system was carried out using Richards' and the VG equations. The pressure head profiles are presented in Figure 7.16. The upper Darcy's velocities at 8.0, 16.0, 24.0 and 52.0 hours, were -1.1×10^{-7}, -6.3×10^{-3}, -7.5×10^{-2} and -5.2×10^{-2} cm/h, respectively. The velocities obtained here also increased non-linearly. The model estimated the movement of the wetting front precisely. The wetting front was observed at the elevations of 16, 14.5 and 5 cm within 16, 24 and 52 hours, respectively. The estimated travel time of water passed the 20-cm deep soil layer was 64-66 hours.

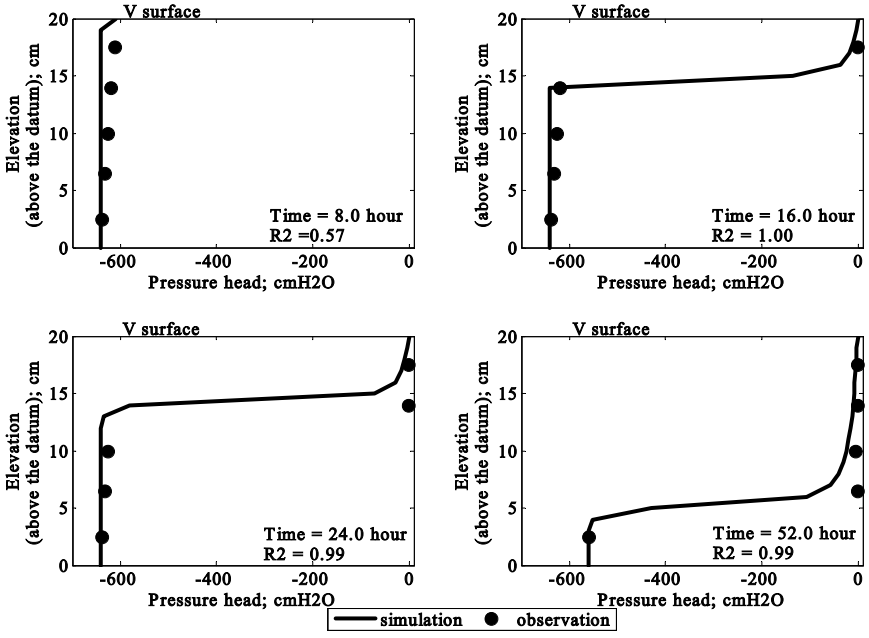

Figure 7.16 Pressure head profiles in a soil infiltration column simulated using Richards' and VG equations (datum at the column base).

Figure 7.17 presents the moisture content profiles obtained from both simulations and observations. The moisture content profiles had the same appearance as the pressure head profiles. The wetting zone was also located at elevations of 18, 16 and 10 cm at the

8, 16 and 52 hours, respectively. The estimated travel time through this 20-cm deep soil layer was 70 hours.

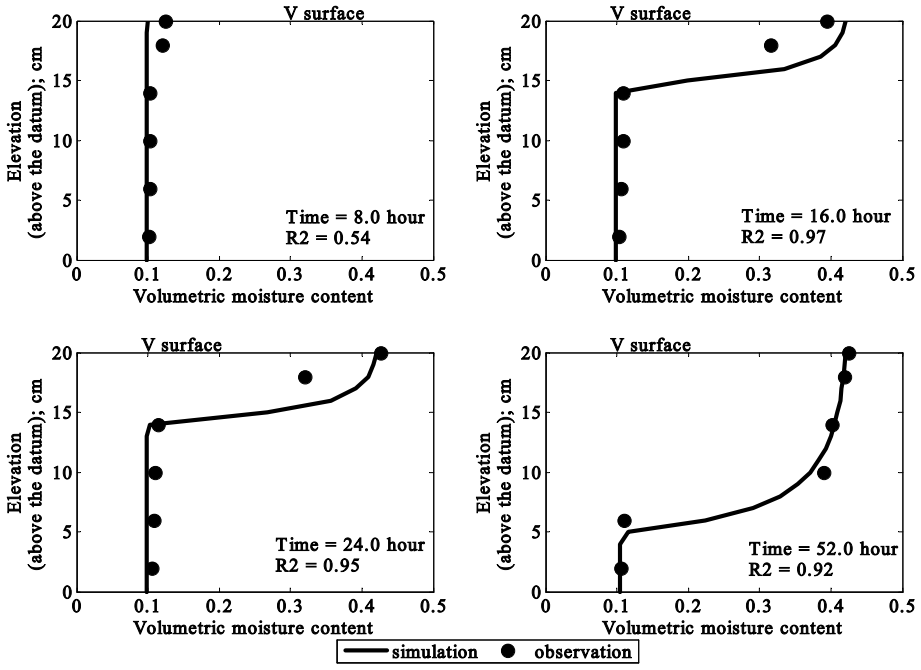

Figure 7.17 Moisture content profiles in a soil infiltration column simulated using Richards' and VG equations (datum at column base).

The distribution of hydraulic pressure head over time is provided in Figure 7.18. An excellent fit was observed at both upper and lower boundary conditions. The whole column might achieve fully saturated conditions within 60-72 hours. The maximum pressure head was -0.005 cmH_2O. It was close to the full saturation hydraulic conductivity. The column nearly reached equilibrium of inflow and outflow.

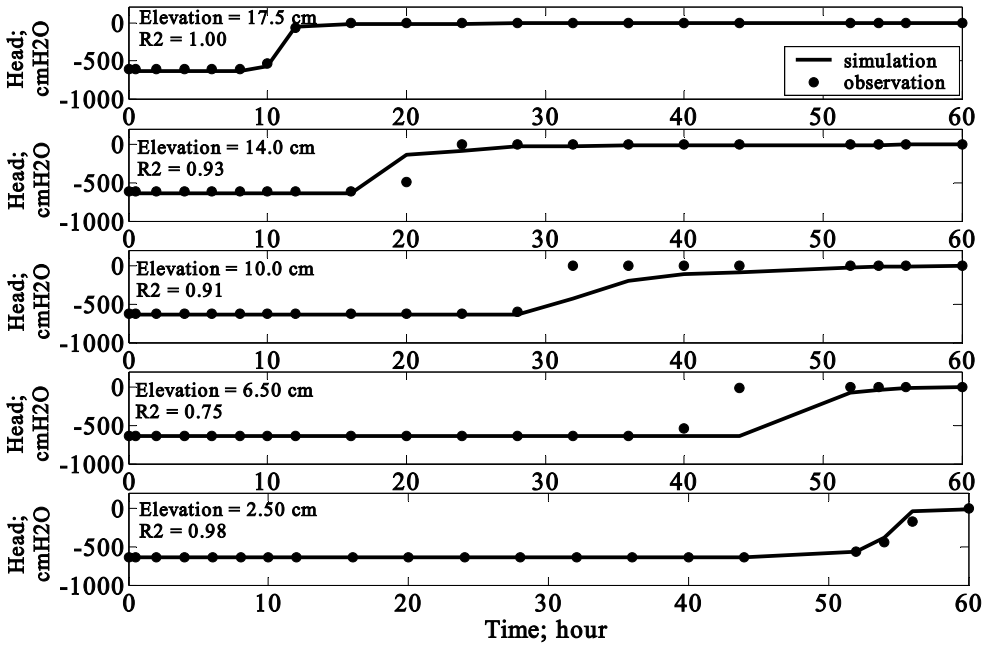

Figure 7.18 Simulation of time series of elevated pressure head in a soil infiltration column using Richards' and VG equations (datum at the column base).

The travel time could be better estimated using pressure head rather than moisture content profiles. The estimated travel time through the 20 cm deep soil layer was 64-66 hours. The travel time of water through the soil column was 18 times longer than sand, whereas the permeability of soil was 10 times lower than sand. The longer travel time might be the result of absorption of water inside soil particles and pores (Wierenga 1995).

7.3.2 Static equilibrium capillary force system

The input parameters for simulations of pressure head and moisture content in the system of static equilibrium of capillary forces are given in Table 7.5.

Table 7.5 Input parameters for static equilibrium of a soil column

Parameters	Values
Domains	20 cm
Boundary conditions	Refer to the pressure head reading
Hydraulic properties	Refer to coefficients of HV and VG equations
Time domain	6 hours
Number of time step; *nt*	Varies from 600 to 2400 steps per hour
Nodal spacing; *dz*	0.25 cm

The simulations and observations are presented in Figure 7.19.

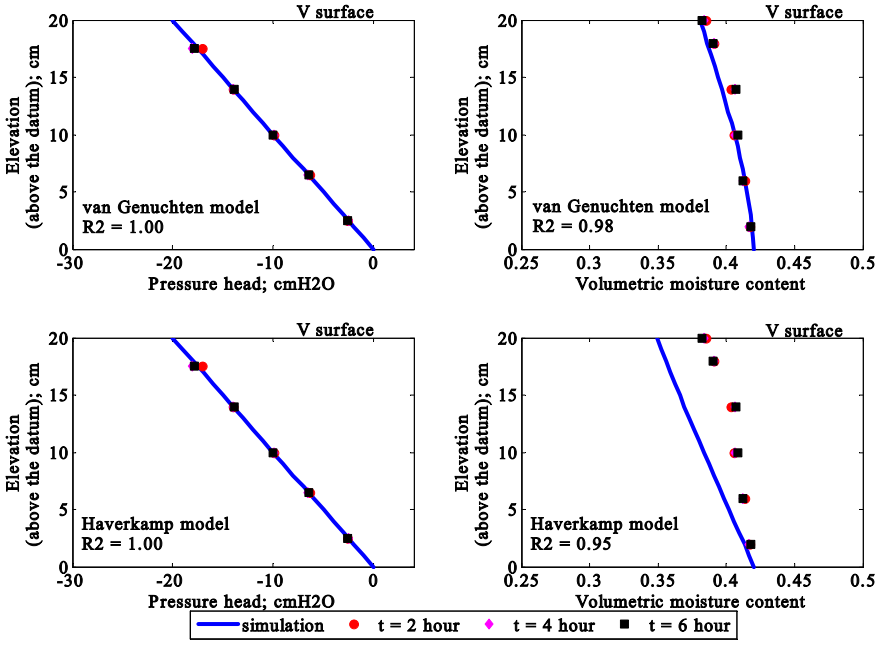

Figure 7.19 Static equilibrium capillary force in a soil column (datum at the column base).

Equilibrium of capillary pressure head was achieved after 2 hours soaking. The maximum hydraulic pressure head was 0 cmH_2O at the datum. The minimum was found at the soil column surface with the value of -19.9 cmH_2O. The distributions of pressure head in soil and sand were same. This confirmed that the static equilibrium condition relies on the capillary height. The capillary height of soil was 47.8 ± 51.2 cmH_2O

(Clapp and Hornberger 1978). The capillary height covered the thickness of the soil layer. It potentially pulled the water from the bottom to the surface of the soil column.

7.3.3 Infiltration-redistribution system

The applied pressure head at the upper boundary condition of the simulation was estimated using the Green-Ampt (1911) equation (cited in Dingman 1994). The saturation pressure head for this soil sample was 47.8±51.2 cmH_2O and the wetting conductivity, k_f was 0.64 (for loam). The observed pressure heads ranged from -17.5 to -10.0 cmH_2O. They were in a possible range. The pressure head at the wetting front was -30.7±27.37 cmH_2O. The input parameters for this simulation are given in Table 7.6.

Table 7.6 Input parameters for water movement through an infiltration and redistribution system in a soil column

Parameters	Values
Domains	20 cm
Boundary conditions	Initial conditions refer to the statical equilibrium of capillary force. The boundaries rely on the pressure head reading.
Hydraulic properties	Refer to coefficients of HV and VG equations
Time domain	8 hours
Number of time step; *nt*	Varies from 800 to 2400 steps per hour
Nodal spacing; *dz*	0.25 cm

The first simulation for this infiltration-redistribution column was undertaken using Richards' and HV equations. The pressure head profiles are presented in Figure 7.20. Water migrated slowly with Darcy's velocities of -9.58×10^{-5}, -1.151×10^{-4}, -1.540×10^{-4} and -2.036×10^{-4} cm/h at 2.0, 4.0, 6.0 and 8.0 hours respectively. Even though the column was fed at the same rate as for the gravitational infiltration tests, the velocities obtained in the current test were lower than the previous one. This same phenomenon occurred in the sand column tests. This confirmed that redistribution could slow down the gravitational flow.

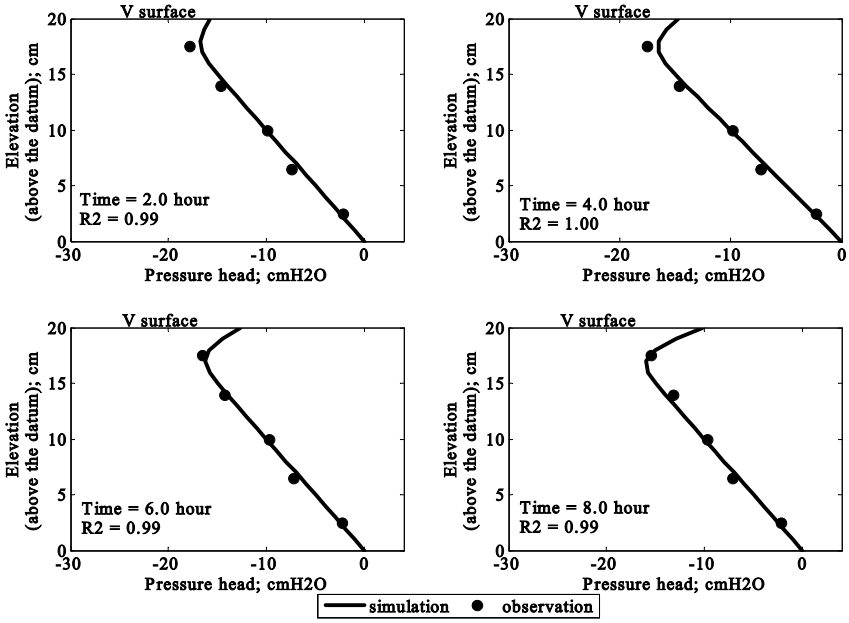

Figure 7.20 Pressure head profiles in a soil infiltration-redistribution column simulated using Richards' and HV equations (datum at the column base).

The simulations for moisture content in this test are presented in Figure 7.21.

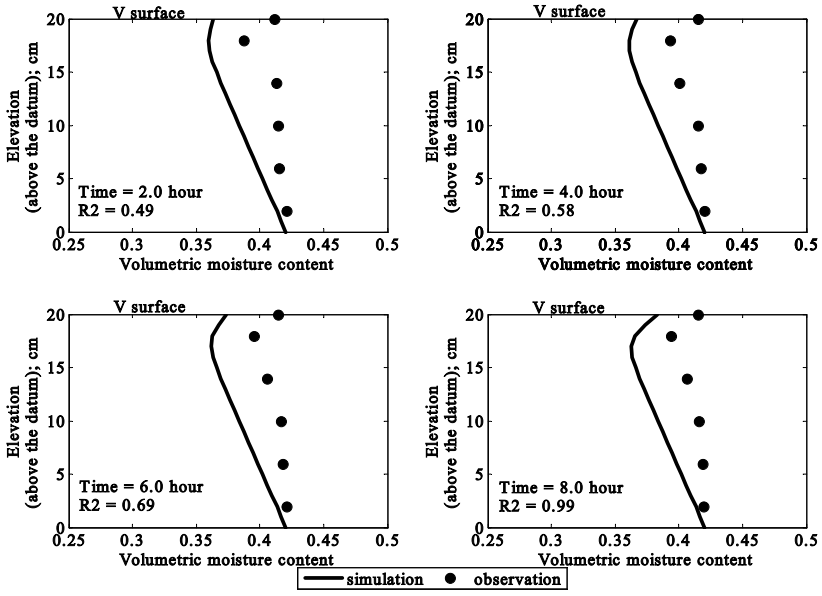

Figure 7.21 Moisture content profiles in a soil infiltration-redistribution column simulated using Richards' and HV equations (datum at column base).

The simulations generated underestimated the moisture content. The same was observed for the sand column. This error might result from the loss of water and the nature of the HV equation to underestimate the results (Haverkamp et al. 1977 and Wierenga 1995).

The second simulation for the infiltration-redistribution soil column test was undertaken using Richards' and VG equations. The pressure head profiles are given in Figure 7.22. Darcy's velocities were -3.843×10^{-5}, -4.796×10^{-5}, -6.840×10^{-5} and -9.672×10^{-5} cm/h at 2.0, 4.0, 6.0 and 8.0 hours, respectively. The velocities increased non-linearly over time. As expected, these velocities were lower than in the soil gravitational infiltration system. Redistribution could pull the water through the soil quicker than infiltration (Wierenga 1995).

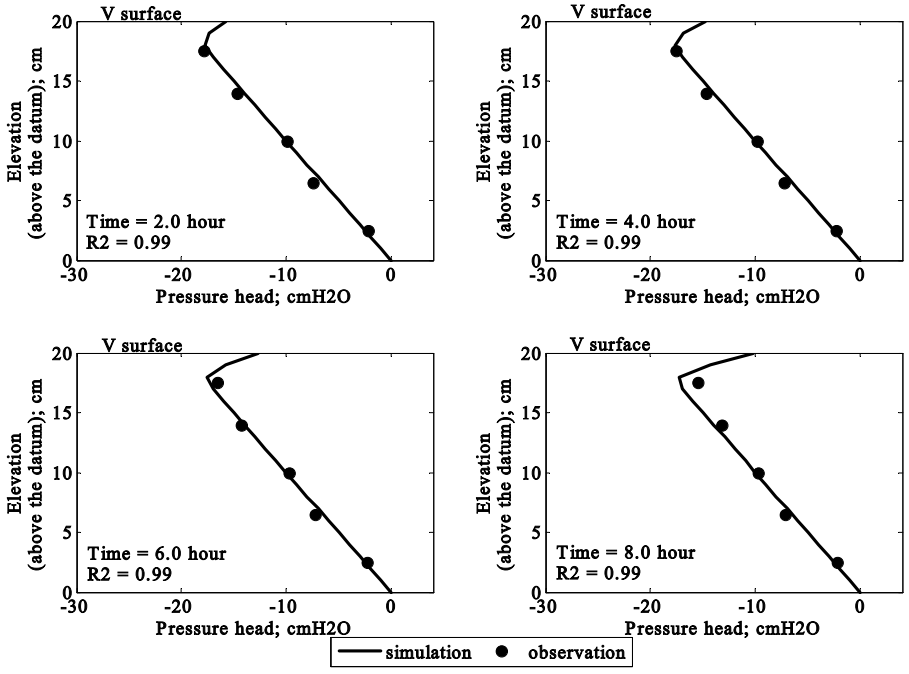

Figure 7.22 Pressure head profiles in a soil infiltration-redistribution column simulated using Richards' and VG equations (datum at column base).

The simulations of moisture content are presented in Figure 7.23. The moisture content changed in a narrow range from 0.38 to 0.42. The lowest moisture content was constant at 0.38 and it was observed at the elevation of 18 cm. The shape of the moisture content profiles was similar to the pressure head profiles.

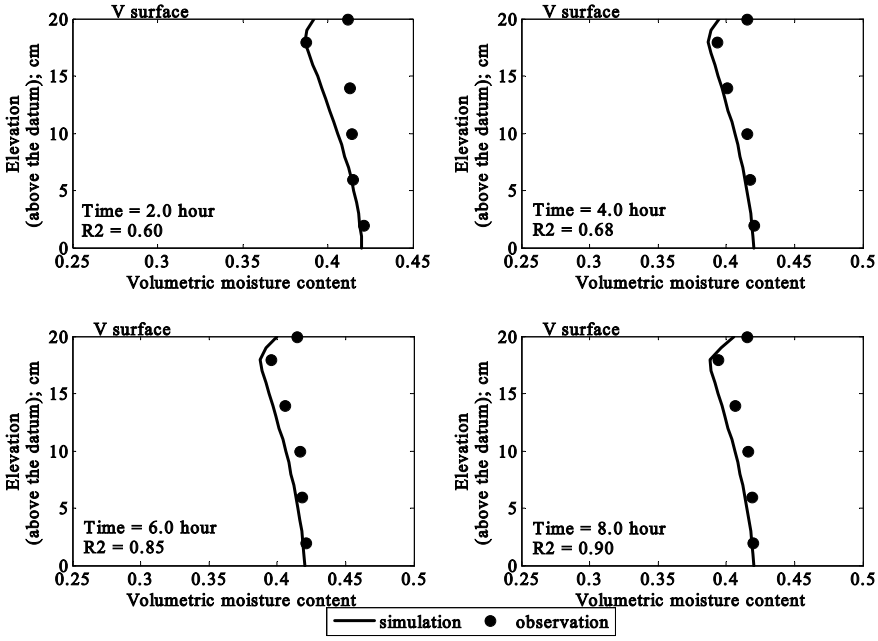

Figure 7.23 Moisture content profiles in a soil infiltration-redistribution column simulated using Richards' and VG equations (datum at column base).

7.4 Dispersion transport in the laboratory scale soil column

The transport under advection-dispersion could be observed using a tracer test. However, it may very difficult if the soil has a high background concentration and the layer is thick. Soil used in this research had a sodium ion concentration of 0.783 meq/L and the measured EC (1:5) was 0.129 mhos/cm. Based on the measured EC(1:5), this background concentration was very high, it equalled 117 mg/L. Shirokava et al. (2000) suggested that EC (1:5) could present 72% of the electroconductivity of soil saturated extract (EC_e at 25 ^oC). Therefore, the concentration of NaCl in the soil saturated extract sample might be 163 mg/L. In order to measure the dispersion transport, three tracer tests were undertaken: low strength tracer applied on a thin soil layer (Test-1); high strength tracer applied on a thin layer (Test-2), and high strength tracer applied on a thick soil layer (Test-3). The observations of the tracer tests are provided in Appendix-A.

7.4.1 Application of a low strength tracer concentration

The simulation was undertaken using a non-reactive contaminants transport mode. Darcy's velocity including mechanical dispersion terms was obtained by Richards' and HV or VG equations. The input parameters for Richards' equation are presented in Table 7.7.

Table 7.7 Input parameters for Richards' equation

Parameters	Values
Domains	5 cm
Boundary conditions	Upper and lower ψare –0.005 and -624 cmH_2O, respectively. Initial ψ is –624 cmH_2O.
Hydraulic properties	Refer to coefficients of HV and VG equations
Time domain	14 hours
Number of time step; *nt*	800 steps per hour
Nodal spacing; *dz*	0.125 cm

The pressure head profiles for the thin soil layer are shown in Figure 7.24. Both simulations obtained by Richards' and HV or VG equations agreed well with the observations. Half of the soil column reached full saturation within 8 hours and it was predicted that the whole column would achieve the fully saturation condition within 16 hours. This statement was remarkably close to the observation, where the first drop of filtered water was percolated out after 18 hours of continuous feeding.

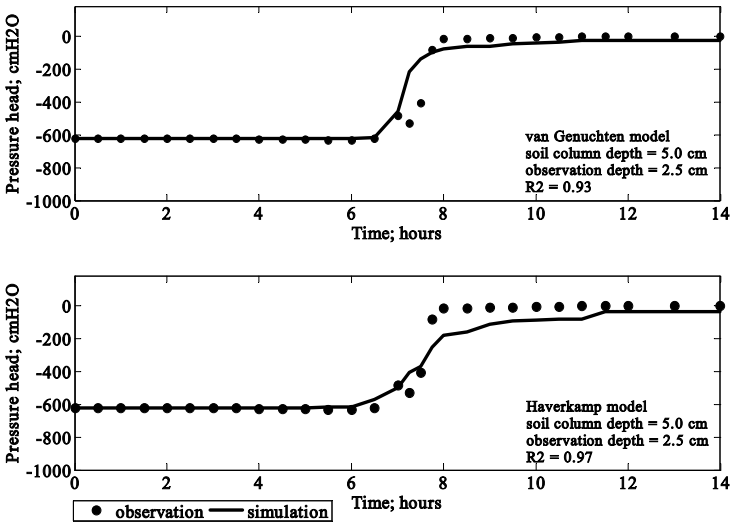

Figure 7.24 Pressure head versus time for Test-1

The nodal Darcy's and the pore velocities were substituted into the tracer transport model. The input parameters for the simulation of tracer transport are provided in Table 7.8.

Table 7.8 Input parameters of the tracer transport model for Test-1

Parameters	**Values**
Domains	5 cm
Tracer concentration	200 mg/L
Nodal Darcy's velocity	Direct load from Richards' and HV or VG equations (Advection transport)
Molecular dispersion	0.04788 cm^2/h (Kemper 1986)
The fraction of D*	0.4
Boundary conditions	Concentrations at the upper and lower boundary are 200 and 0 mg/L, respectively. The initial concentrations are 0 mg/L.
Time domain	14 hours
Number of time step; *nt*	800 steps per hour
Nodal spacing; *dz*	0.125 cm

Firstly, the concentration profiles were obtained by substituting Darcy's velocity governed from Richards' and HV equations. The results are presented in Figure 7.25.

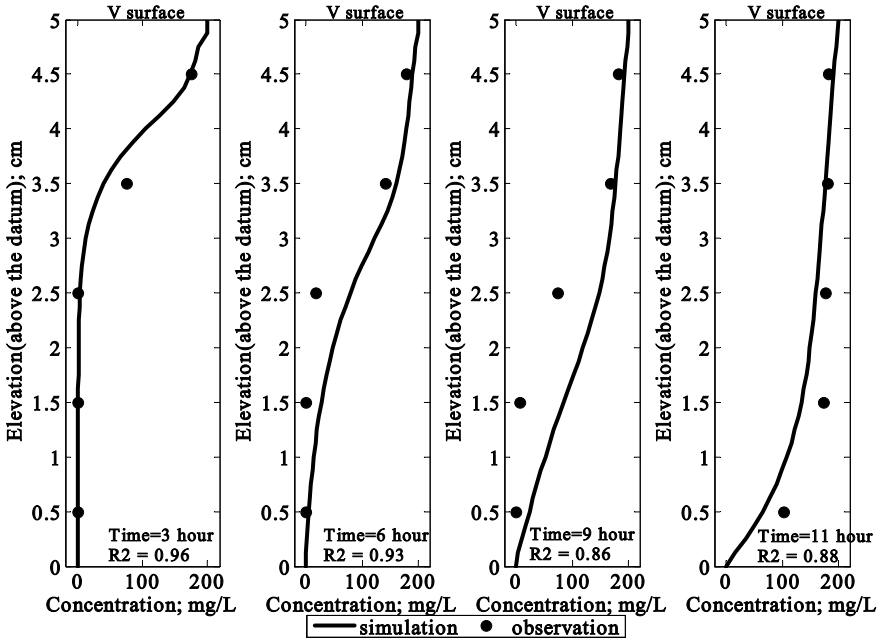

Figure 7.25 Tracer concentration profiles obtained using input from Richards' and HV equations for Test-1 (datum at the column base).

The tracer moved slowly, it took 3, 6, 9 and 11 hours to reach the elevations of 4.5, 3.5, 2.5 and 1.5 cm, respectively. The estimate travel time of tracer was 16 hours. This calculated travel time was close to the water retention time. The maximum tracer concentration was 176 mg/L. Approximately 14% of tracer was lost due to sorption and dispersion processes.

Secondly, the nodal Darcy's velocities obtained from Richards' and VG equations were added as input to the model. The concentration profiles are presented in Figure 7.26. The tracer gradually moved downward and reached elevations of 3.2, 3.0, 2.3 and 1.7 cm, within 3, 6, 9 and 11 hours, respectively. The estimated travel time was in the range of 16-17 hours.

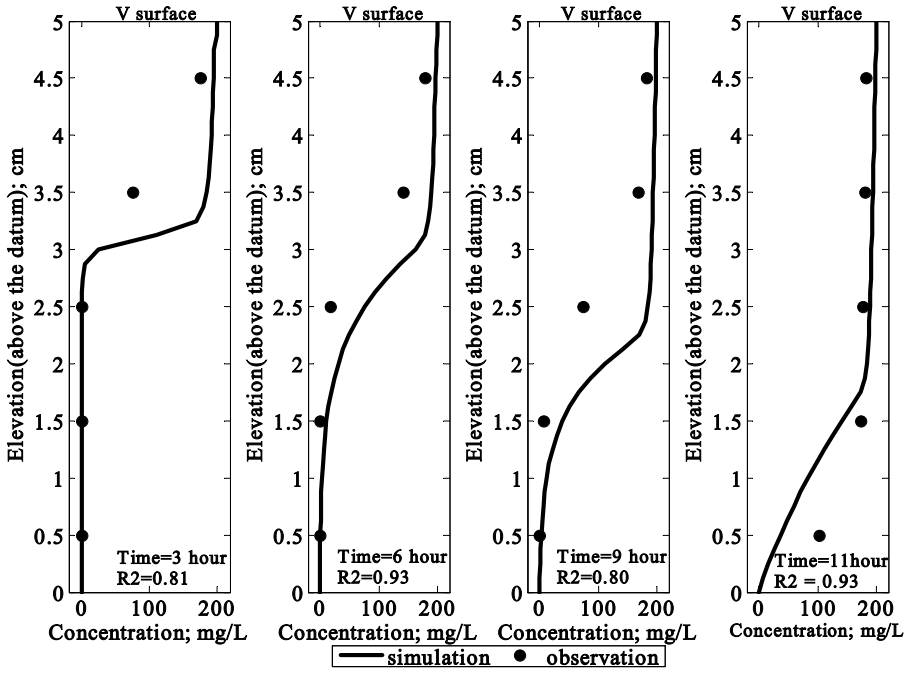

Figure 7.26 Tracer concentration profiles obtained using input from Richards' and VG equations for Test-1 (datum at the column base).

The travel times of the tracer obtained from both simulations equalled the travel time of water. The tracer spreading was negligible if the test took place in a thin soil layer. The average diffusion-dispersion coefficients D_z are given in Table 7.9. The dispersion coefficients governed by substituting Darcy's velocity obtained from Richards' and HV or VG equations, were in the range of 0.01-0.4 and 0.01-0.2 cm^2/h, respectively. The

difference might result from the different estimated pore velocities. However, the D_z value obtained was in the possible range that was proposed by Pickens and Grisak (1981) of 0.037 cm^2/h (or $1.02x10^{-5}$ cm^2/s). The D_z was a time varying and non-linear function, and it relied upon Darcy's and pore velocities (Wierenga 1995). The value of D_z suggests that molecular diffusion was 12-25% of total dispersion, and the mechanical dispersion played a significant role in the dispersion transport.

Table 7.9 Average diffusion-dispersion coefficients for a thin soil layer

Time (hours)	Average diffusion-dispersion coefficient; D_z (cm^2/h)	
	Haverkamp	van Genuchten
3	0.01115	0.00951
6	0.03705	0.01327
9	0.08378	0.03563
11	0.41604	0.19503

7.4.2 Application of a high strength tracer concentration

The nodal Darcy's and the pore velocities obtained from the previous section were substituted into the tracer transport model. The input parameters are presented in Table 7.10.

Table 7.10 Input parameters for the tracer transport model for Test-2

Parameters	Values
Domains	5 cm
Tracer concentration	500 mg/L
Nodal Darcy's velocity	Direct load from Richards and HV or VG equations (Advection transport)
Molecular dispersion	0.04788 cm^2/h (Kemper 1986)
The fraction of D*	0.4
Boundary conditions	Concentrations at the upper and lower boundary are 500 and 0 mg/L, respectively. The initial concentrations are 0 mg/L.
Time domain	14 hours
Number of time step; *nt*	800 steps per hour
Nodal spacing; *dz*	0.125 cm

The nodal Darcy's velocities obtained from Richards' and HV or VG equations were input into the model. The results obtained are presented in Figures 7.27 and 7.28. Both simulations generated the same results. The tracer migrated to the elevations of 4.5, 4.2, 3.5 and 1.5 within 3, 6, 9 and 11 hours, respectively. The estimated travel time was 16

hours, which equalled that obtained in the previous test. The maximum concentration was in the range of 494- 497 mg/L. This indicated that approximately 1% of tracer lost due to the sorption and dispersion processes. The high strength concentration could provide clear profiles of concentration with the least of residual error. Moreover, the values of D_z in these simulations were same as the previous test.

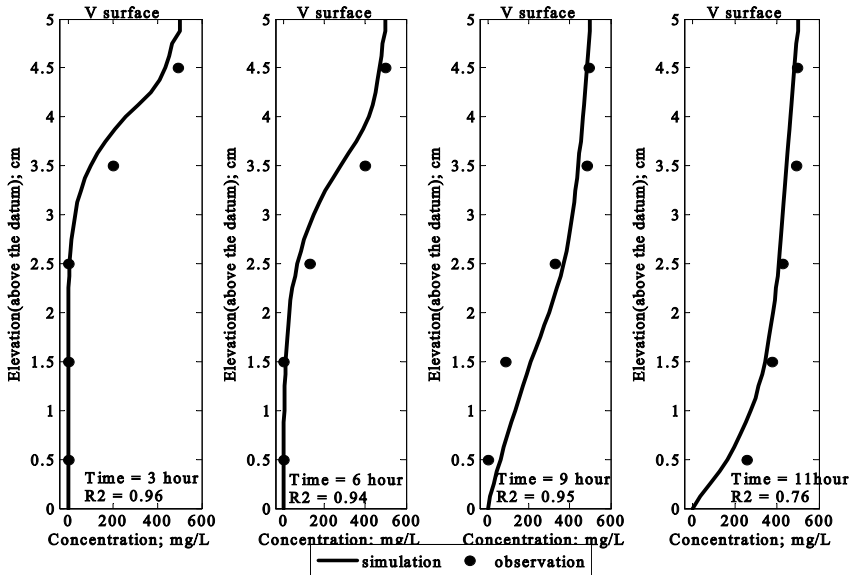

Figure 7.27 Tracer concentration profiles obtained using input from Richards' and HV equations for Test-2 (datum at the column base).

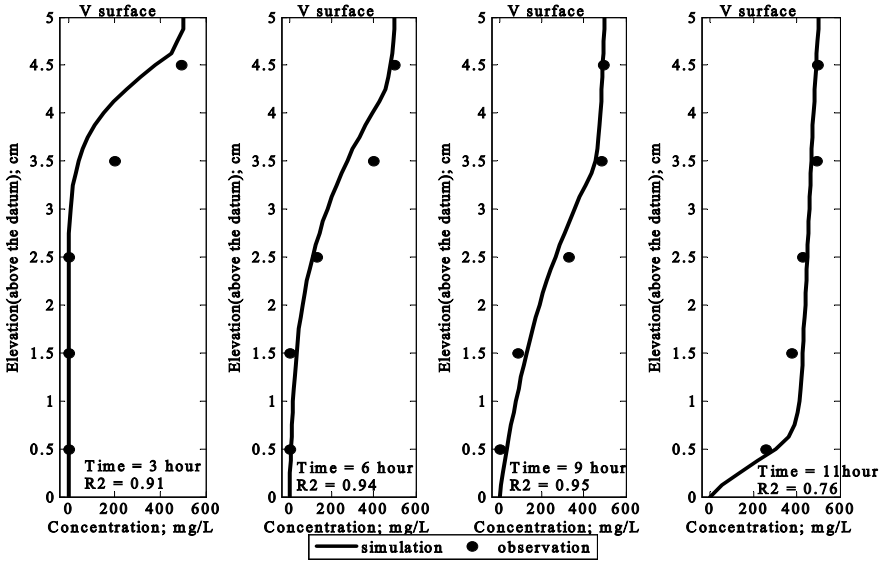

Figure 7.28 Tracer concentration profiles obtained using input from Richards' and VG equations for Test-2 (datum at the column base).

7.4.3 Tracer application in a thick soil layer

The applied Darcy's velocity for this case was presented in Section 7.3.1 Gravitational infiltration system. Darcy's velocity was input to the tracer transport model. The input parameters are summarised in Table 7.11.

Table 7.11 Input parameters for the tracer transport model for Test-3

Parameters	Values
Domains	20 cm
Tracer concentration	500 mg/L
Nodal Darcy's velocity	Direct load from Richards and HV or VG equations (Advection transport)
Molecular dispersion	0.04788 cm^2/h (Kemper 1986)
The fraction of D*	0.4
Boundary conditions	Concentrations at the upper and lower boundary are 500 and 0 mg/L. The initial concentrations are 0 mg/L.
Time domain	72 hours
Number of time step; *nt*	1272 steps per hour
Nodal spacing; *dz*	0.25 cm

The nodal Darcy's velocities obtained from either Richards and HV or Richards and VG equations were input to the simulation of tracer transport. The results are given in Figures 7.29 and 7.30, respectively. Both models simulated the same concentration profiles. The tracer migrated slowly. It reached elevations of 17.5, 15.0, 12.5, 8.0, 5.0 and 2.5 cm within 8, 16, 24, 48, 56 and 72 hours, respectively. The estimated tracer travel time was in the range of 80-82 hours. The tracer travel time was 12-14 hours longer than water travel time. This indicates that the thickness of the soil layer might potentially affect the tracer transport. The maximum tracer concentration was in the range of 488-497 mg/L. Approximately 1.5% of tracer was lost in the soil layer.

The averaged D_z is given in Table 7.12. The value of D_z obtained from a thick soil layer was 0.3-3.5 cm^2/h. It was higher than those observed in a thin soil layer. This confirmed that high spreading of tracer occurs in a thick layer and this could retard the movement of the tracer. The molecular diffusion was 1.1-13% of total dispersion, thus mechanical dispersion also played an important role in the dispersion transport.

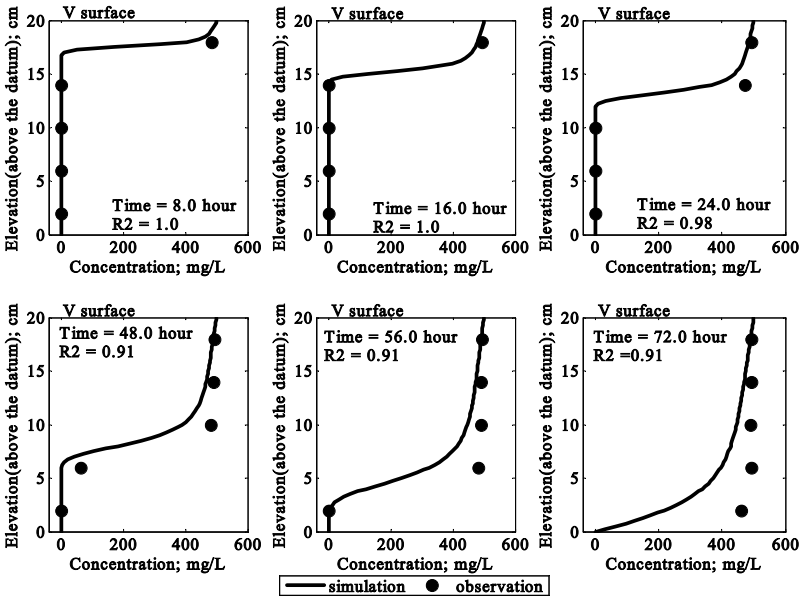

Figure 7.29 Tracer concentration profiles obtained using input from Richards' and HV equations for Test-3 (datum at the column base).

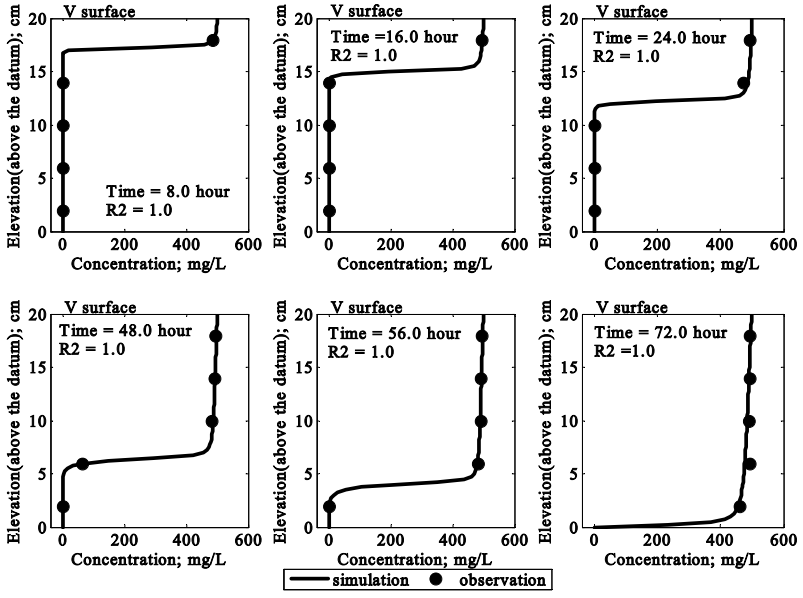

Figure 7.30 Tracer concentration profiles obtained using input from Richards' and VG equations for Test-3 (datum at the column base).

Table 7.12 Average diffusion-dispersion coefficients for a thick soil layer

Time (hour)	Average diffusion-dispersion coefficient; D_z (cm^2/h)	
	Haverkamp	van Genuchten
8	0.385	0.335
16	0.766	0.746
24	1.706	1.703
48	3.056	2.997
56	3.341	3.028
72	3.318	3.489

It was shown that a tracer test could be applied to evaluate the spreading due to advection-dispersion processes. The developed tracer transport model could generate highly accurate simulation results for all tracer transport conditions and it also effectively estimated the diffusion-dispersion coefficients. The high strength tracer concentration and the thin soil layer could be the best approach for the estimation of unsaturated water movement in this soil sample. The high strength tracer concentration could overcome the interference of background concentration contained in the soil sample. In the thick soil layer, the tracer travel time could be extended by the diffusion mechanism and high dispersion could potentially cause large spreading of the tracer.

7.5 Summary

The advection transport in gravitational, capillary and infiltration-redistribution systems could be effectively estimated using Richards' equation. Darcy's velocity obtained during the infiltration flow increased non-linearly over time. The precise time for contaminants transport due to advection can be estimated by the pressure head profiles. Tracer tests using sodium chloride were carried out. The results indicated that high strength concentrations of tracer could be practically applied if the soil had a high background concentration of ions. A thick layer of soil could retard the tracer longer than a thin layer. The travel time of the tracer increases if the layer of soil was thick. The non-reactive solute transport model was applied to simulate the profiles of tracer concentration. The simulations agreed very well with the observations. The model provided many advantages in evaluating nodal mechanical dispersion and dispersion-diffusion coefficients.

CHAPTER 8

PILOT SCALE SOIL COLUMN TESTS

8.1 Introduction

The results obtained from the pilot scale soil column tests are presented and discussed in this chapter. The experiments included studies of contaminants transport with reaction. The developed model gave a good estimation of the contaminant transport coupling retardations. The results revealed that the migration of organic carbon, nitrate, phosphate and *E.Coli* could be retarded by soil minerals and microbes. The developed model effectively estimated the concentration profiles of theses contaminants. The reduction zones of COD, nitrate and phosphate were at the elevation of 105 cm (above the datum). The *E.Coli* reduction zone was 110 cm above the datum. The biological clogging zone was also observed on the column surface, with a thickness of 2 cm. Although this zone could stimulate biological reaction, it has the potential to retard the flow of wastewater. The laboratory data are provided in Appendix-I.

8.2 Advection transport in the pilot scale soil column

The soil column tests were operated under a gravitational system. The readings of pressure head at each tensiometer location are provided in Figure 8.1. The readings were undertaken for a total period of 91 days. The column reached the equilibrium of inflow and outflow after the column had operated for 15 days. The pressure head was constant at –0.2 cmH_2O. The fingerprint readings were observed near the front passes. The front took 0.25, 1.5, 4.5, 5.5 and 8.5 days to reach the elevations of 115, 78, 60, 32 and 5 cm, respectively. The estimated wastewater travel time through the 120-cm deep soil layer was 13-14 days.

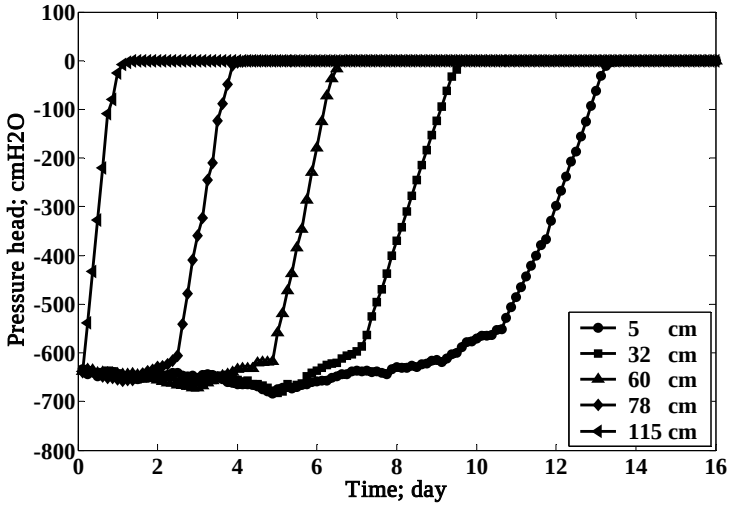

Figure 8.1 Pressure head profiles of the pilot scale soil column

The outflow velocities varied from 0.55 to 1.17 cm/h and the average was 0.77 cm/h. This average rate was close to the full saturation hydraulic conductivity of 0.66 cm/h. The outflow at the equilibrium condition was approximately 0.43 L/d, which is equal to the feeding rate. After one month of continuous feeding, a slime layer was observed at the top of the soil column. Soil was covered with a 2 cm thick dark biofilm. This zone resisted the percolation of wastewater. When the column became clogged, ponding occurred and the percolation rate was reduced to 0.26 L/d. The ponding of wastewater on top of the soil is shown in Figure 8.2.

Figure 8.2 Bio-clogging zone and the wastewater pond

Transport of contaminants was simulated using Richards' equation. The input parameters for the advection transport are given in Table 8.1

Table 8.1 Input parameters for advection transport model

Parameters	Values
Domain	Column depth 120 cm
Boundary conditions	The pressure head at the column surface; ψ_{top} is –0.005 cm, the head at the column base; ψ_{bot} is –624 cm. The initial head; ψ_{int} is 624 cm
Hydraulic properties	Refer to coefficients of HV and VG equations
Time domains	20 days
Number of time step, *nt*	2840
Nodal time spacing, *dz*	1 cm

Firstly, Richards and HV equations were applied to predict the wastewater movement. The pressure head profiles are presented in Figure 8.3. The front moved slowly to the elevations of 115, 78, 60, 32 and 5 cm within 0.25, 1.5, 4.5, 5.5 and 8.75 days, respectively. The equilibrium of inflow and outflow was achieved after the column had operated for 15 days.

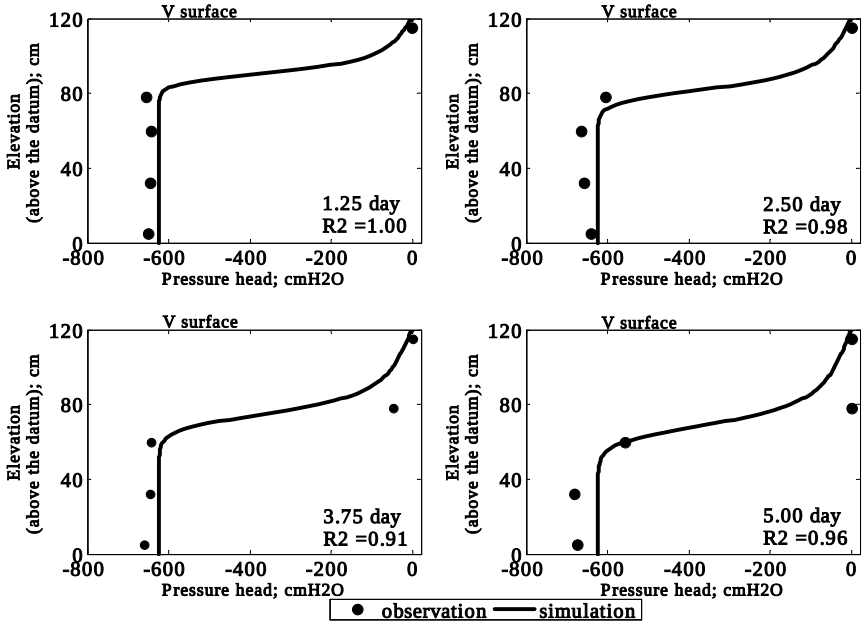

Figure 8.3 Pressure head profiles simulated using Richards' and HV equations (datum at the column base).

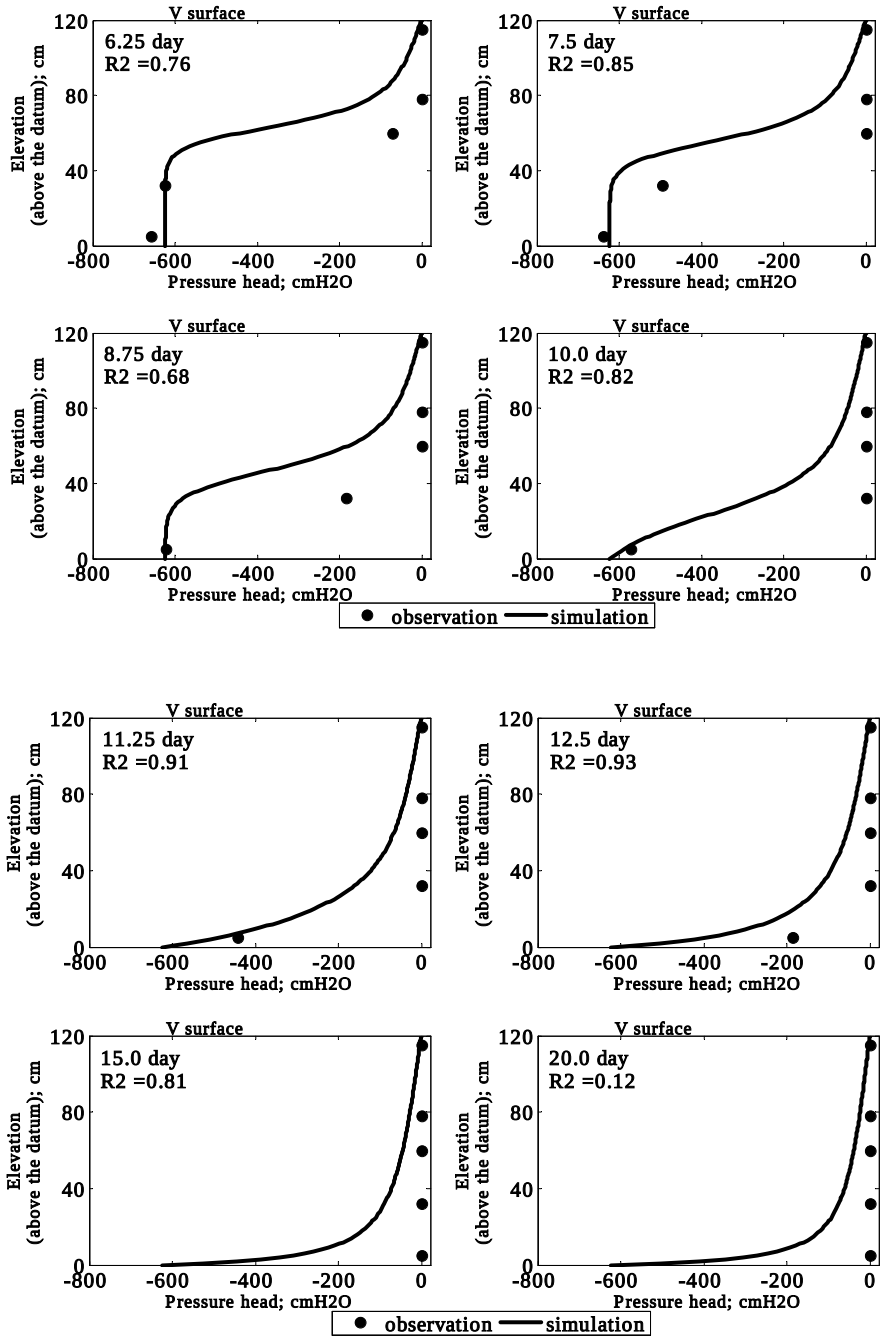

Figure 8.3 (cont.) Pressure head profiles simulated using Richards' and HV equations (datum at the column base).

The pressure head distribution over time was simulated using Richards and HV equation, the results are given in Figure 8.4. The simulations generally agree with the observed

results. However, the wetting front movement observed did not match the simulation. The equilibrium of inflow and outflow estimated in this simulation was 16 days. This was close to the observations.

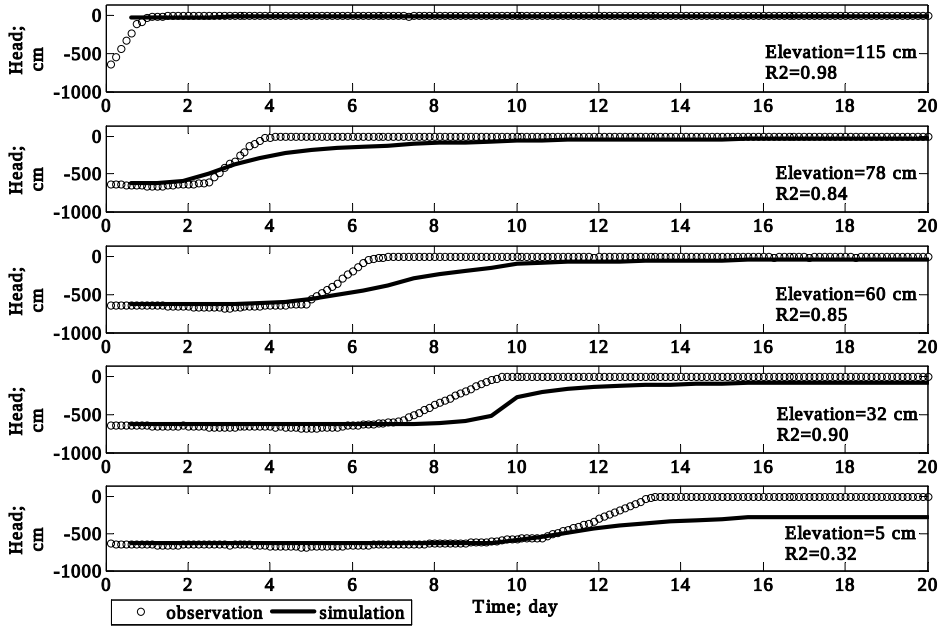

Figure 8.4 Time varying observed and simulated pressure head using Richards' and HV equations (datum at the column base).

Secondly, Richards and VG equations were applied to simulate the wastewater movement. The pressure head profiles are presented in Figure 8.5. The simulations correlated well with the observations. The estimated equilibrium of inflow and outflow of wastewater through the 120 cm deep layer was 14 days.

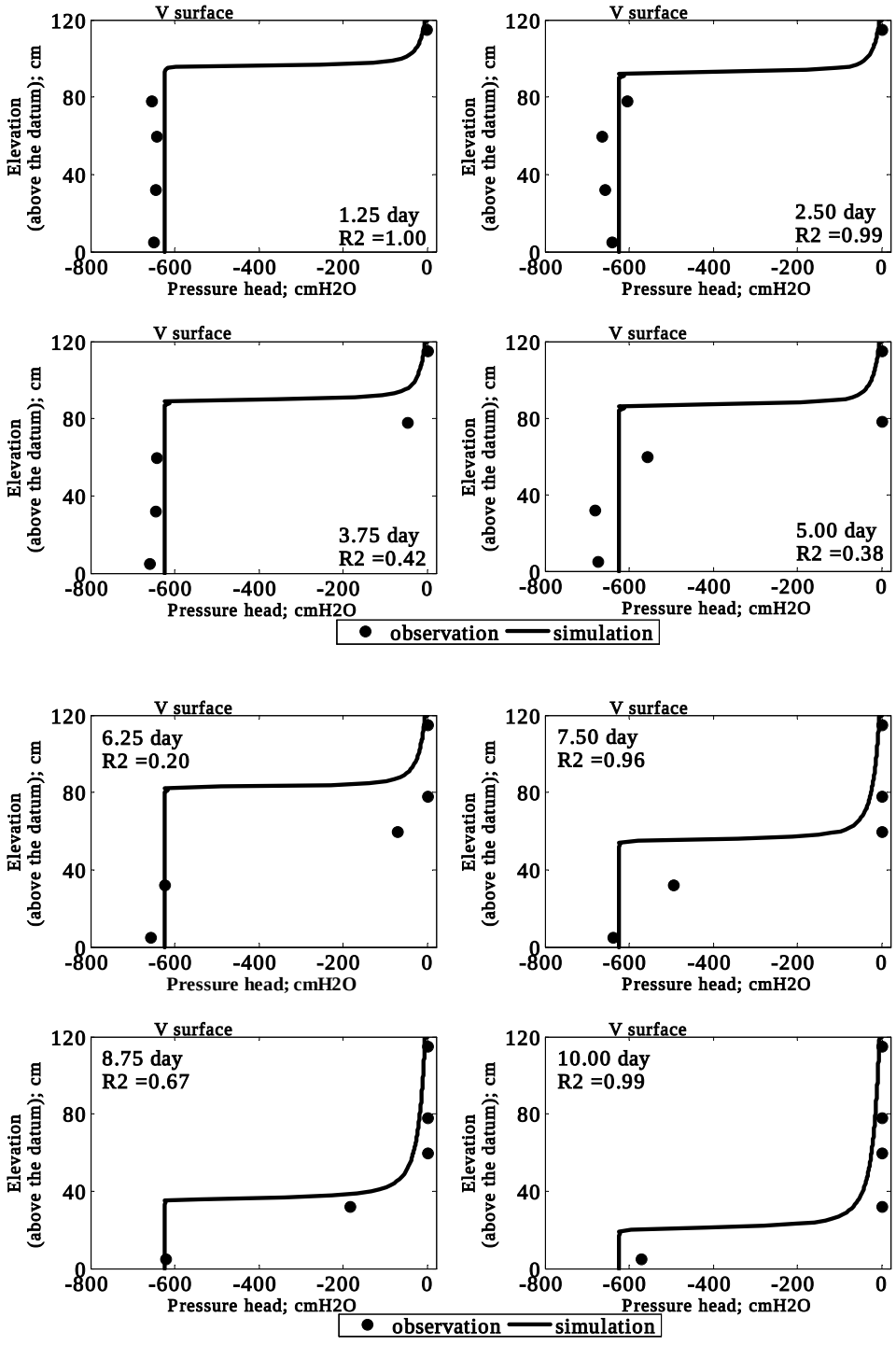

Figure 8.5 Pressure head profiles simulated using Richards' and VG equations (datum at the column base).

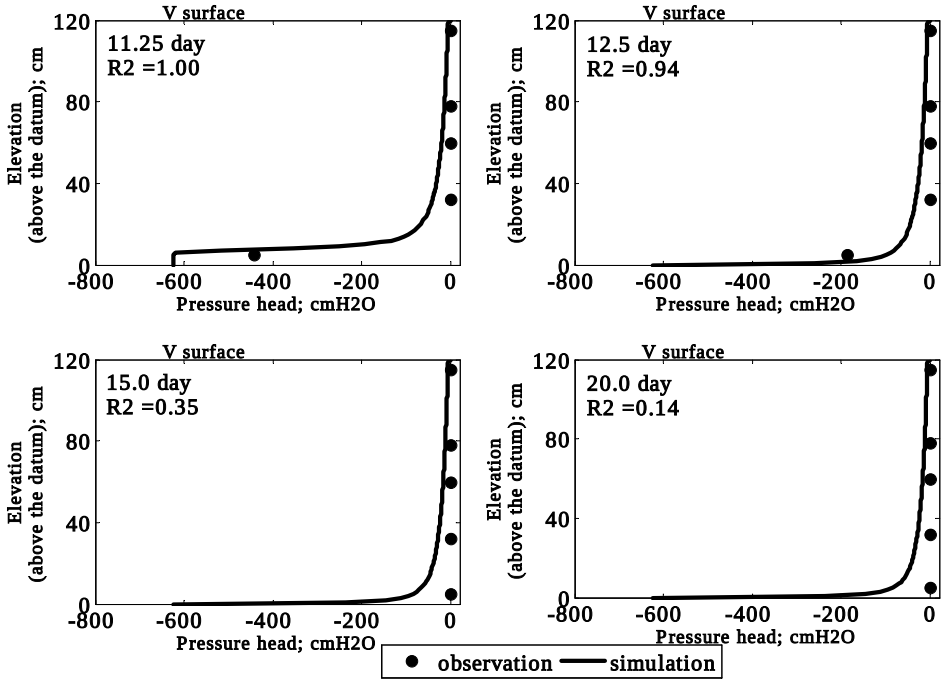

Figure 8.5 (cont.) Pressure head profiles simulated using Richards' and VG equations (datum at the column base).

The distribution of pressure head over time is also estimated using Richards and VG equations, the results are provided in Figure 8.6. The simulations agreed well with the observations. The front passed the elevations of 115, 78, 60, 32 and 5 cm after 0.25, 6.75, 7.75, 9.75 and 12.0 days, respectively. The estimated travel time of contaminants due to advection was 12.3 days.

HV and VG equations have been used very effectively to estimate of the specific moisture content and relative permeability contained in Richards' equation. An advection transport model predicted that the travel times of contaminants passing through a 120-cm deep soil layer would be 12-16 days, which was close to the observations.

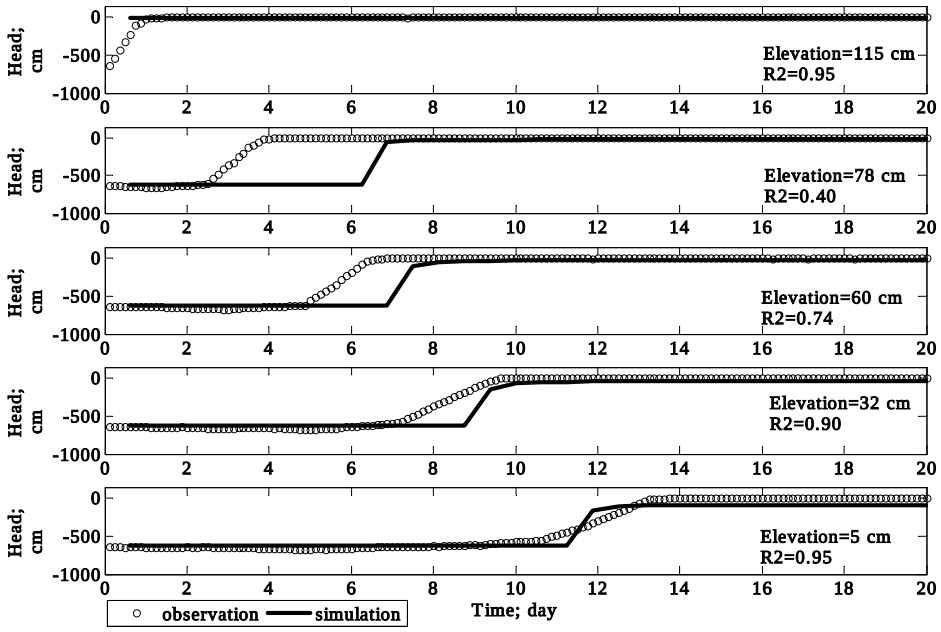

Figure 8.6 Time varying observed and simulated pressure head using Richards' and VG equations (datum at the column base).

8.3 Quality of filtered effluent from soil column

As the soil contained minerals and microbes, some contaminants might be removed during percolation. The quality of wastewater was improved after passing through the soil column and their details are given as follows.

8.3.1 EC and pH

The EC and pH of the filtered effluent are shown in Figure 8.7. The EC of the feed wastewater varied from 483 to 1648 μmohs/cm. The substantial variation was the result of the stormwater dilution during periodic rainfall. The EC observed in the effluent slightly increased compared to the influent. This phenomenon is related to the ion exchange and redox reactions. Clay surfaces have negative charges and these sites are suited for cation exchange. Soil containing humus and metal oxide minerals could stimulate the ion

exchange process (Sparks 1995). The EC values were found to be constant, if the soil column was operated for long periods.

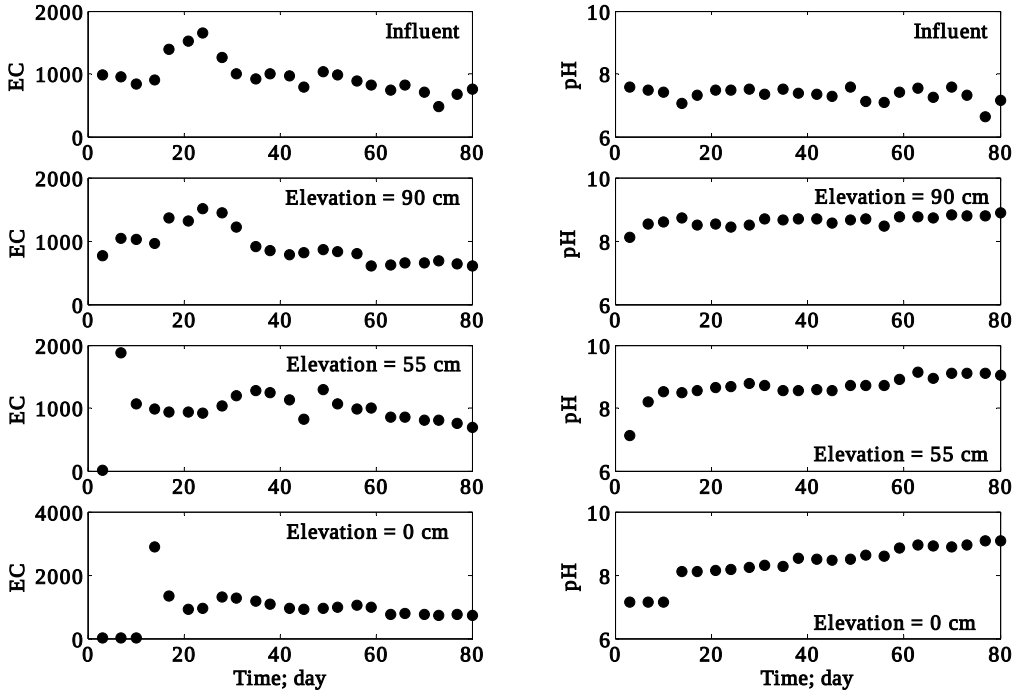

Figure 8.7 EC and pH profiles of the wastewater and the filtered samples (EC was expressed in μmohs/cm and datum was at the column base).

The pH of the influent was found to be neutral. pH increased slightly in filtered samples to between 8 to 9. An increase in pH might result from the dissolution of alkaline minerals, especially, the cations contained in the carbonated buffering system such as Ca^{2+}, Mg^{2+} and Fe^{2+} (Ptacek 1998). A high increase in pH was observed when the column was operated for long periods. According to the EC-pH diagram, cations were less soluble in an alkaline condition. This condition could be conducive for the formation of complexes with contaminants which then precipitate as metal oxides (Watts 1997). Thus, the increase of EC and pH in the system could increase the quantity of precipitates.

8.3.2 Nitrogen compounds

The ammonia (NH_4-N) and nitrate nitrogen (NO_3-N) concentration profiles are shown in Figures 8.8 and 8.9, respectively. The average NH_4-N concentrations in the influent and the effluent were 49 and 4.7 mg/L, respectively. Approximately 90% of NH_4-N was reduced. The ammonia nitrogen can be oxidized by aerobic bacteria to become the stable nitrate nitrogen (Widdowson 1998 and Ptacek 1998). From measurement it has been found that the influent and the effluent NO_3-N concentrations were 1.3 and 2.6 mg/L, respectively confirming the oxidation process. By mass balance calculation, approximately 99% of ammonia was lost in the releasing process. This resulted in the increase of the pH level of the effluent by 1-2 providing the optimum pH for nitrifying bacteria (between pH 7.5 to 8.6) (Metcalf and Eddy 2003). The concentration of nitrate increased due to biodegradation within the top 30 cm of the soil layer.

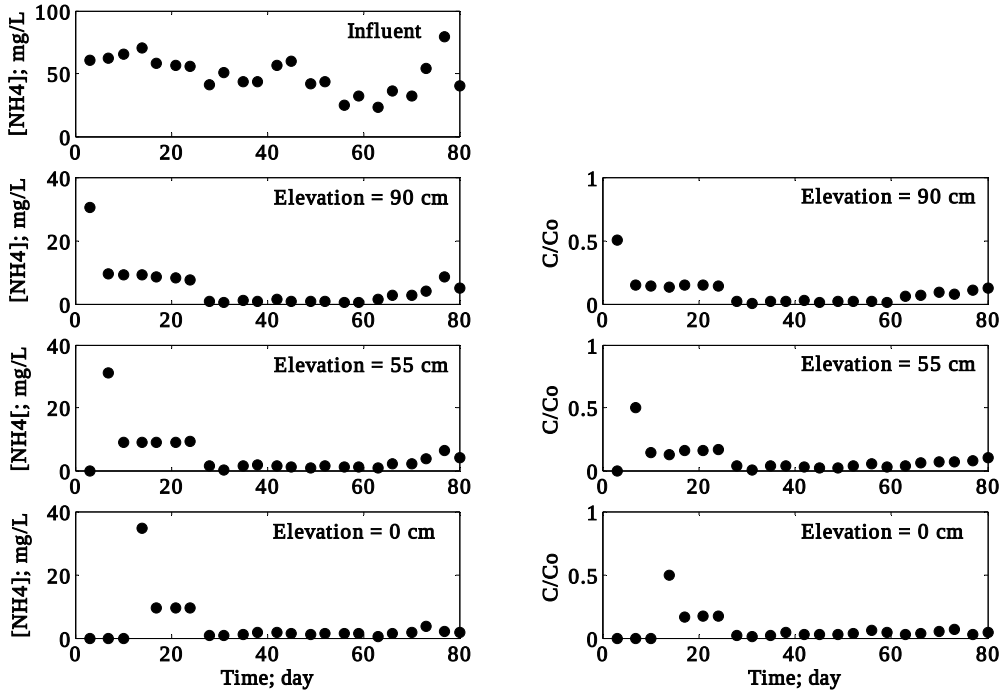

Figure 8.8 Ammonia concentration profiles of the wastewater and the filtered samples (datum at the column base).

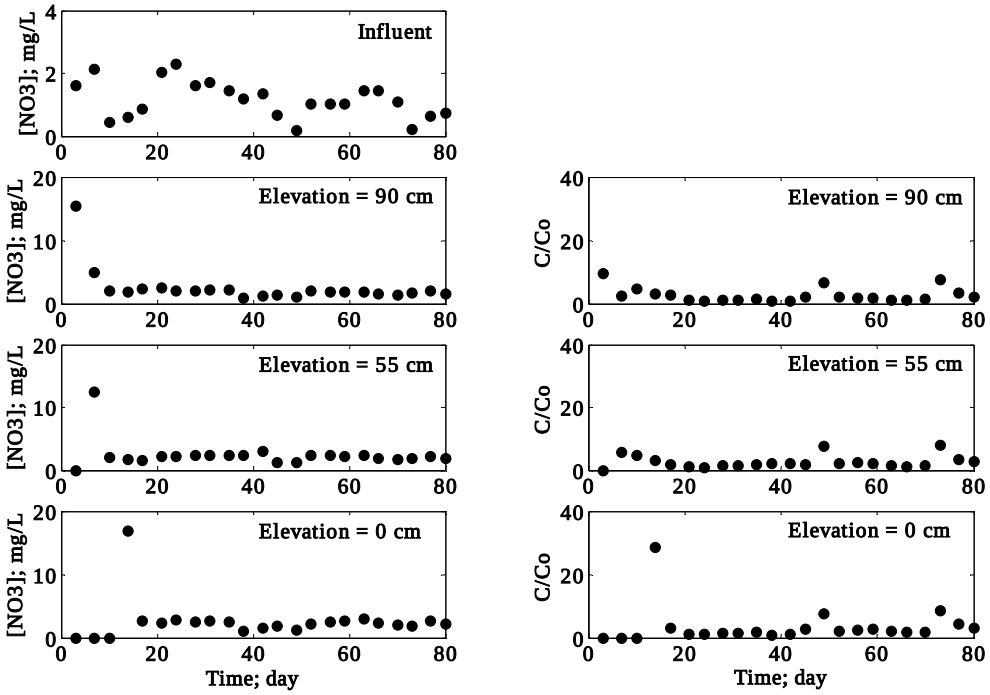

Figure 8.9 Nitrate concentration profiles of the wastewater and the filtered samples (datum at the column base).

The total Kjeldahl nitrogen, TKN, concentration profiles are presented in Figure 8.10. The ratio of C/C_O indicated that the TKN was removed within the upper soil portion. The remaining TKN was not further removed in the lower soil portion. The concentrations of TKN oscillated during testing. The ratios NH_4-N/TKN (or 1/[1+(Org.-N/NH_4-N)])in the raw wastewater and the effluent were 0.95 and 0.87, respectively. This ratio reduced slightly after passing wastewater through the soil column. A decrease of this ratio suggested that NH_4-N and Org.-N might be transformed to be nitrate due to biodegradation process. The ratios Org.-N/TKN in the raw wastewater and the effluent were 0.16 and 0.35, respectively. An increase of this ratio can relate to the leaching of organic nitrogen from the soil. The soil contained total nitrogen 1.76 mg/g soil. This background concentration can have impacted on the measurements of TKN and Org.-N.

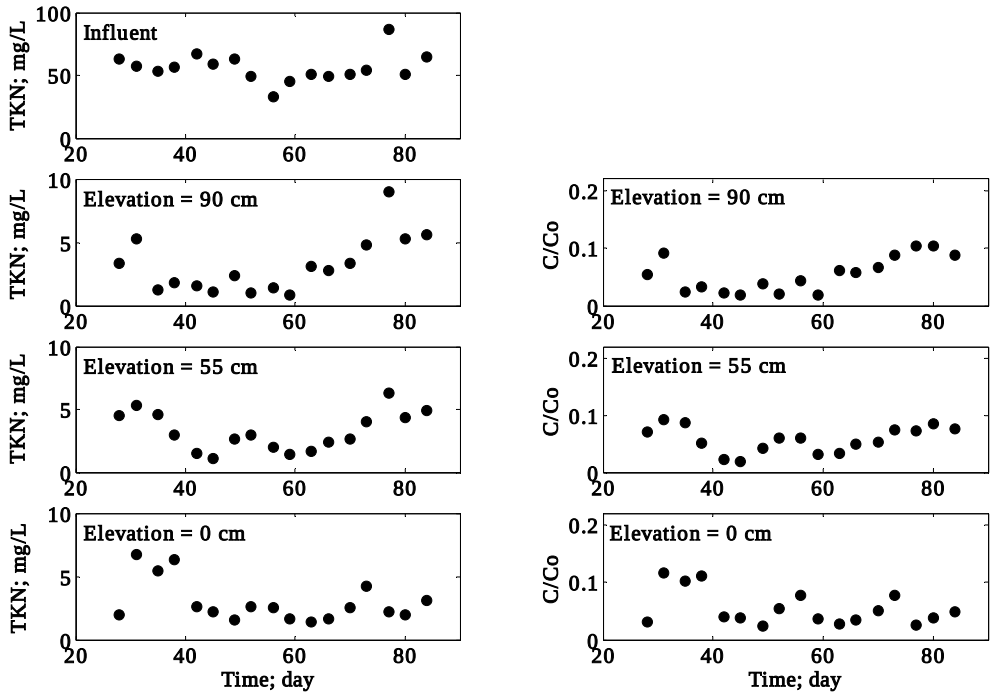

Figure 8.10 TKN concentration profiles of the wastewater and the filtered samples (datum at the column base).

8.3.3 Phosphate compounds

The observations of elevated phosphate concentrations are given in Figure 8.11. The highest phosphate removal was observed at the top portion, close to the column surface. Approximately 40% of the phosphate applied was retarded in this zone. The overall phosphate removal efficiency of this column was 90% of phosphate applied. The high adsorption results from the soil characteristics, where the mineral content could potentially react with phosphate (Wilhelm et al. 1994).

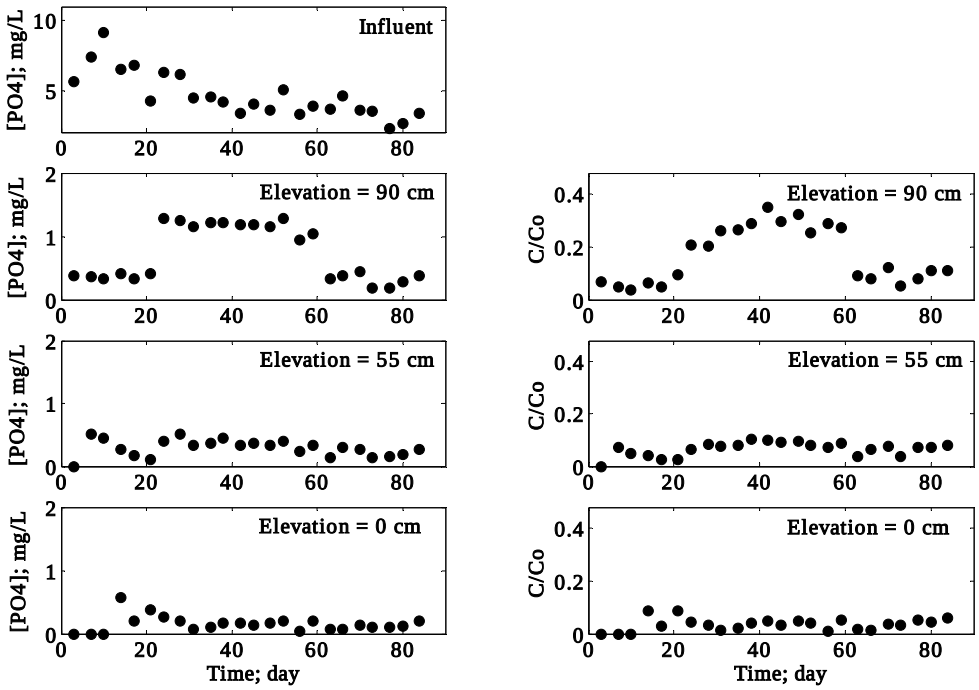

Figure 8.11 Phosphate concentration profiles of the wastewater and the filtered samples (datum at the column base).

8.3.4 Organic carbon compounds

The COD concentration profiles were simulated to describe the variation of concentration of organic carbon compounds. Sawyer et al. (1994) suggested that the COD test was widely used to measure the organic strength of domestic and industrial wastes. This was based upon the fact that all organic carbon compounds, with a few exceptions, could be oxidized by a strong oxidizing reagent under a highly acidic system. The COD is used as a substitute for BOD test in many fields. Metcalf and Eddy (2003) suggested that COD data could interpret the BOD value. For domestic wastewater, BOD/COD was 0.4-0.6. Therefore, it was practical to estimate the organic carbon compounds from COD data.

The COD profiles are presented in Figure 8.12. The average COD concentrations of the influent and the effluent were 245 and 42 mg/L, respectively. The soil column could

remove approximately 83% of COD. The retardation zone was found in the top 30 cm soil. Approximately 80% of COD was reduced in this layer. The COD remaining in the effluent was very low, with a concentration of 37 mg/L, which is equal to the BOD of 14.8-22.2 mg/L. This might be the minimum concentration for utilisation of substrates (20-25 mg/L of BOD for the trickling filter) and thus the microbial activities were inhibited by substrate limitation (McCarty et al. 1981 and Metcalf and Eddy 2003).

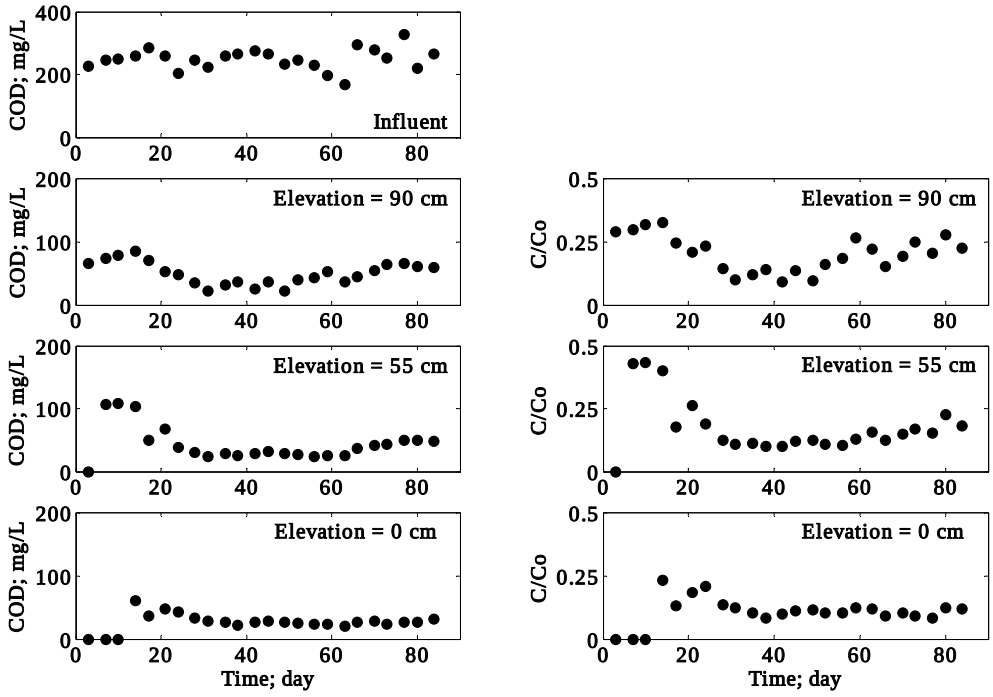

Figure 8.12 COD concentration profiles of the wastewater and the filtered samples (datum at the column base).

8.3.5 DO and temperature

The dissolved oxygen (DO) and temperature profiles are presented in Figure 8.13. The average temperature of the infiltration system was 23 ^{o}C. The DO concentration in the raw and the filtered wastewater were 0.1 and 2.8 mg/L, respectively. The DO in the filtered wastewater increased dramatically due to atmospheric aeration.

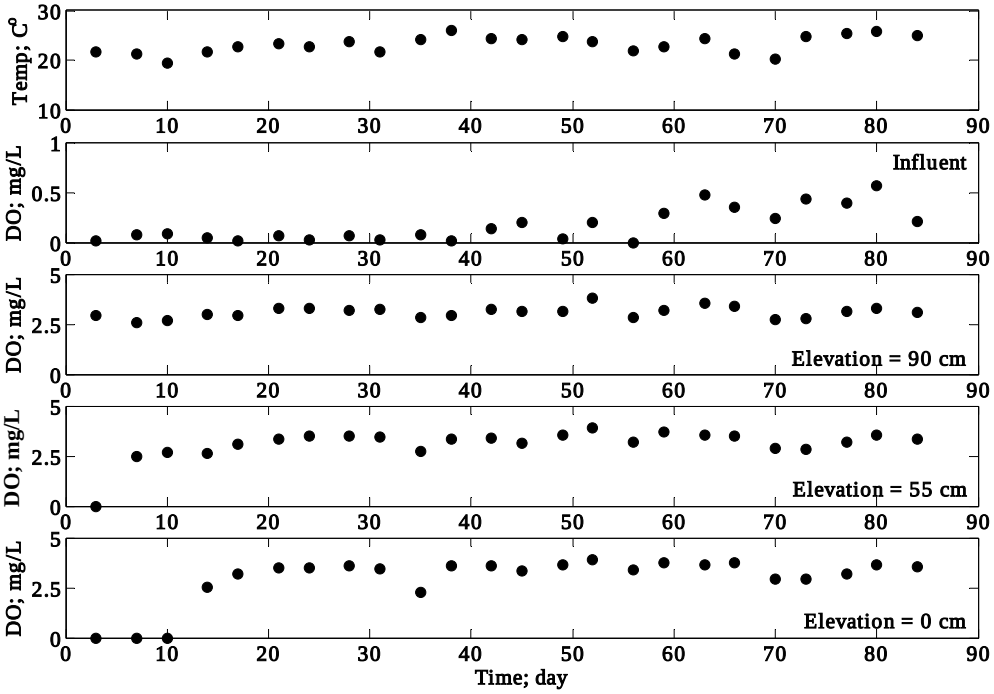

Figure 8.13 Temperature and DO concentration profiles of the wastewater and the filtered samples (datum at the column base).

The dissolved oxygen above 1 mg/L are essential for nitrification. If the DO levels drop below 1 mg/L, nitrification may cease (Metcalf and Eddy 2003), so, the nitrification could be found in the experiment. Moreover, the concentration of COD may reduce due to the aerobic and nitrate respiration processes (MacQuarrie et al. 2001).

8.3.6 *E.Coli*

Average numbers of *E.Coli* in the influent and effluent were 1.70×10^6 and 2.48×10^2 cfu/100 mL, respectively. This soil column could effectively restrain the *E.Coli*. The removal efficiency was 99.999%. Most of the *E.Coli* were trapped at the top portion of soil. The filtered wastewater sample contained *E.Coli* of 1.54×10^3 cfu/100 mL. The removal of *E.Coli* was not significant in the middle and in the low portion of soil column. The *E.Coli* concentration profiles are given in Figure 8.14.

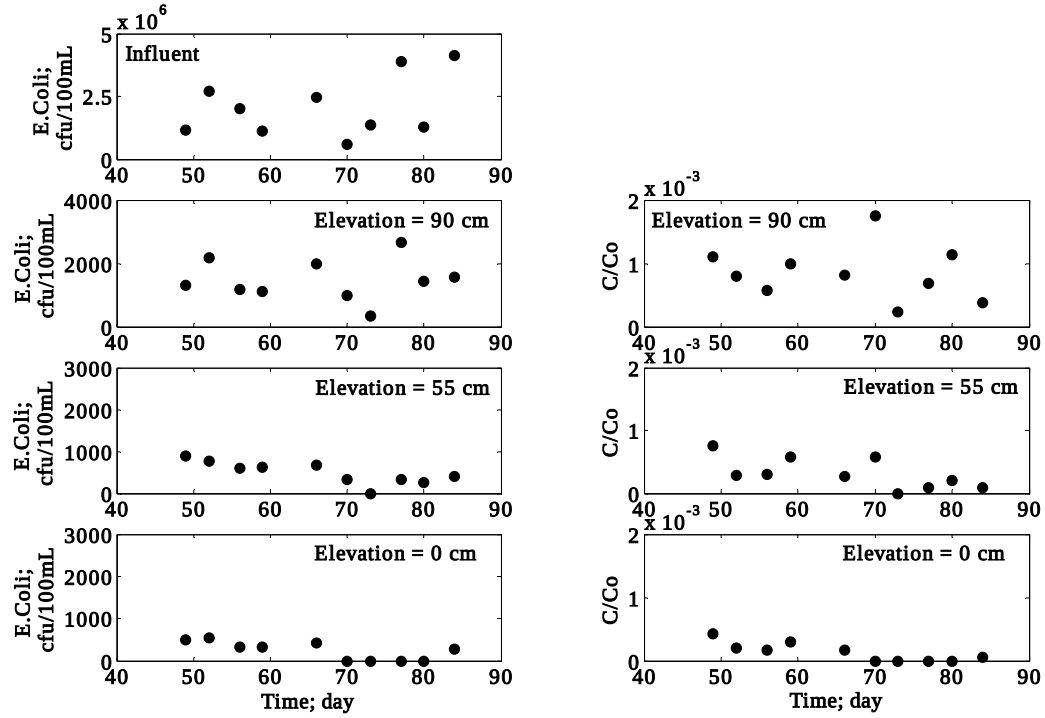

Figure 8.14 *E.Coli* concentration profiles of the wastewater and the filtered samples (datum at the column base).

Based on the above observations of pH, ammonia, nitrate, phosphorous and *E.Coli* concentrations, it is clear that the soil column could effectively improve the quality of domestic wastewater. The effective removal zone for COD, phosphate, ammonia and nitrate reduction was found at the top portion of the soil column. However, the observations were undertaken with a very thick soil layer. The estimated retardation zone presented here was not accurate enough to estimate the safe distance between drainage pipes and the water table. Therefore, the simulations were applied to evaluate the reduction zones of contaminant in unsaturated soil conditions.

8.4 Estimation of contaminant retardation zone

The simulations were undertaken using the contaminants transport model developed in this research. The input parameters used are shown in Table 8.2.

Table 8.2 Input parameters for the contaminant transport model

Parameters	Values
Domain	Column depth 120 cm with a homogenous soil condition
Feeding rate (cm^3/hour)	17.8
The kinetic reaction rates:	
Organic carbon compounds	
Maximum specific growth rate, μ_O (1/h)	74.4 (Widdowson et al. 1988)
Heterotrophic yield coefficient, Y_O	0.45 (Widdowson et al. 1988)
Substrate saturation constant, K_{SO} (g/cm^3)	$4.0x10^{-2}$ (Widdowson et al. 1988)
Oxygen saturation constant, K_O (g/cm^3)	$7.7x10^{-4}$ (Widdowson et al. 1988)
Ammonia saturation constant, K_{AO} (g/cm^3)	$1.0x10^{-3}$ (Widdowson et al. 1988)
Dissolved oxygen concentration, C_O (g/cm^3)	$2.0x10^{-3}$
Ammonia concentration, C_A (g/cm^3)	$5.502x10^{-2}$
Molecular diffusion coefficient, D* (cm^2/h)	0.03924 (Kemper 1986)
Nitrate nitrogen compounds	
Maximum specific growth rate, μ_N (1/h)	69.6 (Widdowson et al. 1988)
Heterotrophic yield coefficient, Y_N	0.5 (Widdowson et al. 1988)
Substrate saturation constant, K_{SN} (g/cm^3)	$4.0x10^{-2}$ (Widdowson et al. 1988)
Nitrate saturation constant, K_N (g/cm^3)	$2.6x10^{-3}$ (Widdowson et al. 1988)
Ammonia saturation coefficient, K_{AN} (g/cm^3)	$1.0x10^{-3}$(Widdowson et al. 1988)
Inhibition coefficient, I[C_O]	0.080
Molecular diffusion coefficient, D* (cm^2/h)	0.0684 (Kemper 1986)
Phosphate phosphorus compounds	
Adsorption coefficient, K_{ad} (cm^3/g)	$2.93x10^4$
Soil bulk density, ρ_B (g/cm^3)	1.25
Molecular diffusion coefficient, D* (cm^2/h)	0.02304 (Kemper 1986)
E.Coli	
Adsorption- desorption rate, K_{ad} (1/h)	56.8 (Schnoor 1996)
Growth and decay rate, K_g (1/h)	0.105 (Stevik et al. 1999b)
Soil bulk density, ρ_B (g/cm^3)	1.25
Molecular diffusion coefficient, D* (cm^2/h)	0.04788 (Kemper 1986)

Table 8.2 (cont.) Input parameters for the contaminant transport model

Parameters	Values
Initial and boundary conditions:	
Organic carbon compounds	The constant concentration at the column surface; C_{top} is 2.494×10^{-4} g/cm^3, the concentration at column base; C_{bot} is 3.773×10^{-5} g/cm^3 and the initial concentration; C_{int} is 3.773×10^{-5} g/cm^3.
Nitrate nitrogen compounds	The constant concentration at the column surface; C_{top} is 1.27×10^{-6} g/cm^3, the concentration at column base; C_{bot} is 2.34×10^{-6} g/cm^3 and the initial concentration; C_{int} is 2.34×10^{-6} g/cm^3.
Phosphate phosphorus compounds	The constant concentration at the column surface; C_{top} is 5.27×10^{-6} g/cm^3, the concentration at column base; C_{bot} is 2.222×10^{-7} g/cm^3 and the initial concentration; C_{int} is 2.222×10^{-7} g/cm^3.
E.Coli	The constant concentration at the column surface; C_{top} is 5.462×10^{-7} g/cm^3 (or 1.93×10^6 cfu/100 mL), the concentration at column base; C_{bot} is 5.911×10^{-11} g/cm^3 (or 210 cfu/100 mL) and the initial concentration; C_{int} is 5.911×10^{-11} g/cm^3 (or 210 cfu/100 mL).
Nodal spacing; cm	1
Maximum time simulation; day	20
Number of time step per hour	2840

Note: Concentration of *E.Coli* estimated based on the microbial weight of 2.83×10^{-8} mg/colony (Widdowson et al. 1988).

The simulation results of each contaminant were obtained as follows.

8.4.1 COD and nitrate compounds

The simulations of COD and nitrate concentration are described in Figures 8.15 and 8.16, respectively. The model could accurately predict the concentrations of COD profile and nitrate under equilibrium conditions. The COD reduction zone was found at an elevation of 105 cm. The concentration of COD remaining in the effluent was 37 mg/L. The NO_3-N concentration profiles indicated that the concentration increased from the surface to an elevation of 105 cm. The nitrate concentration at the base (effluent) was found to be 2-3 mg/L which is less than the critical limit (10 mg/L) used in groundwater supplies. It is clear from these observations that the soil could effectively retard COD and nitrate.

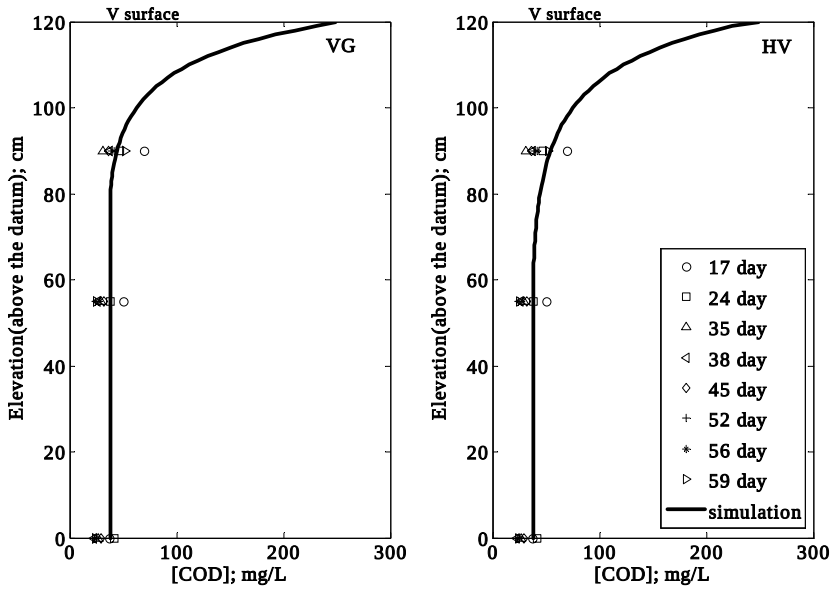

(VG is van Genuchten and HV is Haverkamp et al. hydraulic properties models).

Figure 8.15 COD concentration profiles and the simulations for the pilot scale soil column test (datum at the column base).

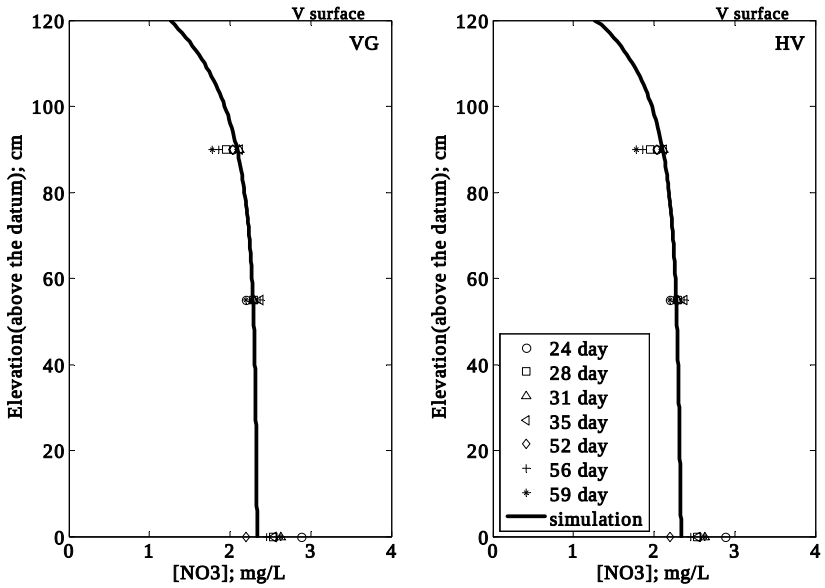

(VG is van Genuchten and HV is Haverkamp et al. hydraulic properties models).

Figure 8.16 Nitrate concentration profiles and the simulations for the pilot scale soil column test (datum at the column base).

8.4.2 Phosphate compounds

Figure 8.17 presents phosphate concentration profiles. The simulations indicated that phosphate was effectively retarded at an elevation of 115 cm. This zone is the phosphate adsorption zone. Even though the column was operated for 91 days, the exhaust zone had not yet been observed. Thus, the presence of soil minerals was sufficient to react with the phosphate. The filtered sample contained phosphate at 0.2 mg/L. The 120 cm deep soil layer could retard the phosphate migration for a very long period. The adsorption capacity used within 91 days was 6.03×10^{-6} mgP/mg soil. The maximum adsorption capacity estimated from the isotherms was 7.62×10^{-4} mgP/mg soil. The soil column had only used 0.79% of the maximum capacity. The estimated breakthrough time of this column was 31.6 years, hence the column can retard phosphate for a long period.

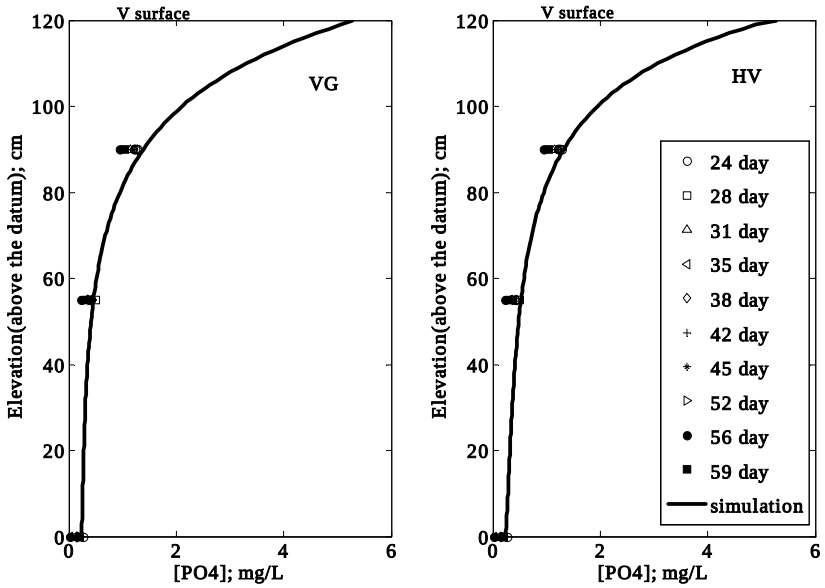

(VG is van Genuchten and HV is Haverkamp et al. hydraulic properties models).

Figure 8.17 Phosphate concentration profiles and the simulations for the pilot scale soil column test (datum at the column base).

8.4.3 *E.Coli*

The simulation results for *E.Coli* are presented in Figure 8.18. Both simulations provided a unique result, which fitted well to the observations. The reduction zone of *E.Coli* was observed at the elevation of 110 cm. However, the amount of *E.Coli* remaining in the filtrated samples was still high. If the *E.Coli* could reach the groundwater, the groundwater would not be safe to drink. A disinfection process will be required.

This topsoil contained fine-grained clay and silt which could extend the contaminant travel time. It also contained high levels of minerals and microbes that could react with the contaminants. The reduction zones of COD, nitrate, phosphate and *E.Coli* were observed on the top of the soil, where aeration occurred. All simulations suggested that the soil could effectively purify domestic wastewater. However, it would transmit water very slowly, and therefore soil might be inappropriate for constructing an absorption field.

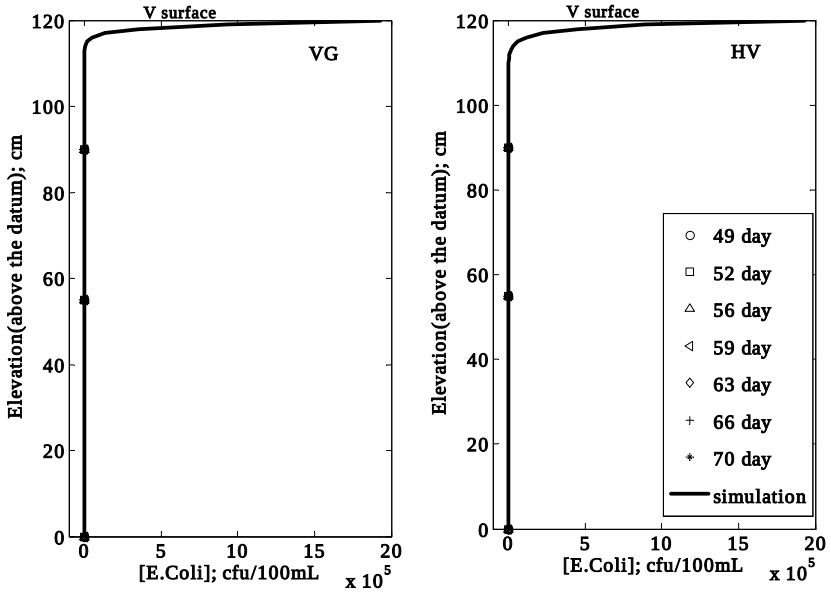

(VG is van Genuchten and HV is Haverkamp et al. hydraulic properties models).

Figure 8.18 *E.Coli* concentration profiles and the simulations for the pilot scale soil column test (datum at the column base).

8.5 Summary

A pilot scale soil column was utilised to study the transport of contaminants in unsaturated soil, and this showed that the contaminants contained in domestic wastewater could be purified by biotransformation and adsorption. The column was operated for three months and performed high levels of wastewater purification. Approximately, 83% of COD was removed with a remaining concentration of 37 mg/L. Ammonia was converted to be nitrate, and then nitrate was consumed due to the nitrate respiration process, and the final concentration of nitrate was 2.3 mg/L. The phosphate compounds were approximately 90% adsorbed and the remaining concentration was 0.2 mg/L. The *E.Coli* could be retarded by 99.999% and remaining *E.Coli* was 210 cfu/100mL.

The simulations of all contaminants across the soil column corresponded well to the respective observations. The reduction zones of COD, nitrate and phosphate were observed at 105 cm above the datum. The *E.Coli* reduction zone was 110 cm above the datum. These

results indicated that 120 cm layer of soil could improve domestic wastewater quality while the remaining contaminants were very low in concentration. This depth of soil is adequate and safe for disposing of domestic wastewater.

CHAPTER 9

MODEL APPLICATIONS AND CASE STUDIES

9.1 Introduction

The model developed using Richards' equation for the gravitational and the infiltration-redistribution systems was verified with four case studies. The case studies included are: Case 9.1.1 Infiltration column experiments with Haverkamp's hydraulic properties model (Haverkamp et al.1977 and Hills et al. 1989), Case 9.1.2 Infiltration column experiments with the van Genuchten hydraulic properties model (Celia et al. 1990), Case 9.1.3 Sharp front infiltration column with an initially dry soil (Paniconi et al. 1991) and Case 9.1.4 Infiltration and redistribution column (Paniconi et al. 1991). The contaminant transport model was verified for four case studies that include both non-reactive compounds (tracer) and reactive compounds. The case studies for the transport of a non-reactive contaminant were, Case 9.2.1 Transport of chloride ion in Delhi sand (James & Rubin 1986) and Case 9.2.2 Warrick et al.'s solute transport in an onsite infiltration system (Warrick et al. 1971). The case studies for the transport of reactive contaminants were, Case 9.2.3 "Movement of contaminants through sandy soil near Perth" (Whelan & Barrow 1984a and 1984b) and Case 9.2.4 "Removal of *E.Coli* from wastewater using lightweight aggregate and activated carbon" (Stevik et al. 1999a and 1999b). The design implications for defining the safe distance between an onsite system and groundwater pumping wells were evaluated. The safe distance for an onsite waste disposal system was calculated and compared with the recommended buffer distance.

9.2 Applications of Richards' equation

The water movement model was verified with the gravitational infiltration and the infiltration-redistribution columns. The water movement through the gravitational infiltration columns was considered in Case 9.1.1, Case 9.1.2 and Case 9.1.3. The water movement through the infiltration-redistribution columns was considered in Case 9.1.4. All simulations are provided in Appendix-J.

Case 9.1.1 Infiltration column experiments with Haverkamp et al.'s hydraulic properties model

One-dimensional experiments were investigated using the soil column with a 70 cm deep bed. Water percolated through the soil column under gravitational force. Richards' and HV equations were applied to this case study. The input parameters are given in Table 9.1.

Table 9.1 Input parameters for Case 9.1.1 (Haverkamp et al. 1977)

Parameters	Values
Domain	Column with depth of 70 cm
Hydraulic properties model	HV
Saturated hydraulic conductivity; K_{zz} (cm/h)	34
Saturated moisture content; θ_s	0.287
Residual moisture content; θ_r	0.075
β	3.96
γ	4.74
α	1.611×10^6
A	1.175×10^6
Boundary and initial conditions	Constant flux at the surface, q_z of 13.69 cm/h. Constant moisture content at the column base, θ_{bot} of 0.1, or pressure head at the column base, ψ_{bot} of -61.5 cm. Constant initial moisture content, θ_{int} of 0.1.
Number of element; *nelem*	70
Increment time interval; *dt* (hour)	0.04
Nodal spacing; *dz* (cm)	1

The Neumann and Dirichlet conditions were applied to the upper and lower boundary, respectively. The simulations of moisture content profiles are presented in Figure 9.1. The developed model fitted the observed data given by Haverkamp et al. (1977) very well. Hills et al. (1989) had also simulated this case study, their simulations and the present model are presented in Table 9.2. The nodal moisture content obtained from the developed model was similar to the one obtained by Hills et al. (1989).

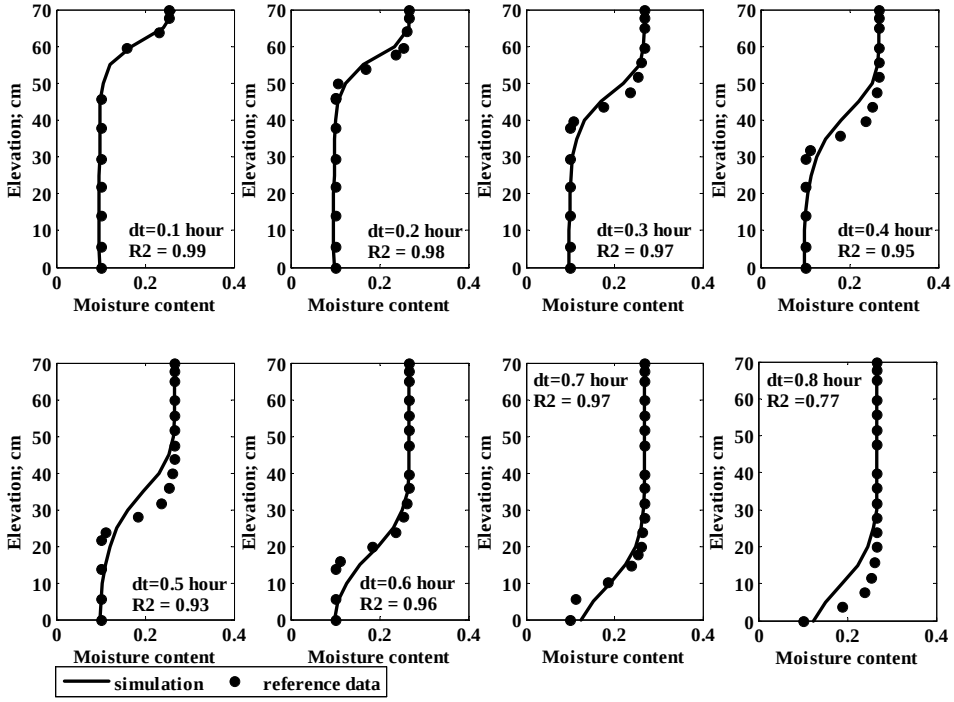

Figure 9.1 Simulations of moisture content profiles for Case 9.1.1 (datum at the base of the column).

Table 9.2 Moisture content profiles at 0.5 hours for Case 9.1.1

Depth (above the datum), z (cm)	Nodal moisture content		
	Present study	Hills et al. (1989)	
		Test case 1*	Test case2**
67.5	0.2670	0.2671	0.2671
62.5	0.2670	0.2669	0.2669
57.5	0.2670	0.2665	0.2664
52.5	0.2670	0.2657	0.2656
47.5	0.2670	0.2642	0.2641
42.5	0.2664	0.2613	0.2611
37.5	0.2638	0.2548	0.2546
32.5	0.2558	0.2369	0.2368
27.5	0.2350	0.1730	0.1743
22.5	0.2012	0.1050	0.1053
17.5	0.1652	0.1001	0.1002
12.5	0.1358	0.1000	0.1000
7.5	0.1153	0.1000	0.1000

Note: * One-step pressure head solution used by Haverkamp et al. (1977)

** Richard's equation ψ-based simulated by Hills et al. (1989)

Case 9.1.2 Infiltration column experiments with van Genuchten's hydraulic properties model

This case study was proposed by Celia et al. (1990). The infiltration column was packed with a homogeneous soil. The hydraulic properties of the soil were observed in field conditions at a site in New Mexico, USA. The input parameters are given in Table 9.3.

Table 9.3 Input parameters for Case 9.1.2 (Celia et al. 1990)

Parameters	Values
Domain	Column with depth of 100 cm
Hydraulic properties model	VG
Saturated hydraulic conductivity; K_{zz} (cm/s)	0.00922
Saturated moisture content; θ_s	0.368
Residual moisture content; θ_r	0.102
p	2
m	0.5
a	0.0335
Boundary conditions	Constant head at the top, ψ_{top} of -75 cm and constant head at the datum ψ_{bot} of -1000 cm.
Initial pressure head; ψ_i (cm)	-1000
Number of element; *nelem*	40
Increment time interval; *dt* (sec)	0.05
Nodal spacing; *dz* (cm)	2.5

Celia et al. (1990) applied the mixed formulation of Richards's equation to evaluate the pressure head profiles. However, for the present research the pressure head based solely on Richards' equation was applied. The known pressure heads were applied to the upper and lower boundaries as the Dirichlet conditions. The simulations of pressure head profiles are presented in Figure 9.2. The simulated results were identical to those given by Celia et al. (1990) despite the fact that different forms of Richards' equation were applied. This implied that convergence has occurred using Richards' equation. It does appear that the developed model is compatible with this kind of boundary condition.

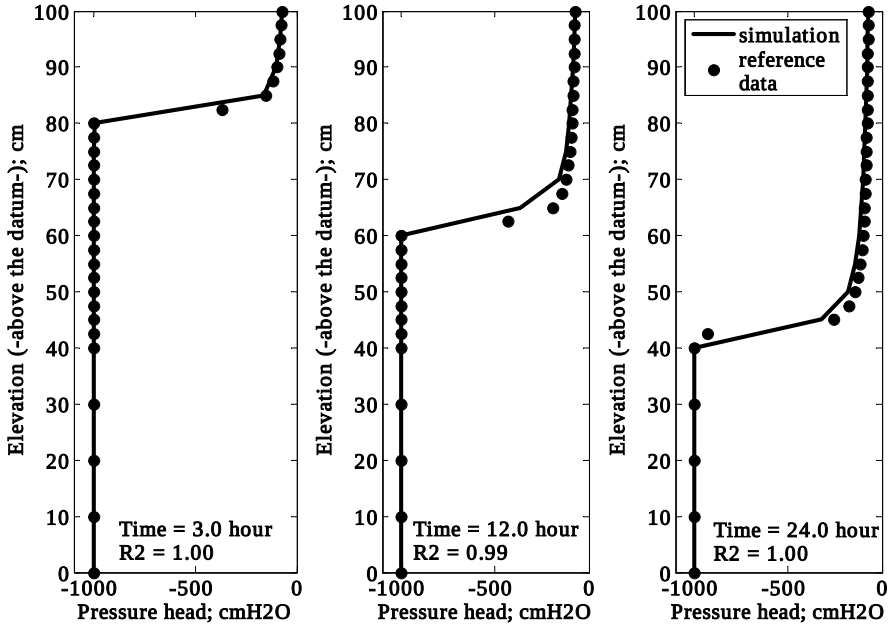

Figure 9.2 Simulations of pressure head profiles for Case 9.1.2 (datum at the base of the column).

Case 9.1.3 Sharp front infiltration column with an initially dry soil

Paniconi et al. (1991) conducted a simulation of water movement through a soil column with a depth of 1.25 m. The column was packed with relatively dry soil to observe the movement of the wetting front. The simulations were obtained using mixed forms of boundary conditions, the lower boundary was defined using the Dirichlet condition, while the upper boundary was controlled by the Neumann condition. The input parameters for this case study are given in Table 9.4.

Table 9.4 Input parameters for Case 9.1.3 (Paniconi et al. 1991)

Parameters	Values
Domain	Column with depth of 125 cm
Hydraulic properties model	VG
Saturated hydraulic conductivity; K_{zz} (cm/h)	0.0004
Air entry pressure; ψ_S (cm)	-120
Saturated moisture content; θ_s	0.38
Residual moisture content; θ_r	0.15
m	0.75
p	4.0
α (1/cm)	0.008333
Specific storage, S_s (1/cm)	0.000001
Boundary and initial conditions	Constant head at the datum, ψ_{bot} of-300 cm, constant head at the surface, ψ_{top} of -6.698246 cm and constant flux at the surface, q_z of 0.08 cm/h. Initial pressure head, ψ_{int} of -300 cm.
Number of element; *nelem*	300
Increment time interval; *dt* (hour)	0.01
Nodal spacing; *dz* (cm)	0.4167

The pressure head based Richards' equation was applied in this research and compared with the original work of Paniconi et al (1991). The specific storage was excluded in this research because this value was considered very small (10^{-6} cm^{-1}). The pressure head and moisture content profiles are presented in Figure 9.3. The result obtained from the developed model agreed well with the one proposed by Paniconi et al. (1991). This revealed that the developed model could effectively predict the movement of water through the relatively dry soil infiltration column.

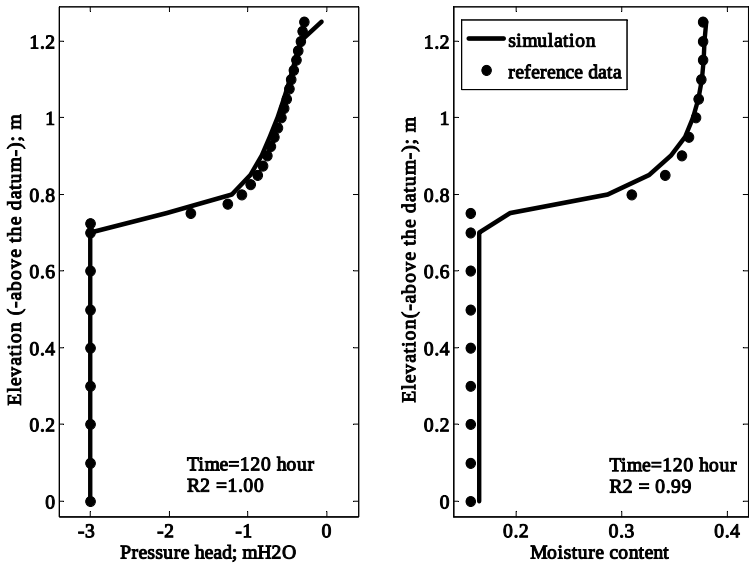

Figure 9.3 Pressure head and moisture content profiles of Case 9.1.3 (datum at the base of the column).

The elevated pressure head profiles obtained from the developed model and Paniconi et al. (1991) are compared in Table 9.5. The nodal pressure head yielded in this research was close to the one presented by Paniconi et al. (1991).

Table 9.5 Pressure head profile for Case 9.1.3

Elevation (m)	Paniconi et al. (1991)*	Present study
0.700	-3.00000	-2.999028
0.750	-1.72850	-2.026748
0.800	-1.08080	-1.199539
0.850	-0.88309	-0.971493
0.900	-0.75763	-0.829035
0.950	-0.66211	-0.719831
1.000	-0.58271	-0.627894
1.050	-0.51314	-0.546206
1.100	-0.45003	-0.471039
1.150	-0.39130	-0.400157
1.200	-0.33563	-0.332108
1.250	-0.28206	-0.066982

Note *Values shown had been obtained by single Picard's iteration technique.

Case 9.1.4 Infiltration and redistribution column

Paniconi et al. (1991) demonstrated a test for the water movement through the infiltration and redistribution column. An initial condition was controlled by a static equilibrium of capillary force. The input parameters for this case study are given in Table 9.6.

Table 9.6 Input parameters for Case 9.1.4 (Paniconi et al. 1991)

Parameters	Values
Domain	Column with depth of 10 m
Hydraulic properties model	VG
Saturated hydraulic conductivity; K_{zz} (m/h)	5
Air entry pressure; ψ_S (m)	-3.0
Saturated moisture content; θ_S	0.45
Residual moisture content; θ_r	0.08
m	0.667
p	3.0
Boundary and initial conditions	Specific flux on the top, q_z of t/64 m/h. Constant head at the column base, ψ_{bot} of 0 m. Constant head at the initial, ψ_{int} of 0 m.
Number of element; *nelem*	100
Increment time interval; *dt* (hour)	1
Maximum simulation time; t (hour)	32

The Neumann and the Dirichlet conditions were applied to the upper and lower boundary, respectively. The pressure head and moisture content profiles are presented in Figures 9.4 and 9.5, respectively. The simulations obtained from the developed model matched very well with the original work of Paniconi et al. (1991). This implied that the developed model was robust, and that it could effectively support the estimation of water movement in the infiltration-redistribution systems.

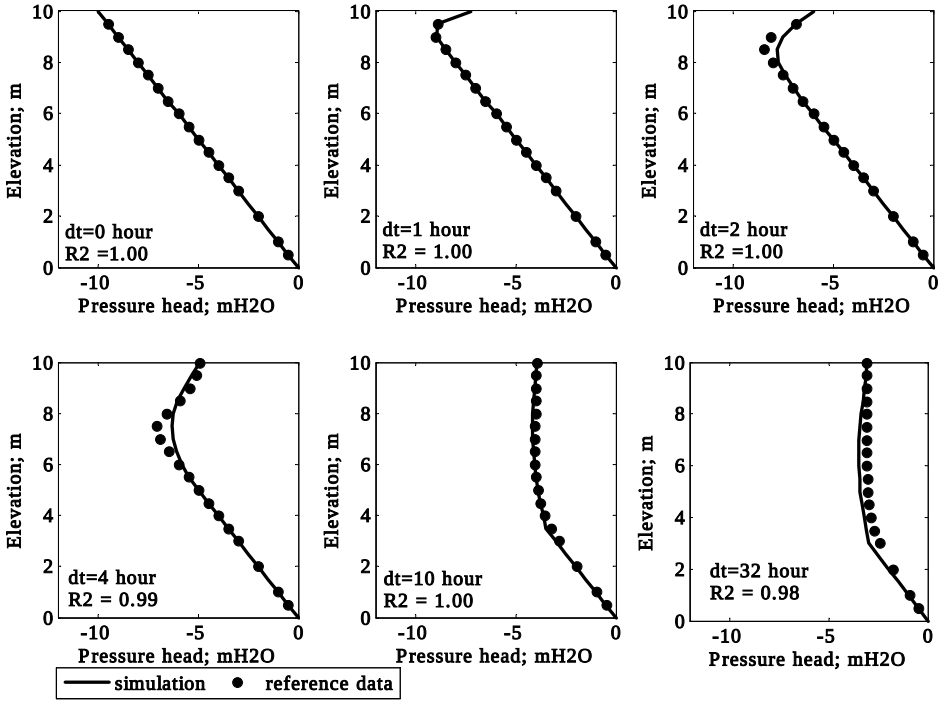

Figure 9.4 Pressure head profiles for Case 9.1.4 (datum was at the groundwater table).

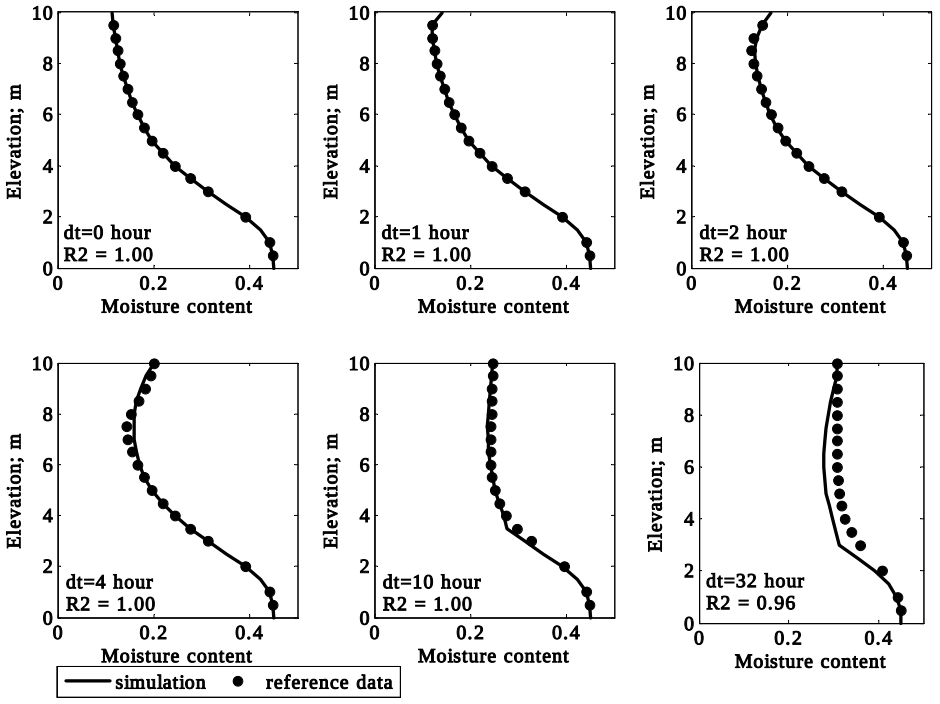

Figure 9.5 Moisture content profiles for Case 9.1.4 (datum was at the groundwater table).

Ségol (1993) presented the data of this case study. The simulations obtained from the developed model were similar to the data given in the reference. The data for the nodal pressure heads and the moisture contents are given in Tables 9.7 and 9.8, respectively.

Table 9.7 Nodal pressure head for Case 9.1.4

Elevation (m)	Ségol (1993)						Present study					
	Time interval (hour)						Time interval (hour)					
	0	1	2	4	10	32	0	1	2	4	10	32
0.50	-0.50000	-0.50000	-0.50000	-0.50000	-0.48816	-0.45052	-0.50000	-0.50000	-0.50000	-0.50000	-0.50000	-0.50000
1.00	-1.00000	-1.00000	-1.00000	-1.00000	-0.97487	-0.89603	-1.00000	-1.00000	-1.00000	-1.00000	-1.00000	-1.00000
2.00	-1.99999	-2.00000	-2.00000	-2.00001	-1.93348	-1.74054	-1.99999	-1.99999	-1.99999	-1.99999	-1.99999	-1.99999
3.00	-2.99999	-3.00000	-3.00000	-2.99999	-2.82685	-2.42854	-2.99999	-2.99999	-2.99999	-2.99999	-2.99999	-2.99999
3.50	-3.49999	-3.50000	-3.50000	-3.49999	-3.21229	-2.67148	-3.49999	-3.49999	-3.49999	-3.49999	-3.49999	-3.09991
4.00	-3.99998	-3.99999	-4.00000	-3.99997	-3.52795	-2.83966	-3.99999	-3.99999	-3.99999	-3.99999	-3.99999	-3.21829
4.50	-4.49998	-4.49999	-4.49999	-4.49991	-3.75877	-2.94492	-4.49999	-4.49999	-4.49999	-4.49999	-3.59615	-3.31658
5.00	-4.9998	-4.99998	-4.99999	-4.99975	-3.90662	-3.00570	-4.99999	-4.99999	-4.99999	-4.99999	-3.74804	-3.39219
5.50	-5.49997	-5.49998	-5.49998	-5.49916	-3.98856	-3.03875	-5.49999	-5.49999	-5.55172	-5.50167	-3.87863	-3.44326
6.00	-5.99997	-5.99997	-5.99997	-5.99663	-4.02636	-3.05586	-5.99998	-5.99999	-6.02369	-5.81432	-3.98533	-3.46893
6.50	-6.49997	-6.49996	-6.49996	-6.48411	-4.03815	-3.06421	-6.49998	-6.49998	-6.50165	-6.07207	-4.06629	-3.46945
7.00	-6.99997	-6.99996	-6.99993	-6.91421	-4.03595	-3.06790	-6.99998	-6.99998	-6.97240	-6.24615	-4.12074	-3.44621
7.50	-7.49996	-7.49995	-7.49967	-7.05589	-4.02684	-3.06914	-7.49998	-7.49981	-7.40426	-6.30683	-4.14910	-3.40160
8.00	-7.99996	-7.99995	-7.99542	-6.57611	-4.01466	-3.06909	-7.99998	-7.99998	-7.72475	-6.22297	-4.51302	-3.33878
8.50	-8.49996	-8.49973	-8.42288	-5.90432	-4.00138	-3.06839	-8.49998	-8.49961	-7.80349	-6.02765	-4.13530	-3.26138
9.00	-8.99995	-8.98282	-8.13040	-5.41940	-3.98795	-3.06738	-8.99998	-8.96860	-7.50750	-5.71085	-4.05014	-3.17319
9.50	-9.49995	-8.87896	-6.85159	-5.10556	-3.97483	-3.06625	-9.49998	-8.90283	-6.84297	-5.32126	-3.99152	-3.07796
10.00	-9.99995	-7.21889	-5.97606	-4.89922	-3.96218	-3.06521	-9.99997	-7.21889	-5.97606	-4.89922	-3.96218	-3.96218

Table 9.8 Nodal moisture content for Case 9.1.4

Elevation (m)	Ségol (1993)						Present study					
	Time interval (hour)						Time interval (hour)					
	0	1	2	4	10	32	0	1	2	4	10	32
0.50	0.44886	0.44886	0.44886	0.44886	0.44894	0.44917	0.44887	0.44887	0.44887	0.44887	0.44887	0.44887
1.00	0.44114	0.44114	0.44114	0.44114	0.44177	0.44357	0.44116	0.44116	0.44116	0.44116	0.44116	0.44116
2.00	0.39122	0.39122	0.39122	0.39122	0.39588	0.40851	0.39136	0.39136	0.39136	0.39136	0.39136	0.39136
3.00	0.31309	0.31309	0.31309	0.31309	0.32671	0.35860	0.31332	0.31332	0.31332	0.31332	0.31332	0.31332
3.50	0.27629	0.27629	0.27629	0.27629	0.29692	0.33913	0.27653	0.27563	0.27653	0.27653	0.27653	0.30562
4.00	0.24460	0.24460	0.24460	0.244460	0.27437	0.32569	0.24483	0.24483	0.24483	0.24483	0.27001	0.29671
4.50	0.21832	0.21832	0.21832	0.21832	0.25920	0.31738	0.21853	0.21853	0.21853	0.21853	0.26012	0.28950
5.00	0.19692	0.19692	0.19692	0.19693	0.25010	0.31264	0.19711	0.19711	0.19711	0.19711	0.25202	0.28407
5.50	0.17958	0.17958	0.17958	0.17961	0.24526	0.31008	0.17975	0.17975	0.17816	0.17970	0.24568	0.28047
6.00	0.16552	0.6552	0.16552	0.16560	0.24308	0.30877	0.16567	0.16567	0.16507	0.17056	0.24104	0.27868
6.50	0.15404	0.15404	0.15404	0.15437	0.24240	0.30812	0.15418	0.15418	0.15414	0.16386	0.23799	0.27864
7.00	0.14461	0.14461	0.14461	0.14610	0.24253	0.30784	0.14473	0.14473	0.14521	0.15972	0.23643	0.28026
7.50	0.13680	0.13681	0.13681	0.14367	0.24305	0.30775	0.13691	0.13691	0.13830	0.15834	0.23622	0.28340
8.00	0.13028	0.13033	0.13033	0.15249	0.24375	0.30775	0.13037	0.13037	0.13383	0.16000	0.23719	0.28789
8.50	0.12479	0.12558	0.12558	0.16799	0.244452	0.30780	0.12487	0.12488	0.13281	0.16497	0.23917	0.29353
9.00	0.12013	0.12876	0.12876	0.18214	0.24529	0.30788	0.12020	0.12048	0.13680	0.17346	0.24195	0.30008
9.50	0.11614	0.14722	0.14722	0.19295	0.24606	0.30797	0.11621	0.12105	0.14750	0.18554	0.24532	0.30731
10.00	0.11271	0.16612	0.16612	0.20088	0.24680	0.30805	0.11278	0.14113	0.16628	0.20107	0.24703	0.30828

9.3 Applications of contaminant transport model

Two types of case studies were selected to verify the contaminants transport model. Case 9.2.1 and Case 9.2.2 were for the transport of a non-reactive contaminant. Case 9.2.3 and Case 9.2.4 were for the transport of reactive contaminants. The simulation data for these case studies are provided in Appendix-J.

Case 9.2.1 Transport of chloride ion in Delhi sand

James and Rubin (1986) conducted an experiment to determine the tracer transport through unsaturated sand. The columns were packed with a sample of Delhi sand that contained 90% sand, 7% silt and 3% clay (by weight). The cation exchange capacity of this sand was 0.05 mol/kg and the organic carbon content was 0.003 g/g. The soil column experiments A and B were operated at the water contents of 0.221 and 0.225, respectively. The average moisture content of the experiments was 0.223 and Darcy's velocity, q_z was 0.397 cm/h. The experimental water content resulting from the feeding tracer (NaCl) solution, θ_{ex} was 0.019. The dimensionless concentrations of chloride were estimated using the analytical solutions. The dispersion coefficient was evaluated using the Pfannukuch (1963) equation (cited in James & Rubin 1986). The equation for the dispersion coefficient was $D_z = 0.0020 + 0.059 q_z$. However, the authors did not provide all the input parameters, and hence the input parameters of the case study were obtained from the related literature as given in Table 9.9.

Table 9.9 Input parameters for Case 9.2.1

Parameters	Values
Domain	Single sand layer with depth of 30 cm.
Hydraulic properties model	VG
Saturated hydraulic conductivity; K_{zz} (cm/h)	9.418 (Carsel et al. 1988)
Saturated moisture content; θ_s	0.430 (Carsel et al. 1988)
Residual moisture content; θ_r	0.045 (Carsel et al. 1988)
Coefficient *a* (1/cm)	0.145 (Carsel et al. 1988)
Coefficient *p*	2.68 (Carsel et al. 1988)
Dispersivity; α_T (cm)	0.075 (James and Rubin 1986)
NaCl Molecular diffusion, D_{mol} (cm^2/h)	0.07308 (James and Rubin 1986)

Table 9.9 (cont.) Input parameters for Case 9.2.1

Parameters	Values
Boundary conditions	
Richards' equation	Constant head ψ_{top}= -8.25 cm at the top and ψ_{bot}= -125 cm at the bottom. (Estimated from Clapp and Hornberger (1978)'s equation)
Contaminant transport	Constant concentration at the surface with C_{top}= 500 meq/L. The concentration gradient is kept at zero (C_{bot}= 0 meq/L). Initial concentration, C_{int}= 0 meq/L.
Number of element; *nelem*	60
Increment time interval; *dt* (min)	0.2
Nodal spacing; *dz* (cm)	0.5

The simulation obtained from the developed model was compared to the one given by James and Rubin (1986), the results of this are given in Figure 9.6. The analytical equation and the developed model gave the residual squares, R^2 of 0.89-0.98 and 0.96, respectively. This indicated that the developed model could effectively estimate the movement of tracer in unsaturated soil conditions. The average Darcy's velocity obtained from this research was 0.365 cm/h. This was 8 % lower than the one estimated by James and Rubin (1986).

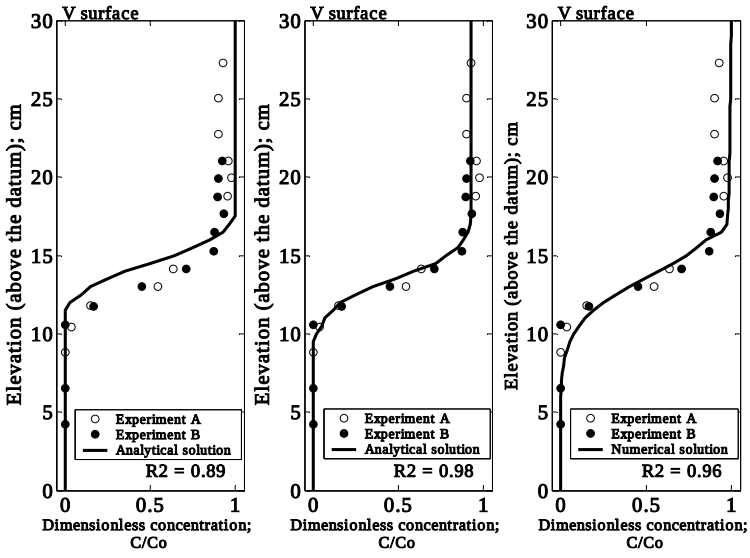

Figure 9.6 Dimensionless concentration profiles for Case 9.2.1 obtained from the various calculation processes (datum at the base of the column).

Case 9.2.2 Warrick et al.'s solute transport in an onsite infiltration system

Warrick et al. (1971) investigated the field scale experiment to determine the advection-dispersion transport of tracer. The experiment was carried out at the University of California West Side Field Station, near Fresno. This site was in a deep alluvial loam soil layer that was classified as the Panoche clay loam type. The experiment was conducted in an area, 6.1m x 6.1m. The sodium chloride solution (0.2 N) was applied as the tracer. The samples of soil water were collected from the centre of the site. This was assumed to be the one dimensional downward flow. The hydraulic properties model was analysed by Warrick et al. (1971) and the equations were expressed as:

$$\theta(\psi) = 0.6829 - 0.09524 \ln(|\psi|) \qquad \psi \le 29.484 \quad cm \tag{9.1}$$

$$\theta(\psi) = 0.4531 - 0.02732 \ln(|\psi|) \qquad -29.484 < \psi \le -14.495 \quad cm \tag{9.2}$$

and

$$K_{zz}(\psi) = 19.34x10^{5}|\psi| \qquad \psi \le -29.484 \quad cm \tag{9.3}$$

$$K_{zz}(\psi) = 516.8|\psi|^{-0.97814} \qquad -29.484 < \psi \le -14.495 \quad cm \tag{9.4}$$

where K_{zz} was in unit cm/d.

The order of these equations changed over pressure head. These hydraulic properties equations were not compatible for the developed model. The hydraulic properties data given by Warrick et al. (1971) were fitted into VG and HV equations. The best fit water retention curves for VG and HV equations are shown in Figure 9.7 and the estimated coefficients for the VG and HV equations are given in Table 9.10.

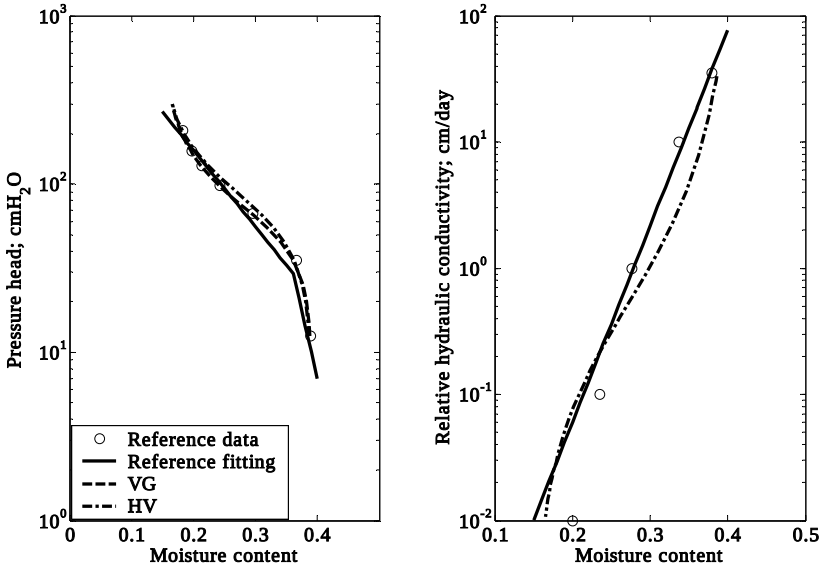

Figure 9.7 Water retention curves for Case 9.2.2 fitted by HV and VG equations

Table 9.10 Hydraulic properties coefficients for Case 9.2.2

Parameters	Values
Saturated moisture content; θ_s	0.38
Residual moisture content; θ_r	0.15
The coefficient for VG equation	
p	2.716
a (1/cm)	0.0163
The coefficient for HV equation	
A	2.31×10^4
a	2.26×10^4
β	2.229
γ	3.194

The authors did not provide all input parameters for the simulation, so the inputs used in this research were obtained from related literature. The input parameters are given in Table 9.11.

Table 9.11 Input parameters for Case 9.2.2

Parameters	Values
Domain	Single soil layer with depth of 200 cm.
Hydraulic properties model	VG and HV
Saturated hydraulic conductivity; K_{zz} (cm/h)	1.575 (Carsel et al. 1988)
Saturated moisture content; θ_s	0.38 (Carsel et al. 1988)
Residual moisture content; θ_r	0.15 (Carsel et al. 1988)
Dispersion ; α_T (cm)	1.026 (Carsel et al. 1988)
Molecular diffusion, D^* (cm^2/h)	0.07308 (James and Rubin 1986)
Boundary and initial conditions	
Richards' equation	Constant head at the top, ψ_{top} of -14.495 cm (or θ =0.38) and constant pressure gradient at the datum ($d\psi/dz$), of 0 (or θ =0.20). Initial moisture content, θ_{int} was constant at 0.20 (estimated using Clapp and Hornberger (1978)'s equation).
Contaminant transport	Constant concentration at the surface, C_{top} of 209 meq/, at t>2.8 hour. The concentration gradient was kept at zero, the concentration at the datum, C_{bot} of 0 meq/L. Initial concentration, C_{int} of 0 meq/L.
Number of element; *nelem*	200
Increment time interval; *dt* (sec)	Variable
Nodal spacing; *dz* (cm)	1

The moisture content profiles are given in Figure 9.8. The moisture content profiles at 2 hours were effectively predicted, however, the moisture content profiles at 17 hours were not satisfactorily predicted. This might be due to the hydraulic properties of this soil sample. The hydraulic properties of soil changed significantly depending upon the moisture content (Ségol 1993). The average Darcy's velocities obtained from Richards' and HV and VG equations at 2 hours were 0.13 and 0.12cm/h, respectively. While, Darcy's velocity at 17 hours obtained from Richards' and HV or VG equation increased to 0.78 and 0.71 cm/h, respectively. Darcy's velocity observed in this case study also increased non-linearly and with time.

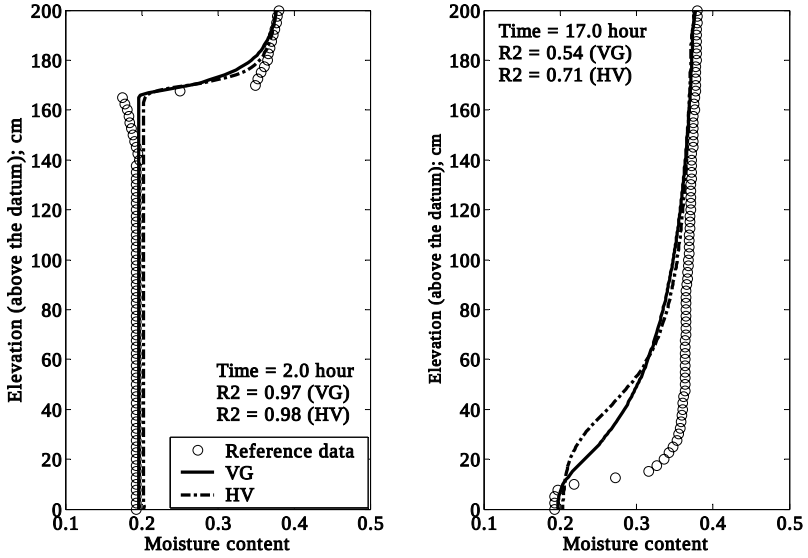

Figure 9.8 Moisture content profiles for Case 9.2.2 (datum at the base of the column).

The tracer concentration profiles are given in Figure 9.9. The model could effectively estimate the tracer concentration profiles at 2 hours. However, it could not estimate the concentration profiles at 17 hours. The background ions in the soil would have disturbed the measurement of tracer concentration as it was found that the measured concentration of the effluent was higher than the feed tracer concentration. This has led to the unpredictable results.

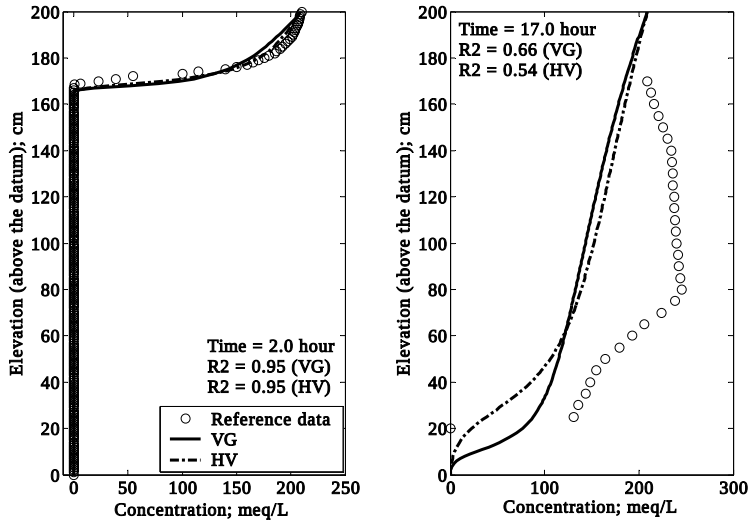

Figure 9.9 Concentration profiles for Case 9.2.2 (datum at the base of the column).

Warrick et al. (1971) assumed the value of D_z was constant at 4.2 cm^2/h (0.07 cm^2/min). The D_z obtained from the developed model was in the range of 3-6 cm^2/h (0.05-0.1 cm^2/min). The values of D_z obtained at 2 and 17 hours were time varying and non-linear. The values obtained for D_z at 2 and 17 hours were 0.71 and 1.42 times of the one given by Warrick et al. (1971).

Case 9.2.3 Movement of contaminants through sandy soil near Perth

Whelan and Barrow (1984a and 1984b) studied the migration of nitrogen and phosphorus compounds released from a septic tank through the sandy soils in Perth, Western Australia. The soil characteristics are provided in Table 9.12.

Table 9.12 Soil textural for Case 9.2.3
(McArthur & Bettenay 1964, cited in Whelan & Barrow 1984b)

Soil name	Great soil group	USA classification	CEC (C/g)	pH	Fe (%)	Coarse sand[1] (%)	Fine sand[2] (%)	Silt[3] (%)	Clay[4] (%)
Bassendean	Iron-humus	Spodosol Grey sand	0.1	6.0	0.02	97	1	1	2
dune system.	podzol	Iron Band	0.2	6.2	0.39	90	5	1	3
Jandakot sand									
Spearwood	Podzolized								
dune system.	aeolian sand	Inceptisol	0.5	6.8	0.26	77	18	2	3
Karrakatta sand									

Note: [1]The coarse sand with a particle size 0.2-2 mm, [2] The fine sand with the particle size 0.2-0.02 mm,
[3] The silt with the particle size 20-2 μm, and [4] The clay with the particle size less than 2 μm.

The total texture of Spodosal grey sand was 101% and the iron band was 99%. So the portions of soil textures were adjusted to 100%. Spodosal grey contained sand, clay and silt at 97, 2 and 1%, respectively. Spodosal iron band contained 96% sand, 1% silt, and 3% clay. Inceptisol contained 95% sand, 2% silt, and 3% clay.

The hydraulic properties data of these soils were not provided in the reference. Thus, these data were obtained using the Saxton et al. (1986) equations. The estimated hydraulic properties data of these soils are given in Figure 9.10. The USDA textural classes of all these samples were sand.

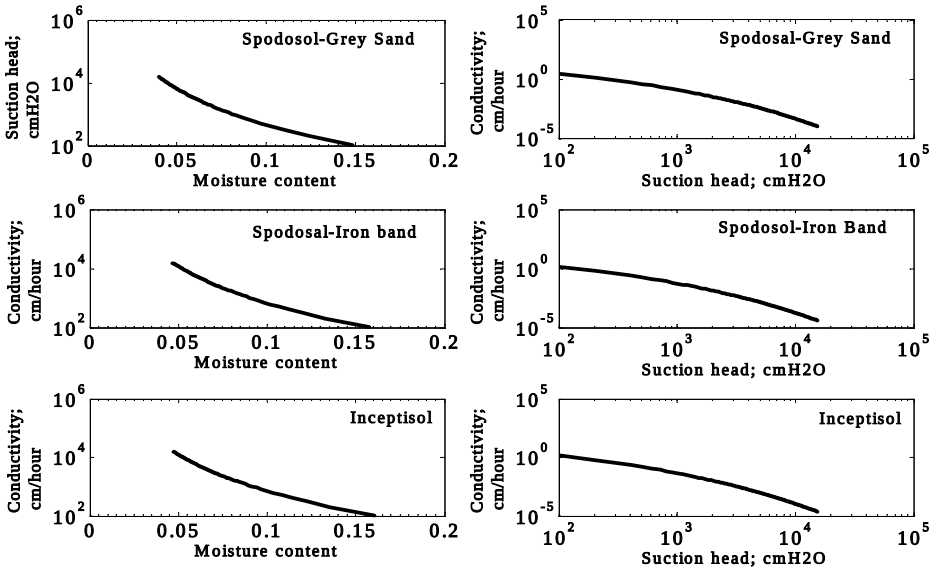

Figure 9.10 Soil water retention curves for Case 9.2.3

HV and VG equations were applied to fit these estimated soil hydraulic properties data. The water retention curves fitted using HV and VG equations were presented Figures 9.11 and 9.12, respectively. The water retention curves of these soil samples were same. This might be the result of the similarity of the soil textures. The coefficients of the soil hydraulic properties were given in Table 9.13. The hydraulic properties coefficients of these soil samples were similar and the differences were not significant.

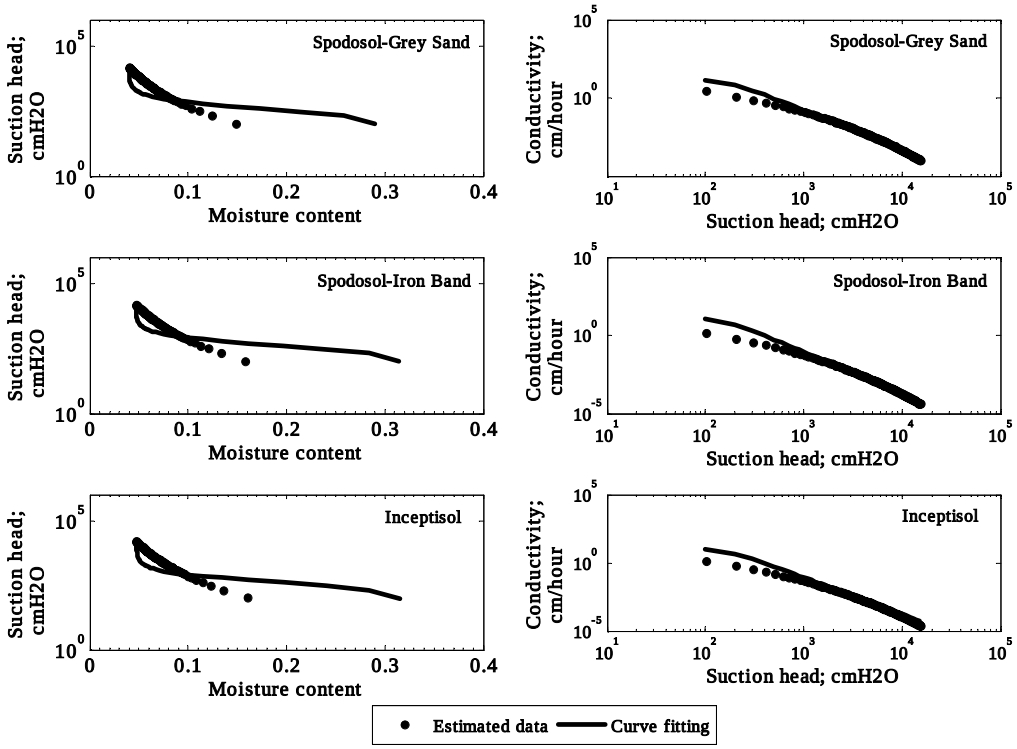

Figure 9.11 Water retention curves of Case 9.2.3 fitted using HV equations

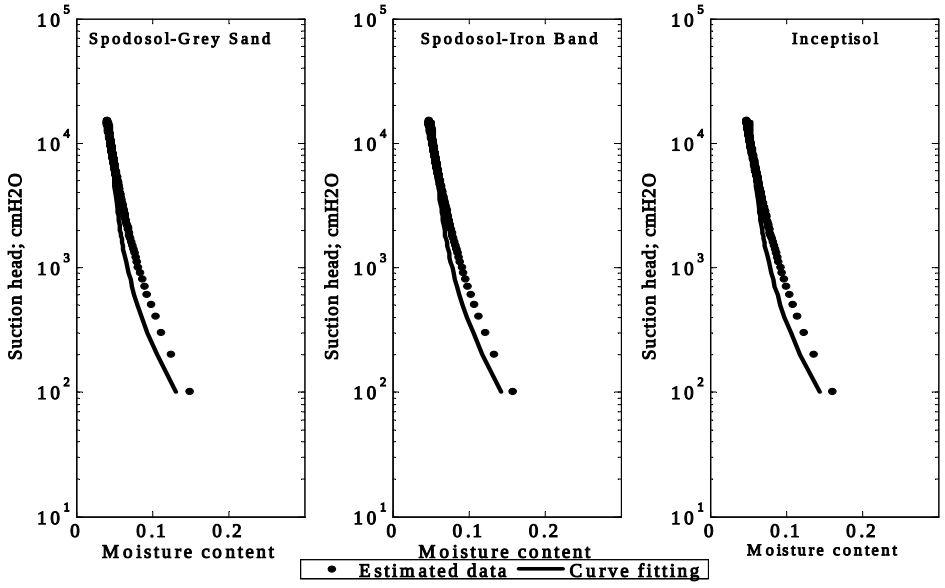

Figure 9.12 Water retention curves of Case 9.2.3 fitted using VG equations

Table 9.13 Coefficients of hydraulic properties for Case 9.2.3

Parameters	Values		
	Spodosal-grey sand	Spodosal-iron band	Inceptisol
θ_s	0.300	0.323	0.323
θ_r	0.040	0.047	0.047
$K_{zz}k_{rw}$ (cm/h)	17.3	13.7	13.3
ψ_s (cm)	5.79	2.28	2.53
Hydraulic properties			
HV			
A	7.14×10^5	7.21×10^5	7.35×10^5
α	1.12×10^6	1.28×10^6	1.31×10^6
β	2.317	2.318	2.322
γ	2.634	2.684	2.688
VG			
p	1.6627	1.6178	1.6246
a (1/cm)	0.0253	0.0275	0.0272

The migrations of organic carbon compounds and nitrate were observed at the drainage field that located on Bassendean sand layer. The septic tank received a combination of black and grey water. It was operated for 16 years. A sand sample from this site contained the background concentrations of ammonium and nitrate of 10-37 and 0-13 μg/g, respectively. Samples of filtered wastewater were collected at the far end of each drainage system (3 m away from the drainage pipe). The migrations of phosphate were observed in two different sites. One was located at Bassendean Janakot and another was at Spearwood-Karrakatta. The phosphate migrations were observed at the layer of 6 cm of Spearwood-Karrakatta and 2 m of Bassendean Janakot sand. The septic tanks installed in these sites received a combination of black and grey water. The tank located on the Bassendean Janakot sand had operated for 16 years, and the other installed on the Spearwood-Karrakatta sand had operated for 4 years. The background concentrations of inorganic phosphate in these sands varied widely from 0.5-300 μg/g. The averages of soil inorganic and organic phosphorus concentration were 90 and 5 μgP/g soil, respectively. The authors provided the data for phosphate adsorption capacities of 1.5 m thick Bassendean white sand layer, 0.5 m thick Spodozol sand layer and the 10 m thick Spearwood sand layer, and there were 10, 80 and 35 μgP/g soil, at 2, 5 and 40 months, respectively (Whelan and Barrow 1984a and 1984b).

The boundary and initial conditions for Richards' equation were not identified in the reference, so, the boundary conditions were assumed to be the same as that presented in

Section 7.1.1 for the gravitational infiltration system. The time for collecting the soil pore water was not given in the reference. So too, the equilibrium flow condition was considered. The input parameters for the case study are given in Table 9.14.

Table 9.14 Input parameters for Case 9.2.3

Parameters	Values
Domain	Single layer with depth of 0.8 m (organic carbon and nitrate), 6 cm (phosphate- Spearwood sand) and 2.0m (phosphate-Bassendean sand).
Hydraulic properties model	HV and VG
Saturated hydraulic conductivity; K_{zz} (cm/h)	Refer to the Table 9.13
Saturated moisture content; θ_s	Refer to the Table 9.13
Residual moisture content; θ_r	Refer to the Table 9.13
Dispersivity; α_T (cm)	3.25 (organic carbon), 7.54 (nitrate) and 1.57 (phosphate)
Molecular diffusion; D^* (cm^2/h)	
Nitrate	0.06840 (Kemper 1986)
Ammonium	0.07055 (Kemper 1986)
Phosphate	0.02304 (Kemper 1986)
Boundary conditions	
Richards' equation	Constant head at the top, ψ_{top} of -2.54 cm (or θ = 0.323), at the datum, ψ_{bot} of -125 cm and constant pressure gradient at the datum, $d\psi/dz$ of 0 (or θ = 0.047). Initial pressure head ψ_{int}, -125 cm.
Contaminant transport	Organic carbon compounds Constant concentration at the surface, C_{top} of 1.25% and at the datum, C_{bot} of 0.39%. Initial concentration, C_{int} of 0.39%. Nitrate nitrogen compounds Constant concentration at the surface, C_{top} of 2 mg/L and at the datum, C_{bot} of 83 mg/L. Initial concentration, C_{int} of 2 mg/L.

Table 9.14 (cont.) Input parameters for Case 9.2.3

Parameters	Values
Contaminant transport	Phosphate phosphorus compounds Spearwood sand: Constant concentration at the surface, C_{top} of 15 mg/L and at the datum, C_{bot} of 0.72mg/L. Initial concentration, C_{int} of 0.72 mg/L. Bassendean sand: Constant concentration at the surface, C_{top} of 19.5 mg/L and at the datum, C_{bot} of 0.50mg/L. Initial concentration, C_{int} of 0.50 mg/L.
The kinetic parameters	
Organic carbon and nitrate nitrogen compounds (Widdowson et al. 1988):	
μ_O (1/h)	74.4
μ_N (1/h)	69.6
Y_O	0.45
Y_N	0.50
K_{SO} (mg/cm^3)	0.040
K_{SN} (mg/cm^3)	0.040
K_O (mg/cm^3)	0.00077
K_N (mg/cm^3)	0.00260
K_{AO} (mg/cm^3)	0.0010
K_{AN} (mg/cm^3)	0.0010
C_A (mg/L)	50
C_O (mg/L)	2
I[Co]	0.0802
Phosphate phosphorus compounds:	
K_d (cm^3/g)	Varies from 1.22×10^{-9} (Spearwood sand, thickness of 10 m) to 6.49×10^{-9} (Bassendean sand, thickness of 1.5 m)
ρ_B (g/cm^3)	1.70
Number of element; *nelem*	80
Increment time interval; *dt* (sec)	1.5×10^{-4} (organic carbon and nitrate) and 1.5×10^{-7}(phosphate)
Nodal spacing; *dz* (cm)	1.000(organic carbon and nitrate), 0.075 (phosphate-Spearwood sand) and 2.5 (phosphate-Bassendean sand)

The simulations of nitrate and organic carbon transport are presented in Figures 9.13. The simulations were close to the observations of Whelan and Barrow (1984a and 1984b). The organic carbon biodegradation zone was found at the elevation of 0.6 m above the datum. The ammonium was converted to nitrate by the nitrifying bacteria. Nitrate increased from 2 mg/L (at the surface) to 83 mg/L (at the biodegradation zone). The concentration remained constant until the filtered sample reached the datum. The nitrate concentration in the filtered samples was higher than the acceptable concentration (>10 mg/L), if it is used as a water supply source. The groundwater at this site needed a suitable unit process to remove nitrate before consumption.

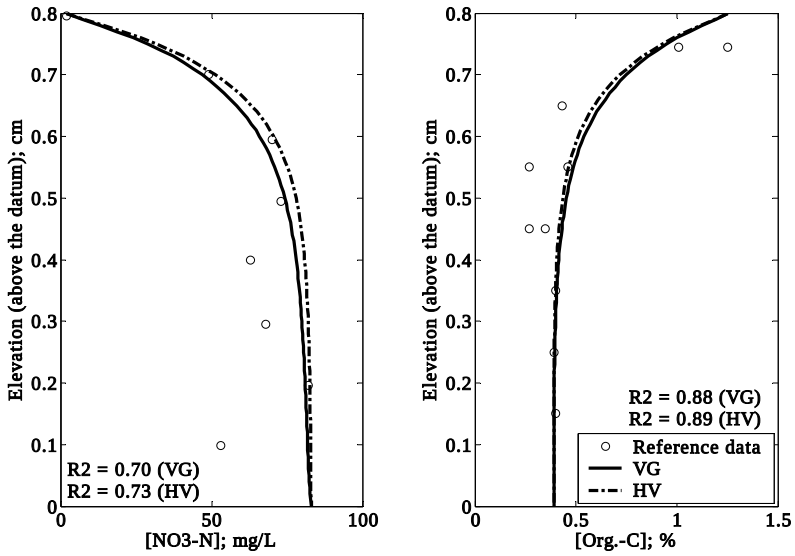

Figure 9.13 Simulation of organic carbon and nitrate nitrogen concentration profiles (datum at the end of soil layer).

Phosphate concentration profiles on the Spearwood and the Bassendean sand layers are given in Figures 9.14 and 9.15, respectively. The concentration profiles were observed in the slime layer of the Spearwood sand. The maximum phosphate concentration was 15 mg/L. The adsorption zone was found at the elevation of 5.8 cm above the datum. The adsorption could retard more than 95% of the initial phosphate concentration. The migration of phosphate was very fast in the Bassendean sand. The maximum phosphate concentration was 19.5 mg/L. Phosphate adsorption zone was observed at the elevation of 1.15 m above the datum. The Bassendean sand could adsorb approximately 98% of the initial phosphate concentration. The different depth of the adsorption zone might be

a result of iron content. The iron might adsorb and react to the phosphate (Zanini et al. 1998). The Spearwood sand contained 0.26 %Fe, while the Bassendean sand (Spodosal gray sand) contained 0.02 %Fe. As mentioned, phosphate migrated very slowly in the Spearwood sand.

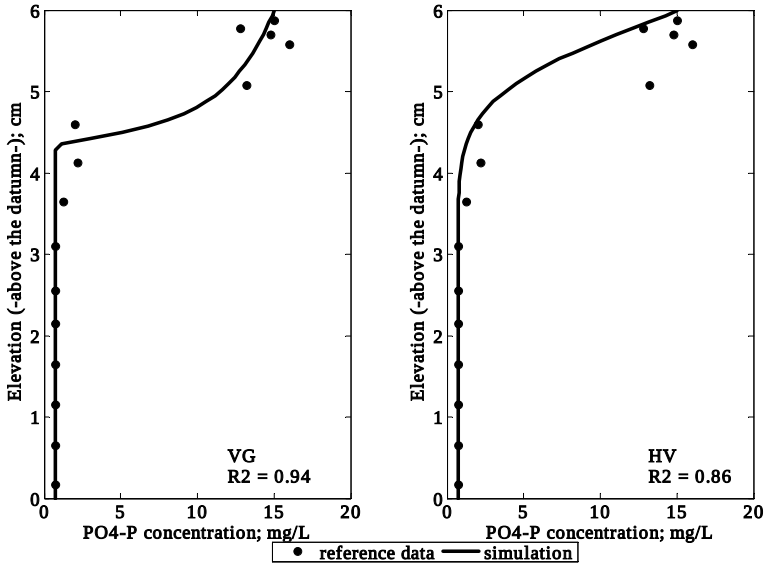

Figure 9.14 Phosphate concentration profiles on the Spearwood sand (datum at the end of sand layer).

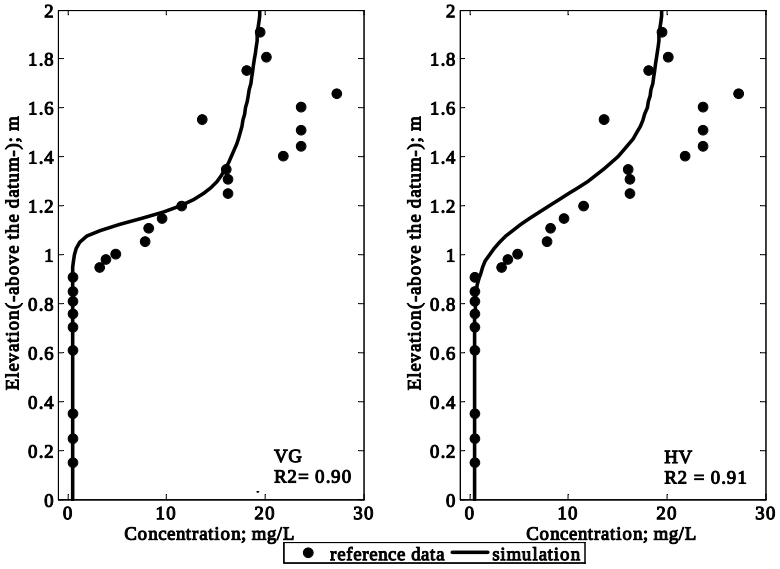

Figure 9.15 Phosphate concentration profiles on the Bassendean sand (datum at the end of sand layer).

Case 9.2.4 Removal of *E.Coli* from wastewater by light weight aggregate and activated carbon

Stevik et al. (1999a) studied the transport and retardation of *E.Coli* in unsaturated infiltration columns. The porous media utilised in this study included light weight aggregate (LWA) and activated carbon (AC). The LWA was classified into two categories, spherical and crushed LWA. The porosity of the crushed LWA, the spherical LWA and the AC were 0.15, 0.13 and 0.13, respectively. The characteristics and the pore radius distribution of these media are given in Table 9.15.

Table 9.15 Properties of the media and distribution of the pore radius (Stevik et al. 1999a)

Filter media	Chemical properties			Pore radius distribution (%)			
	CEC (meq/100g)	pH	Specific surface area* (m^2/g)	R** >0.13mm	R** 0.07-0.13mm	R** 0.01-0.07mm	R** <0.01mm
Crushed LWA	5.27	7.0	0.545	0.28	0.17	0.28	0.30
Spherical LWA	2.40	10.0	0.240	0.18	0.19	0.15	0.47
Activated Carbon	3.80	7.0	900	0.05	0.30	0.18	0.47

Note: * The specific surface area was determined by BET method (Brunauer et al. 1983, cite in Stevik et al. 1999a).
** The pore radius.

A 15 cm diameter by 100 cm long plastic cylinder was fabricated for the infiltration column test. All the media were packed to a height of 80 cm. The column was placed inside a dark room at a temperature of 7 $\pm$1 ^{o}C. The artificial wastewater was prepared with 0.5 g/L glucose, 0.1 g/L potassium hydrogen phosphate, 0.1 g/L ammonium nitrate and 0.1 g/L magnesium sulphate heptahydrate and 10mL of incubated *E.Coli.* The incubated *E.Coli* was prepared and the culture of *E.Coli* (stain DH5α) was dissolved in beef extract (0.3% Bacto beef extract, 0.5% Bacto peptone and 0.05% yeast extract (v/w)). The *E.Coli* solution was kept at the temperature of 37 ^{o}C for 24 hours. The artificial wastewater contained *E.Coli* of 5.0x10^8 cfu/mL (9.05 log*E.Coli*/100 mL). The wastewater was poured into the column at a rate of 25 mm/day (Stevik et al. 1999a).

The authors provided the hydraulic properties data for these media. These data were fitted using VG equations. The water retention curves of these media are given in Figure 9.16 and the empirical coefficients are given in Table 9.16.

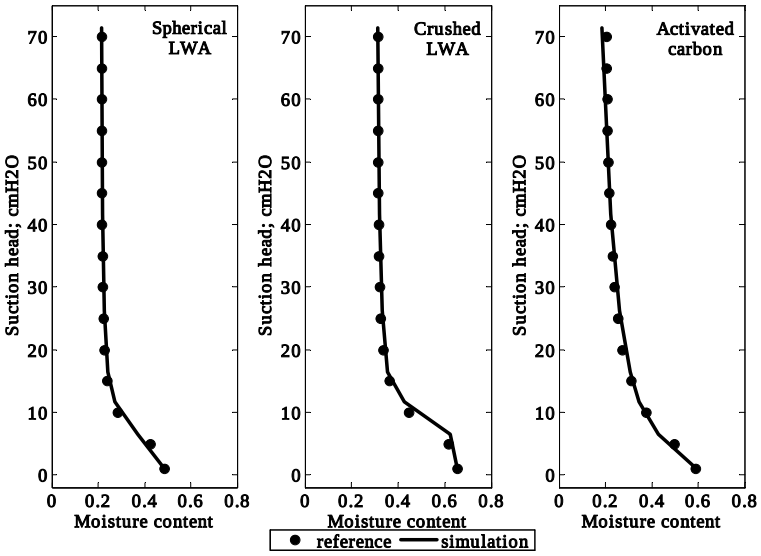

Figure 9.16 Calculated water retention curves for all utilised media

Table 9.16 Hydraulic properties coefficients of the utilised media

Parameters	Filter media		
	Crushed LWA	Spherical LWA	AC
Saturated moisture content; θ_s	0.655	0.485	0.593
Residual moisture content; θ_r	0.312	0.215	0.183
Saturated moisture content; K_{zz} (cm/h)	0.681	0.779	0.783
Coefficient *p*	3.8122	3.7264	2.2561
Coefficient *a*	0.1284	0.1581	0.1615
Effective size; d_{10} (mm)	0.15	1.10	0.70
d_{50} (mm)	1.50	1.75	1.05
Ratio of d_{50}/d_{10}	10.0	1.59	1.50
Uniformity ($=d_{60}/d_{10}$)	13.3[A]	1.59[B]	1.95[C]

Note: [A] Crushed LWA, 0-3 mm with an effective size 0.15, [B] LWA, 2.5-5 mm with an effective size 2.20 and [C] AC with an effective size 0.59.

The initial moisture contents of these media were 4% by weight. Lo and Cui (2006) and Degal (2006) estimated the residual moisture contents of LWA and the AC were less than 5% by weight. This indicated that the columns were initially dry state. A hydraulic

properties test might be obtained from the wetting cycle (Fetter 1992). In the wetting process, water loss might occur due to absorption. This water loss might lead to an underestimate of the hydraulic properties data (Klute 1986). Water retention curves of the crushed and spherical LWA were different because of uniformity of material and grain size. Uniform grain size material resulted in a narrow range of change of pressure head over moisture content (Fetter 1992). Changes in moisture content of the crushed LWA were narrower than spherical LWA, but wider than AC. The order of uniformity should be crushed LWA>spherical LWA>AC. This observation corresponded to the sequence of the ratio of d_{50}/d_{10}.

The moisture content profiles of the infiltration column at a feeding rate of 25 mm/d were estimated using the developed model. The input parameters for this case study are shown in Table 9.17.

Table 9.17 Input parameters for the movement of wastewater in Case 9.2.4 (Stevik et al. 1999a and 1999b)

Parameters	Values
Domain	Column with depth of 80 cm. The solution feeding rate was 0.104 cm/h.
Hydraulic properties coefficients	Refer to Table 7.16.
The boundaries conditions	The initial moisture contents were 0.313 (crushed LWA), 0.215 (spherical LWA) and 0.204 (AC). The moisture contents at the column surface were 0.655 (crushed LWA), 0.485 (spherical LWA) and 0.593 (AC). The moisture contents at the column base were 0.313 (crushed LWA), 0.215 (spherical LWA) and 0.204 (AC).
Time domain (min)	From 0 to 180
Number of time step; *nt*	1800
Time interval; *dt* (min)	0.1
Nodal spacing; *dz* (cm)	1

The moisture content profiles of the spherical LWA are presented in Figure 9.17. The simulation matched well with the observation presented by Stevik et al. (1999a). The

wetting zone migrated to the elevation of 70 cm within 10 minutes. The simulation implied that a fast moving wetting front reached the upper portion (at the elevations of 60-75 cm) within 60 minutes. The unsaturated flow was observed in the lowest portion (at the elevation of 40 cm) of the infiltration column.

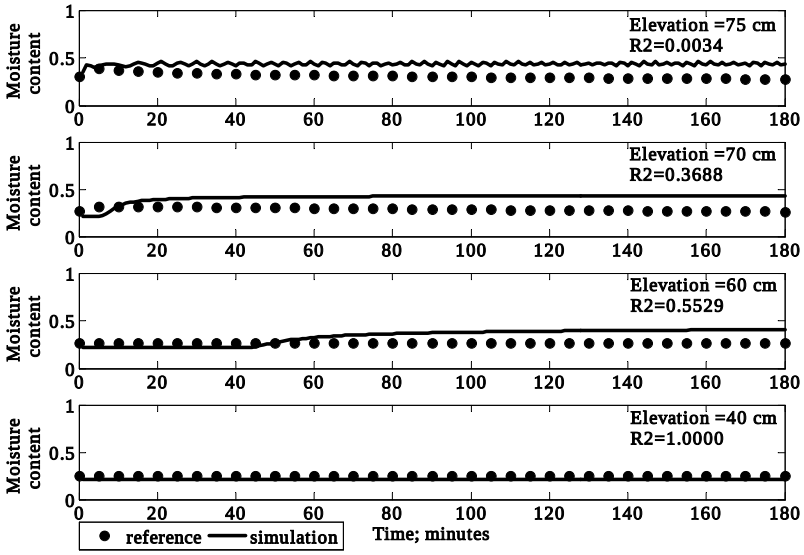

Figure 9.17 Moisture content profiles of a spherical LWA infiltration column (datum at the base of column).

The simulations of moisture content profiles of the crushed LWA infiltration column are shown in Figure 9.18. The wetting zone was observed at the elevation of 70 cm within 10 minutes. The wetting front moved very fast in the upper portions of the column (at the elevations of 60-75 cm) within 65 minutes. The unsaturated flow was found at the elevation of 40 cm.

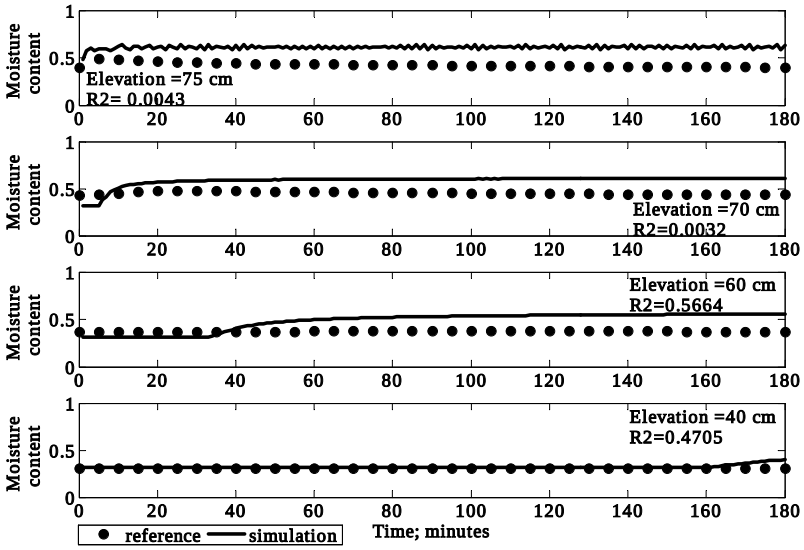

Figure 9.18 Moisture content profiles of a crushed LWA infiltration column (datum at the base of column).

The simulations of moisture content profiles of the AC infiltration column are provided in Figure 9.19. The wetting front reached the elevation of 70 cm within 10 minutes. The wetting front extended very fast from surface to the elevation of 60 cm within 60 minutes. The unsaturated flow was found at the elevation of 40 cm.

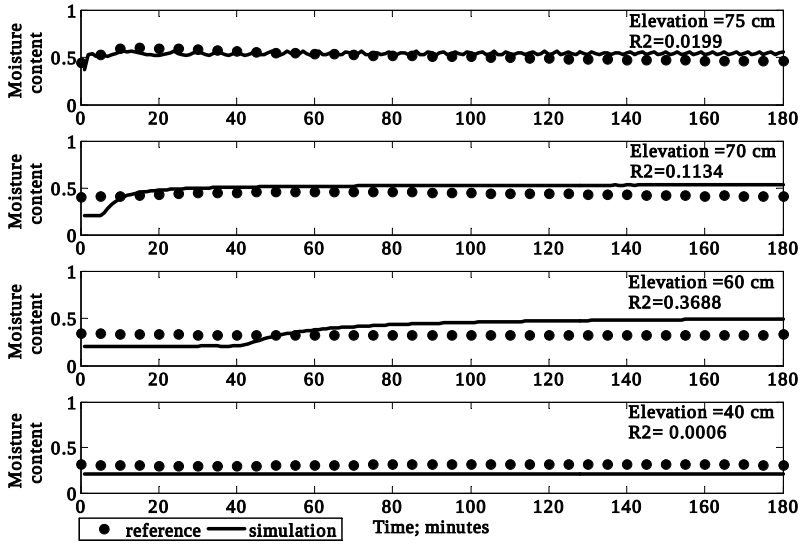

Figure 9.19 Moisture content profiles of an activated carbon infiltration column (datum at the base of column).

The time for the wastewater to pass through the columns could be written in the following order: Crushed LWA>Spherical LWA=AC. This order was related to the sequence of the saturated permeability, K_{zz}.

The authors stated that the experiments were carried out for three months in the dark and at cold temperature (7 ±1 ^{o}C). The time required for 90 percent of the initial *E.Coli* to die is 19 days (Based on the die-off constant 0.12 d^{-1}) (Metcalf & Eddy 2003). Therefore, it could be assumed that the *E.Coli* was inhibited by low temperatures and might reach a declining phase. The input parameters are given in Table 9.18.

Table 9.18 Input parameters for Case 9.2.4

Parameters	Values
Domain	Column with depth of 80 cm
	The solution feeding rate was 0.0104 cm/h
Hydraulic properties coefficients	Refer to Table 7.16
Hydraulic conductivity (cm/h)	0.681(crushed LWA), 0.779 (spherical LWA) and 0.783 (AC)
Boundaries conditions	The initial microbial concentration 0 cfu/g. The microbial concentration at the column surface and base were $9.12x10^{7}$ and $1.318x10^{3}$cfu/g.
Adsorption rate (1/h)	0.015 (Stevik et al 1999b)
Growth-decay rate (1/h)	56.8 (Schnoor 1996)
Bulk density (g/cm^{3})	0.84 (LWA) and 0.35 (AC)
Microbial molecular diffusion (cm^{2}/h)	0.04788 (Kemper 1986)
Molecular faction	0.1
Transverse dispersion (1/cm)	7.59
Final time domain (day)	180
Number of time step	1800
Time interval; dt (min)	0.1
Nodal spacing; dz (cm)	1

The authors provided the concentration profile of *E.Coli* observed in the spherical LWA infiltration test. Simulations for the other porous media were carried out with the same boundary conditions as the spherical LWA. The simulations of *E.Coli* migration through these columns are presented in Figure 9.20.

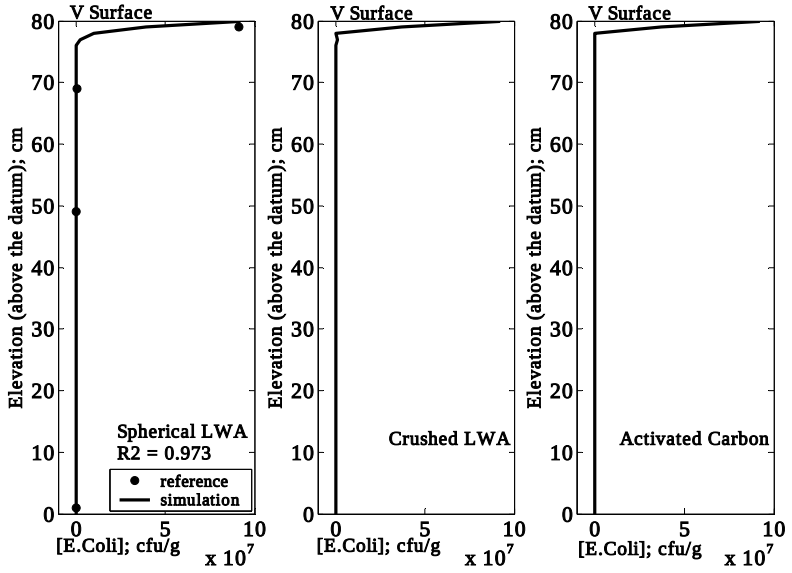

Figure 9.20 *E.Coli* concentration profiles for Case 9.2.4 (datum at the base of column).

Stevik et al. (1999a) suggested that these porous materials were relatively coarse. The retardation due to the pore filtration process might be less effective than the adsorption. The *E.Coli* could adhere to the active absorption site of these porous media. Among these media, AC has the largest surface area of 900 m^2/g. The crushed LWA and the spherical LWA had surface areas of 0.54 and 0.24 m^2/g, respectively. The retention time for *E.Coli* was much longer in the AC than the crushed LWA, and the shortest was in the spherical LWA infiltration column. The authors claimed that the crushed LWA, the spherical LWA, and the AC could retard 100, 99.999, and 100% of *E.Coli*, respectively. The developed model also confirmed these findings. The *E.Coli* reduction zones of the crushed LWA, the spherical LWA, and the AC infiltration column were at the elevations of 75, 72 and 75 cm, respectively. The developed model also implied that the removal of *E.Coli* depended on the density of media. The *E.Coli* could be restrained on the LWA longer than the AC.

9.4 Implication for design of septic tank

After the contaminants were loaded from the septic tank to the drainage field they could migrate through the unsaturated soil, and eventually pollute the groundwater. The safe

distance was defined as the distance between the drainage field and the pumping well as shown in Figure 9.21.

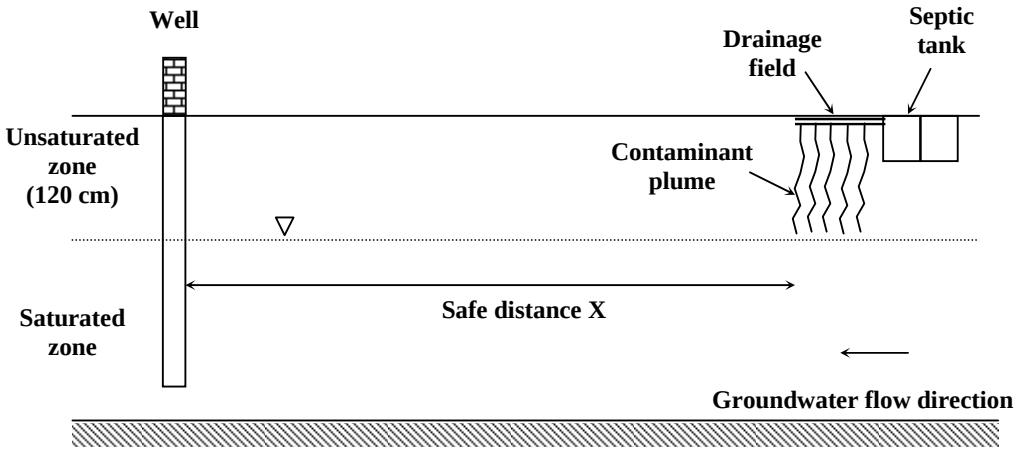

Figure 9.21 Schematic diagram of groundwater contamination from an onsite waste disposal systems

Predictions were in two stages:

1. To predict contaminant transport in the unsaturated zone below the drainage field and aquifer (presented in Section 8.1 and 8.3).
2. To predict contaminant transport in the saturated zone.

The contaminant transport with sorption and biodegradation processes was estimated using the one-dimensional advection-dispersion equation for reactive contaminants. The equation was presented as follows (Watts 1997).

$$\frac{\partial C}{\partial t} = \frac{D_x}{\kappa}\frac{\partial^2 C}{\partial x^2} - \frac{v}{\kappa}\frac{\partial C}{\partial x} - \frac{k_F C}{\kappa} \qquad (9\text{-}5)$$

where

C = Contaminant concentration in the aqueous phase [ML^{-3}]

κ = Retardation factor $\left(=1+\frac{\rho_B K_d}{n}\right)$ [-]

D_x = Groundwater dispersion coefficient [L^2T^{-1}]

v = Pore velocity [LT^{-1}]

k_F = First-order rate constant for contaminant degradation [T^{-1}]

t = Time [T]

x = Safe distance [L]

The analytical solution of the advective-dispersive equation was obtained by using the Laplace Transform. The solution was given as (Watts 1997):

$$\frac{C(x,t)}{C_o} = \frac{1}{2}\left[\exp(A_1)\cdot erfc(A_2) + \exp(B_1)\cdot erfc(B_2)\right] \quad (9\text{-}6)$$

where

$$A_1 = \frac{x}{2D_x'}\left(v_x' - \sqrt{v_x'^2 + 4D_x'k_F'}\right) \qquad A_2 = \frac{x - t\sqrt{v_x'^2 + 4D_x'k_F'}}{2\sqrt{D_x't}}$$

$$B_1 = \frac{x}{2D_x'}\left(v_x' + \sqrt{v_x'^2 + 4D_x'k_F'}\right) \qquad B_2 = \frac{x + t\sqrt{v_x'^2 + 4D_x'k_F'}}{2\sqrt{D_x't}}$$

$$D_{xx}' = D_x/\kappa \qquad v_x' = v_x/\kappa \qquad k_F' = k_F/\kappa$$

The *B* terms in Equation 9-6 were often negligible. The simplified analytical solutions were given as follows:

$$\frac{C(x,t)}{C_o} = \frac{1}{2}\left[\exp(A_1)\cdot erfc(A_2)\right] \quad (9\text{-}7)$$

The calculations were considered in the three different conditions. The estimated conditions are provided in the Table 9.19. The first site was an area which has low pore velocity (0.06 m/d) and high dispersion (0.085 m^2/d). The second site was an area which has a high pore velocity (0.08 m/d) and high dispersion (0.085 m^2/d), while the third site was an area which has high pore velocity (0.08 m/d) and low dispersion (0.04 m^2/d). The pumping stations were 10, 20, 30, 50, 70, 100, 150 and 200 m away from the drainage fields. The initial contaminant concentrations were assumed from Section 8.4-Estimation of contaminants retardation zone. The kinetics parameters were estimated based on the properties of Dimethyl Phatalate, a chemical which could be adsorbed and biodegraded by soil minerals and microbes and is also non-toxic (Watts 1997).

Table 9.19 Conditions of the study sites (Watts 1997)

Parameters	Value
Pore water velocity; v_x (m/day)	0.06-0.08
Groundwater dispersion coefficient; D_x (m^2/day)	0.04-0.085
Soil distribution coefficient; K_d (mL/g)	0.10
Soil bulk density; ρ_B (g/cm^3)	1.25
Porosity; n	0.11
First order degradation constant; k_F (day^{-1})	0.0011
Concentrations of contaminants at the end of unsaturated zone:	
COD (mg/L)	37.73
Nitrate compounds (mg/L)	2.34
Phosphate compounds (mg/L)	0.22
E.Coli (mg/L)*	5.91×10^{-5}mg/L (or 210 cfu/100mL)
Time span (day)	5475 (15 years)

Note: * Based on the microbial weight of 2.83×10^{-8} mg/colony (Widdowson et al. 1988).

The concentrations of COD, nitrate, phosphate and *E.Coli* observed at the various pumping wells are presented in Figures 9.22, 9.23, 9.24 and 9.25, respectively. The results indicated that the contaminants could be retarded for a long period, if the pore water velocity was low and dispersion was high as observed at site-1. The low pore velocity might reduce the transport of contaminant due to advection. The high dispersion might spread the contaminants. The concentrations of the contaminant also reduced over time and distance. As the travel time of the contaminant increased, the concentrations of the contaminants reduced. When the distance between the contaminant plume and the observation well, *X*, increased, the maximum contaminant concentration decreased.

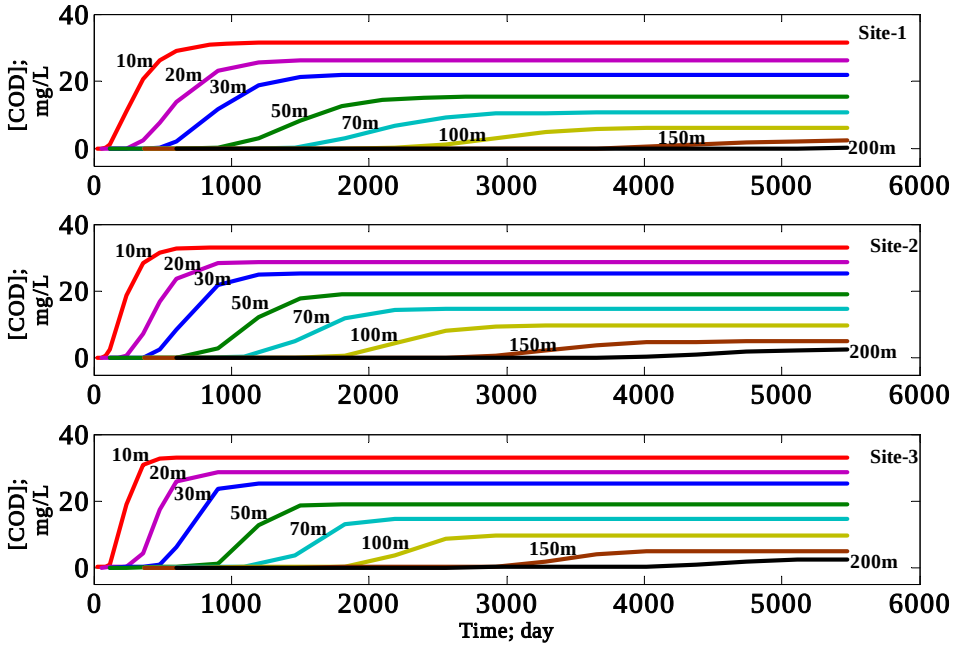

Figure 9.22 Migration of COD from drainage field to various locations of pumping wells (C_O =37.73 mg/L)

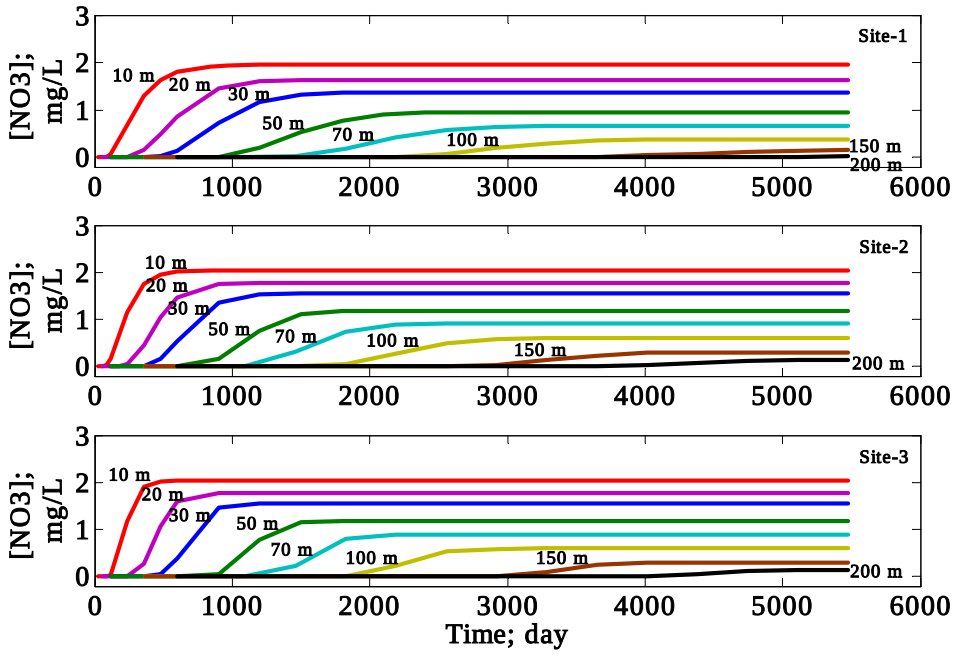

Figure 9.23 Migration of nitrate from drainage field to various locations of pumping wells (C_O =2.34 mg/L)

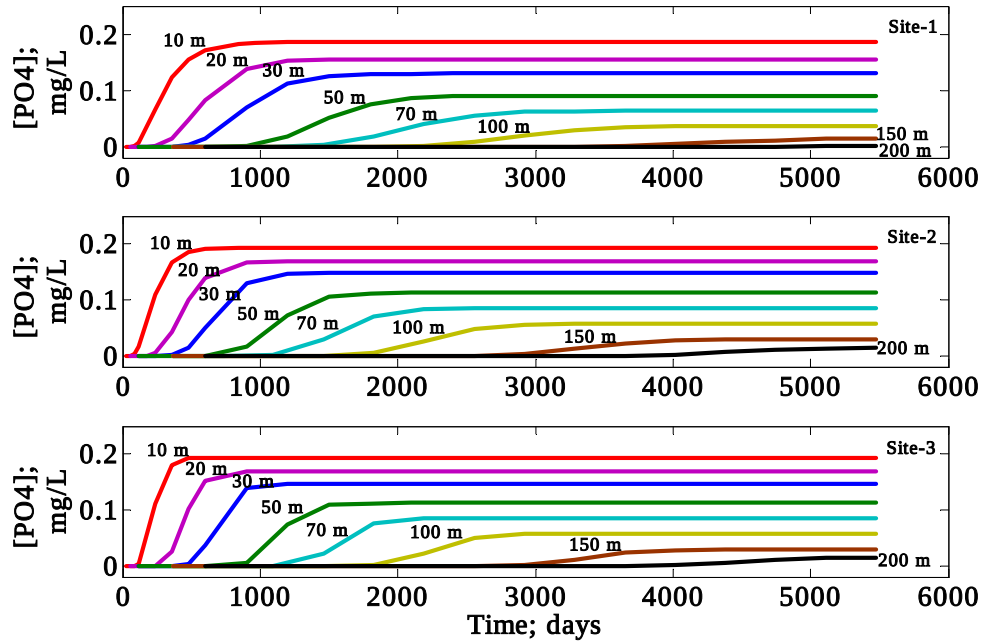

Figure 9.24 Migration of phosphate from drainage field to various locations of pumping wells (C_O =0.22 mg/L)

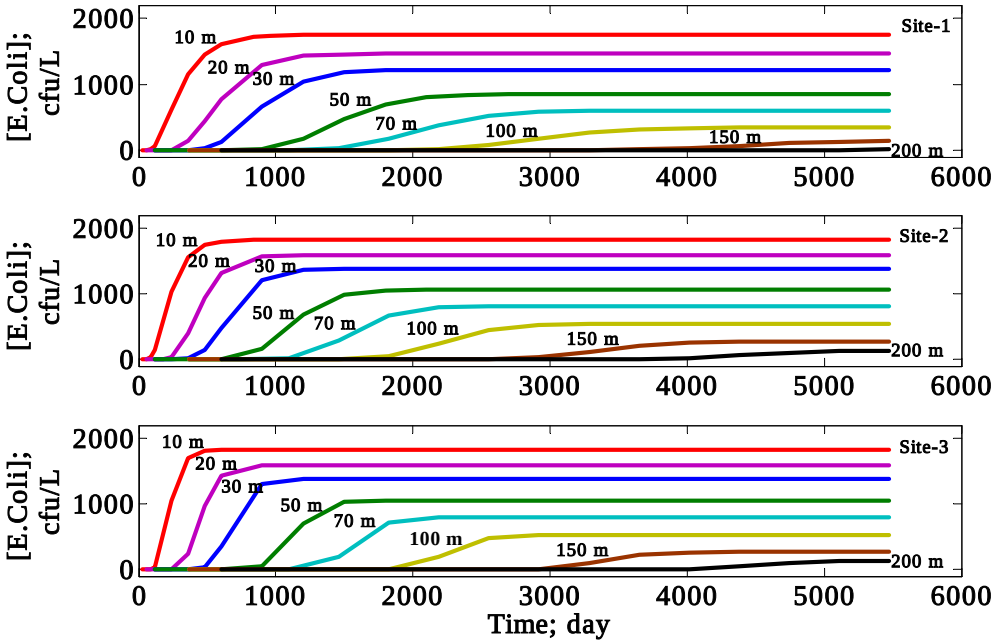

Figure 9.25 Migration of *E.Coli* from drainage field to various locations of pumping wells (C_O =5.91x10^{-5} mg/L or 2090 cfu/L)

The travel times and the maximum concentrations observed at each pumping well are provided in Table 9.20.

Table 9.20 Contaminant travel times and their maximum concentrations

Site		Distance between drainage field and pumping well (m)							
		10	20	30	50	70	100	150	200
Time (day)	Site-1	90	240	480	900	1460	2190	3650	5475
	Site-2	60	180	360	480	1095	1460	2555	4015
	Site-3	90	240	360	480	1095	1825	2920	4015
COD (mg/L)	Site-1	31.55	26.38	22.07	15.43	10.79	6.30	2.46	0.31
	Site-2	32.95	28.77	25.12	19.16	14.61	9.73	4.94	2.46
	Site-3	32.91	28.71	25.05	19.06	14.50	9.63	4.86	2.45
NO_3 (mg/L)	Site-1	1.96	1.64	1.37	0.96	0.67	0.39	0.15	0.02
	Site-2	2.04	1.78	1.56	1.19	0.91	0.60	0.31	0.15
	Site-3	2.04	1.78	1.55	1.18	0.90	0.60	0.30	0.15
PO_4 (mg/L)	Site-1	0.19	0.16	0.13	0.09	0.06	0.04	0.01	0.001
	Site-2	0.19	0.17	0.15	0.11	0.09	0.06	0.03	0.01
	Site-3	0.19	0.17	0.15	0.11	0.09	0.06	0.03	0.01
E.Coli (cfu/100 mL)	Site-1	175	146	122	85	60	35	14	1.8
	Site-2	182	159	139	106	81	54	27	14
	Site-3	182	159	139	106	80	53	27	14

The recommended buffer distances in onsite systems are given in Figure 9.21. The buffer distance given by NSW Department of Local Government (DoL) (1998) was in the range of 100-250 m. This was enough to preserve the natural subsurface water and groundwater resources. Based on the results calculated, the required safe distance should be more than 150 m to cover the life span of the drainage field (10-15 years). The calculated safe distance is higher than the lower value proposed by the NSW DoL. However, the safe distance might be changed in accordance with the geo-hydrological and the biochemical conditions. The contaminant concentrations might reduce slightly in the fully saturation zone due to the dispersion, adsorption and biodegradation processes.

Table 9.21 Recommended buffer distances for onsite systems
(Department of Local Government 1994)

System	Recommended buffer distances
All land application systems	1) 100 m to permanent surface waters (e.g. river, streams, lakes etc.). 2) 250 m to domestic groundwater well. 3) 40 m to other waters (e.g. farm dams, intermittent waterways and drainage channels, etc.).
Surface spray irrigation	1) 6 m if area up-gradient and 3 m if area down-gradient of driveways and property boundaries. 2) 15 m to dwellings. 3) 3 m to paths and walkways. 4) 6 m to swimming pools.
Surface drip and trickle irrigation	6 m if area up-gradient and 3 m if area down-gradient of swimming pools, property boundaries, driveways and buildings.
Subsurface irrigation	6 m if area up-gradient and 3 m if area down-gradient of swimming pools, property boundaries, driveways and buildings.
Absorption system	1) 12 m if area up-gradient and 6 m if area down-gradient of property boundary. 2) 6 m if area up-gradient and 3 m if area down-gradient of swimming pools, driveways and buildings.

9.5 Summary

The models developed for Richards' equation and contaminant transport were verified by comparison with case studies obtained from the literature. Four case studies were applied to the various infiltration systems: Case 9.1.1-Infiltration column experiments with Haverkamp et al.'s hydraulic properties model, Case 9.1.2-Infiltration column experiments with van Genuchten's hydraulic properties model, Case 9.1.3-Sharp front infiltration column with an initially dry soil and Case 9.1.4-Infiltration and redistribution column. The model developed in this research was shown to provide very accurate simulation results for all case studies.

In a similar fashion the contaminant transport model was verified using four case studies. The case studies for the non-reactive contaminant transport were, Case 9.2.1-Transport of chloride ion in Delhi sand and Case 9.2.2-Warrick et al.'s solute transport in an onsite infiltration system. The reactive contaminant transport case studies included

Case 9.2.3-Movement of contaminants through sandy soil near Perth, and Case 9.2.4-Removal of *E.Coli* from wastewater by light weight aggregate and activated carbon. The contaminant transport model could effectively predict the concentration profiles for all these case studies. The model was highly flexible with regard to the various boundary conditions.

The safe distance between the drainage field and the pumping wells was calculated and compared to the buffer distance for onsite systems recommended by the NSW Department of Local Government (1994). The safe distance obtained from the simulation was 150 m, whereas the recommended buffer distance was 100-250 m. However, the safe distance might be either increased or decreased depending upon the hydro-geological or biochemical conditions of the local sites. High dispersion and low pore velocity conditions could provide a benefit to contaminant retardation.

CHAPTER 10

CONCLUSIONS AND RECOMMENDATIONS FOR FURTHER WORK

10.1 General approaches

Groundwater contamination is an important problem on a global scale because it results in pollution of drinking water supplies and results in outbreaks of waterborne diseases. The conservation and protection of groundwater from various pollution sources is necessary if our water resources are to be sustainably managed. Onsite disposal systems were proven to be a major source of groundwater pollutants because of their failures. Monitoring the migration of the reactive contaminants from them is possible but it is expensive and time consuming, while modelling is an innovative tool that can be used to monitor, predict and implement the fate and migration of these reactive contaminants. To achieve all these purposes, a comprehensive mathematical and numerical model was developed in this research using the fundamentals of geo-hydrology and eco-toxicology, which covered the fate and transport of contaminants in the infiltration zone. The governing equations were defined and modified based on the input and response relationships described in the mathematical model. This mathematical model was solved numerically using finite element techniques. The numerical model was coded using MATLAB software. The computational codes obtained were inexpensive, user friendly and well suited to assist in finding a solution for the serious problems associated with the migration of contaminants into the infiltration zone.

Computational features in this model include:

- Incorporates the effects of soil hydraulic properties.
- Provides an estimation of the soil hydraulic properties according to Haverkamp et al. (1977)'s equations, van Genuchten (1980)'s equations and Saxton et al. (1986)'s equations.
- Supports various infiltration boundaries such as gravitational flow, static equilibrium capillary flow and infiltration redistribution flow.

- Supports a varying boundary in real time that could be entered from the actual observation records.
- Integrates the flow and transport model to evaluate the dispersion of contaminants.
- Determines the non-reactive tracer transport in variably saturated soil.
- Supports the multi-species contaminant transport with the multiplicative kinetics processes.
- Integrates the microbial transport model with the filtering and metabolism processes.
- Supports the contaminant transport coupled to the adsorption process.
- Optimises the round-off error in the calculated results using the mass balance function.
- Provides a profile of the graphical plots of the pressure head, moisture content, concentration, Darcy's velocity, pore velocity, dispersion, relative hydraulic conductivity, and kinetics reaction rate.
- Displays the time respondent graphical plots of the pressure head, moisture content and concentration.
- Visualises a final report with the calculated results complete.

The capabilities of the model for professional applications include:

- Estimating a profile of the pressure head and moisture content for the movement of wastewater under gravity, in unsaturated soil conditions;
- Estimating a head of pressure and distribution of moisture content under a static equilibrium capillary in unsaturated soil conditions;
- Estimating the profile of a head of pressure and moisture content for the movement of wastewater in unsaturated infiltration and redistribution soil conditions;
- Estimating the transport of non-reactive (tracer) in unsaturated soil conditions;
- Estimating the transport of nitrate and organic carbon compounds in unsaturated soil conditions;
- Estimating the transport of phosphate compounds in unsaturated soil conditions;
- Estimating the transport of *E.Coli* in unsaturated soil conditions; and
- Estimating the properties of unsaturated soil from the texture of the soil.

10.2 Specific approaches

This study focused on modelling the transport of contaminants in onsite waste disposal systems. The process of developing a model, the experimental results, calibration, application of the model, are summarised as follows:

10.2.1 Development of a conceptual model

The specific contaminants emanating from a septic tank which contaminate groundwater includes nitrate, organic carbon, phosphate compounds, and *E.Coli*. When these contaminants released to a drainage field, they were subjected to a large number of simultaneous physical, chemical, and biological processes including filtration, adsorption, and biodegradation. The conceptual model was divided into transport and retardation processes.

(a) Contaminant transport processes

- The contaminants migrated in the unsaturated zone due to advection and dispersion. Advection affected the flow of discharging effluent while diffusion influenced the concentration and spread of contaminant. Dispersion could be quantified by the hydrodynamic and concentration gradients.

(b) Contaminant retardation processes

- Aerobic and nitrate respiration processes contributed to the retardation of organic carbon and nitrate compounds.
- Phosphate compounds could be adsorbed onto the surface of the soil.
- The removal of *E.Coli* relied on both biodegradation and filtration.

10.2.2 Development of mathematical and numerical models

The mathematical model was constructed as follows.

(a) Contaminant transport processes

- The advection flow of the discharging effluent was estimated by Darcy's velocity. This was obtained from the non-linear Richards' equation.

- Richards' equation contains ideal soil hydraulic parameters including relative hydraulic conductivity $(K_{zz}k_{rw})$, and specific soil moisture content (M_C). These non-measurable parameters were evaluated using the equations proposed by Haverkamp et al. (1977), van Genuchten (1980) and Saxton et al. (1986).
- Dispersion of the contaminants was estimated using Fick's law. Advection and dispersion transports were changed in terms of Darcy's and pore velocities.

(b) Contaminant retardation processes

- The process of nitrate and organic carbon biotransformation was described using the multiplicative Monod's equation.
- The phosphate adsorption process was evaluated using the Langmuir adsorption isotherm formulation.
- Removal of *E.Coli* was examined using the microbial metabolism kinetics reaction and linear sorption equations.

The governing equations contained in the mathematical model were the non-linearity partial differential equations. A numerical approach technique was used to calculate the approximate solution. The numerical model was constructed as follows.

- Gelerkin's finite element method was used to support the time and space discritisation of Richards' and contaminant transport equations. This led to the transformed ordinary differential equations.
- The algebraic stiffness matrices were linearised using the Lagrange linear interpolation function. The elements were controlled as a uniform grid system.
- The developed numerical models were solved using Picard's single iteration schematic.
- The algorithm of these routine simulations had been prepared with regard to the numerical solutions. Both models for Richards' equations and contaminants transport were coded with MATLAB software that might provide an efficient and robust process for calculation.

10.2.3 Model calibration processes

Experimental data obtained in this research was used to calibrate the model. Two porous media were applied, including samples of sand and topsoil. Sand is a uniform

and non-reactive porous media which provided an effective permeability for infiltration. Topsoil is a non-uniform and reactive porous media which provided infiltration with retardation. The infiltration columns were investigated on a laboratory (20 cm) scale and on a pilot (120 cm) scale. The laboratory scale sand and soil columns were used to determine the properties of the sand and soil hydraulics, and the advection transport and dispersion transport. A pilot scale column of soil was used to examine the transport of contaminants in field conditions. In addition, the phosphate adsorption isotherm and the suitability of using a fibreglass wick on wastewater sampling were investigated using batch tests.

(a) Hydraulic properties of sand and soil

- The data were fitted with Haverkamp et al. (1977)'s and van Genuchten (1980)'s model. The coefficients of the hydraulic properties were determined and applied further as input into Richards' equation.

(b) Water movement under gravitational force

- The simulation was investigated under real time, with various boundary conditions. The results agreed with the observation data.
- Darcy's velocities presented in both sand and soil columns were non-linear and time varying.

(c) Water movement in a static equilibrium capillary force

- The data for both the sand and soil columns indicated that water moved upwards due to the capillary force and the pressure head was distributed linearly.
- The same profiles for capillary pressure were observed in both sand and soil columns because the capillary height relates to the pore diameters. This statement corresponded well to the physical model of capillarity inside the capillary tube proposed by Fredlune and Rahardjo (1940).
- The highest moisture content was near the water table, the lowest was at the surface of the column, but it reduced along the elevation.
- The column of soil was in a state of equilibrium longer than the column of sand which indicated that a higher storage capacity was obtained and there was a higher void ratio.

(d) Water movement in an infiltration and redistribution system

- The driest points of both sand and soil columns were at the elevations of 15-17.5 cm above the datum.
- The simulation results obtained for both sand and soil columns agreed with the observation data.
- Darcy's velocity estimated in the infiltration and redistribution system was lower than under the flow of gravity. It might be concerned that the upward flow of redistribution could affect the velocity of the gravitational flow.

(e) Tracer test

- The data indicates that the interfering effect of soil could be reduced if concentrated tracer was applied. Retardation of the tracer could be seen when the layer of soil was thick. This statement reflects to the high spreading of tracer due to the diffusion-dispersion mechanism.
- Molecular diffusion in porous soil media was approximately 40% of the diffusion in pure water.
- Mechanical dispersion varied over time according to the pore velocity. Dispersion increased in the same pattern as Darcy's velocity.

(f) Soil phosphate adsorption isotherm

- A soil phosphate adsorption isotherm test was used to determine the coefficient of adsorption. The Langmuir adsorption isotherm best fitted the observation data. The coefficients k_L and k_M were 0.00384 and 7.634, respectively.

(g) Suitability of fibreglass wick on soil contaminant sampling technique

- The fibreglass wick could completely remove the suspended solids but soluble COD, phosphate, nitrate, ammonia and *E.Coli* contained in filtrate samples could possibly be determined. It was concluded that the filtration mechanism in the fibreglass wick did not affect the concentration of the dissolved contaminants.

(h) Contaminant transport

- During 3 months of operation the column of soil successfully removed all contaminants.
- Interaction between the soil and contaminants could purify and improve the quality of discharging wastewater.

- The organic carbon compounds were evaluated with COD and a reduction zone was seen 105 cm above the datum so the COD was removed by approximately 83%. The filtrated concentration of COD was 37 mg/L.
- Approximately 90% of NH_4-N was reduced. The ammonia nitrogen can be oxidized by aerobic bacteria to become stable nitrate nitrogen. The nitrate in the filtered samples obtained from the soil column had a concentration of 2.3 mg/L which was 4 times lower than the critical concentration (10 mg/L).
- The phosphate compounds were reduced approximately 90% by the adsorption process. The remaining concentration in the filtered samples was 0.22 mg/L. A phosphate reduction zone was seen 105 cm above the datum.
- *E.Coli* was reduced approximately by 99.999% through the soil and trapped in the soil pores. The filtered samples of soil contained *E.Coli* with an average concentration of 200 cfu/100mL. An *E.Coli* reduction zone was seen 110 cm above the datum.

10.2.4 Model applications

Richards' equation (advection transport) and the contaminant transport model were validated using the historical data published in the reviewed literature.

(a) Richards' equation (advection transport)
The model was used for four case studies.

- The model was operated using gravitational infiltration flow and support by Haverkamp's hydraulic properties equations. The moisture content simulations were presented in Case 9.1.1 Infiltration column experiments with Haverkamp's hydraulic properties model. The model could effectively predict the moisture content.
- The gravitational infiltration flow and the supporting van Genuchten hydraulic properties model was presented in Case 9.1.2 Infiltration column experiments with the van Genuchten hydraulic properties model. The model could generate an identical result to the one proposed in the literature.
- The gravitational infiltration flow and supporting van Genuchten hydraulic properties model was also presented in Case 9.1.3 Sharp front infiltration

column with an initially dry soil. The developed model could effectively predict the profiles of pressure head and the moisture content.

- The model was used for the water movement into the infiltration and redistribution system, as given in Case 9.1.4 Infiltration and redistribution test. The simulations generated from the model were close to the data obtained from the literature.

(b) Non-Reactive contaminant transport model

- The solute transport model was used to determine the movement of tracer into Delhi sand. As presented in Case 9.2.1 Transport of Chloride ions in Delhi sand and its measured concentrations could be estimated using this model.
- A classical tracer test under field conditions was acknowledged in Warrick et al.'s experiment. The data from the hydraulic properties was fitted with van Genuchten's and Haverkamp's hydraulic properties models. The non-reactive transport model in this research could describe this field case study well.

(c) Reactive contaminant transport model

- The movement of nitrogen and organic carbon compounds in sandy soil were predicted using the developed model. The simulation results for this case study were presented in Case 9.2.3 Movement of septic tank contaminants through sandy soil near Perth.
- The movement of phosphate in sandy soil was effectively simulated with the developed model. The result of simulating concentrated phosphate was illustrated in Case 9.2.3 Movement of septic tank contaminants through sandy soil near Perth.
- The transport of *E.Coli* in porous media was estimated using the developed model. The model gave good simulation results to this reference case study, as presented in Case 9.2.4 Removal of *E.Coli* from wastewater by light weight aggregate and activated carbon.

All the models developed in this research were able to successfully predict results for all case studies. The model could be adjusted for various initial and other boundary conditions and could demonstrate an alternative approach for predicting the hydraulic properties of soil texture.

10.3 Recommendations for future research

This research consisted of a complete model development processes. The model obtained in this work was reliable and it could predict the transport of contaminants emanating from an onsite waste disposal system through a soil absorption field. Although the model achieved its goals, its evolution should be dynamically driven. The model should be improved as follows:

- The model development for estimating the transport of contaminants in unsaturated soil conditions is progressing with respect to its ability to represent mathematically the hydrogeological and geochemical phenomena controlling wastewater flow and contaminant fate. The field or laboratory data are often insufficient to warrant model calibration especially in the infiltration and redistribution systems. Based on these premises, the cases considered in the mathematical model depended upon mass balance equations, suitably modified to reflect the specific conditions relating to homogeneity, isotropy and non-deformation porous medium. For the lack of proven field data, the contaminant transport in the infiltration-redistution system could not be verified. However, the reason for the lack of applications the model in infiltration and redistribution systems is that the available sampling techniques are still impractical.
- Although the model was developed for estimating the contaminants movement in unsaturated soil, it does not cover the trace organic or xenobiotic or synthesis compounds such as trichloroethylene, 1,1,1-trichloroethane, Polychlorinated Biphenyls (PCBs), Nonaqueous-phase liquid (NAPL) and Benzene, Toluene, Ethylbenzene and Xylene (BTEX). It was felt that surface and groundwater were also subject to contamination with these compounds from contaminated locations resulting from hazardous waste disposal, accidental spills and leaking storage tanks. In order to predict the transport of these hazardous substances, the removal processes such as hydrolysis, oxidation-reduction, volatilization and bio-uptake (bioconcentration) might be considered. By increasing the number of contaminants the model will be able to support the transport of contaminants in other areas such as underground storage tanks, heavy industry and municipal industry complexes, from spills which result from accidents and from uncontrolled use of these substances in agriculture and forestry operations.

- The developed model was concerned only with one-dimensional flow systems, such as where the commonly used septic drainage field distributed the patch of inflow contaminant. The model dimension could be extended to be two or three dimensions and the improved model will be better applicable to the contaminant plume in unsaturated soil condition.
- The model developed in this research was only concerned with a single onsite waste disposal system; it may not be suitable for the transport of contaminant in areas where a lot of septic systems were installed. This problem could be addressed if the non-point sources were accounted for.
- The impact of dilution due to rainfall precipitation, evaporation, and transpiration could be added resulting in an improved model will be readily applied to real absorption field conditions.

REFERENCES

American Public Health Association, APHA. (1998). Standard methods for the examination of water and wastewater, 20th ed. Washington, DC: APHA.

American Society for Testing and Materials International, ASTM. (1999). Annual book of ASTM Standards. Pennsylvania: ASTM international.

Australia/ New Zealand Standard. (2000). On-site domestic-wastewater management, AS/NZS 1547. Strathfield: Standard Australia International.

Australian and New Zealand Environment and Conservation Council (ANZECC/ARMCANZ) (2000). Water quality guidelines for fresh and marine waters. Canberra: ANZECC and ARMCANZ.

AWT. Ensight (1997). Karuah sewerage scheme microbial (viral) risk assessment to human health from oysters, Report No. 97/73. Prepared for ERM Mitchell McCotter, Hunter Water Corporation, Department of Land & Water Conservation, 78 p.

Baek, N.H., Clesceri, L.S. and Clesceri, N.L. (1989). Modeling of enhanced biodegradation in unsaturated soil zone. Journal of Environmental Engineering **115**(1): 150-172.

Baker, M.J. (1996). Laboratory and field studies on the transport and treatment of phosphorus from on-site wastewater disposal systems. Msc Thesis, University of Waterloo, Ontario, 195 p.

Bauters, T.W.J., DiCarlo, D.A., Steenhuis, T.S. and Parlange, J.Y. (1998). Preferential flow in water-repellent sands. Soil Science Society of America Journal **62**:1185-1190.

Bear, J. (1972). Dynamics of fluids in porous media. New York: Elsevier Publishing Company, 764 p.

Bear, J. (1979). Hydraulics of groundwater. New York: McGraw-Hill, 567 p.

Bear, J. and Verrujit, A. (1987). Modelling groundwater flow and pollution, Dordrecht: D Reidel Publishing Company, 414 p.

Benefield, L.D. and Molz, F.J. (1984). A model for the activated sludge process which considers wastewater characteristics, flux behaviour and microbial population. Biotechnology Bioengineering **26**: 352-361.

Boll, J., Steenhuis, T.S. and Selker, J.S. (1992). Fiberglass wicks for sampling of water and solutes in the vadose zone. Soil Science Society of America Journal **56**: 701-707.

Borden, R.C., Bedient, P.B., Lee, M.D., Ward, C.H. and Wilson, J.T. (1986). Transport of dissolved hydrocarbons influences by oxygen-limited biodegradation, 2. Field applications. Water Resources Research **22** (13): 1983-1990.

Borden, R.C. and Bedient, P.B. (1986). Transport of dissolved hydrocarbons influenced by oxygen–limited biodegradation, 1. Theoretical development. Water Resources Research **22** (13): 1973-82.

Boulding, J. R. and Ginn, J.S. (2004). Practical handbook of soil, vadose zone and ground water contamination: assessment, prevention and remediation, 2nd ed. Florida: CRC Press LLC., 691 p.

Bouwer, E.J. and McCarty, P.L. (1984). Modeling of trace organics biotransformation in the subsurface. Ground Water **22** (4): 433-440.

Bowles, J.E. (1992). Engineering properties of soils and their measurement, 4th ed. New York: McGraw-Hill, Inc., 240 p.

Brady, N. C. (1974). The nature and properties of soil, 8th ed. New York: Macmillan, 740 p.

Bremner, J.M. and Mulvaney, C.S. (1982). Nitrogen-total, *In* A.L. Page et al. (eds.) Methods of soil analysis, Part 2 Chemical and microbiological properties. Agronomy **9**, p.595-624.

Broadbridge, P. and White, I. (1988). Constant rate rainfall infiltration: A versatile nonlinear model 1. Analytical solution. Water Resources Research **24** (1): 145-154.

Brooker, B. (1999). The source of faecal coliforms in Wallis Lake. NSW Annual Coastal Conference Proceedings, Forster, NSW Coastal Council, 38-57.

Brouwer, J. (1983). Land capacity for septic tank effluent absorption field. Canberra: Department of Resources and Energy, Australian Water Resources Council, 339 p.

Brouwer, J. and Bugeja, R.M. (1983). Land application for septic tank effluent absorption fields. Report of Australian Water Resource Council. Research Project 79/118. Australian Water Resource Council Technical Publication No. 80, part 2. Canberra: Australian Government Publishing Service, 177 p.

Brouwer, J., Willatt, S.T., and van der Graaff, R. (1979). The hydrology of on-site septic tank effluent disposal on a yellow duplex soil. *In* Hydrology and Water Resources Symposium, 10-12 Sept 1979, Perth. Canberra: ACT IEAust.

Brunauer, S., Emmertt, P.H. and Teller, E. (1938). Adsorption of gases in multimolecular layers. Journal of the American Chemical Society **60**:39.

Bunnell, J.F., Zampella, R.A., Morgan, M.D. and Gray, D.M. (1999). A comparison of nitrogen removal by subsurface pressure dosing and standard septic systems in sandy soils. Journal of Environmental Management **56** :209-219.

Butler, D. and Payne, J. (1995). Septic tanks: Problems and practice. Building and Environment **30**(3): 419-425.

Canter, L.W. and Knox, R.C. (1985). Ground water pollution from septic tank systems. *In* Septic tank system effects on ground water quality. Michigan: Lewis Publishers Inc. 333 p.

Carsel, R. F., and Parrish, R. S. (1988). Developing joint probability distributions of soil-water retention characteristics. Water Resources Research **24**(5): 755-769.

Celia, M.A., Boulotas, E.T. and Zarba, R.L. (1990). A general mass-conservative numerical solution for the unsaturated flow equation. Water Resources Research **26**(7): 1483-1496.

Characklish, W.G., Turakhia, M.H. and Zelver, N. (1990). Transport and interfacial transfer phenomena, Biofilms. *In* W.G. Characklish and K.C. Marshall (eds.) New York: John Wiley, pp.341-394.

Clapp, R. B. and Hornberger, G.M. (1978). Empirical equations for some soil hydraulic properties. Water Resources Research **14**: 601-604.

Clement, T.P., Sun, Y., Hooker, B.S. and Petersen, J.N. (1998). Modeling multispecies reactive transport in ground water. Groundwater Monitoring Remediation Journal **18**: 72-92.

Codd, M. (1997) Public inquiry into the management of sewage and sewage by products in the NSW Coastal zone. NSW Environment Protection Authority.

Coley, R.L. (1983). Some new procedures for numerical solution of variably saturated flow problems. Water Resources Research **19**(5): 1271-1285.

Cullen, S.J. and Everett, L.G. (1995). Estimating the storage capacity of the vadose zone. *In* L.G. Wilson et al. (eds.), Handbook of vadose zone characterization & monitoring. Florida: CRC Press, Inc., 730 pp.

Cuyk, S.V., Siegrist, R., Logan, A., Masson, S., Fischer, E. and Figueroa, L. (2001). Hydraulic and purification behaviors and their interaction during wastewater treatment in soil infiltration systems. Water Research **35**(4): 953-964.

Czigány, S., Flurt, M., Harsh, J.B., Williams, B.C. and Shira, J.M. (2005). Suitability of fibreglass wicks to sample colloids from vadose zone pore water. Vadose Zone Journal **4**:175-183.

Degel, H. J. (2006). Purification of air, water and off gas: solvent recovery activated carbon solvent recovery. http:www.activated-carbon.com/sol/recintro.html [accessed: 12 January 2006].

Department of Local Government. (1998). Environmental & health protection: Guideline on-site sewage management for single households. Bankstown: Department of Local Government, 190 p.

Desimone, L.A. and Howes, B.L. (1996). Denitrification and nitrogen transport in a coastal aquifer receiving wastewater discharge. Environmental Science and Technology **30**(4): 1152-1162.

Dingman, S. L. (1994). Physical hydrology. New Jersey: Prentice Hall, 575 p.

Earth Summit. (2002). Freshwater: A global crisis of water security and basic water provision. http://www.earthsummit2002.org [accessed: 28 August 2002].

Fetter, C.W. (1992). Contaminant hydrogeology. New York: Macmillan Publishing Company, 458 p.

Fredlune, D.G. and Rahardjo, H. (1940). Soil mechanics for unsaturated soils. New York: John Wiley & Sons, Inc., 517 p.

Geary, P.M. (1992). Diffuse pollution from wastewater disposal in small unsewered communities. Australian Journal Soil and Water Conservation **5**(1): 28-33.

Geary, P.M. (2003). On-site treatment system failure and shellfish contamination in Port Stephens, NSW. NSW Department of Local Government, Enchantment Grant Project E08 report.

Gee, G.W. and Bauder, J.W. (1986). Particle size analysis, *In* A. Klute et al. (eds.) Method of soil analysis, Part 1 Physical and mineralogical methods. Agronomy **9**, p. 383-411.

Gee, G.W., Zhang, Z.F., Ward, A.L. and Keller, J.M. (2004). Passive-wick water fluxmeters: theory and practice. Proceeding of SuperSoil 2004: 3rd Australian New Zealand Soils conference, 5-9 December 2004, University of Sydney, Australia.

Ginn, T.R., Wood, B.D., Nelson, K.E., Scheibe, T.D., Murphy, E.M. and Clement, T.P. (2002). Processes in microbial transport in the natural subsurface. Advances in Water Resources **25**: 1017-1042.

Green, R.E. and Corey, J.C. (1971). Calculation of hydraulic conductivity a further evaluation of some predictive methods. Soil Science Society of America Proceeding **35**: 3-8.

Green, W.H. and Ampt, G.A. (1911). Studies on soil physics, 1: The flow of air and water through soil. Journal of Agricultural Science **4**(1): 1-24.

Hackney, C.R. and Pierson, M.D. (1994). Environmental indicators and shellfish safety. New York: Chapman and Hall, pp. 92-153.

Hagedorn, C. (1981). The potential for groundwater contamination from septic effluents. Journal of Environmental Quality **10**: 1-8.

Hamilton, G.J., Howes, K.M. and Attwater, R. (eds.) (1992). Proceeding of the 5th Australian Soil Conservation Conference, Perth, W.A., Australia. March 1990.

Harman, J., Robertson, W.D., Cherry, J.A. and Zanini, L. (1996). Impacts on a sand aquifer from an old septic system: nitrate and phosphate. Ground Water **34**(6): 1105-1114.

Harvey, R.W., Smith, R.L. and George, L. (1984). Effect of organic contamination upon microbial distribution and heterotrophic uptake in Cape Cod, Mass., aquifer. Applied and Environmental Microbiology **48**: 1197-1202.

Haverkamp, R., Vauclin, M., Touma, J., Wierenga, P.J. and Vachaud, G. (1977). A comparison of numerical simulation models for one-dimensional infiltration. Soil Science Society of America Journal **41**: 285-294.

Hills, R.G., Porro, I., Hudson, D.B. and Wierenga, P.J. (1989). Modeling one-dimensional infiltration into very dry soils, 1. Model development and evaluation. Water Resources Research **25** (6): 1259-1269.

Holder, M., Brown, K.W., Thomas, J.C., Zabcik, D. and Murray, H.E. (1991). Capillary-wick unsaturated zone pore water sampler. Soil Science Society of America Journal **55**: 1195-1202.

Huyakorn, P.S. and Pinder, G.F. (1983). Computational methods in subsurface flow. New York, Academic Press, 473 p.

Huyakorn, P.S., Mercer, J.M. and Ward, D.S. (1985). Finite element matrix and mass balance computational schemes for transport in variably saturated porous media. Water Resources Research **21** (3): 346-358.

Huyakorn, P.S., Thomas, S.D. and Thompson, B.M. (1984). Technique for making finite element competitive in modeling flow in variably saturates porous media. Water Resources Research **20**(8): 1099-1115.

James, R.V. and Rubin, J. (1986). Transport of chloride ion in a water-unsaturated soil exhibiting anion exclusion. Soil Science Society of America Journal **50**: 1142-1149.

Jewett, D.G., Hilbert, T.A., Logan, B.E., Arnold, R.G. and Bales, R.G. (1995). Bacterial transport in laboratory columns and filters: influence of ionic strength and pH on collision efficiency. Water Research **29**(7): 1673-1680.

Kaplan, O.B. (1991). Septic System Handbook, 2 nd ed. Michigan: Lewis Publisher, 434 p.

Kemper, W.D. (1986). Solute Diffusivity *In* A. Klute et al. Methods of soil analysis part1 Physical and mineralogical methods, 2nd ed. Agronomy **9** (1):1007-1024.

Killingstad, M.W., Widdowson, M.A. and Smith, R.L. (2002). Modeling enhanced in situ denitrification in groundwater. Journal of Environmental Engineering **128**(6): 491-504.

Kinzelbach, W., Schafer, W. and Herzer, J. (1991). Numerical modeling of natural and enhanced denitrification processes in aquifer. Water Resources Research **27**(6): 1123-1135.

Kirkner, D.J. and Reeves, H. (1988). Multicomponent mass transport with homogeneous and heterogeneous chemical reactions: effect of the chemistry on the choice of numerical algorithm 1. Theory. Water Resources Research **24**(10): 1719-1729.

Klute, A. (1986). Water retention: laboratory methods, *In* A. Klute et al. (eds.) Method of soil analysis, Part 1 Physical and mineralogical methods. Agronomy **9**, p.635-662.

Knutson, J.H., Lee, S.B., Zhang, W.Q. and Selker, J.S. (1993). Fibreglass wick preparation for use in passive capillary wick soil pore-water samplers. Soil Science Society of America Journal **57**: 1474-1476.

Kunze, R.J., Uehara, G. and Graham, K. (1968). Factors important in the calculation of hydraulic conductivity. Soil Science Society of America Proceedings **32**: 760-765.

Lee, S., McAvoy, D.C., Szydlik, J. and Schnoor, J.L. (1998). Modeling the fate and transport of household chemicals in septic systems. Ground Water **36**(1): 123-132.

Lo, T.M. and Cui, H.Z. (2006). Properties of green lightweight aggregate concrete: International workshop on sustainable development and concrete technology 113-118. http:www.ctre.iastate.edu/pubs/sustainable/logreen.pdf [accessed: 12 January 2006].

MacQuarrie, K.T.B. and Sudicky, E.A. (2001). Multicomponent simulation of wastewater-derived nitrogen and carbon in shallow unconfined aquifers I. Model Formulation and Performance. Journal of Contaminant Hydrology **47**: 53-84.

MacQuarrie, K.T.B., Sudicky, E.A. and Frind, E.O. (1990). Simulation of biodegradable organic contaminants in groundwater 1. numerical formulation in principal directions. Water Resources Research **26**(2): 207-222.

MacQuarrie, K.T.B., Sudicky, E.A. and Robertson, W.D. (2001). Multicomponent simulation of wastewater-derived nitrogen and carbon in shallow unconfined aquifer II. Model application in a field site. Journal of Contaminant Hydrology **47**: 85-104.

McArthur, W.M. and Bettenay, E. (1964). The development and distribution of the soils of Swan Coastal Plain, Western Australia. CSIRO Australian Soil Publishing. No. 16. Melbourne: CSIRO, 55 p.

McCarty, P.L., Reinhard, L.M. and Rittman, B.E. (1981). Trace organics in groundwater. Environmental Science and Technology **15** (1): 40-51.

McKay, L.D., Layton, A., Rietti-Shati, M. and Driese, S. (2002). Transport of pathogen surrogates in saprolite subsoils in East Tennessee. 12th Tennessee Water Resource Symposium, Montgomery Bell State Park, TN. April 3-5, 2002.

Metcalf and Eddy, Inc. (2003). Constituents in wastewater, *In* Tchobanoglous, G. (eds.) Wastewater engineering: treatment and reuse, 4th ed. New York: McGraw-Hill, pp.27-151.

Miller, R.E., Hazard, J. and Howes, S. (2001). Precision, accuracy and efficiency of four tools for measuring soil bulk density or strength. Oregon: U.S. Department of Agriculture, USDA.

Nelson, D.W. and Sommers, L.E. (1982). Total carbon, organic carbon and organic matter, *In* A. L. Page et al. (eds.) Methods of Soil Analysis, Part 2 Chemical and microbiological properties. Agronomy **9**, p.539-579.

Neralla, S., Weaver, R.W., Lesikar, B.J. and Persyn, R.A. (2000). Improvement of domestic wastewater quality by subsurface flow constructed wetlands. Bioresource Technology **75**: 19-25.

New South Wales Environmental Protection Authority (NSW EPA.) (1995). Environmental guidelines for industry -the utilisation of treated effluent by irrigation. Sydney: NSW EPA.

Noss, R.R. (1989). Septic systems cleaners: A significant threat to groundwater quality. Journal of Environmental Health **51**(4): 201-204.

Nützmann, G., Maciejewski, S. and Joswig, K. (2002). Estimation of water saturation dependence of dispersion in unsaturated porous media: experiments and modelling analysis. Advance in Water Resources **25**: 565-576.

O'Neill, R., Roads, G. and Weise, R. (1993). On-site wastewater treatment and disposal in N.S.W., report prepared for Department of Water Resources and the University of Technology Sydney.

Olsen, S.R. and Sommers, L.E. (1982). Phosphorus, *In* A.L. Page et al. (eds.) Methods of soil analysis, Part 2 Chemical and microbiological properties. Agronomy **9**, p.403-430.

Orhon, D. and Artan, N. (1994). Modeling of activated sludge systems. Lanchester: Technomic Publication, 589 p.

Paniconi, C., Aldama, A.A. and Wood, E.F. (1991). Numerical evaluation of iterative and noniterative methods for solution of the nonlinear Richards equation. Water Resources Research **27**(6): 1147-1163.

Parker, W.F. and Mee, B.J. (1982). Survival of *Salmonella Adelaide* and *Fecal Coliforms* in coarse sands of the Swan Coastal Plain, Western Australia. Applied and Environmental Microbiology **43**(5): 981-986.

Pfannukuch, H.O. (1963). Contribution a l'e'tude des displacements de fluids miscibles dans un milieu poreux. Paris Institut Francais due Petrol Revue **18**: 215-270.

Pickens, J.F. and Grisak, G. E. (1981). Scale-dependent dispersion in stratified granular aquifer. Water Resources Research **17**(4): 1191-1211.

Pierzynski, G.M., Sims, J.T. and Vance, G.F. (2000). Soils and environmental quality, 2nd ed. Boca Raton: CRC Press, 459 p.

Poletika, N.N., Roth, K. and Jury, W.A. (1992). Interpretation of solute transport data obtained with fiberglass wick soil solution samplers. Soil Science Society of America Journal **56**: 1751-1753.

Ptacek, C.J. (1998). Geochemistry of septic-system plume in a coastal barrier bar, Point Pelee, Ontario, Canada. Journal of Contaminant Hydrology **33**: 293-312.

Rawls, W.J., Brakensiek, D.L. and Miller, N. (1983). Green-Amp infiltration parameters from soil data. Journal of Hydraulic Engineering **109** (1): 62-70.

Rayment, G.E. and Higginson, F.R. (1992). Australian laboratory handbook of soil and water chemical methods. Melbourne: Inkata Press, 330 p.

Reeves, H. and Kirkner, D.J. (1988). Multicomponent mass transport with homogeneous and heterogeneous chemical reactions: Effect of the Chemistry on the choice of numerical algorithm 2. Numerical results. Water Resources Research **24** (10): 1730-1739.

Rimmer, A., Steenhuis, T.S. and Selker, J.S. (1995). One-dimensional model to evaluate the performance of wick samplers in soils. Soil Science Society of America Journal **59**: 88-92.

Robertson, W.D. (1995). Development of steady-state phosphorus concentration in septic system plumes. Journal of Contaminant Hydrology **19**: 289-305.

Robertson, W.D. and Blowes, D.W. (1995). Major ion and trace metal geochemistry of an acidic septic system plume in silt. Ground Water **33**(2): 275-283.

Robertson, W.D. and Cherry, J.A. (1992). Hydrogeology of an unconfined sand aquifer and its effect on the behavior of nitrogen from a large-flux septic system. Applied Hydrogeology **1**: 32-44.

Robertson, W.D. and Harman, J. (1999). Phosphate plume persistence at two decommissioned septic system sites. Ground Water **37**(2): 228-236.

Robertson, W.D., Blowes, D.W., Ptacek, C.J. and Cherry, J.A. (2000). Long-term performance of in-situ reactive barrier for nitrate remediation. Ground Water **38**(5): 689-695.

Robinson, R.A. and Stokes, R. H. (1965). Electrolyte solutions: the measurement and interpretation of conductance, chemical potential and diffusion in solutions of simple electrolytes**,** 2nd ed. London: Butter Worth Press, 570 p.

Russell, J. and Reinken, J. (1984). Focus about PRZM: General information. http://viso.ei.jrc.it/focus/gw/models/PRZM/index.html [accessed: 5 December 2002].

Sawyer, C.N., MaCarty, P.L. and Parkin, G.F. (1994). Chemistry for environmental engineering, 4th ed. New York: McGraw-Hill, Inc., 658 p.

Saxton, K.E., Rawls, W. J., Romberger, J.S. and Papendick, R.I. (1986). Estimating generalised soil water characteristics from texture. Soil Science Society of America Journal **50**: 1031-1036.

Schaap, M.G., Leij, F.J. and van Genuchten, M. Th. (2001). Rosetta: A computer program for estimating soil hydraulic parameters with hierarchical pedotransfer functions. Journal of Hydrology **251**:163-176.

Scheidegger, A. (1960). The physics of flow through porous media. Toronto: University of Toronto Press, 313 p.

Schijven, J.F., Hassanizadeh, S.M. and de Bruin, H.A.M. (2002). Column experiment to study nonlinear removal of bacteriophages by passage through saturated dune sand. Journal of Contaminant Hydrology **58**: 243-259.

Schnoor, J.L. (1996). Environmental modeling: fate and transport of pollutants in water, air and soil. New York: John Wiley & Sons, Inc., 682 p.

Segerlind, L.J. (1984). Applied finite element analysis. New York: John Wiley & Sons, Inc., 422 p.

Ségol, G. (1993). Classical groundwater simulations: Proving and improving numerical models. New Jersey: PTR Prentice Hall, 53 p.

Shah, D.B., Coulman, G.A., Novak, L.T. and Ellis, B.G. (1975). A mathematical model for phosphorus movement in soils. Journal of Environmental Quality **4**(1): 87-92.

Shirokova, Y., Forkutsa, I. and Sharafutdinova, N. (2000). Use of electrical conductivity instead of soluble salts for soil salinity monitoring in Central Asia. Irrigation and Drainage Systems **14**: 199-205.

Sierra, J. and Renault, P. (1998). Temporal pattern of oxygen concentration in a hydromorphic soil. Soil Science Society of America Journal **62**:1398-1405.

South Australian Health Commission. (1968). Septic tank effluent drainage schemes, Public Health Inspection Guide 6.

Sparks, D.L. (1995). Environmental soil chemistry. San Diego: Academic Press, pp. 1-202.

Standards Association of Australia (1980-2003). The Australian standards. Journal of the Standard Association of Australia: North Sydney.

Stevik, T.K., Ausland, G., Hansseb, J.F. and Jessen, P.D. (1999b). The influence of physical and chemical factors on the transport of *E.Coli* through biological filters for wastewater purification. Water Research **33**(18): 3701-3706.

Stevik, T.K., Ausland, G., Jenssen, P.D. and Siegrist, R.L. (1999a). Removal of *E.Coli* during intermittent filtration of wastewater effluent as effected by dosing rate at media type. Water Research **33**(9): 2088-2098.

Sydney Water (2005). Our systems and operations: Wastewater treatment plants, http://www.sydneywater.com.au/OurSystemsAndOperations/WastewaterTreatmentPlants/ [accessed: 15 December 2005].

Thomas, G.W. (1982). Exchangeable cations, *In* A. Klute et al. (eds.) Method of soil analysis, Part 1. Physical and mineralogical methods, Agronomy **9**, p.159-165.

U.S. Environmental Protection Agency (EPA). (1977). The report to congress, waste disposal practices and their effects on ground water. EPA/570/9-77/001, 512 p.

U.S. Environmental Protection Agency (EPA). (1983a). Surface impoundment assessment national report. EPA 570/9-84.002.

U.S. Environmental Protection Agency (EPA). (1983b). Nitrogen, ammonia method 350.1 (Colorimetric, Automated, Phenate). *In* Methods for chemical analysis of water and wastewater, EPA-600/ 4-79-020. pp.350-1.1-350-1.4.

U.S. Environmental Protection Agency (EPA). (1986). Septic systems and groundwater protection: A program manager's guideline and reference book. Washington, DC.: Office of Groundwater Protection.

U.S. Environmental Protection Agency (EPA). (1990). National water quality inventory: 1988 Report to Congress, EPA-440-4-90-003.

U.S. Environmental Protection Agency (EPA). (2005). *Escherichia Coli* (*E.Coli*) in water by membrane filtration using modified membrane-Thermotolerant Escherichia coli agar (modified mTEC). EPA-821-R-04-025.

U.S. Geological Survey (USGS). (1993). Methods for analysis by the U.S. Geological Survey National Water Quality Laboratory--Determination of inorganic and organic constituents in water and fluvial sediment, File Report 93-125.

United States Department of Agriculture (USDA) (2001). Soil classification standards. Washington D.C: USDA.

Vachaud, G. and Thony, J.L. (1971). Hysteresis during infiltration and redistribution in a soil column at different initial water content. Water Resources Research **7**: 111-127.

van Genuchten, M. Th. (1980). A closed-form equation for predicting the hydraulic conductivity of unsaturated soils. Soil Science Society of America Journal **44**: 892-898.

Vaughn, J.M., Landry, E.F. and Thomas, M.Z. (1983). Entrainment of viruses from septic tank leach fields through a shallow, sandy soil aquifer. Applied and Environmental Microbiology **45**:1474-1480.

Vinod, T. and Bokil, S.D. (1982). Wastewater treatment by soils: Role of particle-size distribution. Journal of Environmental Quality **11**(4): 596-602.

Walker, W.G., Bouma, J.J., Kenney, D.R. and Olcott, P.G. (1973). Nitrogen transformations during subsurface disposal of septic tank effluent in sands: II Ground water quality. Journal of Environmental Quality **2**(4): 521-525.

Wang, H.F. and Anderson, M.P. (1982). Introduction to groundwater modelling: Finite differences and finite element methods. San Francisco: W.H. Freeman, 237 p.

Wanner, O. and Gujer, W. (1986). A multispecies biofilm model. Biotechnology Bioengineering **28**: 314-328.

Warrick, A.W., Biggar, J.W. and Nielsen, D.R. (1971). Simultaneous solute and water transfer for an unsaturated soil. Water Resources Research **7**(5): 1216-1225.

Warrick, A.W., Islas, A. and Lomen, D.O. (1991). An analytical solution to Richards' equation for time varying Infiltration. Water Resources Research **27**(5): 763-766.

Warrick, A.W. (1991). Numerical approximations of Darcian flow through unsaturated soil. Water Resources Research **27** (6): 1215-1222.

Watson, K.K. (1966). An instantaneous profile method for determining the hydraulic conductivity of unsaturated porous material. Water Resources Research **2**: 709-715.

Watts, R. J. (1997). Hazardous wastes: Resources, pathways, receptors. New York: John Wiley & Sons, Inc, 764 p.

Weiskel, P.K. and Howes, B.L. (1992). Differential transport of sewage-derived nitrogen and phosphorus through a coastal watershed. Environmental Science and Technology **26**(2): 352-360.

Whatman (2005). Glass microfibre filters-typical properties of binder free glass microfibre filters. http://www.whatman.com/products/?pageID=7.25.6 [accessed: 24 December 2005].

Whelan, B.R. (1988). Disposal of septic tank effluent in calcareous sands. Journal of Environmental Quality **17**(2): 272-277.

Whelan, B.R. and Barrow, N.J. (1984a). The movement of septic tank effluent through sandy soils near Perth. II movement of phosphorus. Australian Journal Soil Research **22**: 293-302.

Whelan, B.R. and Barrow, N.J. (1984b). The movement of septic tank effluent through sandy soils near Perth. I Movement of nitrogen. Australian Journal Soil Research **22**, 283-292.

White, I. (2001). Safeguarding environmental conditions for oyster cultivation in New South Wales. Centre for Resource and Environmental Studies, ANU, Canberra. Reported to Healthy Rivers Commission.

White, I. and Broadbridge, P. (1988). Constant rate rainfall infiltration: A versatile nonlinear model 2. Applications of solutions. Water Resources Research **24** (1): 155-162.

Widdowson, M.A., Molz, F.J. and Benefield, L.D. (1988). A numerical transport model for oxygen- and nitrate respiration linked to substrate and nutrient availability in porous media. Water Resources Research **24**(9):1553-1565.

Wierenga, P.J. (1995). Water and solute transport and storage. *In* L.G. Wilson et al. (eds.), Handbook of vadose zone characterization & monitoring. Florida: CRC Press, Inc., pp. 41-60.

Wilhelm, S.R., Schiff, S.L. and Cherry, J.A. (1994). Biogeochemical evolution of domestic waste water in septic systems: 1 conceptual model. Ground Water **32**(6): 905-916.

Wilhelm, S.R., Schiff, S.L. and Robertson, W.D. (1996). Biogeochemical evolution of domestic waste water in septic systems: 2 application of conceptual model in sandy aquifers. Ground Water **34**(5): 853-864.

Winneberger, J.H.T. (1984). Septic-tank system a consultant's toolkit. Boston: Butterworth Publisher, 123 p.

World Summit on Sustainable Development (2002). A framework for action on water and sanitation. http://www.undp.org/seed/water [accessed: 22 February 2002].

Wurbs, R.A. and James, W. P. (2001). Water resources engineering. New Jersey: Prentice Hall, pp.534-621.

Yang, J.E., Skogley, E.O., Schaff, B.E. and Kim, J.J. (1998). A simple spectrophotometric determination of nitrate in water, resin and soil extracts. Soil Science Society of America Journal **62**:1108-1115.

Zanini, L., Robertson, W.D., Ptacek, C.J., Schiff, S.L. and Mayer, T. (1998). Phosphorus characterization in sediments impacted by septic effluent at four sites in Central Canada. Journal of Contaminant Hydrology **33**:405-429.

Zysset, A., Stauffer, F. and Dracos, T. (1994). Modeling of reactive groundwater transport governed by biodegradation. Water Resources Research **30**(8): 2423-2434.